(NASA-CR-135239-Vol-2) ACOUSTIC TESTS OF DUCT-BURNING TURBOFAN JET NOISE SIMULATION: COMPREHENSIVE DATA REPORT. VOLUME 2: MODEL DESIGN AND AERODYNAMIC TEST RESULTS Final Report (General Electric Co.) 229 p HC G3/07 27187

N78-28097

Unclas

ACOUSTIC TESTS of DUCT-BURNING TURBOFAN JET NOISE SIMULATION

COMPREHENSIVE DATA REPORT

VOLUME II

MODEL DESIGN AND
AERODYNAMIC TEST RESULTS

P.H. HECK
D. LATHAM
J.F. BRAUSCH
E.J. STRINGAS
P.S. STAID
P.R. KNOTT

General Electric

NATIONAL AERONAUTICS AND SPACE ADMINISTRATION
LEWIS RESEARCH CENTER
21000 BROOKPARK ROAD
CLEVELAND, OHIO 44135

NASA CONTRACT: NAS3-18008

ACOUSTIC TESTS of DUCT-BURNING TURBOFAN JET NOISE SIMULATION

COMPREHENSIVE DATA REPORT

VOLUME II

MODEL DESIGN AND
AERODYNAMIC TEST RESULTS

P.H. HECK
D. LATHAM
J.F. BRAUSCH
E.J. STRINGAS
P.S. STAID
P.R. KNOTT

General Electric

NATIONAL AERONAUTICS AND SPACE ADMINISTRATION
LEWIS RESEARCH CENTER
21000 BROOKPARK ROAD
CLEVELAND, OHIO 44135

NASA CONTRACT: NAS3-18008

INTRODUCTION

The following two reports represent detailed discussions of model design and aerodynamic performance test results in support of the Final Technical Report on NASA Contract NAS3-18008.

VOLUME II

Table Of Contents

1. "Concept Screening and Model Design For Acoustic Tests of Duct-Burning Turbofan Jet Noise Simulation", J F. Brausch and P.S. Staid, General Electric AEG TM-74-270, June 1974.

2. "Hot/Cold Flow Model Tests To Determine Static Performance of Duct Noise Suppression Nozzles", R.A. Kirschbaum and R.G. Brasket, FluiDyne Engineering Corporation Report 1008, July 1974.

GENERAL ELECTRIC

TECHNICAL MEMORANDUM

OPERATION Acoustic Design Technology

PROJECT NAS3-18008 T.M. NO. 74-270

G. E. CLASS 2

TITLE:

Concept Screening and Model Design for Acoustic Tests of Duct-Burning Turbofan Jet Noise Simulation

PREPARED BY J.F. Brausch & P.S. Staid 6/12/74 DATE

APPROVED BY P.H. Heck P.H Heck 6/12/74 DATE

DISTRIBUTION:

A.J. Albright	V.G. Harris	C.T. Savell
R.D. Allan	P.H. Heck	F.V. Scheffel
C. Ball	J. Johnson	J.J. Schloemer
R.G. Beavers	P.R. Knott	R.G. Siegfried
B. Brimelow	D. Latham	E.J. Stringas
O.T. Castells	R. Lee	R.W. Whittaker
W.S. Clapper	P.W. Mossey	Evendale TIC (3)
V.L. Doyle	J.R. Savage	

Table of Contents

Section		Page
1.0	SUMMARY	1
2.0	INTRODUCTION	2
3.0	DESIGN OBJECTIVES	4
4.0	SYSTEM CONCEPT SELECTION	7
	4.1 GENERAL APPROACH	7
	4.2 CYCLE ANALYSIS AND SELECTION OF PRIMARY TO SECONDARY AREA RATIO	13
5.0	BASELINE ENGINE/SCALE MODEL COANNULAR NON-COPLANAR SYSTEM	23
	5.1 DEVELOPMENT OF BASELINE ENGINE FLOWPATH	23
	5.2 SCALE MODEL SYSTEM DEFINITION	28
6.0	DUCT MULTI-ELEMENT SUPPRESSOR SYSTEMS	32
	6.1 STUDY AND DESIGN OF MULTI-TUBE DUCT SUPPRESSOR SYSTEM	33
	6.1.1 Area Ratio	33
	6.1.2 Tube Number	41
	6.1.3 Analytical Prediction Procedure - Area Ratio and Tube Number	45
	6.1.4 Tube Size Equality and Spacing Uniformity	54
	6.1.5 Tube Length	54
	6.1.6 Baseplate and Tube Exit Plane Stagger	65
	6.1.7 Tube Nozzle Aerodynamic Performance Correlation	74
	6.1.8 Selection of Multi-Tube Duct Suppressor Design	79
	6.2 STUDY AND DESIGN OF MULTI-CHUTE DUCT SUPPRESSOR SYSTEM	84
	6.2.1 Acoustic/Aerodynamic Review	84
	6.2.2 Aerodynamic Correlation	99
	6.2.3 Selection of Multi-Chute Duct Suppressor Design	101
7.0	EJECTORS - HARDWALL AND ACOUSTICALLY TREATED	108
	7.1 HARDWALL EJECTOR DESIGN	108
	7.2 ACOUSTICALLY TREATED EJECTOR DESIGN	112
8.0	COANNULAR COPLANAR BASELINE SYSTEM	117

Table of Contents (concluded)

Section		Page
9.0	MODEL HARDWARE DESIGN DEVELOPMENT	119
10.0	MODEL INSTRUMENTATION	130
	REFERENCES	132
	NOMENCLATURE	134
	APPENDIX A	136

SECTION 1.0

SUMMARY

Under contract with NASA-Lewis (NAS3-18008), the concept of a dual flow turbojet engine operating at takeoff with an over-extracted core and afterburning duct cycle was to be investigated for acoustic and aerodynamic performance; particularly for possible acoustic refraction benefits. A system concept study resulted in selection of a coannular dual flow plug nozzle and from a detailed parametric cycle analysis, an A_{e8}/A_{e18} ratio of 1.55 was chosen. An engine exhaust nozzle flowpath was designed and scaled to model size, a representative baseline nozzle for the study. Upon thorough review of available literature and test data, multi-element tube and chute jet noise suppressor concepts were selected for the augmented duct. Additionally, a secondary ejector concept was selected allowing for evaluation of both hardwall and acoustically treated ejector flowpaths. A coannular coplanar nozzle system without center plug was also selected as a standard acoustic baseline. A thorough mechanical design effort resulted in a well integrated detailed model nozzle system capable of withstanding the wide range of pressure and temperature test conditions planned for a thorough investigation of the concepts acoustic/aerodynamic feasibility. The nozzle system provides smooth nozzle external flowlines and is readily adaptable for use in wind tunnel acoustic/aerodynamic performance evaluation.

This memorandum documents the concept selection and model design effort of the contract. Upon completion of the planned test effort, additional reports will document the acoustic and aerodynamic performance evaluation.

SECTION 2.0

INTRODUCTION

During the course of the United States Supersonic Transport Program, the urgent necessity to aggressively attack the jet noise problem was clearly established. As studies of Advanced Supersonic Transport (AST) systems progress, increased emphasis on noise reduction technology will be mandatory if a new, viable AST program is to become a reality. Furthermore, the potential establishment of Federal noise regulations below those of FAR Part 36 will require a broad investigation of various engine cycles and jet noise suppressors. Currently, the duct-burning turbofan (DBTF) cycle is a potential candidate.

Heretofore, most of the jet noise suppression work accomplished for high speed aircraft has been aimed at turbojet and mixed flow turbofan cycle systems. Very little jet noise suppression effort has been applied to separated flow turbofan cycles.

There are several considerations which indicate the existence of acoustic source noise reduction through the advantage of refractive characteristics of duct-burning turbofan jet streams. Preliminary acoustic refraction calculations indicate that noise produced by the lower velocity core stream of a separated flow duct-burning fan engine, including the upstream core engine noise, may be focused away from the sideline. If lined ejectors are used with duct-burning coannular nozzles, the relative location of the dominant noise sources are nearer to the ejector walls than are the dominant noise sources of turbojet and mixed flow turbofan systems. This closer proximity of the noise sources will most likely enhance the lined ejector suppression effectiveness and lower the ejector length requirement. Moreover, locating the suppressor elements in the noise-dominant annular stream may simplify the deployment and stowage problem. Suppressor ventilation may also be enhanced by virtue of its location.

While these potential advantages attributed to the DBTF concept remained unproven, NASA Lewis recognized the need for design study and confirming experimental investigation. On August 22, 1973, the General Electric Company

became recipient of a NASA contract to investigate such a concept, namely, NAS3-18008, "Acoustic Tests of Duct Burning Turbofan Jet Noise Simulation." Work scope within the contract includes a) design and development of a simulated DBTF exhaust nozzle system in model hardware, both unsuppressed and mechanically suppressed in the duct stream and with and without hardwall/ acoustically treated ejector systems, b) acoustic, aerodynamic and plume velocity evaluation of the performance of the model systems, and c) analysis of the resultant test data in terms of acoustic phenomena and acoustic/ aerodynamic performance trades.

This technical memorandum documents the engineering design study performed to conceptually develop the DBTF exhaust nozzle system, the duct nozzle multi-element jet noise suppressors and the hardwall and acoustically treated ejector systems. It also documents the basic criteria for hardware mechanical design as well as the resultant detailed final hardware.

SECTION 3.0

DESIGN OBJECTIVES

The objectives of the model system selection, conceptual definition of duct suppressors and ejector systems, and hardware mechanical design and detail were delineated in the RFP and the subsequent contract and work plan as follows:

1.0 Model Design and Fabrication

- The Contractor shall design the nozzle/suppressor/ejector for each of the two preselected multi-chute and multi-tube annular stream suppression concepts. The Contractor shall apply state-of-the-art noise suppression, aerodynamic and engine design information, as well as quick, inexpensive test procedures to refine the potentially large number of design variables present in such concepts. In addition, the Contractor shall design two baseline models; an unsuppressed coannular non-coplanar nozzle with center plug and an unsuppressed coannular coplanar nozzle without center plug.
- The Contractor shall fabricate the test models for use in hot static tests. Test models shall include ejectors, ejector acoustic liners, instrument connections at the test models and adapters to fit test facilities.
- All test models shall have a common primary to secondary area ratio and primary flow area. Models shall be sufficiently large to allow scaling to full size AST duct-burning turbofan engines. In no case shall models have an equivalent diameter smaller than six inches. Models shall be of flight-type configuration to allow possible future study of external flow effects.

2.0 Test

- The Contractor shall perform static tests for noise and aerodynamic performance on the suppressed and baseline configurations. The parametric test matrix shall cover a range of temperature and velocity combinations sufficiently wide to investigate the effects of the two suppressor concepts, with and without ejectors and acoustic liners on the generation, redirection and absorption of jet noise, and to compare them with the baseline coannular non-coplanar and coplanar nozzle characteristics. The minimum ranges of variables required for testing are:

  a) Temperature:

  Primary Stream, T_8 = amb to 1460° R
  Annular Stream, T_{18} = amb to 1960° R
  $\Delta T = T_{18} - T_8$ = 0 to 1000°

  b) Velocity:

  Primary Stream, V_9 = 1000 to 1400 ft/sec
  Annular Stream, V_{19} = 550 to 2800 ft/sec
  Velocity Ratio, V_{19}/V_9 = 0.4 to 2.0

- The Contractor shall notice that even though the prime concept under investigation is based on the annular stream having higher velocities and temperatures than the primary stream, ($V_{19}/V_9 > 1.0$, $(T_{18} - T_8) > 0$), and in the supersonic range for the annular flow, some data are still required at $V_{19}/V_9 < 1.0$, $T_{18} - T_8 \leq 0$ and subsonic velocities in the annular stream.

- Data shall be taken, as a minimum, for the two suppressed-annulus test models without ejector, with hardwall ejector, and with lined ejector, as well as for the two baseline configurations. These models are as follows:

Model No.	Description
1	Coannular, Non-coplanar, Annular Multi-chute Suppressor
2	Coannular, Non-coplanar, Annular Multi-tube Suppressor
3	Model 1 with Hardwall Ejector

4 Model 1 with Acoustically Treated Ejector

5 Model 2 with Hardwall Ejector

6 Model 2 with Acoustically Treated Ejector

7 Coannular, Non-coplanar, Unsuppressed

8 Coannular, Coplanar, Unsuppressed

- The Contractor shall provide sufficient instrumentation to measure thrust, weight flow and total temperature and pressure sufficient to calculate the ideal velocities. In addition, jet plume velocity distributions will be documented. Static pressure profiles shall be measured along ejector walls.

3.0 Data Analysis

- The Contractor shall process the data obtained on all tests and analyze the results. The results shall, as a minimum, show the measured effect of the two suppressed coannular nozzle concepts, with and without ejector, lined and unlined, upon noise generation as indicated by sound power levels and comparisons with the baselines, both on a total and spectral basis. The measured effect of velocities on power generation shall also be analyzed. Effect of configuration and velocities upon sound propagation, as indicated by directivity and sound pressure level spectra shall be analyzed. Effectiveness of the different configurations on noise suppression shall be compared as indicated by changes in thrust and perceived noise level along the sideline. All noise spectral data shall be handled on the basis of 1/3-octave band analysis. The Contractor shall examine noise data and aerodynamic data and correlate the results obtained.

- The above mentioned analyses, in addition to any others that the Contractor may deem expedient, shall be combined to evaluate the worth of the suppression concepts studied on applications to DBTF cycles, and provide methods for more realistically including noise considerations in the cycle screening procedures. In addition, suggestions shall be provided on the need and nature of further studies on DBTF nozzle suppressor performance.

SECTION 4.0

SYSTEM CONCEPT SELECTION

4.1 GENERAL APPROACH

Recent studies on advanced cycles applicable to military and commercial high Mach aircraft indicate potential system advantages for multiple-flow engines, such as duct-burning turbofans and variable cycle engines. Plug nozzles, and in particular, dual flow plug nozzles, integrate well with these type of engine systems and possess both performance and mechanical advantages over other types of exhaust systems.

The main internal performance advantage of the single or dual flow plug nozzle is that it provides the necessary expansion area for the high Mach conditions with minimum weight and complexity, while maintaining high levels of installed performance at transonic and subsonic flight conditions. The plug nozzle also exhibits an installed performance payoff. At high flight Mach numbers, the exhaust gases fill the available expansion area and the drag is, therefore, very low. In subsonic flight the jet plume does not fill the available projected area behind the engine, resulting in an effective aerodynamic boattail, potentially more shallow than equivalent realistic C-D nozzle boattails, and less drag.

Exhaust system weight becomes increasingly more important as the design Mach number increases. This trend is due primarily to the extra nozzle length and complexity required by the large expansion ratios necessary for high performance at high Mach conditions, and also to high nozzle pressure loadings. The plug nozzle offers potential weight advantages because of the structural characteristics of the cylindrical shroud (i.e., the single piece cylindrical shroud carries its pressure loading as hoop stress) as compared to the individual segments of a long flap C-D type exhaust nozzle.

In recent years the sliding shroud plug nozzle concept has emerged. This design translates the outer shroud, varying the nozzle internal area ratio to match that required by the nozzle pressure ratio. This results in high internal performance over a large range of nozzle pressure ratios with minimum complexity and weight.

General Electric has integrated the dual flow translating shroud plug nozzle concept with advanced engine cycles and demonstrated high performance characteristics through scale model nozzle testing. Under the Navy "High Mach Nozzles Program" (Reference 1) and General Electric's Independent Research and Development Program (Reference 2), static and wind tunnel tests were conducted and detailed design methods, criteria, and evaluation techniques were developed. In addition, under the Air Force "Turbine Engine Exhaust Nozzle Performance Investigation," further design studies and both static and installed performance tests are currently being made. Static test results of this program are reported in Reference 3. Furthermore, General Electric has conducted studies over a wide range of aircraft/engine/exhaust nozzle systems for supersonic transport application under the NASA Advanced Supersonic Propulsion System Technology Study (AST). Results of these studies for duct-burning turbofan engines utilizing dual flow plug nozzle exhaust systems are reported in Reference 4.

Through engine exhaust nozzle conceptual design studies, the dual flow plug nozzle system (alternately referred to as the annular internal/external expansion nozzle system) has also been shown amenable to mechanical implementation of jet noise suppressors. System designs have been performed to incorporate multi-element chute and tube suppressors both in the core and duct streams. Typical schemes are shown as a) Figure 4-1, GE21/F3B1 Duct-Burning Turbofan engine with over-extracted core and a 36 chute duct suppressor, b) Figure 4-2, a typical annular internal/external expansion nozzle system utilizing a multi-spoke core suppressor, stowable within the core plug, c) Figure 4-3, GE21/F3B1 Duct-Burning Turbofan with a multi-chute suppressor used for both core and duct suppression, stowable within the core plug, and d) Figure 4-4, GE21/F3B1 Duct-Burning Turbofan engine with a multi-tube duct suppressor, stowable within the duct plug.

These numerous studies formed a base upon which the exhaust nozzle for the NASA DBTF jet noise program was designed. The parametric cycle deck developed for the NASA Advanced Supersonic Propulsion program was utilized to define the basic engine cycle and in particular the exhaust conditions of interest to this program.

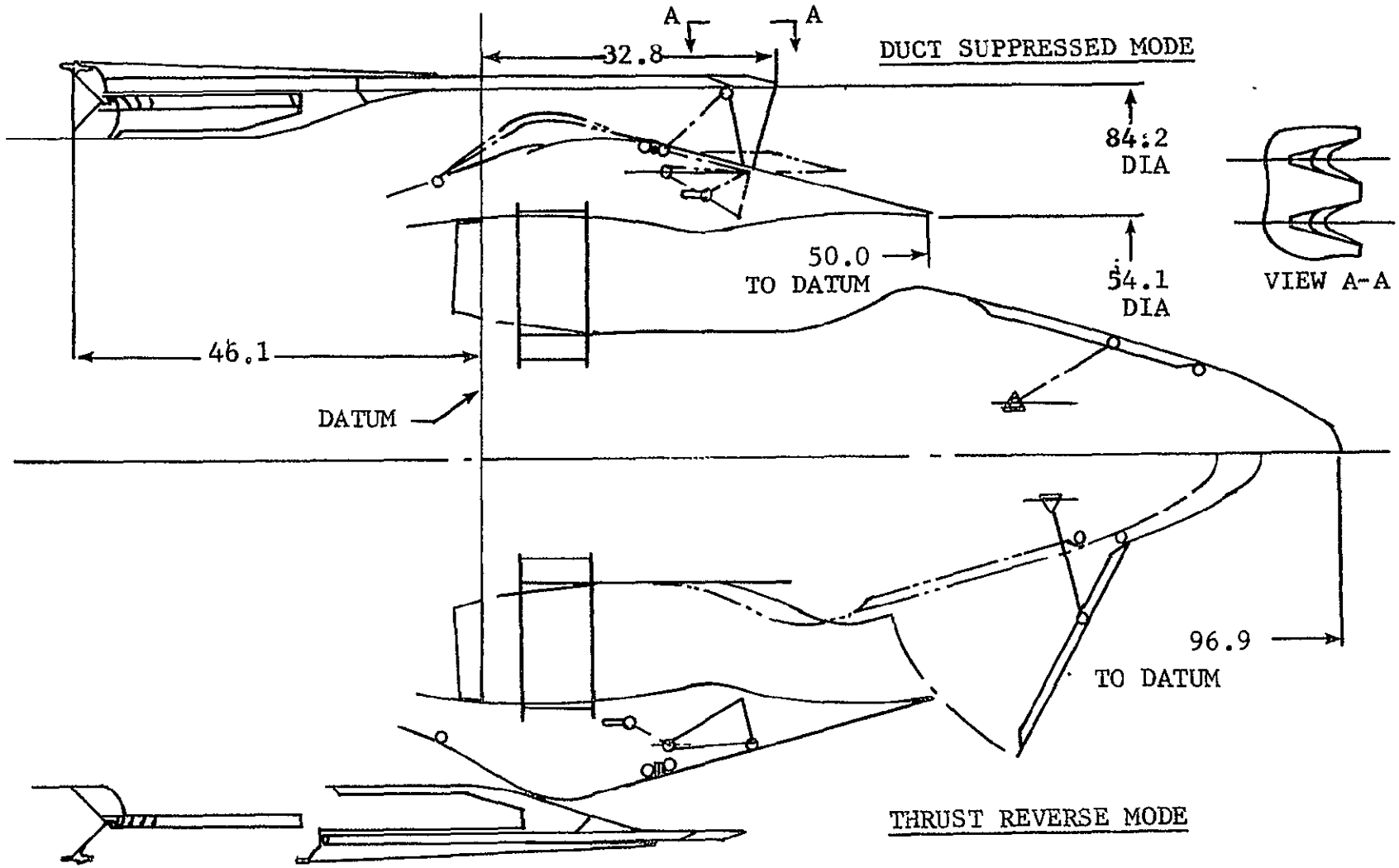

Figure 4-1 DUCT-BURNING TURBOFAN GE21/F3B1 OVER-EXTRACTED CORE, 36 CHUTE DUCT SUPPRESSOR

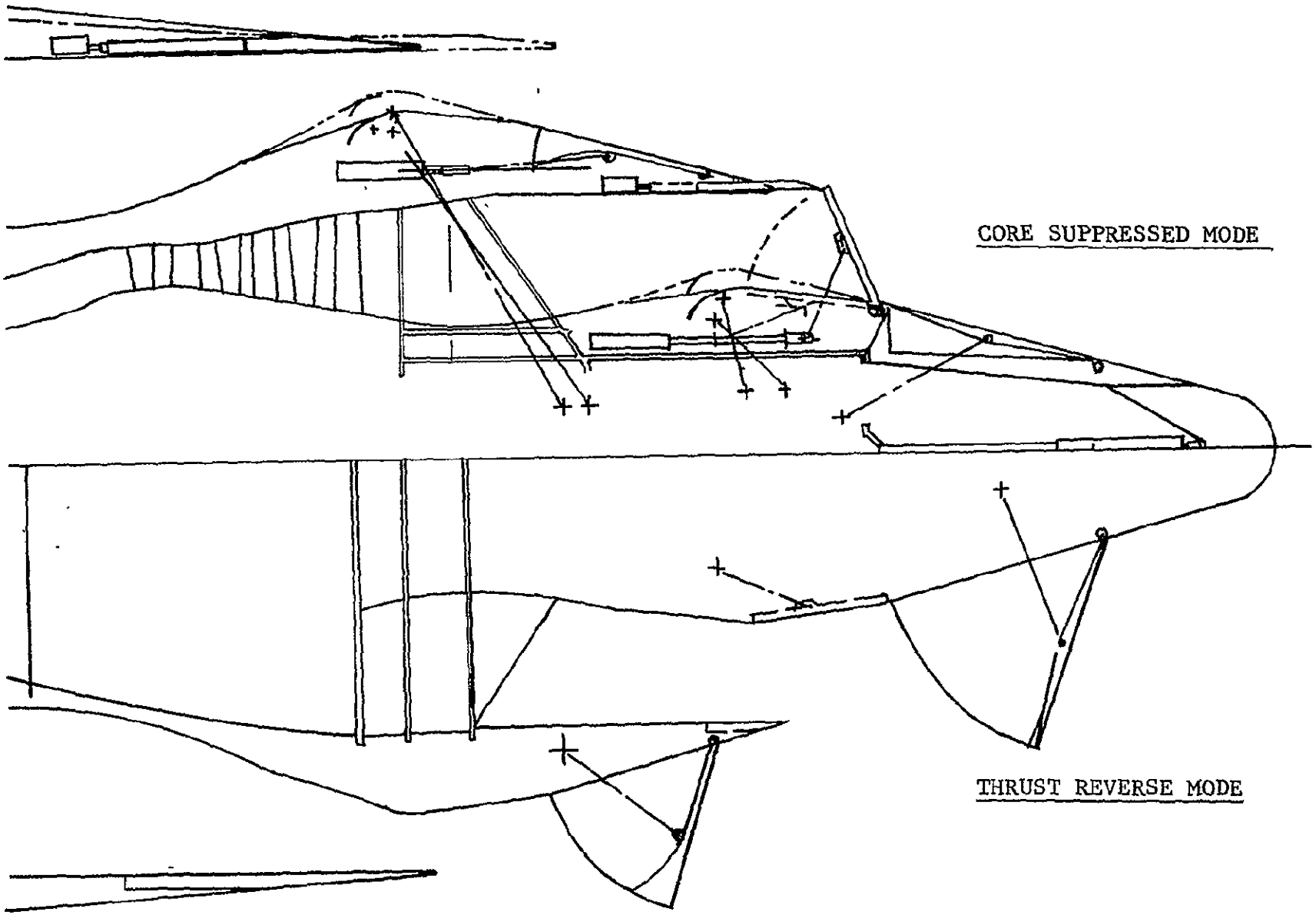

igure 4-2 TYPICAL ANNULAR INTERNAL/EXTERNAL EXPANSION NOZZLE WITH CORE MULTI-SPOKE SUPPRESSOR

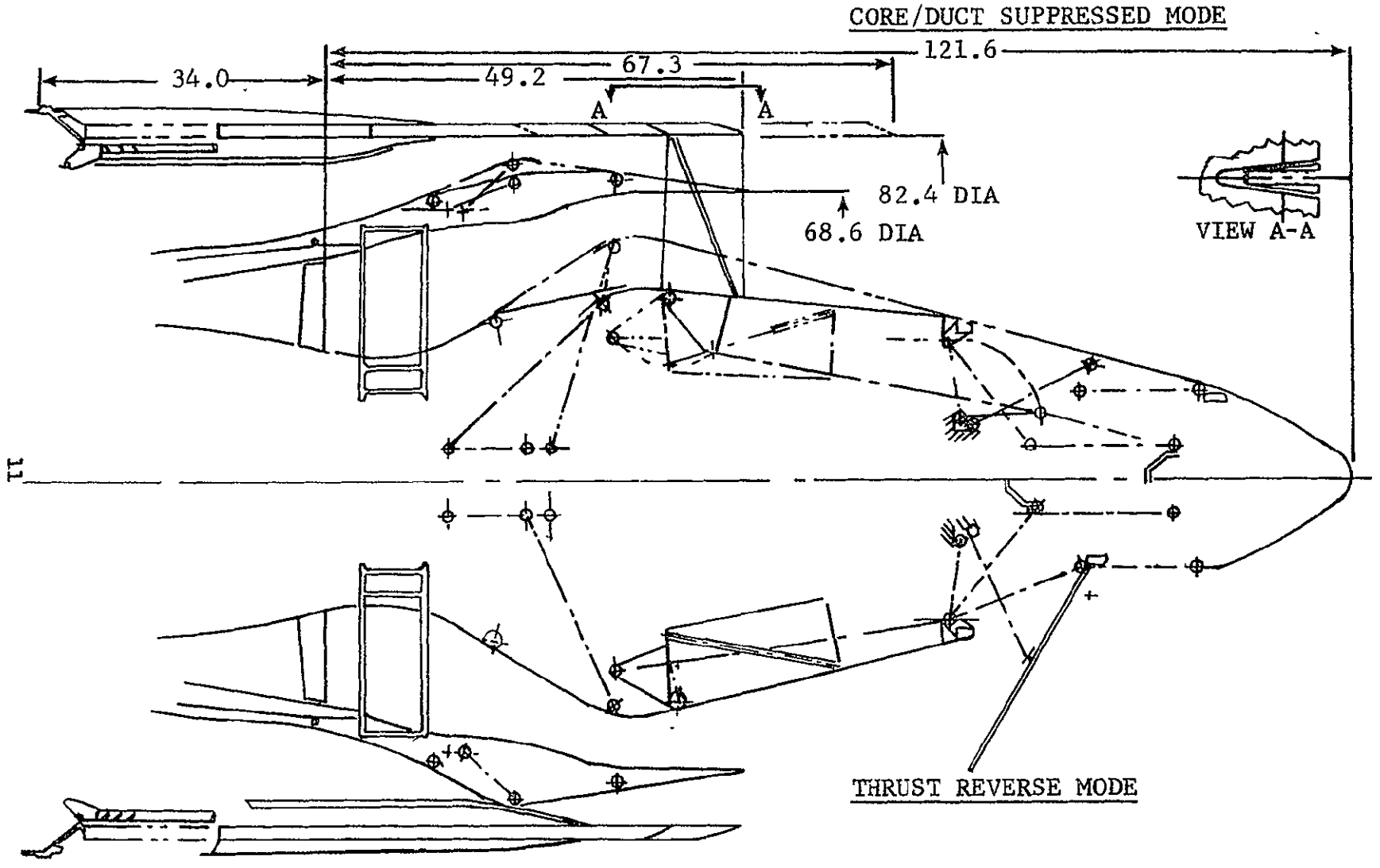

Figure 4-3 DUCT-BURNING TURBOFAN GE21/F3B1, MULTI-CHUTE INTEGRAL CORE/DUCT SUPPRESSOR

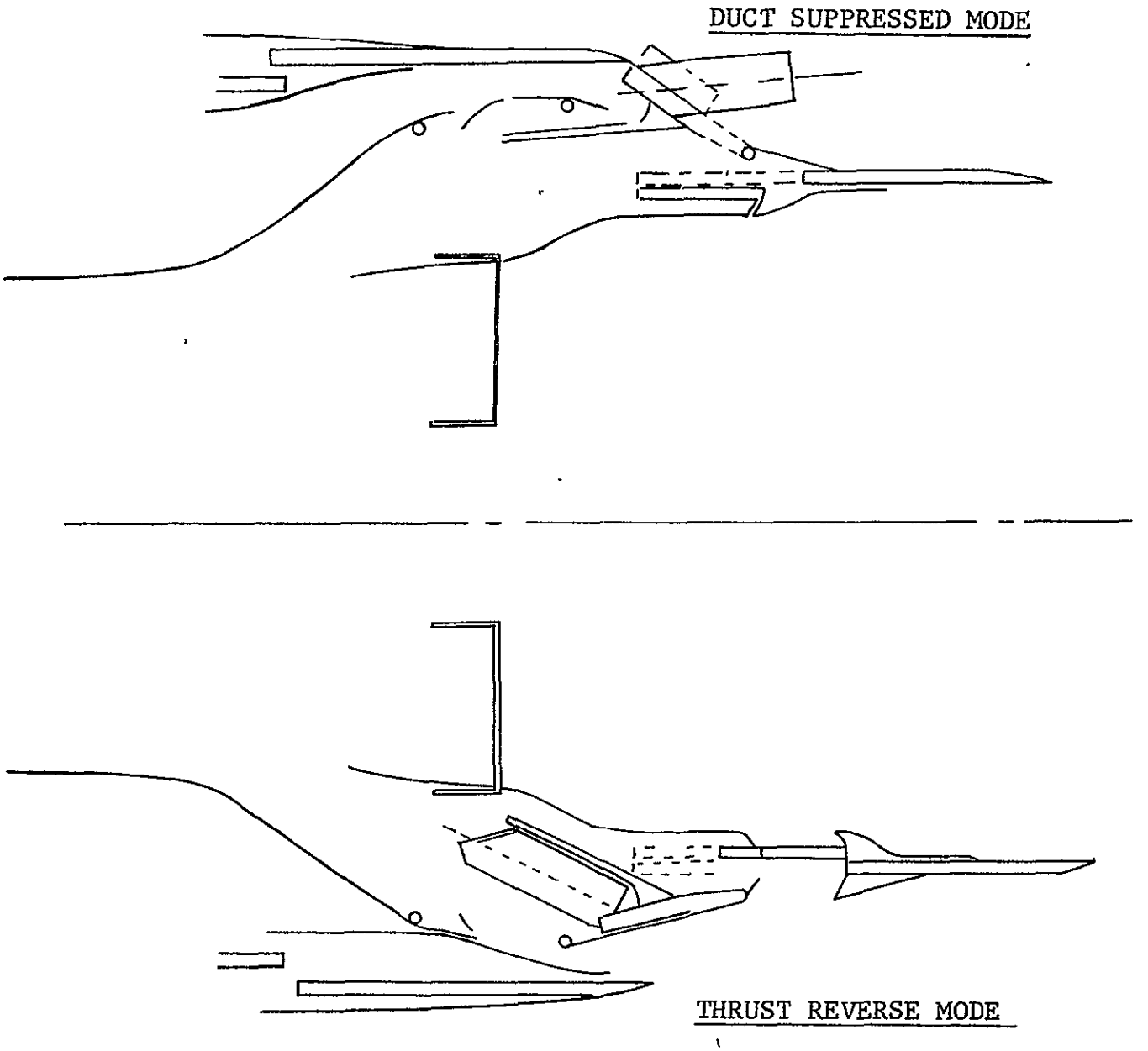

Figure 4-4 DUCT BURNING TURBOFAN GE21/F3B1,
MULTI - TUBE DUCT SUPPRESSOR

The design data and methods developed in References 1, 2, and 3, were used to define the unsuppressed dual flow exhaust nozzle for the selected engine cycle. The result is a representative advanced supersonic technology exhaust system on which to conduct jet noise investigations.

4.2 CYCLE ANALYSIS AND SELECTION OF PRIMARY TO SECONDARY AREA RATIO

The NASA Lewis/GE Advanced Supersonic Propulsion System Technology Study (AST) has conducted detailed investigations of DBTF engine cycles with primary emphasis on non-duct burning during takeoff, but with peripheral studies using duct augmentation at takeoff. From the study, two viable DBTF engine systems precipitated; the F3B1 reported in References 5 and 6 and the F3B2 reported in Reference 7.

The AST parametric DBTF cycle deck was used to study the duct burning cycle with high core energy extraction, to provide insight into selection of the core/fan area ratio (A_{e8}/A_{e18}). Additionally, the selection was influenced by a) considering the maximum core total temperature and jet velocity (T_8 = 1460° R, V_9 = 1400 f/s) and the maximum duct total temperature (T_{18} = 1960° R) within the requested (RFP) matrix as basic engine cycle design criteria, and b) feasibility of mechanically implementing and operating such an engine with a reasonable $\beta(W_{18}/W_8)$ ratio. For the basic cycle study using afterburning takeoff, the duct was considered augmented to the maximum limit of 1960° R. The fan pressure ratio (PR_F) was set at three values, i.e., 2.7, 3.2 and 4.2, while at an engine overall pressure ratio (OAPR) of 15. This resulted in duct exhaust nozzle pressure ratios (P_{18}/P_o) of approximately 2.5, 3.0 and 3.9, respectively, and duct exhaust ideal jet velocities of approximately 2360, 2540 and 2800 ft/sec, respectively. The engine thrust was held constant at about 53.3K lb. for the M = 0.3 sea-level application, therefore, β ratio and subsequent core cycle parameters were allowed to fluctuate at each of the fan pressure ratio points to generate an engine cycle matrix. Pertinent cycle parameters of core total temperature (T_8), duct to core exhaust velocity ratio (V_{19}/V_9), core to duct exhaust nozzle area ratio (A_{e8}/A_{e18}), and bypass ratio (β) are cross plotted in Figure 4-5 for the matrix studies at the three fan pressure ratio settings. On this graph the location of the maximum limit of the RFP core jet velocity,

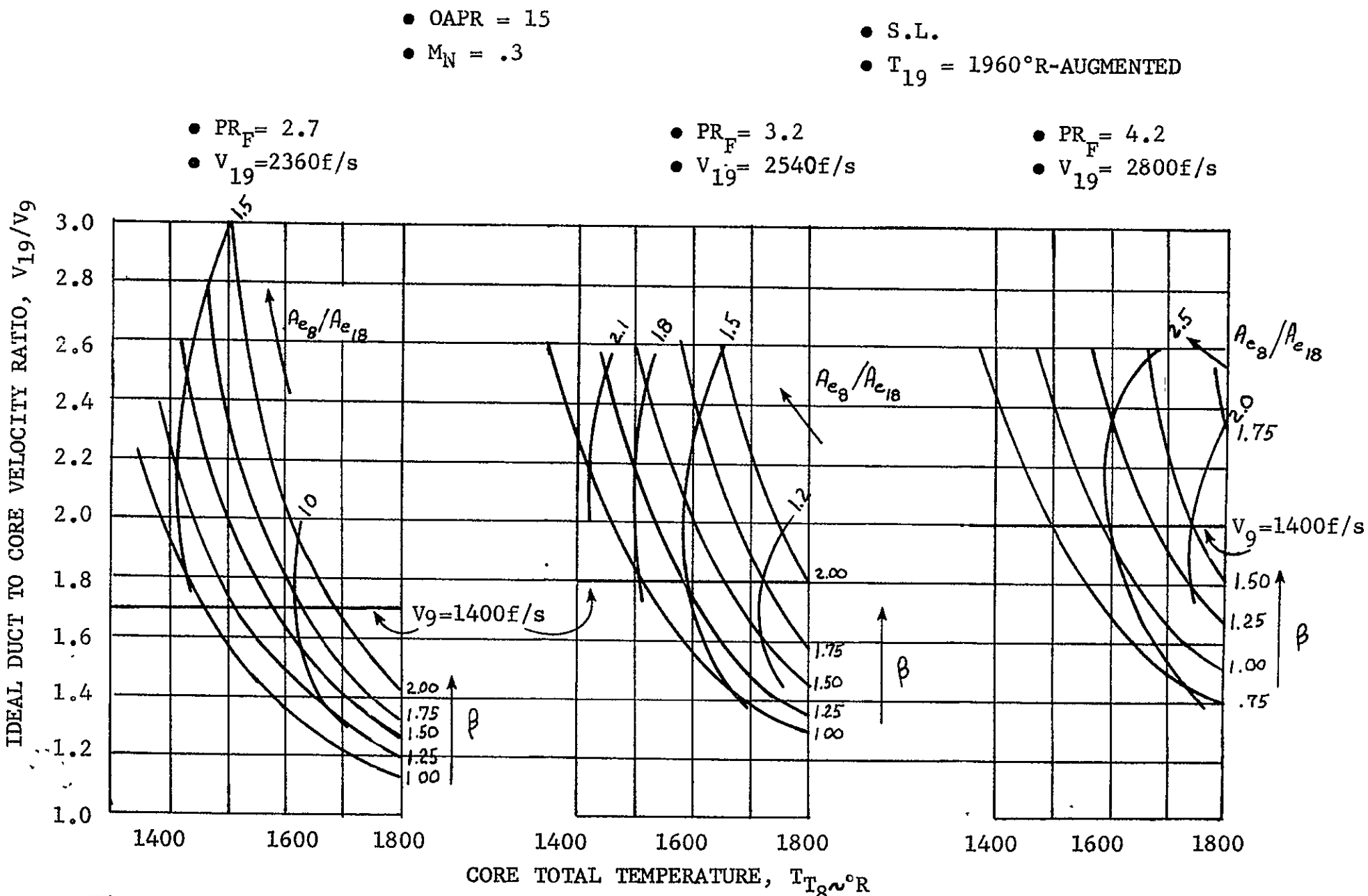

Figure 4-5 OVER EXTRACTED CORE-DBTF CYCLE STUDY, FAN PRESSURE RATIO VARIATION-AUGMENTED

at V_9 = 1400 ft/sec, is indicated on the V_{19}/V_9 scale. At this core velocity the relationship between Ae_8/Ae_{18} and β was then further considered for the eventual selection of the Ae_8/Ae_{18} value for which the exhaust system aerodynamic flowpath would be designed.

In addition to the augmented duct takeoff design cycle at OAPR = 15, a non-augmented duct cycle study was performed holding the same PR_F values of 2.7, 3.2 and 4.2. The resultant pertinent cycle parameters interdependency is cross-plotted in the same manner in Figure 4-6. It becomes clear that, for a selected Ae_8/Ae_{18} value, to generate the same engine thrust level with a non-augmented duct requires a substantially higher β ratio machine than the augmented duct cycle.

To further investigate the effect of engine overall pressure ratio, similar cycle matrices were generated at OAPR values of 10 and 25 at the fan pressure ratios of 2.7 for the augmented duct takeoff application, engine overall pressure ratios of 25, 15 and 10 are representative of Mach 2.2, 2.7 and 3.2 aircraft designs at altitude cruise, respectively. Results of the study are presented in similar format in Figure 4-7.

Based on these cycle studies and on mechanical model and engine considerations, the best selection of core to duct area ratio was chosen at approximately 1.5. This evolved from a) consideration of OAPR = 15 for a Mach 2.7 aircraft to be the most representative engine/aircraft system selection, b) comparison of other engine cycles at takeoff power as is done in Figure 4-8, and c) consideration of the 1400 ft/sec jet velocity at takeoff as the core design point and selecting the best mechanical/aerodynamic trade between Ae_8/Ae_{18} and β.

The selected approximate design point is shown on the OAPR = 15, PR_F = 2.7, T_{18} = 1960° R - augmented takeoff matrix plot, repeated as Figure 4-9. Using this base point as input, more detailed cycle analysis was performed using the AST parametric cycle deck but in an off design mode. Cycle data were thus generated for the base design over-extracted core engine at various pertinent mission points; namely, takeoff, community, approach, subsonic cruise/divert, hold/loiter, climb/acceleration and supersonic cruise. The resulting cycle data are presented in Table 4-1. Honeing-in on the takeoff

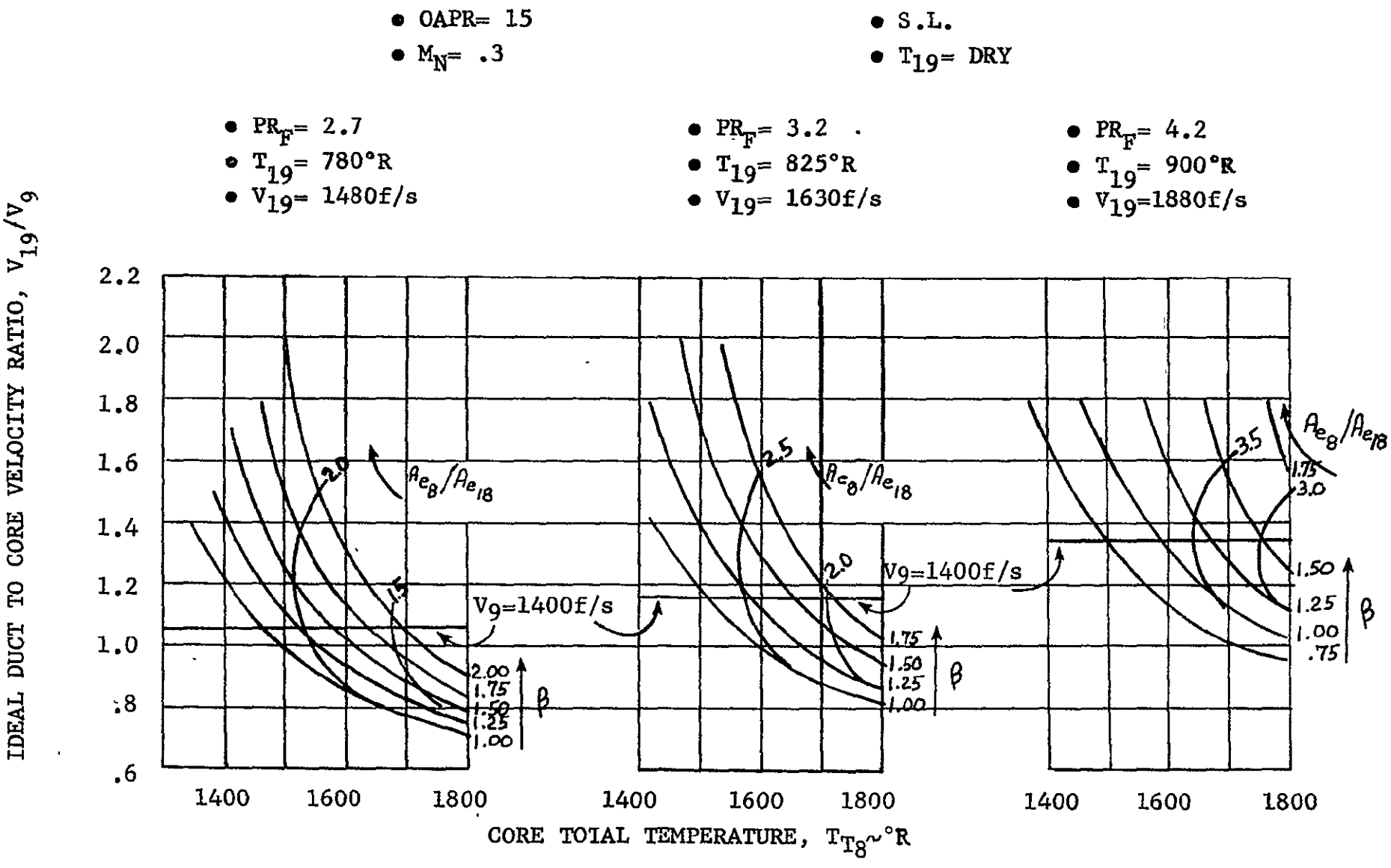

Figure 4-6 OVER EXTRACTED CORE-DBTF CYCLE STUDY, FAN PRESSURE RATIO VARIATION-DRY

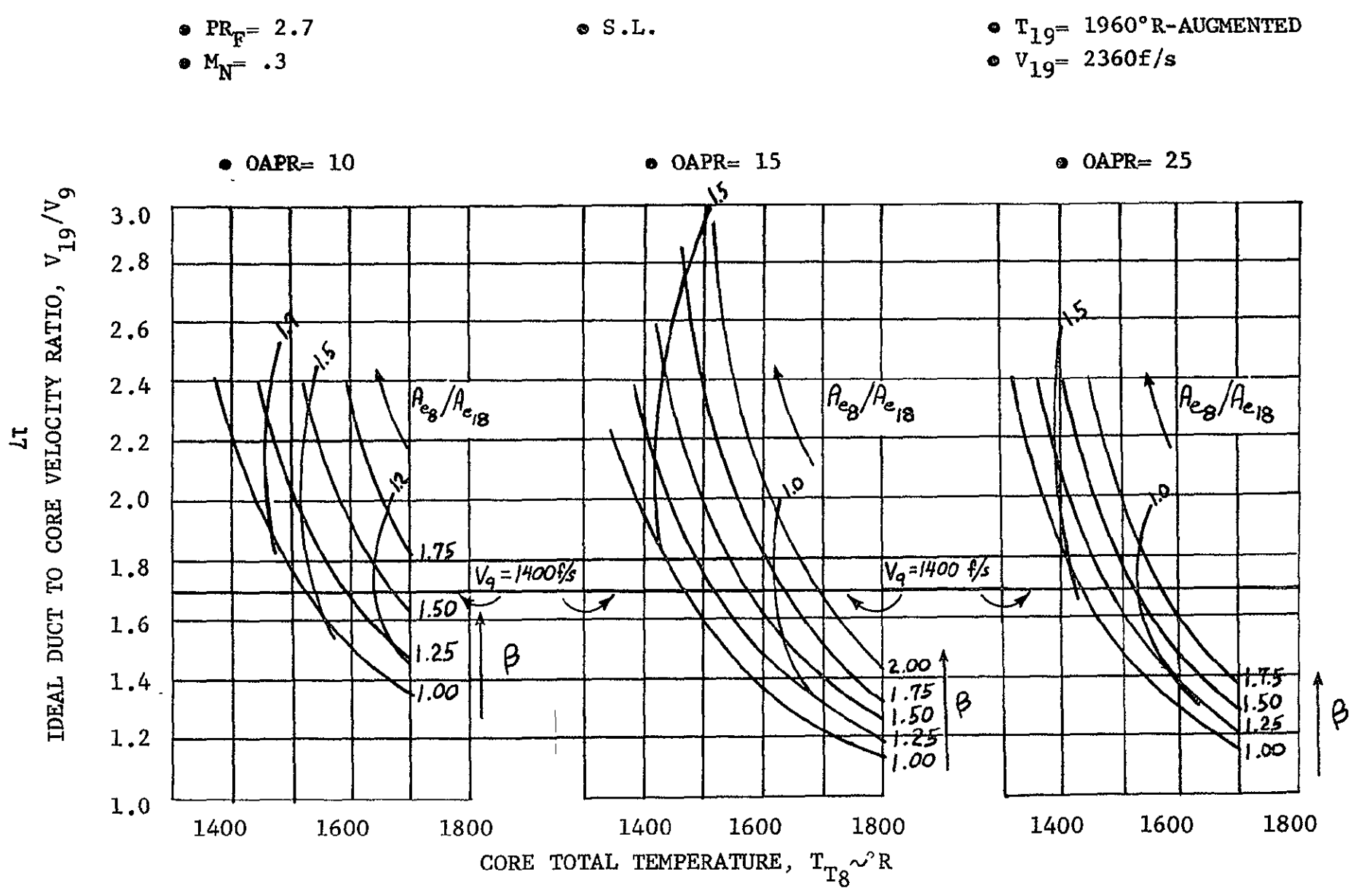

Figure 4-7 OVER EXTRACTED CORE-DBTF CYCLE STUDY, OVERALL PRESSURE RATIO VARIATION-AUGMENTED

- Over-Extracted Core Study Based on Perturbed F3B1 Cycle

⊗ AST Triple Rotor Engine Cycle (Dual Flow at T/O) at T/O Power with M = .3, 500 Ft. Alt., β = 1.22

⊠ AST Variable Cycle, TJ/TF at T/O Power with M = .3, 500 Ft. Alt., β = 1.79

⬡ Study-Selected Approximate Design Point at T/O Power M = .3, Sea Level

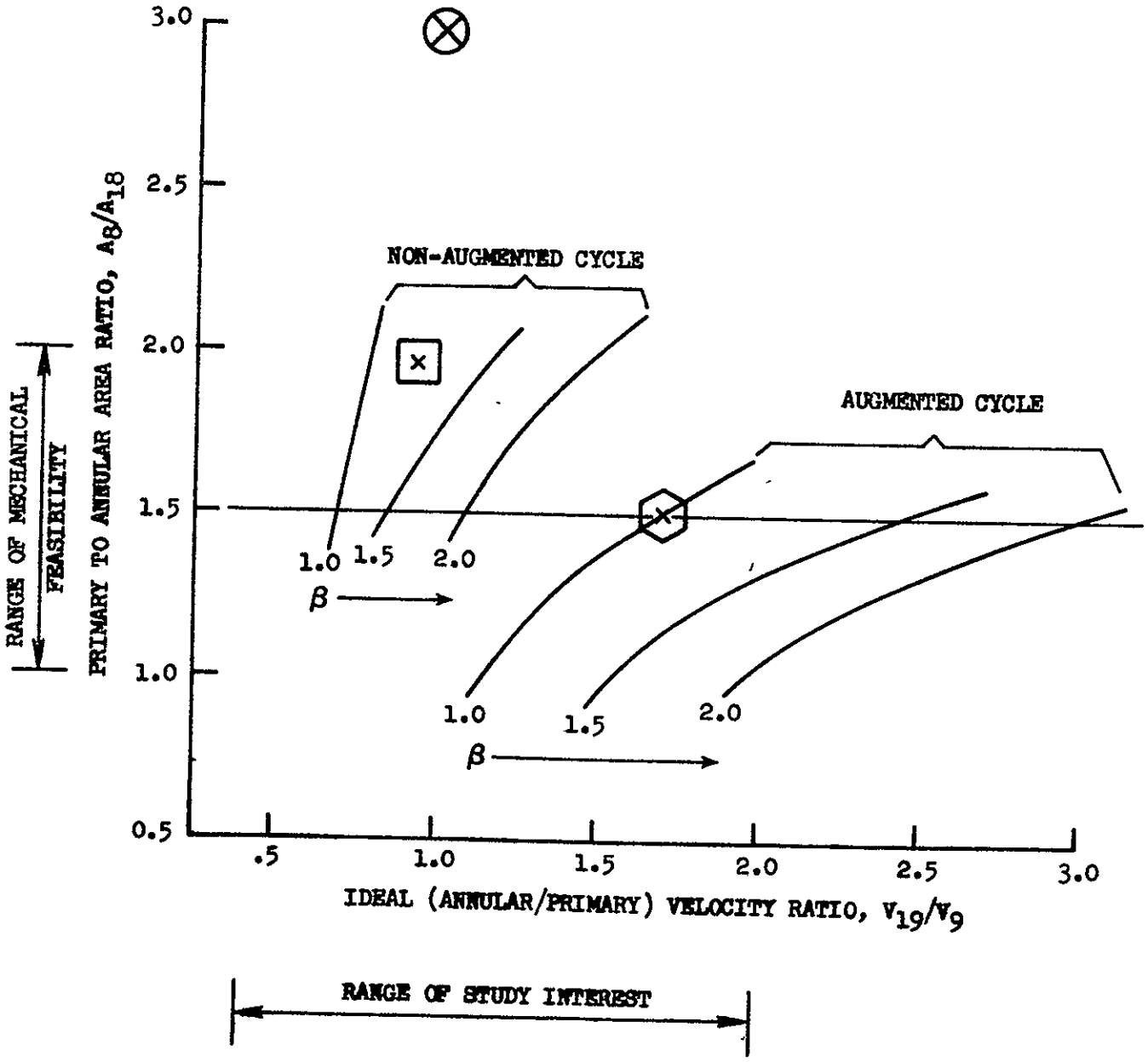

FIGURE 4-8 DESIGN POINT RELATIVE TO DBTF ENGINE CYCLES

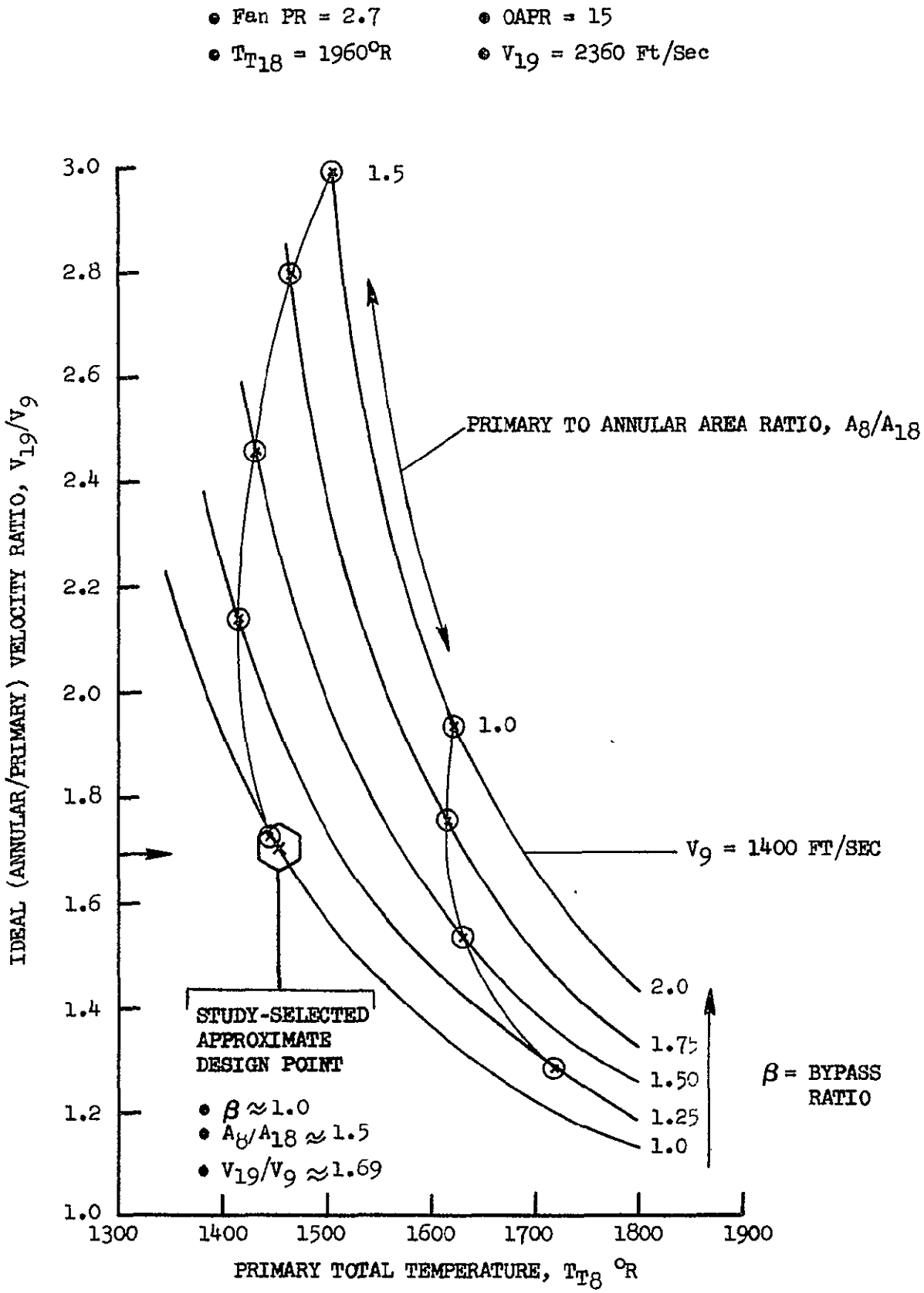

FIGURE 4-9 OVER-EXTRACTED CORE-DBTF CYCLE STUDY

ORIGINAL PAGE IS OF POOR QUALITY

Table 4-1. Cycle Data, Over-Extracted Core DBTF Mission Analysis.

	Takeoff							Community/ Approach			Subsonic Cruise/Divert			
Case	1	2	3	4	5	6	7	8	9	10	11	12	13	14
% Spd	100	90	80	70	60	50	40	70.6	56.2	47.5	43.0	50	39.9	36.8
Alt, ft	0	0	0	0	0	0	0	1500	1500	1500	370	35K	35K	35K
M_o	.3	.3	.3	.3	.3	.3	.3	.4	.4	.4	.221	.95	.95	.95
F_N, lbf	53594	50207	46510	42514	37790	30652	17212	40342	30345	20344	17109	25657	16938	13010
P_{amb}, psia	14.696	14.696	14.696	14.696	14.696	14.696	14.696	13.917	13.917	13.917	14.501	3.458	3.458	3.458
T_{amb}, °R	546	546	546	546	546	546	546	540	540	540	544	408	408	408
P_{18}/P_o	2.656	2.543	2.410	2.257	2.068	1.845	1.519	2.479	2.071	1.738	1.423	4.411	3.717	3.362
T_{18}, °R	1954	1735	1506	1271	1015	761	704	1585	1001	733	696	684	644	623
W_{18}, pps	592	605	616	631	650	675	568	584	620	615	513	225	200	190
Ae_{18}, in^2	1286	1286	1287	1286	1286	1294	1320	1286	1286	1302	1328	726	744	769
V_{19}, F/S	2415	2226	2017	1787	1514	1212	976	2100	1505	1135	895	1775	1702	1645
P_8/P_o	1.510	1.487	1.467	1.452	1.437	1.381	1.211	1.432	1.394	1.300	1.189	7.441	5.505	4.574
T_8, °R	1460	1471	1494	1536	1612	1597	1401	1400	1502	1470	1421	2420	2028	1848
W_8, pps	585	572	557	541	520	491	399	527	487	435	371	258	209	183
Ae_8, in^2	1994	1998	2001	2003	2005	2014	2040	2006	2012	2026	2043	952	952	952
V_9, f/s	1400	1381	1369	1370	1385	1304	947	1284	1282	1131	908	3652	3120	2836

Table 4-1. Cycle Data, Over-Extracted Core DBTF Mission Analysis. (Concluded)

	Hold/Loiter		Climb/Acceleration						Supersonic Cruise							
Case	15	16	17	18	19	20	21	22	23	24	25	26	27	28	29	3
% Spd	29	27	100	100	100	100	100	100	100	90	80	70	60	50	45	4
Alt, ft	15K	1500	1500	20K	345K	41.3K	48.1K	54.9K	58640	58640	58640	58640	58640	58640	58640	58
M_o	.5	.5	.4	.8	1.20	1.6	2.0	2.4	2.62	2.62	2.62	2.62	2.62	2.62	2.62	2
F_N, lbf	10150	10661	84982	56699	47430	43906	41185	38185	36471	33234	29677	25727	21180	16262	15468	14
P_{amb}, psia	8.294	13.917	13.917	6.753	3.541	2.555	1.843	1.329	1.110	1.110	1.110	1.110	1.110	1.110	1.110	1.
T_{amb}, °R	480	528	528	462	410	404	404	404	404	404	404	404	404	404	404	
P_{18}/P_o	1.779	1.622	2.709	3.699	5.893	8.708	13.331	21.387	28.247	28.294	28.338	28.383	28.429	28.473	26.464	24.
T_{18}, °R	602	643	2452	2452	2452	2452	2452	2452	2453	2211	1959	1697	1416	1138	1111	1
W_{18}, pps	263	397	566	378	317	332	364	420	457	455	453	451	449	447	406	
Ae_{18}, in^2	825	853	1434	1448	1451	1425	1415	1413	1392	1309	1221	1125	1016	901	871	
V_{19}, f/s	1552	1583	2738	3083	3498	3780	4003	4004	4018	3862	3681	3469	3212	2915	2861	2
P_8/P_o	1.882	1.538	3.831	5.585	8.533	10.80	14.014	16.957	18.858	18.884	18.900	18.915	18.931	18.946	21.045	22
T_8, °R	1463	1419	2381	2393	2382	2374	2359	2253	2197	2196	2196	2196	2197	2197	2260	2
W_8, pps	205	284	590	405	333	315	300	290	289	289	290	290	290	290	274	
Ae_8, in^2	956	980	1043	1014	1039	1075	1089	1176	1247	1246	1245	1245	1244	1244	1075	
V_9, f/s	1713	1409	3073	3414	3715	3855	3988	3985	3980	3979	3980	3981	3981	3982	4090	4

design point therefore precipitated the following cycle conditions, around which the basic unsuppressed nozzle system was designed:

System	Duct	Core
OAPR = 15	P_{18}/P_o = 2.66	P_8/P_o = 1.51
SL + 18°	T_{18} = 1954° R	T_8 = 1460° R
M_N = .3	W_{18} = 592 pps	W_8 = 585 pps
PR_F = 2.7	Ae_{18} = 1286 in^2	Ae_8 = 1994 in^2
β = 1.0	V_{19} = 2415 ft/sec	V_9 = 1400 ft/sec
Ae_8/Ae_{18} = 1.55		

The cycle data at other than takeoff were generated for several purposes. The first was to determine the extent of throat area variation required within the complete engine/aircraft mission. Knowing the minimum and maximum areas, plus other criteria such as A_{19}/A_{18} and A_9/A_8 expansion requirements for good aerodynamic performance throughout the mission, the hinged flap system selected for nozzle throat control could be developed into an engine aerodynamic flowpath and reasonably simulated in model hardware. The second purpose was to generate part power cycle data for both the core and duct streams, around which to establish a representative test matrix for acoustic and aerodynamic performance evaluation.

SECTION 5.0

BASELINE ENGINE/SCALE MODEL COANNULAR NON-COPLANAR SYSTEM

5.1 DEVELOPMENT OF BASELINE ENGINE FLOWPATH

The baseline engine nozzle flowpath was established using the detailed cycle data (presented in Table 4-1) obtained at various mission points for the base engine cycle selected at takeoff in Section 4.2. Additionally the design was influenced by the criteria set forth in References 1, 2 and 3. A schematic of the engine aerodynamic flowpath, showing the minimum, maximum and supersonic cruise area variations, is presented as Figure 5-1.

Core and duct throat area variations required by the engine cycle are accomplished by flap and seal arrangements on the respective plugs, forming a "collapsing plug" scheme. The external area ratios (refer to Figure 5-2 for terminology illustration) of the core and duct plugs were sized to give complete expansion at the supersonic cruise point. This plug sizing established the outer nozzle diameter. This diameter was then checked with the engine maximum diameter as calculated in the parametric cycle deck and was found to be compatible with the engine size, having room for shroud and nacelle thickness and requiring very little boattailing.

Maximum internal area ratio (see Figure 5-2) of the fan nozzle is sized to give peak external thrust coefficient at supersonic cruise. The minimum internal area ratio of the fan nozzle was sized to give peak internal thrust coefficient at subsonic cruise/divert operation. Figures 5-3 and 5-4 illustrate this concept of internal and external peak thrust coefficient. This variation in fan internal area ratio is accomplished by means of a translating shroud.

The core nozzle internal area ratio illustrated in the schematic of Figure 5-1 is fixed at a value giving peak internal thrust coefficient at subsonic operation. This results in some core thrust loss at supersonic cruise when the core nozzle is operating at the peak external thrust coefficient. This can be avoided by using variable core internal area ratio, obtainable through use of a translating shroud on the core outer flowpath or by combining the core throat area variation with throat plane axial location variation.

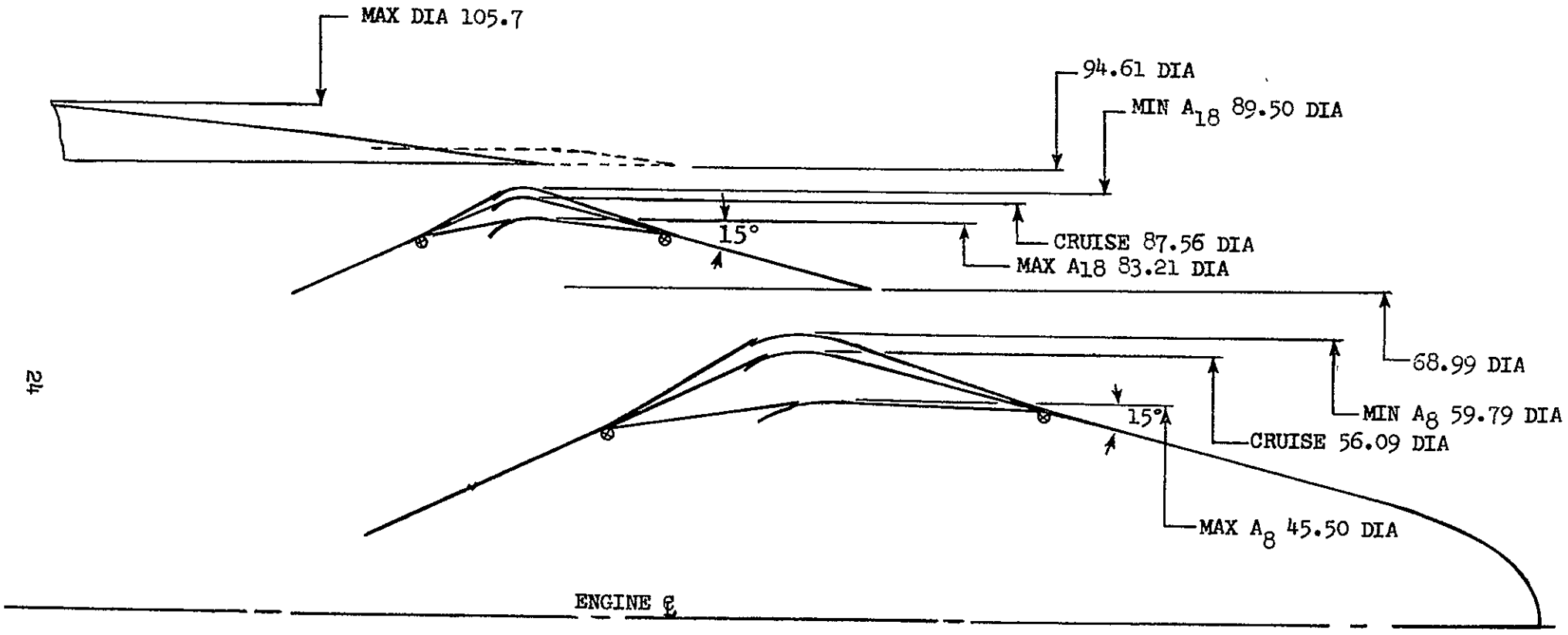

Figure 5-1 ENGINE FLOWPATH SCHEMATIC-BASELINE COANNULAR NON-COPLANAR SYSTEM

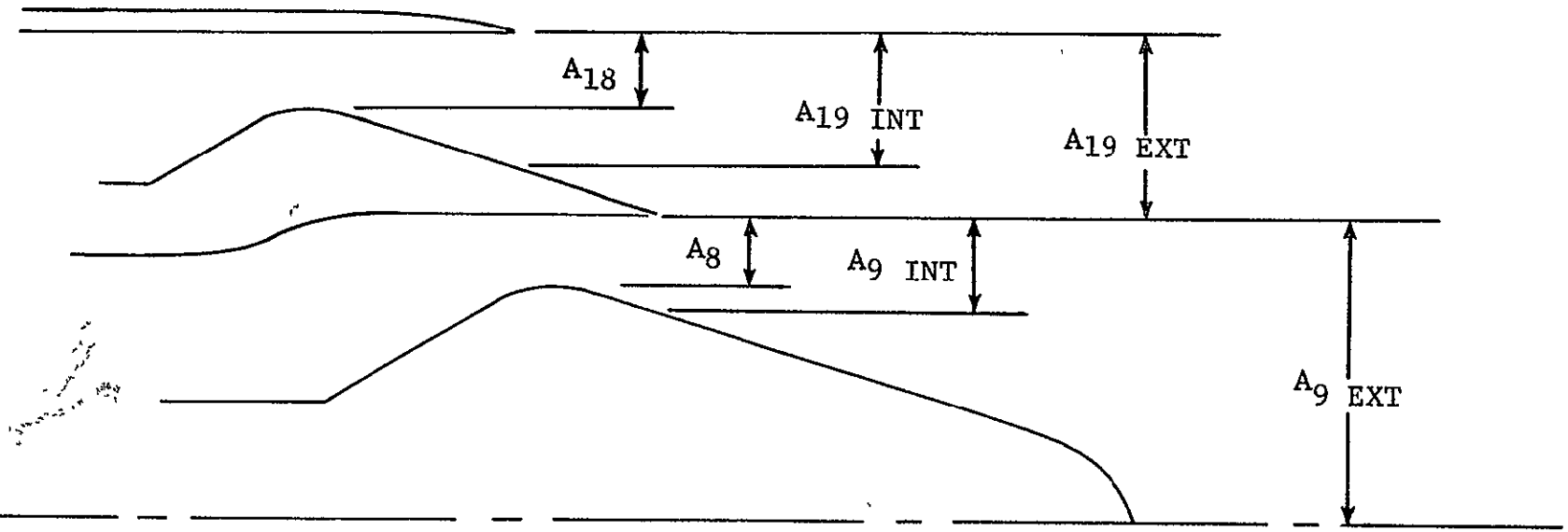

FAN INTERNAL AREA RATIO = $A_{19\ INT}/A_{18}$
FAN EXTERNAL AREA RATIO = $A_{19\ EXT}/A_{18}$
CORE INTERNAL AREA RATIO = $A_{9\ INT}/A_8$
CORE EXTERNAL AREA RATIO = $A_{9\ EXT}/A_8$

Figure 5-2 DEFINITION OF NOZZLE AREA RATIOS

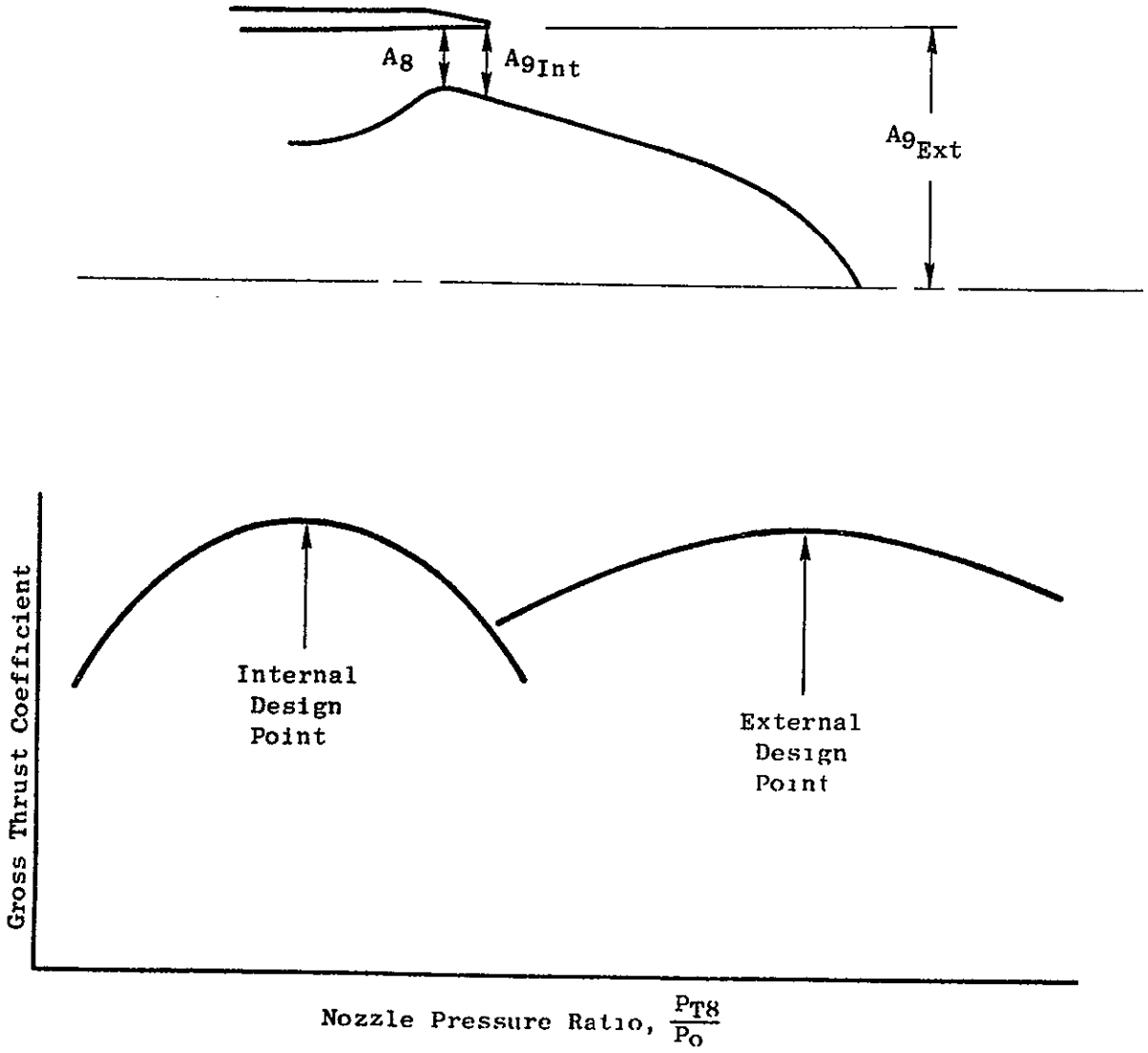

Figure 5-3 Internal and External Peak C_{f_g} Schematic.

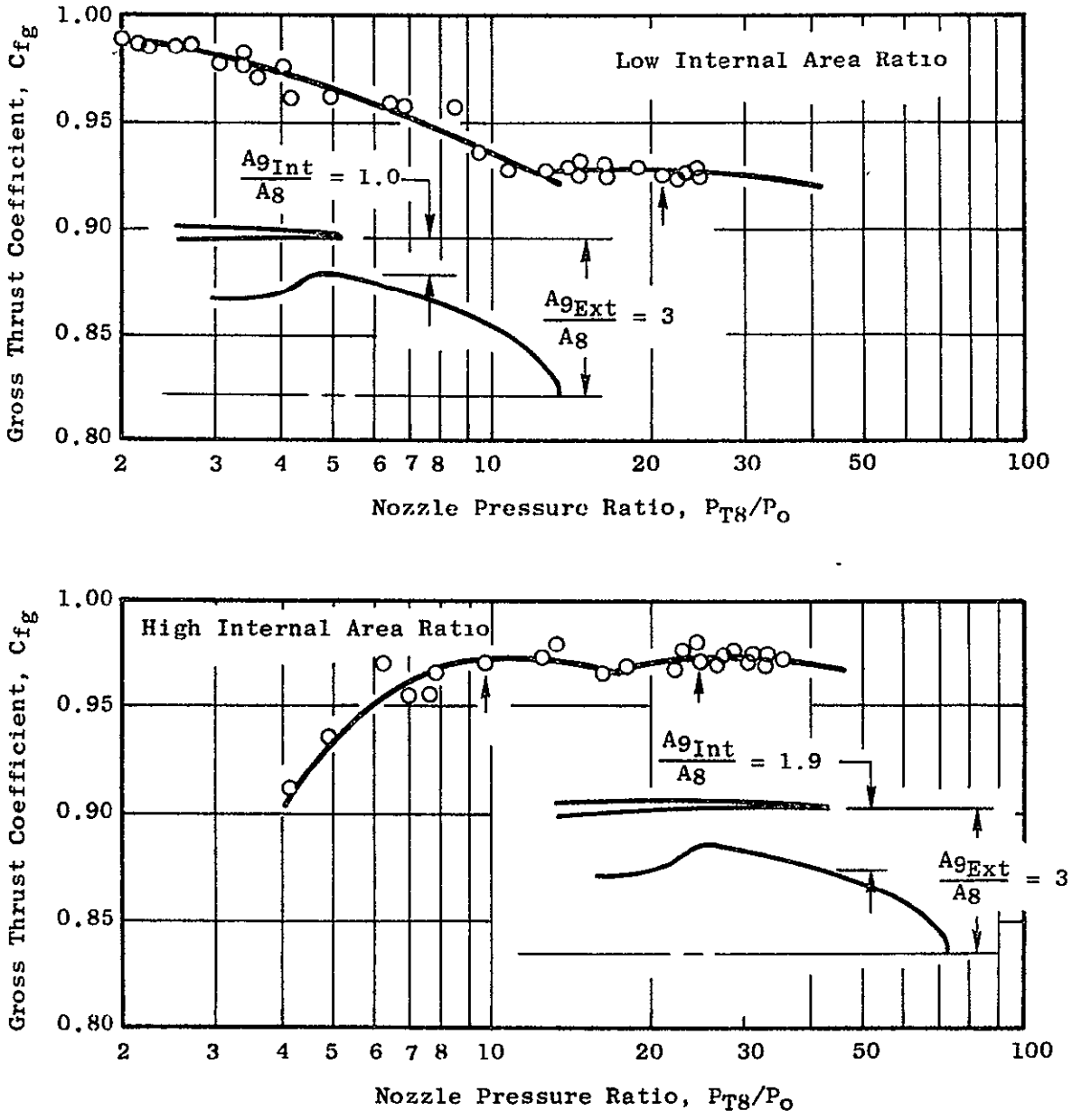

Figure 5-4 Sample Data Showing Internal and External Peak C_{f_g} Data.

Both of these systems are mechanically complex. As they are unnecessary for the subject noise study, they were not included in this design. A schematic illustrating the nozzle concept and resulting thrust characteristics is shown in Figure 5-5 for the key operating points.

It is not within the scope of the program to conduct detailed mechanical design of the selected nozzle system. However, the baseline nozzle flowpath utilizes and is compatible with typical mechanical schemes from previous dual flow plug nozzle mechanical designs as depicted previously in Figures 4-1 through 4-4.

5.2 SCALE MODEL SYSTEM DEFINITION

The scale model nozzle combined core and duct aerodynamic flow area was selected as that equivalent to a six inch diameter nozzle system. The selection was influenced by the following three criteria.

- Requirements within the NASA request-for-proposal were established as "all test models shall have a common primary to secondary area ratio (A_8/A_{18}) and primary flow area. Models shall be sufficiently large to allow scaling to full size AST duct-burning turbofan engines. In no case shall models have an equivalent diameter smaller than six inches."
- The models are to be tested for aerodynamic static performance at elevated temperature at the FluiDyne Engineering Corporation. FluiDyne's hot flow static thrust stand is a blowdown facility utilizing a pebble bed heater. The maximum temperature that can be run for any given weight flow is limited by the heater capacity. In order to investigate the temperature effects on ejector performance, as high of temperatures as possible are desired. The highest model flow rate of interest in the test matrix is core pressure ratio of 2.0 and fan pressure ratio of 4.0. For a 6" equivalent diameter nozzle this results in a total nozzle weight flow of approximately 15.5 lbs/sec at a fan and core temperature of 1460° R. This flow rate is very near FluiDyne's capability of 16-18 lbs/sec at 1460° R. Any significant increases in model size would require the hot static thrust testing to be run at lower exit temperatures.

SUPERSONIC CRUISE

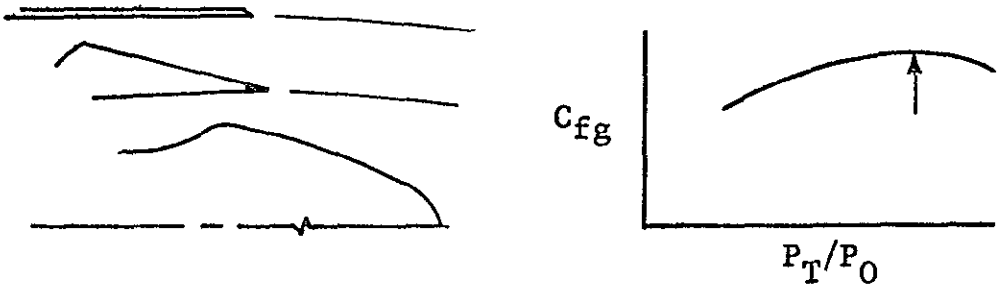

SUBSONIC CRUISE

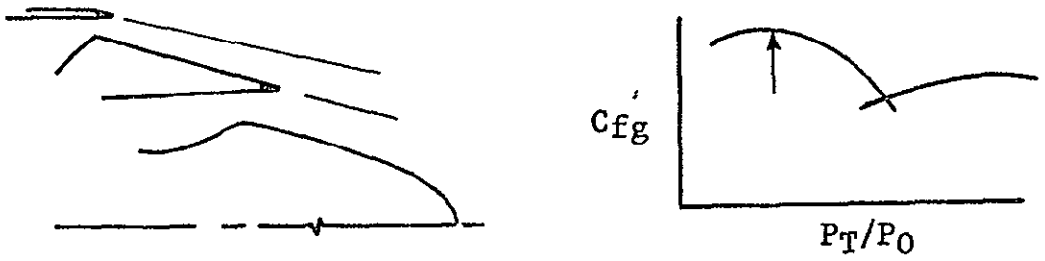

ACCELERATION

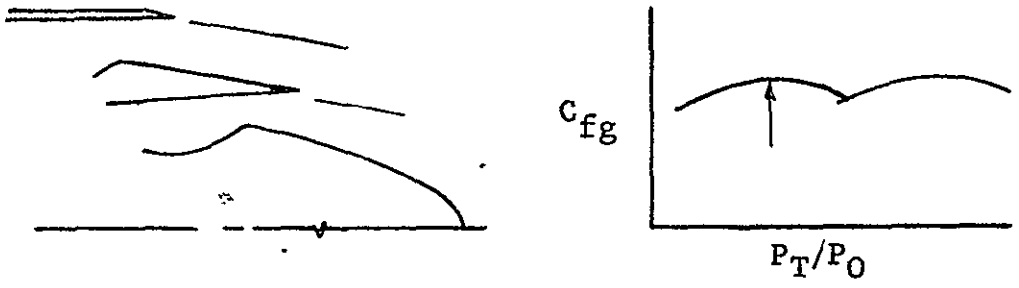

Figure 5-5 DUAL FLOW PLUG NOZZLE APPLICATION FOR SUPERSONIC TRANSPORT

- For acoustic evaluation, the 6" equivalent diameter nozzle size and the Ae_8/Ae_{18} selection sets the core and duct equivalent to 4.63" and 3.72" diameter nozzles respectively. These equivalent nozzle sizes are directly compatible with efficient operation of the core and duct burner systems over the wide range of planned test cycle conditions. Additionally, the chosen nozzle size allows incorporation of multi-element suppressor systems whose characteristic frequency range of interest falls well within the 80 KHz measuring capability of the facility equipment.

Scaling the baseline coannular non-coplanar engine flowpath from Figure 5-1 to model size was accomplished using a linear scale factor. The flowpaths were duplicated to an axial station where adaptation to the facility hardware dictated variance.

A schematic of the model system is presented as Figure 5-6, also showing adaptive hardware to the acoustic test facility. A tabulation of the design areas and discharge coefficients is in Table A-1 of Appendix A. A sketch of the model system showing all related miscellaneous assembly hardware is also included in Appendix A, as well as the hardware detailed drawings.

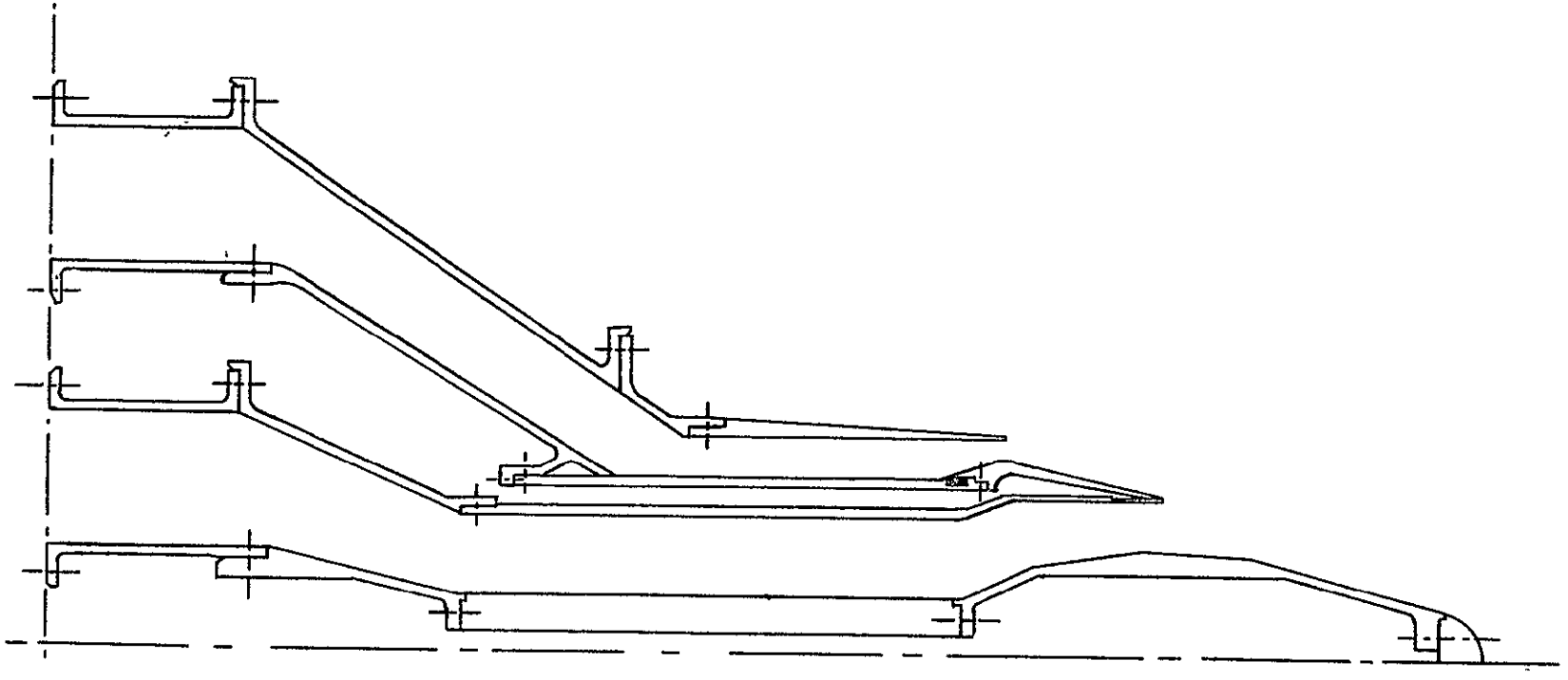

Figure 5-6 BASELINE COANNULAR NON-COPLANAR MODEL SYSTEM

SECTION 6.0

DUCT MULTI-ELEMENT SUPPRESSOR SYSTEMS

Within the proposal P73-27 to NASA-Lewis on the DBTF program, the development of jet noise suppressors for supersonic exhaust systems were reviewed in detail under the following major categories:

- Basic Hardwall Ejectors
- Primary Suppressors
- Secondary Suppressors
- Fluidynamic Injection
- Multi-Tube/Hole Nozzle Suppressors
- Plug/Annular Nozzle Suppressors (Multi-Spoke/Chute)

All of the above systems have their unique suppression characteristics in terms of peak suppression magnitude, suppression level versus jet velocity, and related performance penalties. In order to meet the stringent noise goals of current/future AST applications, the more complex suppressor systems, i.e., the multi-tube and multi-spoke/chute, capable of attaining reasonably high suppression levels, were preselected for application to the DBTF annular stream. To implement the selections into practical model designs in terms of acoustic/aerodynamic performance trade, all available pertinent literature and data on the two suppressor concepts were reviewed. These data and sources consisted of the following:

- Internal General Electric data for multi-tube and multi-spoke/chute configurations generated under the a) SST Engine Development Contract FA-22-67-7, b) Supersonic Transport Noise Reduction Technology Summary Phase I, Contract FA-SS-71-13, and c) Supersonic Transport Noise Reduction Technology Program Phase II, Contract DOT/FA72WA-2894. These data are documented in various General Electric internal reports and contract interim and final reports as referenced with the text.

- o The Boeing Company's a) SST Technology Follow-On Program - Phase I, Contract DOT-FA-SS-71-12, b) SST Follow-ON Program Phase II, Contract DOT-FA-72WA-2893 and c) Contract NAS3-15570 work on acoustically lined ejector technology. These data and results are also documented in contract interim and final reports and referenced herein.
- o Other available open literature reports.

The following sections document the pertinent information used from these sources and their subsequent influence on the annular jet noise suppressor designs.

6.1 STUDY AND DESIGN OF MULTI-TUBE DUCT SUPPRESSOR SYSTEM

To effect a well integrated multi-tube duct suppressor design, the acoustic/aerodynamic trade dependencies on the following geometric parameters were considered.

- o Area Ratio
- o Tube Number
- o Analytical Prediction Procedure - Area Ratio and Tube Number
- o Tube size equality and spacing uniformity
- o Tube length
- o Baseplate and tube exit plane stagger
- o Tube end geometry, i.e., straight versus convergent
- o Tube cant from axial centerline

6.1.1 Area Ratio

- o The General Electric test series and results (Reference 8), presented in Figures 6-1, 6-2 and 6-3, indicate in the design ideal jet velocity range of 2400 to 2500 ft/sec that Area Ratio (A/R) = 2.5 to 3.5 nozzle designs obtained 12.5 to 13.5 PNL suppression, the spread favoring higher A/R. Increasing A/R above 3.5 nets minor additional

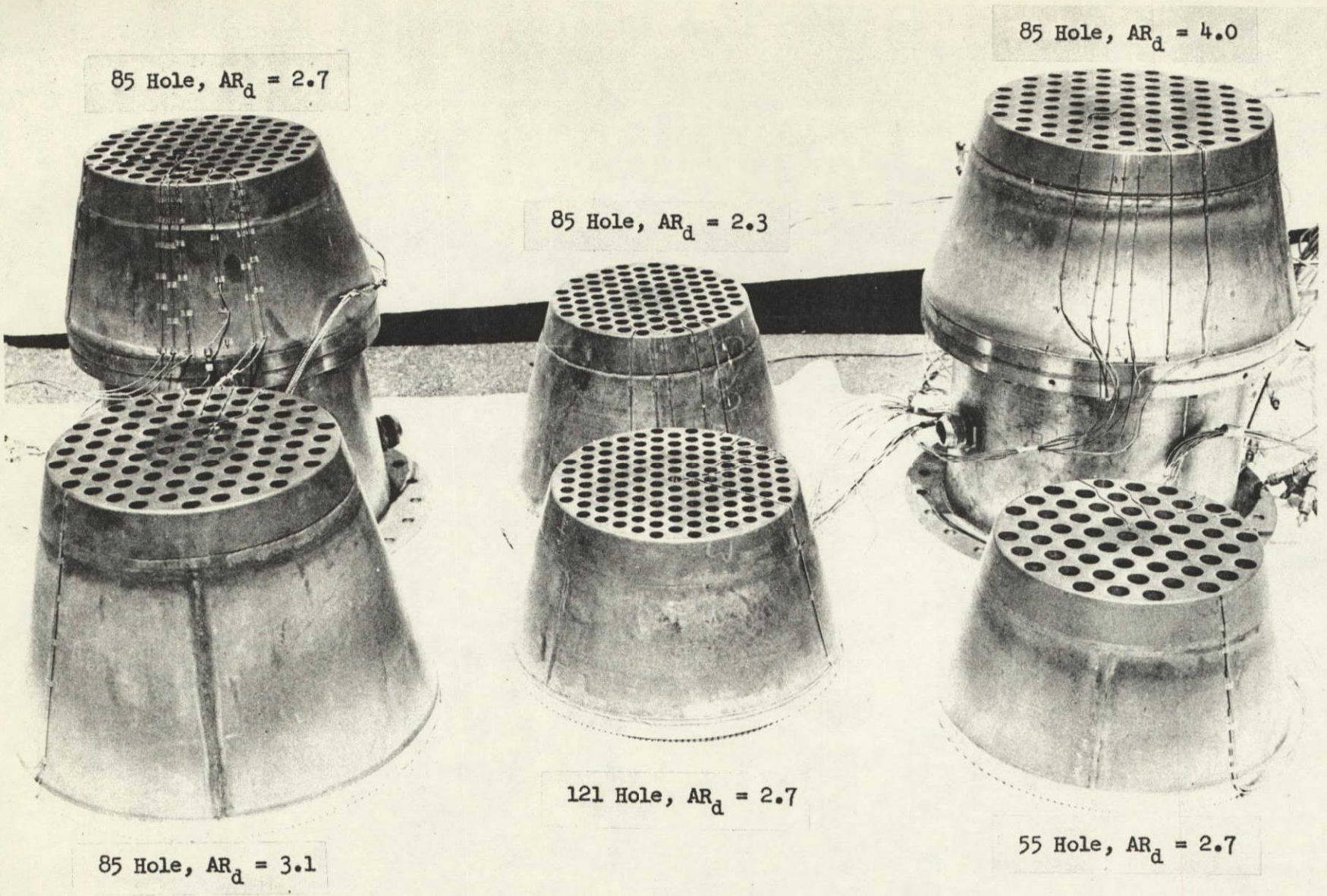

FIGURE 6-1 MULTI-HOLE NOZZLE HARDWARE USED IN PARAMETRIC INVESTIGATIONS OF AREA RATIO AND HOLE NUMBER

ORIGINAL PAGE IS
OF POOR QUALITY

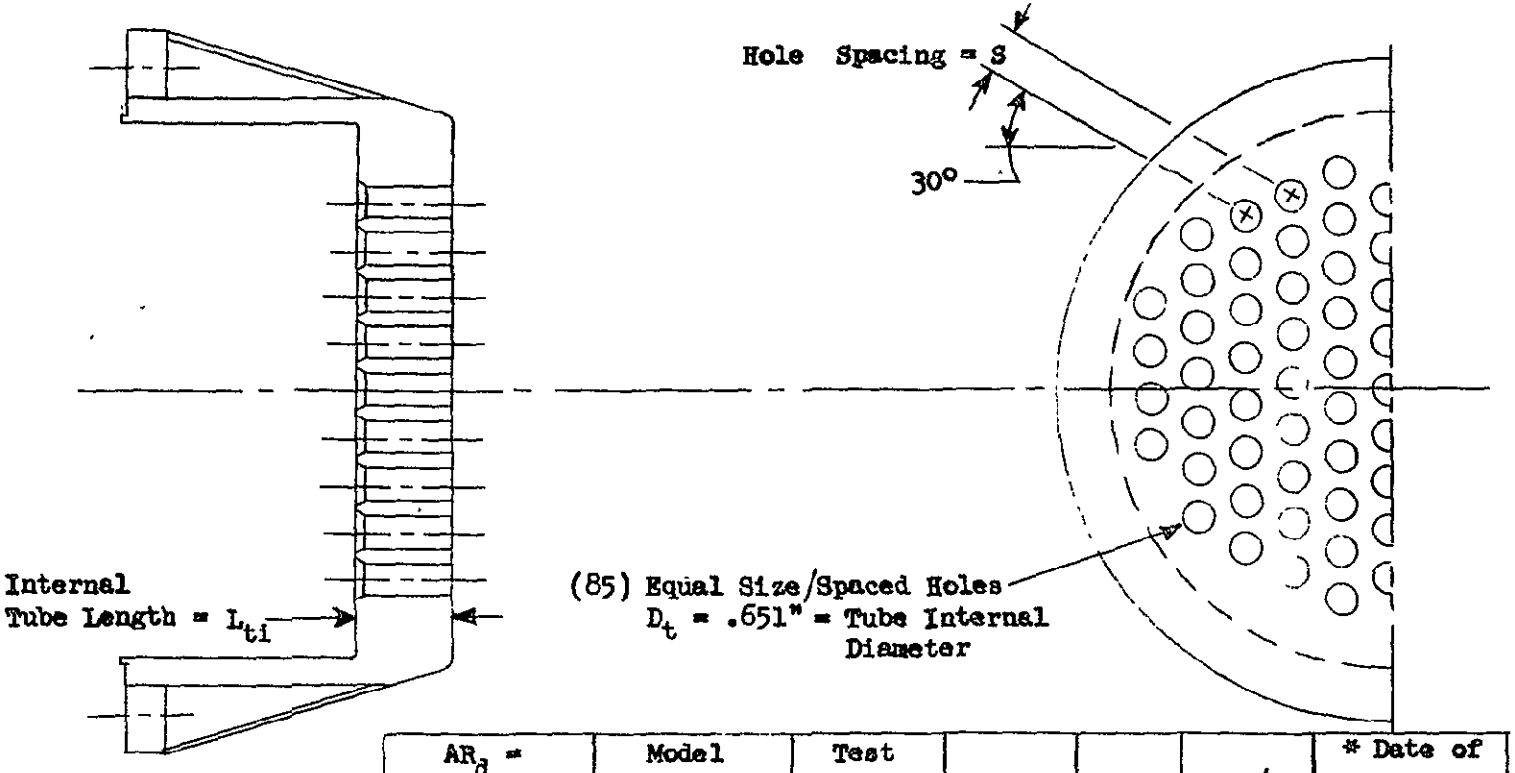

AR_d = Area Ratio	Model No.	Test Date	S	L_{ti}	L_{ti}/D_t	* Date of Repeat Run
2.0	6.0H85-2.0	4-02-69*	.741"	1.45	2.23	6-17-69
2.3	6.0H85-2.3	3-18-69	.799"	1.45	2.23	
2.7	6.0H85-2.7	3-06-69	.870"	1.49	2.29	
3.1	6.0H85-3.1	3-19-69	.937"	1.45	2.23	
4.0	6.0H85-4.0	4-03-69*	1.072"	1.49	2.29	5-14-69

FIGURE 6-2 SCHEMATIC OF 85 HOLE NOZZLE USED IN PARAMETRIC INVESTIGATION OF AREA RATIO

ORIGINAL PAGE IS
OF POOR QUALITY

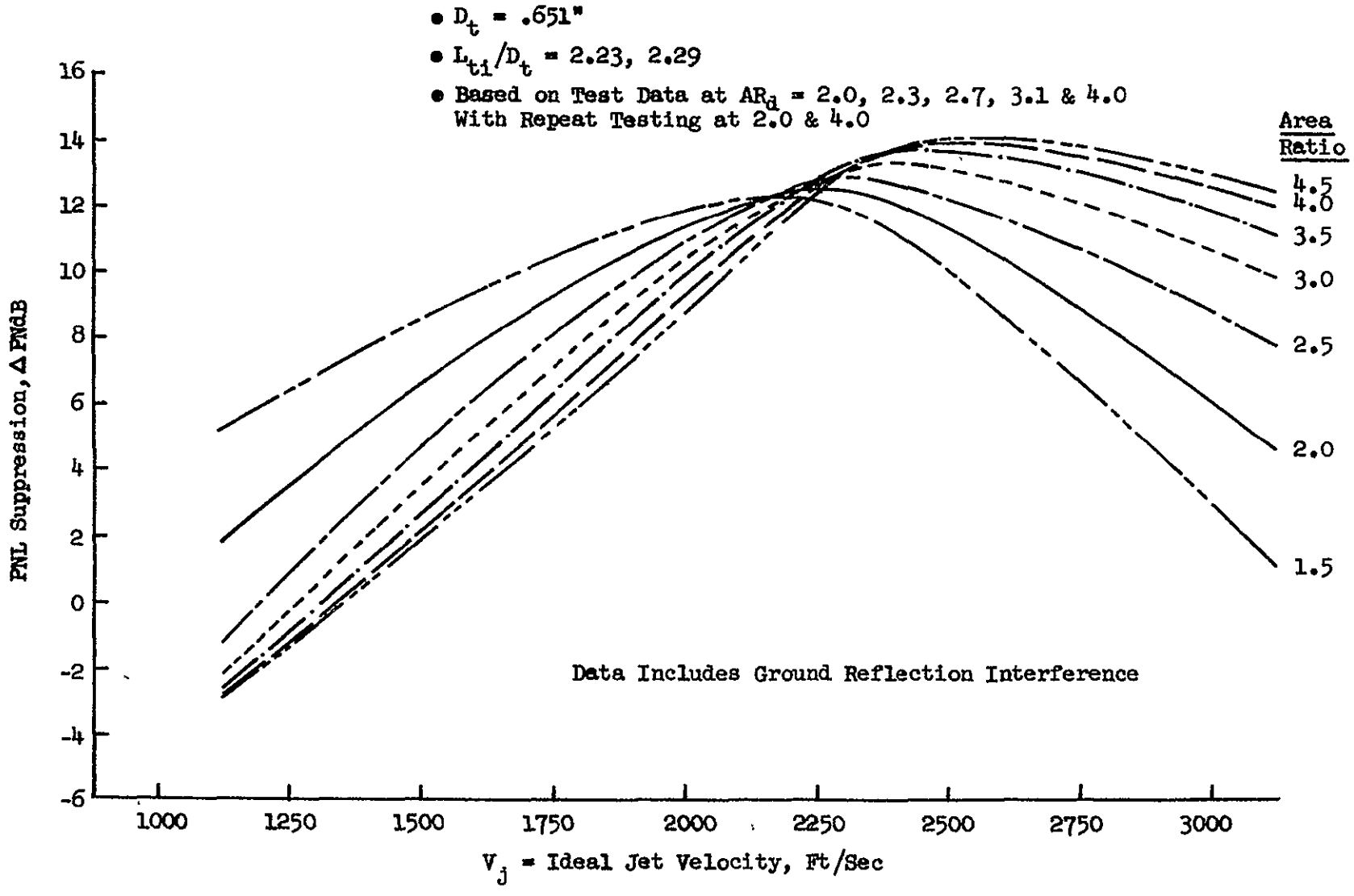

FIGURE 6-3 EFFECT OF AREA RATIO ON 1500 FT. SIDLINE PNL SUPPRESSIONS FOR 85 HOLE NOZZLES

suppression. Typical spectra and PNL directivity data, shown at V_j = 2350 ft/sec in Figure 6-4, indicate a) increased A/R decreases the low frequency noise generation substantially due to wider tube spacing delaying the jet coalescence and thereby allowing velocity decay before merging and a subsequently shorter merged jet region, b) increased A/R generally allows for greater high frequency noise levels due to the delay of coalescence allowing increased length for the region of high frequency noise generation, and c) increased A/R improves suppression primarily in the aft quadrant toward the jet axis.

- From Boeing data (Reference 9), replotted to directly show A/R effect as a function of V_j in Figure 6-5, in the design velocity range of V_j = 2400-2500 ft/sec, high levels of noise suppression are obtained and a spread of 2 to 2.5 ΔPNL is seen, higher suppression favoring higher A/R. Increased A/R above 2.5 for the 37 tube array shows several additional PNL suppression but at the expense of mechanical practicality. Therefore, the trends of General Electric and Boeing data agree well and a selection near A/R = 2.5 to 3.0 seems best for acoustic/mechanical implementation trade.

- Boeing PWL data (Reference 9) Figure 6-6 indicates that, at 1610° R and with nozzle pressure ratios of 2, 3 and 4 for a 37 tube array, increase in area ratio tends to decrease high frequency jet premerging noise suppression slightly but low frequency jet coalescing noise suppression levels are increased quite rapidly. The combination of the high and low frequency suppression in terms of total noise PWL suppression is also shown and indicates only slight suppression increase at PR = 3.0, T_T = 1610° R, V_j = 2300 ft/sec for area ratio increase from 2.0 to 4.0. Above 4.0 area ratio no increase in suppression is evident.

Conclusions from reviewing the data associating noise to multi-tube area ratio, as applicable to the selected design velocity of V_{19} = 2415 ft/sec, are:

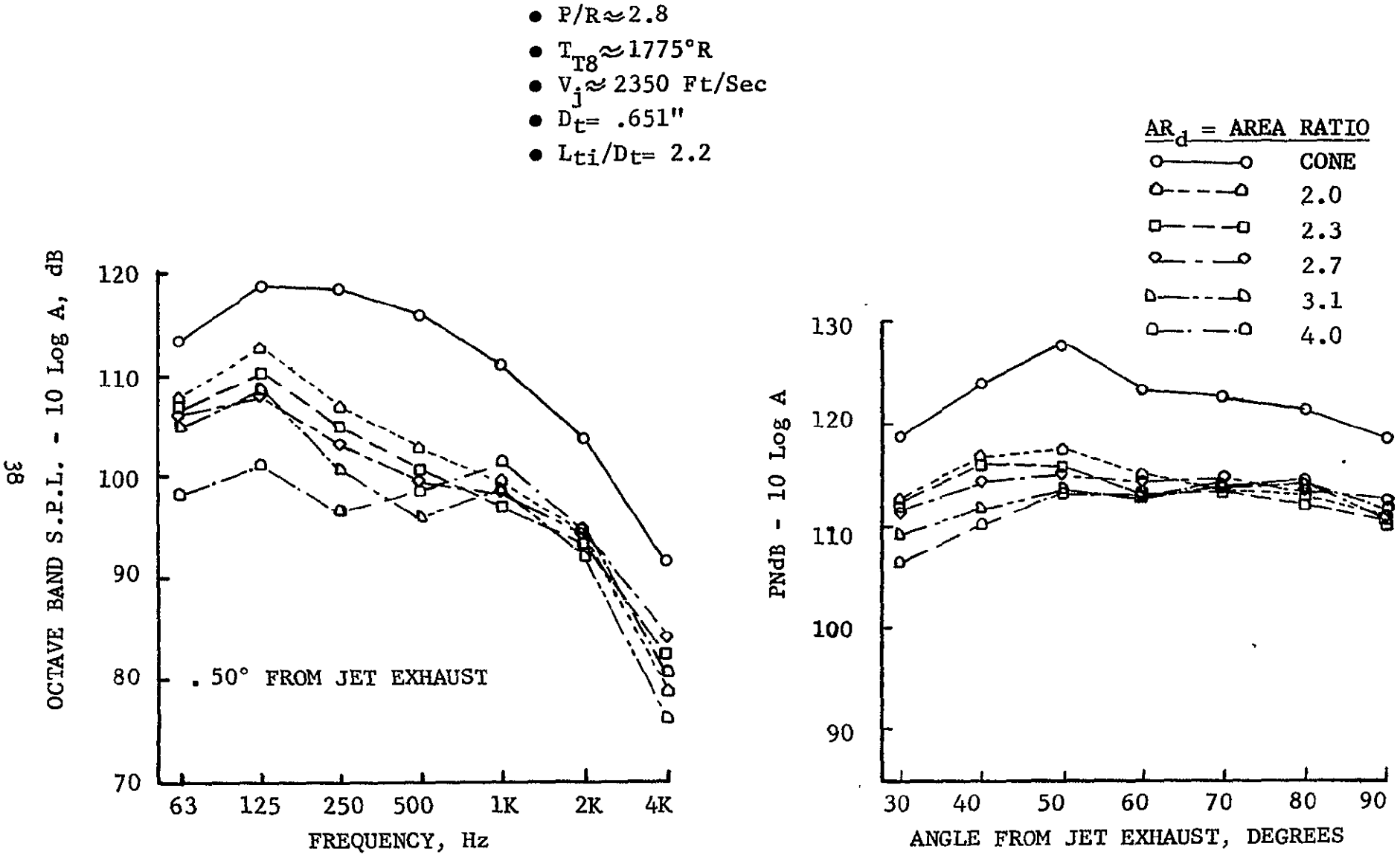

Figure 6-4 EFFECT OF AREA RATIO ON 1500 FT. SIDELINE SPRECTRA AND DIRECTIVITY

- 37 TUBE NOZZLES
- ELLIPTICAL TUBES CLOSE PACKED
- 2128'S.L. re:R.C. NOZZLE
- T_{T8}= 1610°R

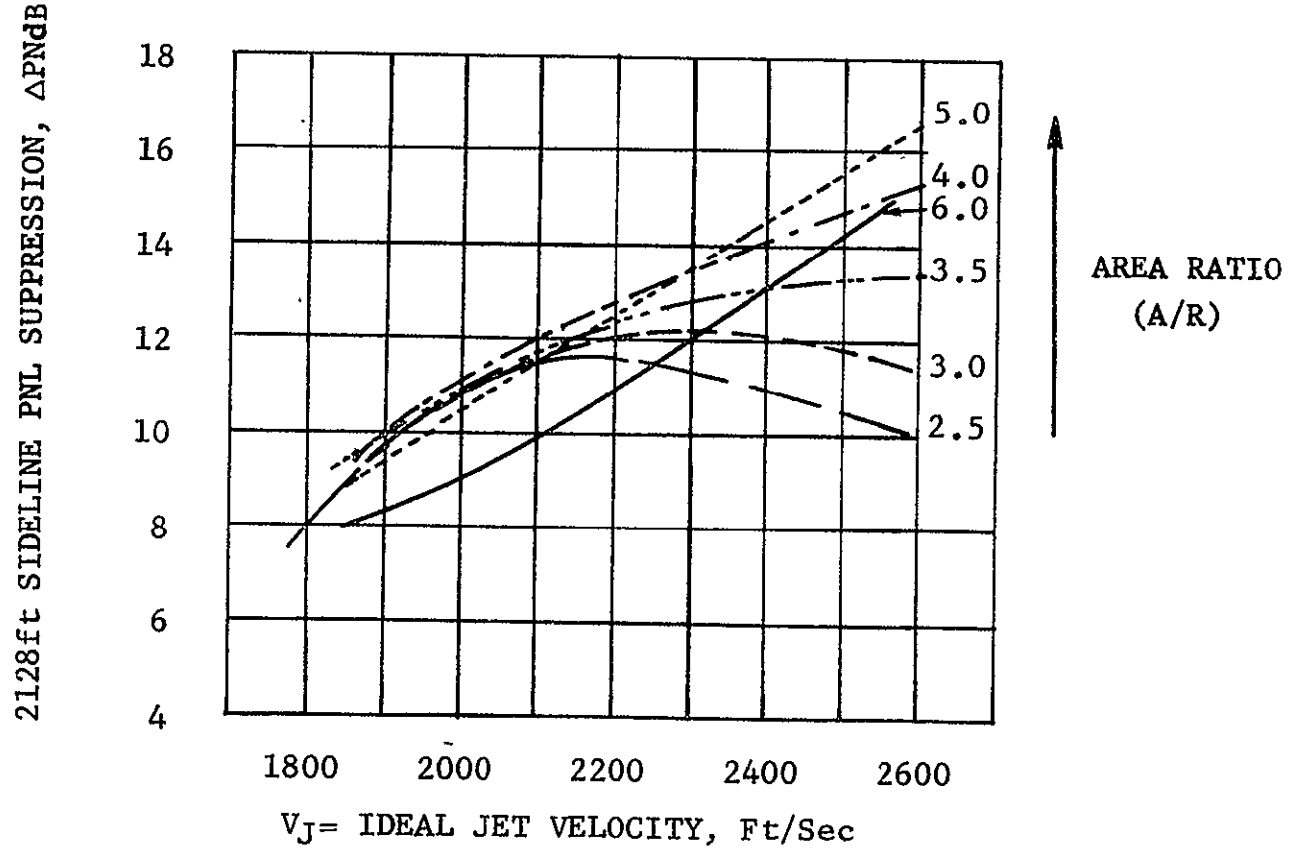

Figure 6-5 BOEING PARAMETRIC TUBE STUDY-AREA RATIO VARIATION

- 37 TUBE NOZZLES
- T_T = 1610°R

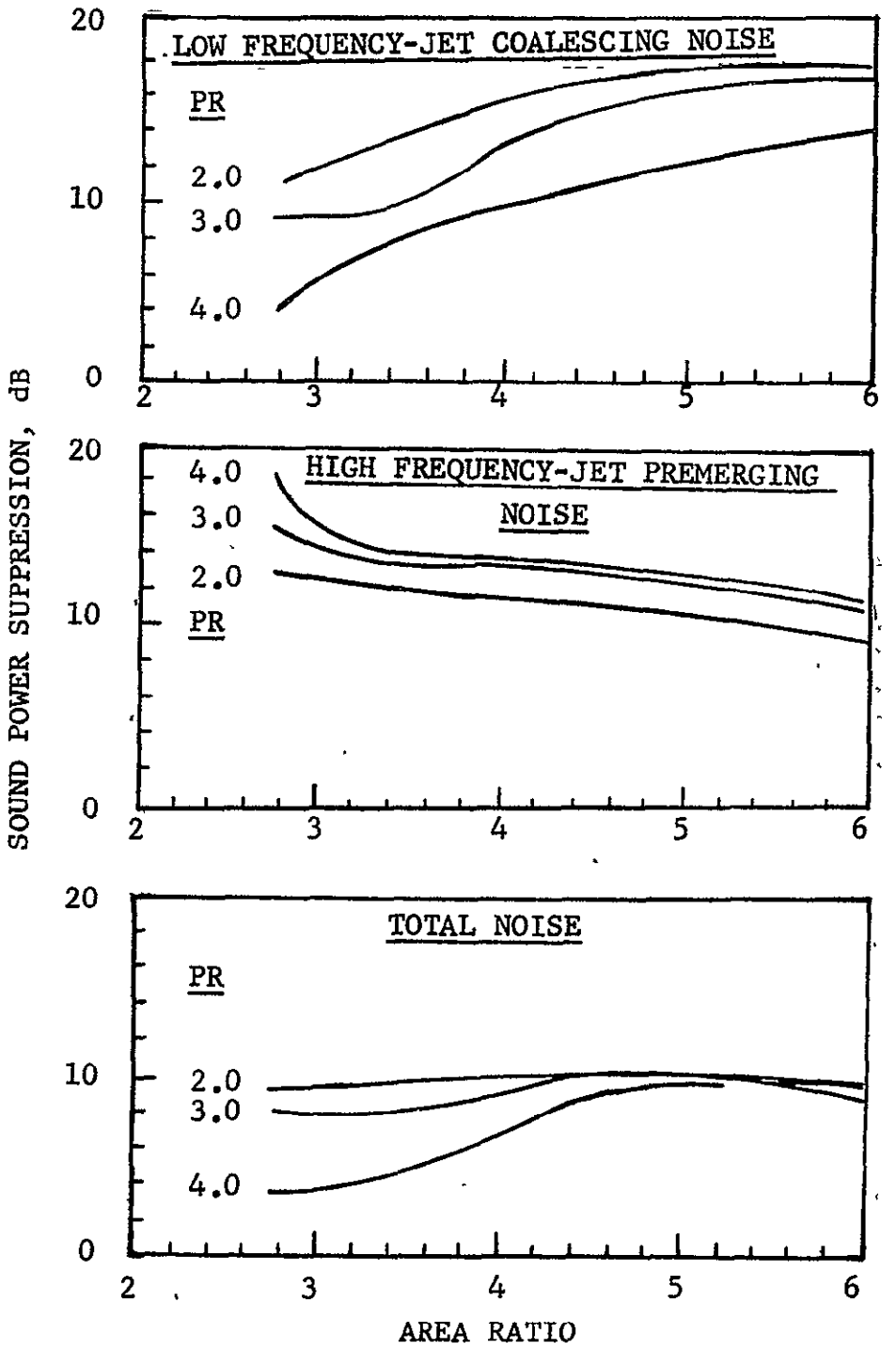

Figure 6-6 EFFECT OF AREA RATIO ON LOW AND HIGH FREQUENCY PLUS TOTAL PWL NOISE SUPPRESSION

- Favoring moderately high area ratio will gain slight suppression increase at this V_j point, however, very high A/R gains very little additional suppression and also becomes mechanically impractical.

- In order to achieve significant reduction of low frequency noise content, the area ratio must be relatively high. As A/R is increased, ambient air has an easier path into the internal portions of the main jet stream. The A/R determines the merged velocity of the flow from individual elements relative to the velocity of the jet at the nozzle exit and, thereby, determines the low frequency noise content.

- For the high V_j design range, an increase in area ratio causes more high frequency noise generation. This can nullify the effect of reducing the low frequency noise. The area ratio should be selected to balance the penalizing increase in high frequency noise against the beneficial decrease in low frequency noise.

- If the optimum study design is considered as the acoustically treated ejector/duct suppressor system, the area ratio should be chosen to generate more high frequency noise than that optimum for an unejected design. The high frequency noise generation location is close to the nozzle exit plane. An acoustically treated ejector has the potential of reducing the penalizing high frequency noise so that, together with the low frequency noise reduction achieved by the higher area-ratio, greater overall suppression of PNL should result.

6.1.2 Tube Number

- The General Electric (Reference 8) test series, to isolate the effect of hole/tube number using 55, 85 and 121 holes at area ratio = 2.7, and results are documented in Figures 6-7, 6-8 and 6-9. The graph of Figure 6-9 indicates, in the V_j = 2400-2500 ft/sec range, approximately 1 ΔPNL variance between 50 and 100 tubes. True magnitude of PNL variance is somewhat nondiscernable as PNL change with tube number is non-uniform from 50 to 125 tubes. However, typical spectra

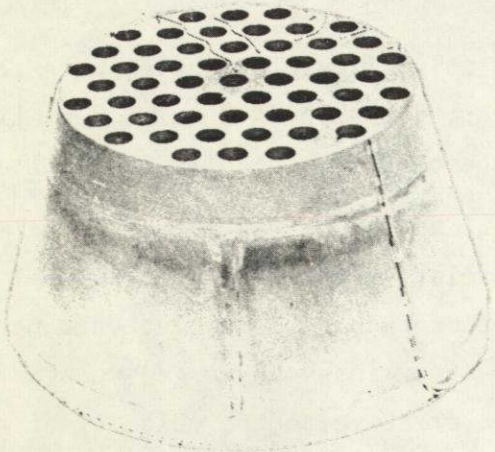

55 Holes

AR_d = 2.7

(Model No. 6.0H55-2.7)

85 Holes

AR_d = 2.7

(Model No. 6.0H85-2.7)

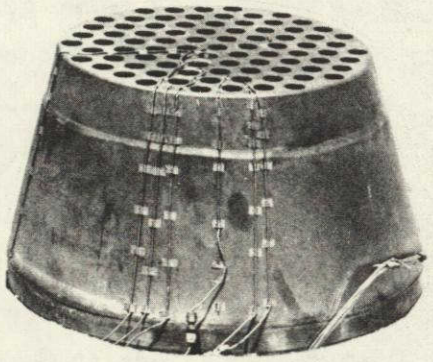

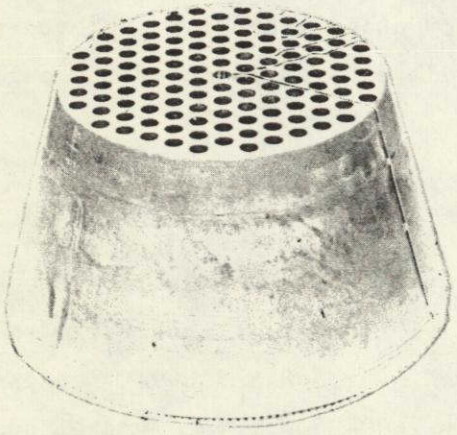

121 Holes

AR_d = 2.7

(Model No. 6.0H121-2.7)

FIGURE 6-7 MULTI-HOLE NOZZLE HARDWARE USED IN PARAMETRIC INVESTIGATION OF HOLE NUMBER

ORIGINAL PAGE IS
OF POOR QUALITY

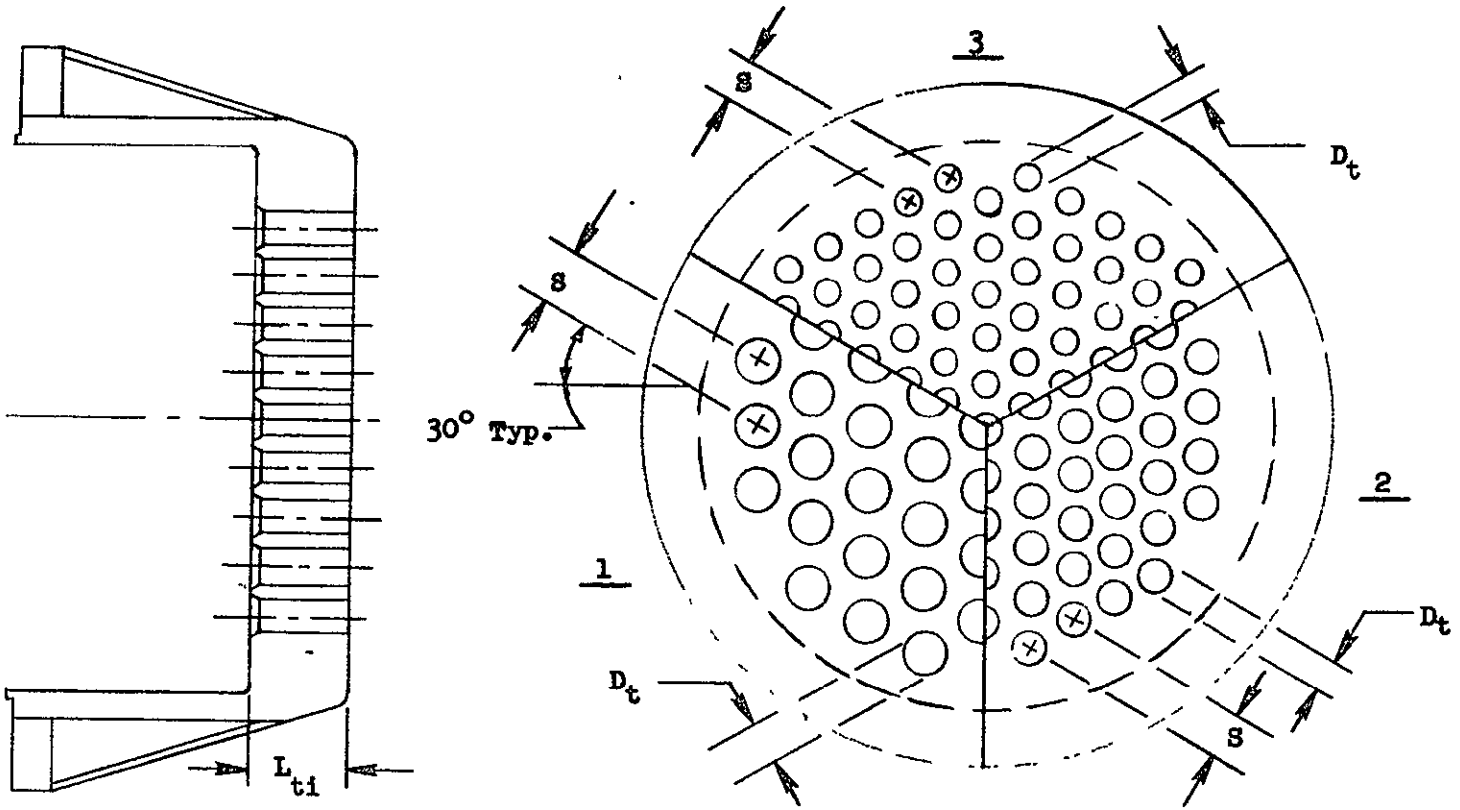

*Repeat Run on 6-26-69

	Number of Holes	Model No.	Test Date	Area Ratio	S	D_t	L_{ti}	L_{ti}/D_t
1	55	6.0H55-2.7	4-07-69*	2.7	1.087"	.809"	1.49"	1.84
2	85	6.0H85-2.7	3-06-69	2.7	.870"	.651"	1.49"	2.29
3	121	6.0H121-2.7	4-08-69	2.7	.725"	.546"	1.49"	2.73

FIGURE 6-8 SCHEMATIC OF 55,85, AND 121 HOLE NOZZLES FOR PARAMETRIC INVESTIGATION OF HOLE NUMBER AT CONSTANT AREA RATIO, AR_d = 2.7

ORIGINAL PAGE IS
OF POOR QUALITY

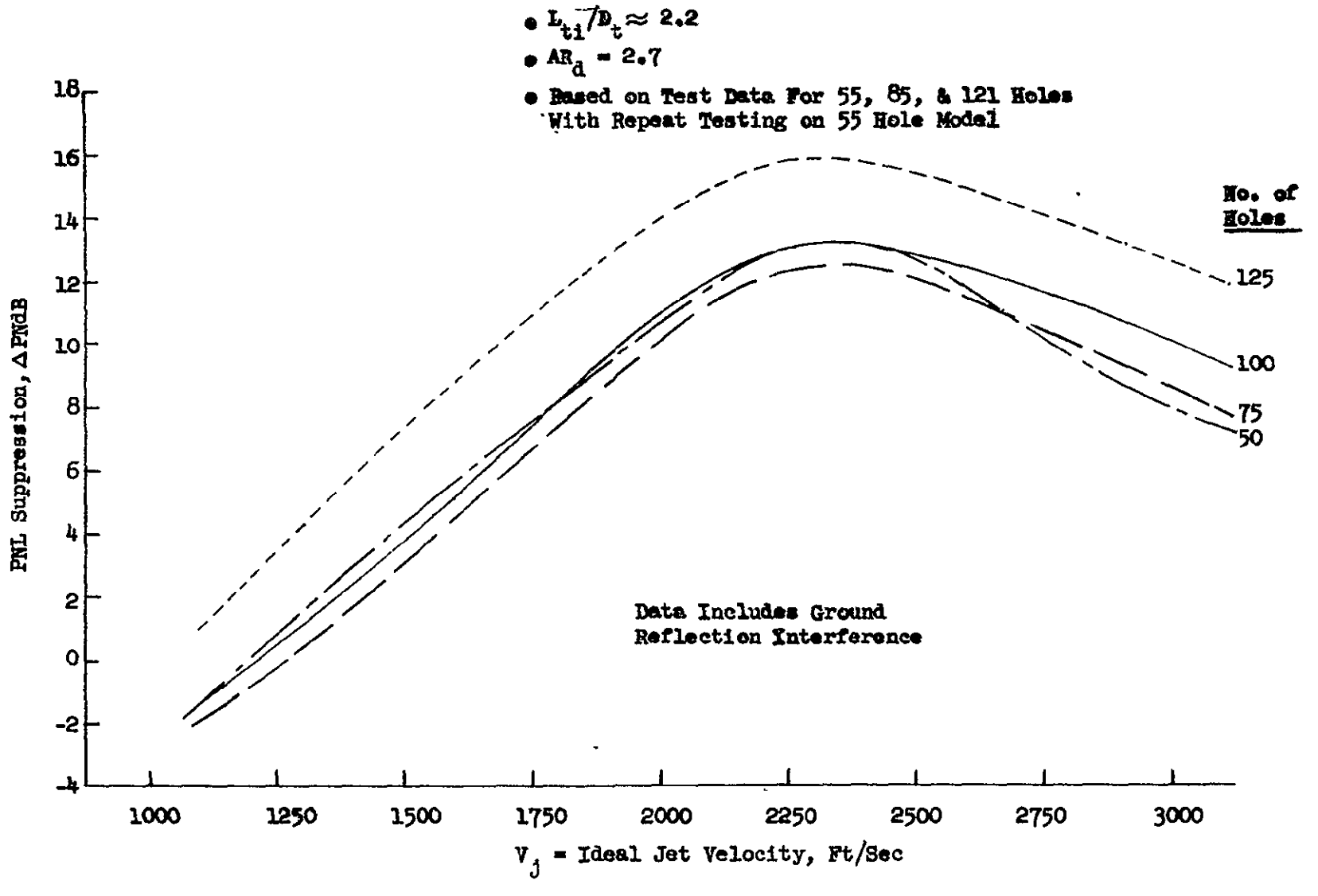

FIGURE 6-9 EFFECT OF HOLE NUMBER ON 1500 FT. SIDELINE PNL SUPPRESSIONS FOR MULTI-HOLE NOZZLES

and PNL directivity data, at 2350 ft/sec in Figure 6-10, show a definite trend of slightly higher suppression with increase in tube number.

- Boeing test data (Reference 9), isolating the effect of tube number at area ratio of 3.3 while using 7, 19, 37 and 61 tube arrays, is replotted in Figure 6-11. The data show tube number to be a predominant parameter at low element number but with only 0.5 ΔPNL increase in suppression from 37 to 61 tubes in the V_j range of 2400 to 2500 ft/sec. The trend, however, is clear; that higher tube number yields greater suppression, at least within the 37 to 61 tube range.

- Boeing PWL data (Reference 9) in Figure 6-12 indicates that, at 1610° R and for nozzle pressure ratios of 2, 3 and 4 and for an area ratio of 3.3 tube array, increase in tube number tends to rapidly increase suppression of high frequency jet premerging noise but suppression of low frequency jet coalescence noise remains nearly constant. The combination of high and low frequency PWL suppression, in terms of total noise (OAPWL) suppression, is also shown and again indicates the trend of noise suppression increase with higher tube numbers.

Conclusions from review of data associating noise to multi-tube element number, as applicable to the design velocity of 2415 ft/sec, are:

- For a reasonably high element number, necessary to form a respectable annular array for a duct suppressor using a minimum of three tube rows, and particularly in the A/R range of 2.5 to 3.0, tube number is not an extremely important parameter if maintained in the reasonably high range, i.e., 50 to 90.

- All trends indicate that within this range the higher tube numbers slightly increase suppression.

6.1.3 Analytical Prediction Procedure - Area Ratio and Tube Number

The General Electric Company has developed an analytical procedure for predicting the jet noise from multi-tube suppressors (Reference 10). The prediction method was developed as a result of extensive experience accumulated with multi-element suppressor configurations tested during the SST program

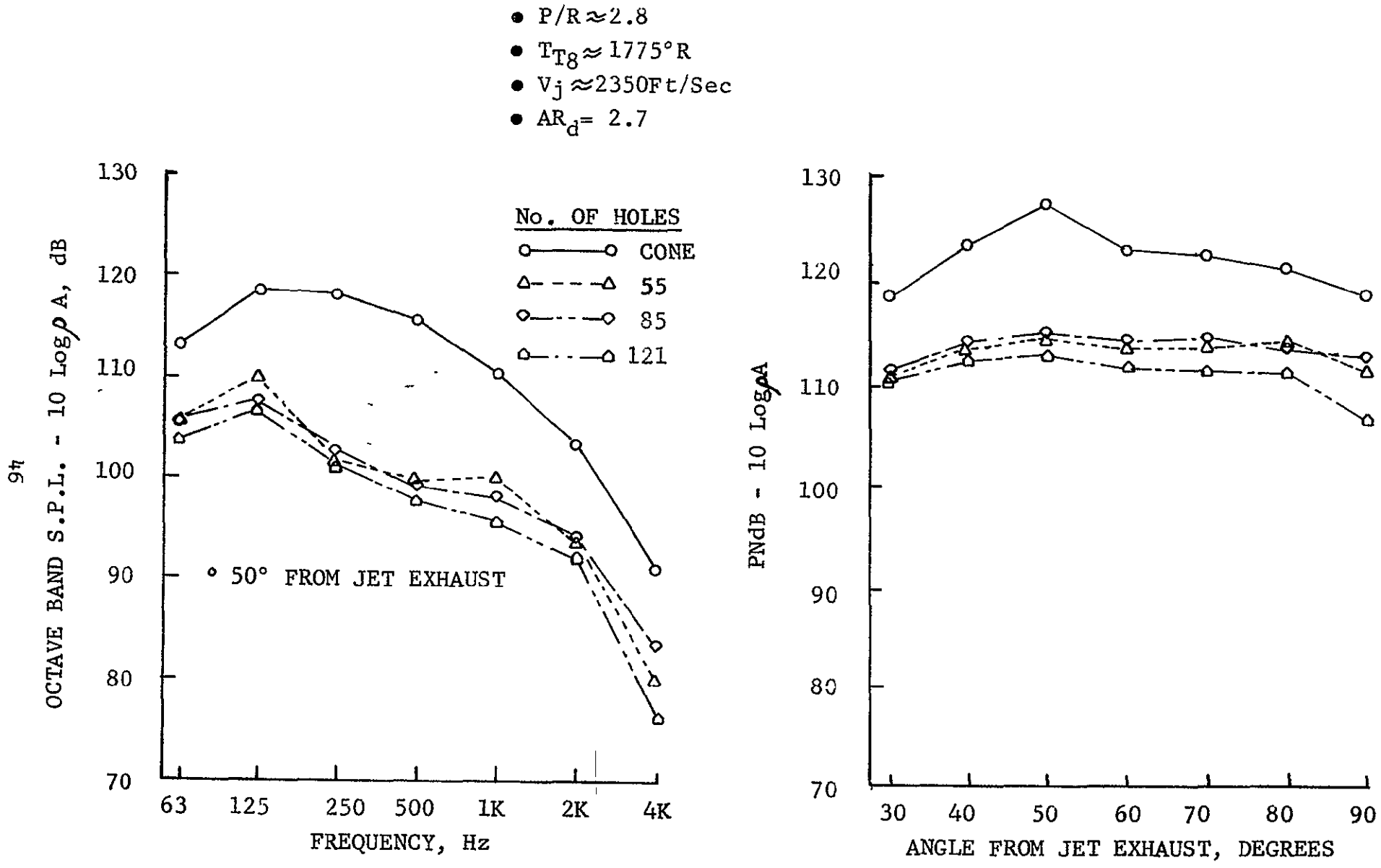

Figure 6-10 EFFECT OF TUBE/HOLE NUMBER ON 1500FT. SIDELINE SPECTRA AND DIRECTIVITY

- AREA RATIO = 3.3
- 2128'S.L. re: R.C.NOZZLE
- T_T = 1610°R

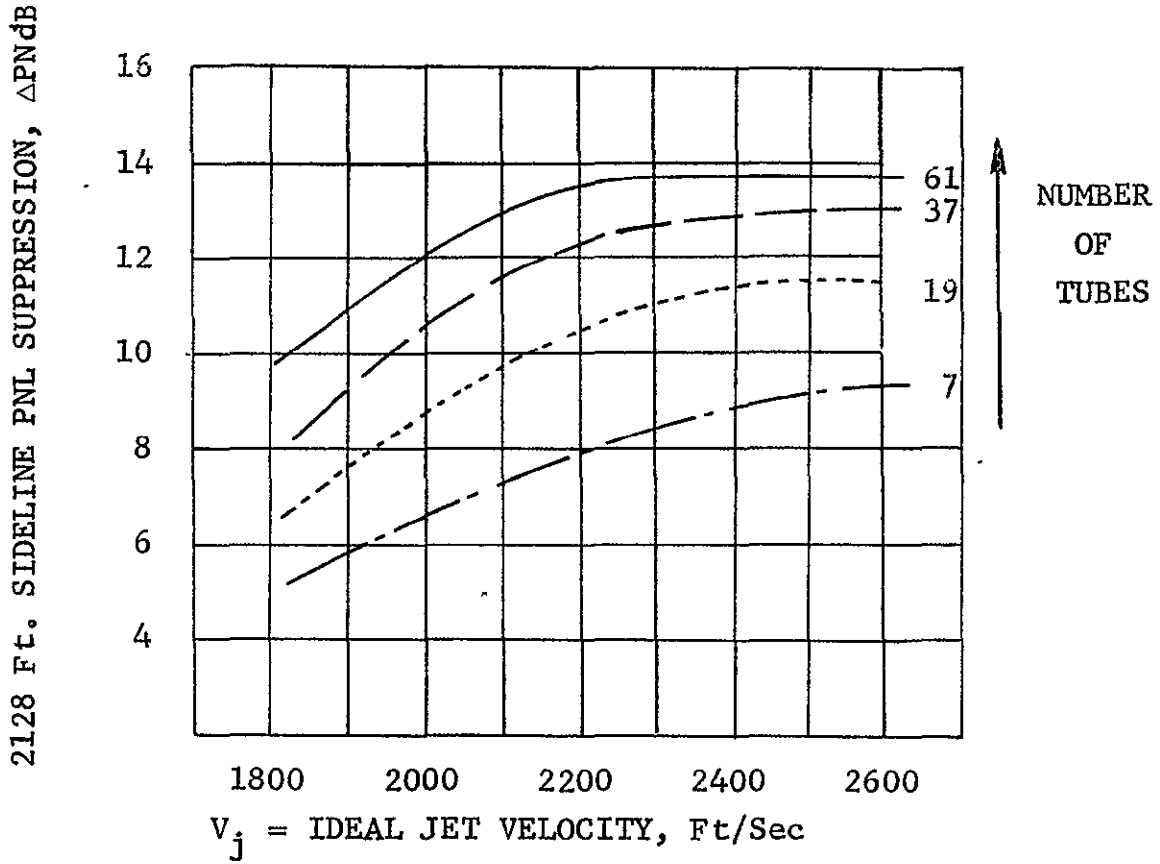

Figure 6-11 BOEING PARAMETRIC TUBE STUDY-TUBE NUMBER VARIATION

- A/R= 3.3
- T_T= 1610°R

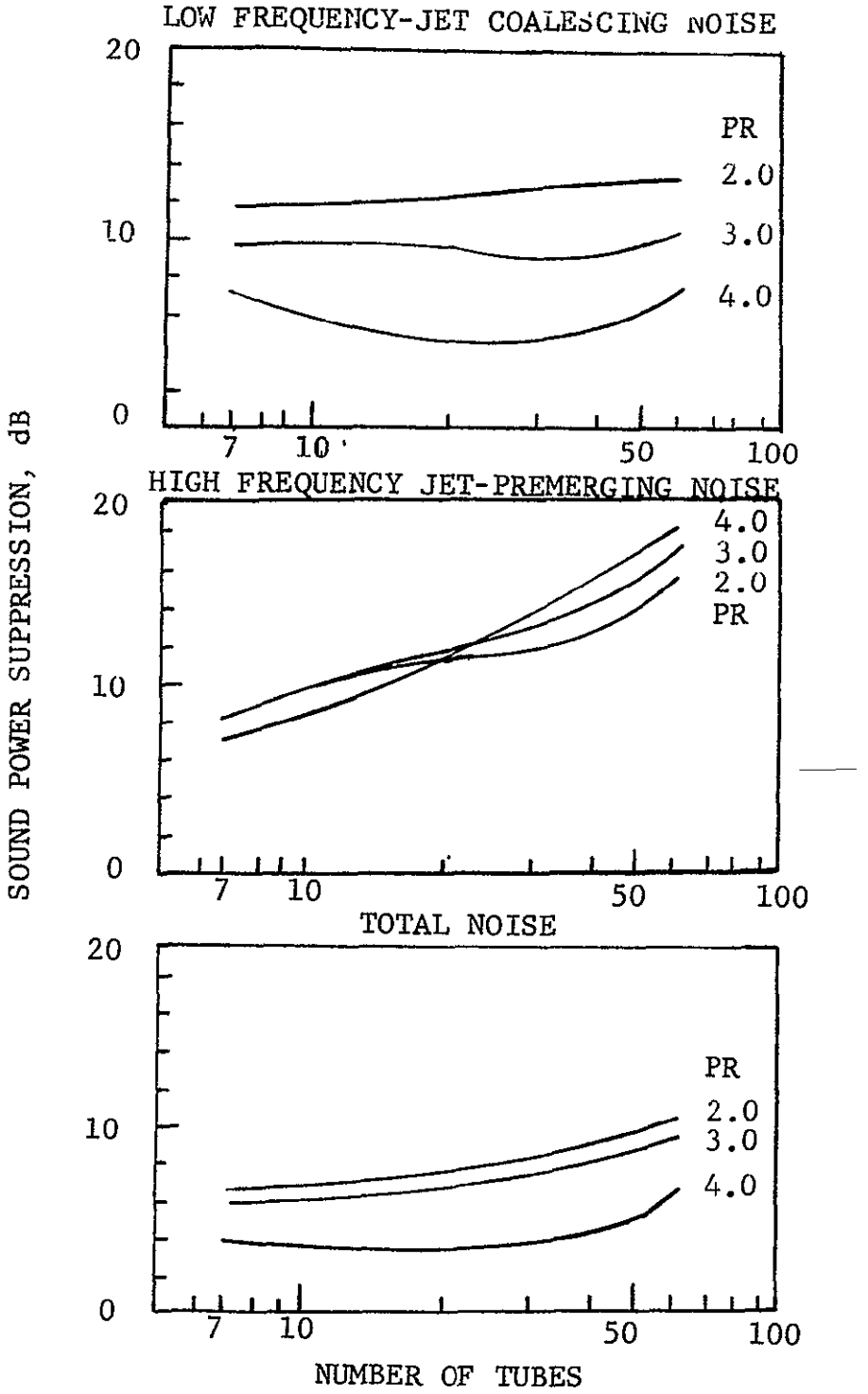

Figure 6-12 EFFECT OF TUBE NUMBER ON LOW AND HIGH FREQUENCY PLUS TOTAL PWL NOISE SUPPRESSION

and as a result of the continuing effort at General Electric under current contracts for the development of supersonic transport noise reduction technology. This development has led to the understanding of the phenomenological characteristics of supersonic jet noise source levels, source locations within the jet, and the important factors to achieve reduction of such noise.

The following method is used in determining the noise levels:

1. The maximum angle OASPL and octave band spectral distribution are determined. These data are used for an individual tube based on the nozzle exit conditions, and on the flow conditions and area calculated for the merged jet.

2. Noise is calculated for the flow from the tubes, prior to merging, as follows:

   a) The axial location of peak noise generation is determined for each octave band. Using the octave band midpoint frequency, the value of $(X/D)_{peak}$ for each octave band is determined.

   b) The axial location, $(X/D)_{cut\ off}$, at which noise is no longer generated by flow from the individual tubes is determined.

   c) The ratio of the value determined in b to that in a, above, is used to determine the SPL level relative to the overall octave band SPL (determined in Step 1); this determines the SPL in the octave band for noise from an individual tube.

   d) The noise from all the tubes is then determined using the effective number of tubes radiating sound.

3. Noise for the merged flow (determined in Step 1) is then added to that from the individual tubes (Step 2) for each octave band. These data are then used to determine the Perceived Noise Level by standard procedure.

This analysis has been programmed for computation and the method has been successfully checked against measured data for many model configurations within the following range of variables:

- o $2.0 \leq$ Area Ratio ≤ 8.0
- o $37 \leq$ Tube Number ≤ 253
- o $1600 \leq$ Ideal Jet Velocity, ft/sec ≤ 3400

The criteria for acoustic design of multi-element suppressors, as evolved through improved understanding, can be summarized as follows:

- o The multi-element suppessor achieves its purpose by two mechanisms:
  - Rapid entrainment of ambient air into the high velocity stream, causing the velocity of the mixed stream to be reduced to subsonic levels much closer to the exit plane.
  - Generation of high frequency noise from the individual streams whose acoustic radiation efficiency is greatly reduced because of the interaction among adjacent streams and because of the disruption of the propagation path from those regions of the jet which are shielded by the outermost portion.

Prior to selection of the final DBTF design point, an acoustic parametric study was conducted (Reference 11 and 12), using the analytical prediction procedure, to define the maximum attainable PNL suppression for a given area ratio and tube number over a specified range of cycle conditions. The major study effort was done at $P_T/P_o = 3.0$, $T_T = 1880°$ R, $V_j = 2485$ ft/sec and results are shown in Figures 6-13 and 6-14 on a 320 ft arc. Figure 6-13 shows the individual jets and merged jet contributions in terms of PNL as a function of area ratio and tube number. Figure 6-14 shows the total PNL when the individual spectra are combined. When evaluated on a 1500 ft sideline the variations in ΔPNL with tube number and area ratio are as shown in Figure 6-15. The results, as follows, are consistent with those previously discussed for the area ratio and tube number studies.

- o In general, increase in tube number at reasonably high area ratio results in a low level of suppression increase.
- o Increase in area ratio at the design point increases suppression slightly for the higher area ratio range but major suppression gain is from low to high A/R (2.0 to 2.8).

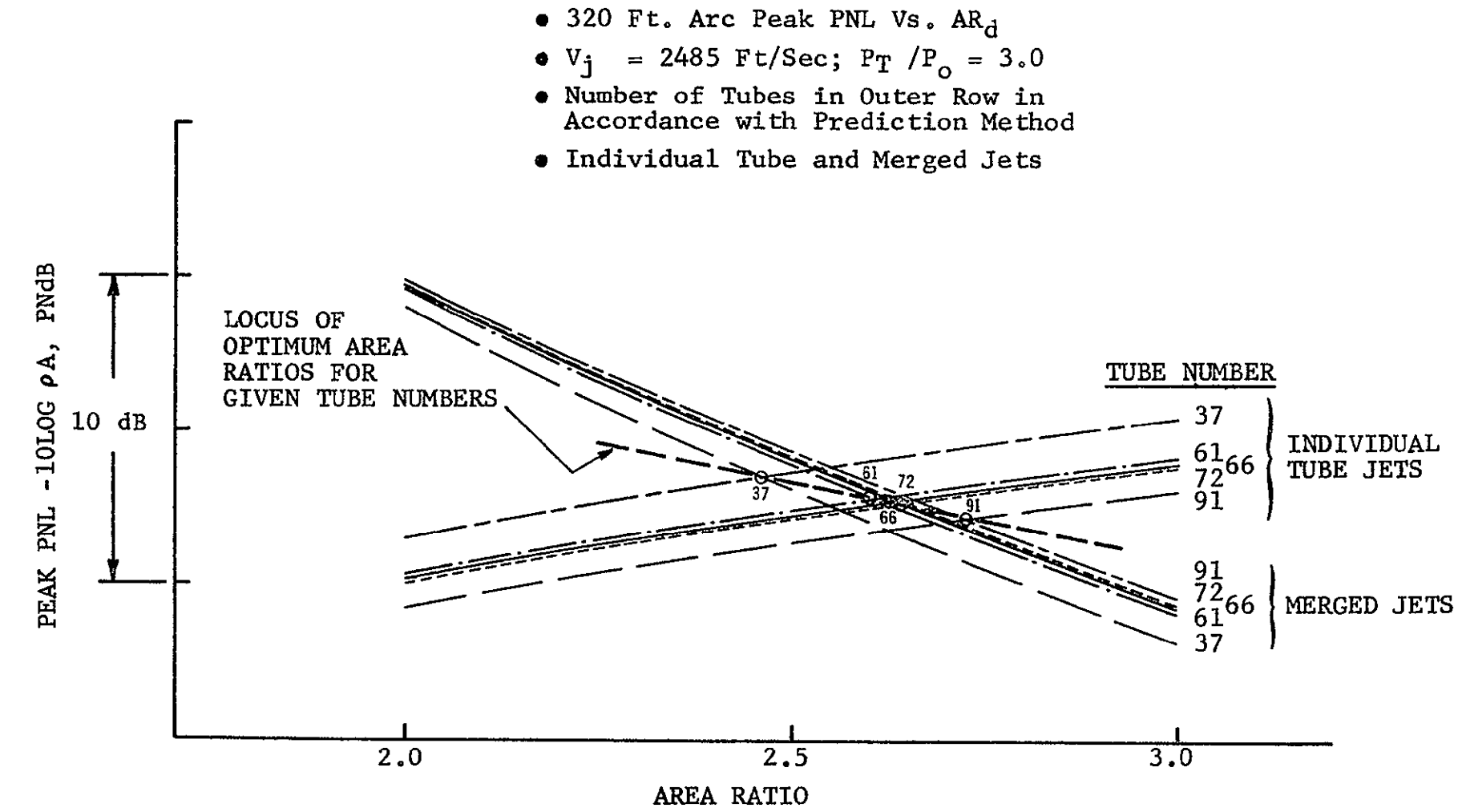

FIGURE 6-13 MULTI-TUBE PREDICTION RESULTS

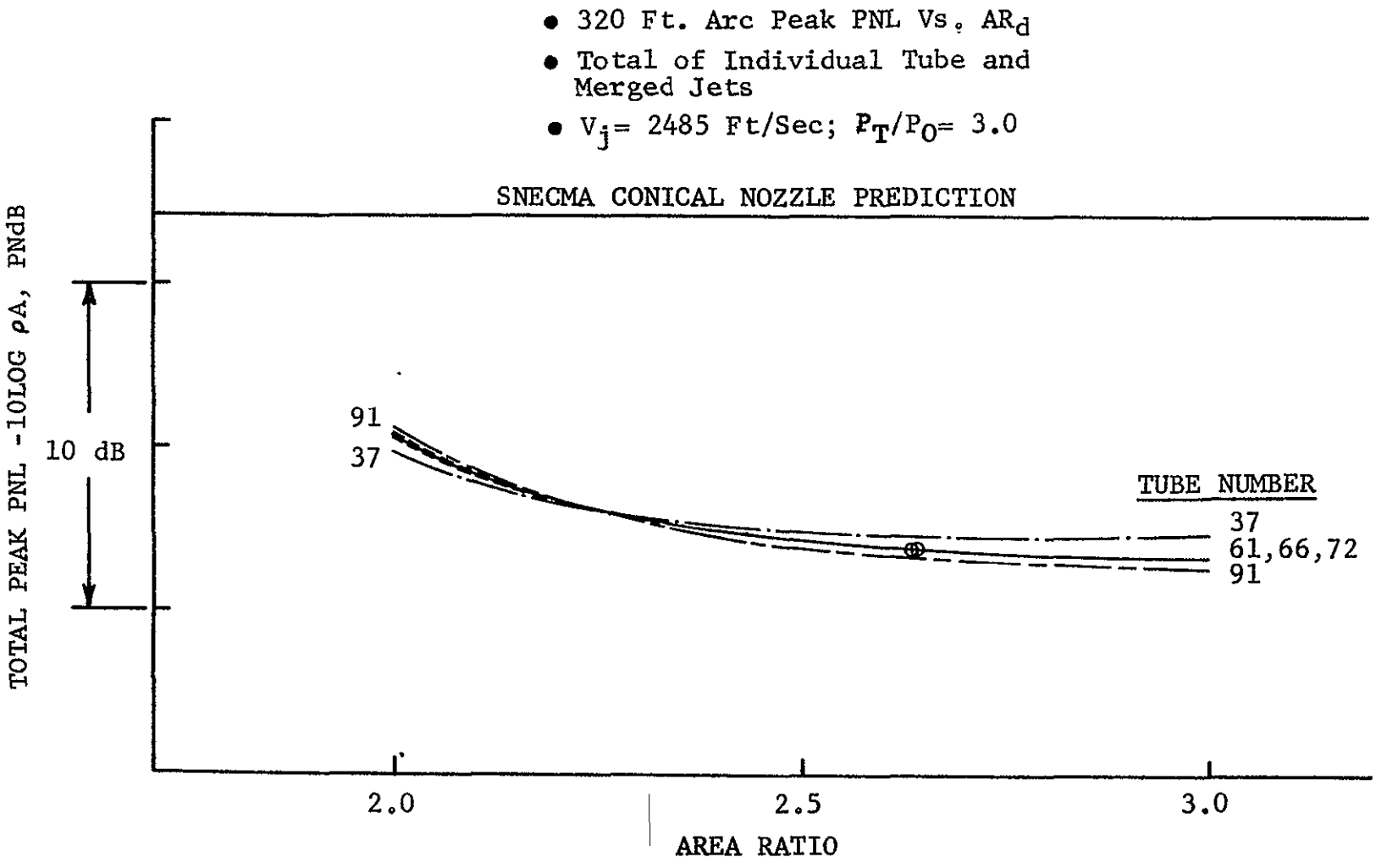

FIGURE 6-14 MULTI-TUBE PREDICTION RESULTS

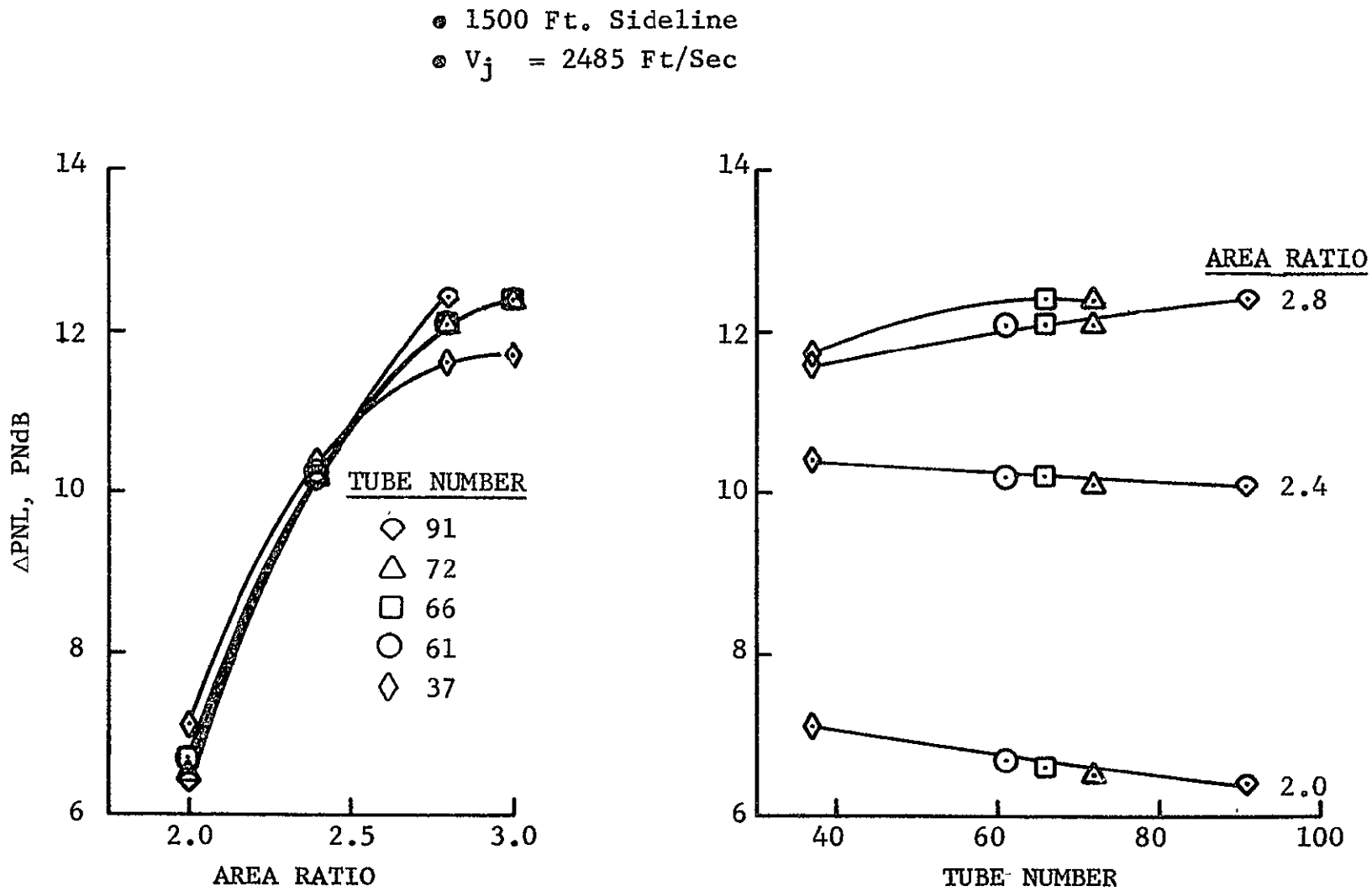

FIGURE 6-15 1500 FT. SIDELINE MULTI-TUBE PREDICTION RESULTS

- Suppression variance with ideal jet velocity is shown in Figure 6-16 and indicates that for a relatively high area ratio (2.8) essentially no change in ΔPNL occurs over the range of 2200 to 2500 ft/sec.

6.1.4 Tube Size Equality and Spacing Uniformity

- General Electric data (Reference 8) shows that three flat baseplate models were tested to evaluate suppression effects of equal/unequal hole size and uniform versus random spacing. Each model had 97 holes and was of A/R = 2.0 as shown schematically in Figure 6-17. The first model (4.88H121-97) had equal hole size and uniform spacing. The second (4.2H97) and third (4.39H97) models used hole patterns of unequal size and non-uniform spacing. From test results shown in Figure 6-18 as 300 and 1500 ft sideline PNL suppression, the equal size and uniform spacing configuration yielded 2 to 6 PNL greater suppression in the medium-to-high velocity range over the non-equal size and random spacing configurations.

- From Boeing data (Reference 13), Figure 6-19 presents the acoustic results for the extremes of simple arrays, i.e., close packed and radially aligned tubes. The close packed array is seen to be consistently better showing ΔPNL increases of approximately 1.0 to 1.5 for 37 tube area ratio of 3.3 and 4.5 arrays, respectively.

  The major conclusion from the review of data associating noise to multi-tube size equality and spacing uniformity was that equality of hole/tube size and uniformity of spacing between tubes/holes appears to be a major parameter in refining a suppressor design. An equal sized and more uniformly spaced tube bundle produces significantly higher suppression than a randomly sized and spaced array.

6.1.5 Tube Length

- General Electric data (Reference 8) indicates an investigation was performed to isolate the effects of tube internal length-to-diameter ratio (L_{ti}/D_t) on multi-tube suppression. An 85 tube nozzle with 0.430" I.D. tubes of 4.5" initial length (L_{ti}/D_t = 10.47) and of area

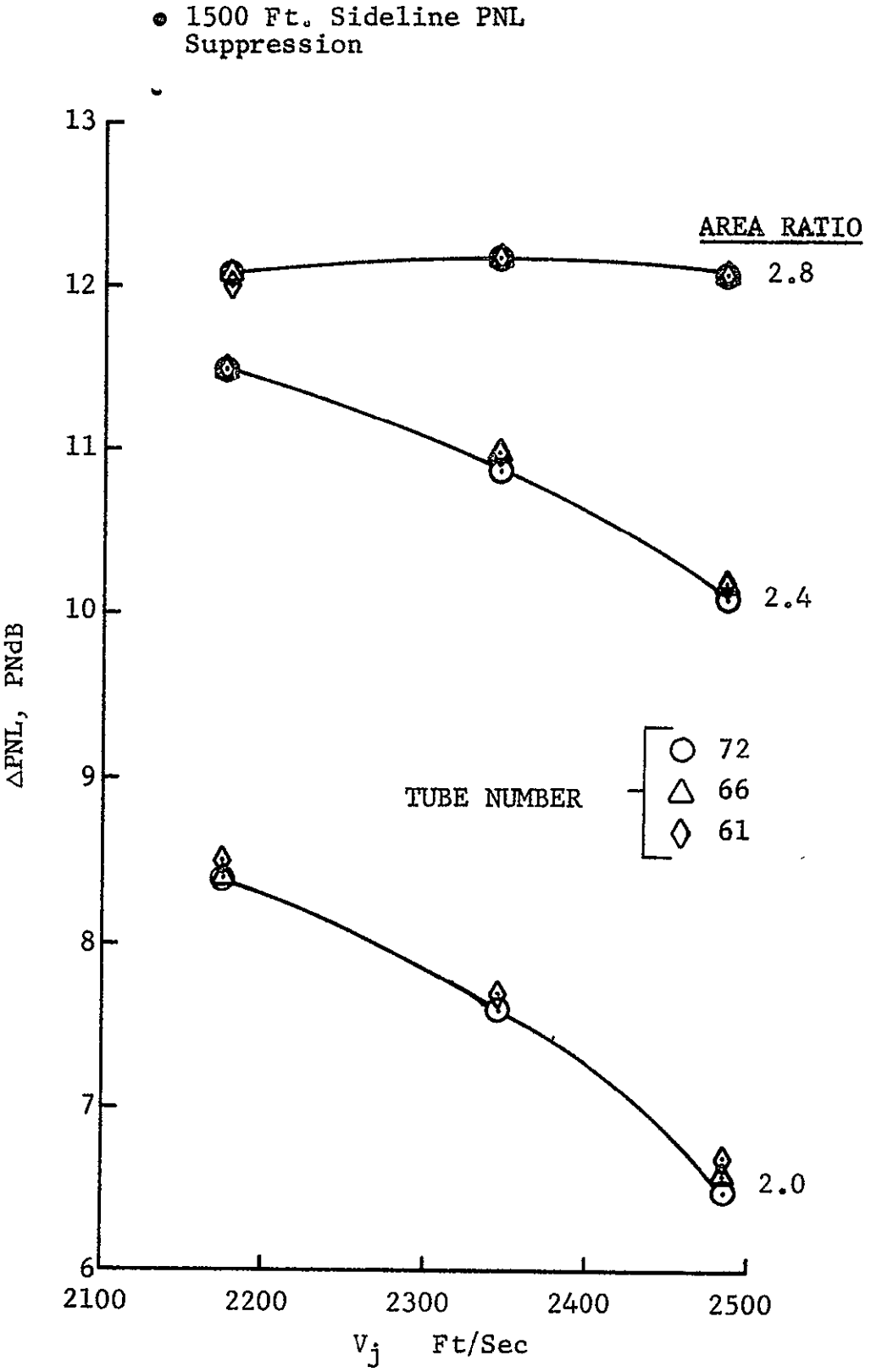

FIGURE 6-16 1500 FT. SIDELINE MULTI-TUBE PREDICTION RESULTS

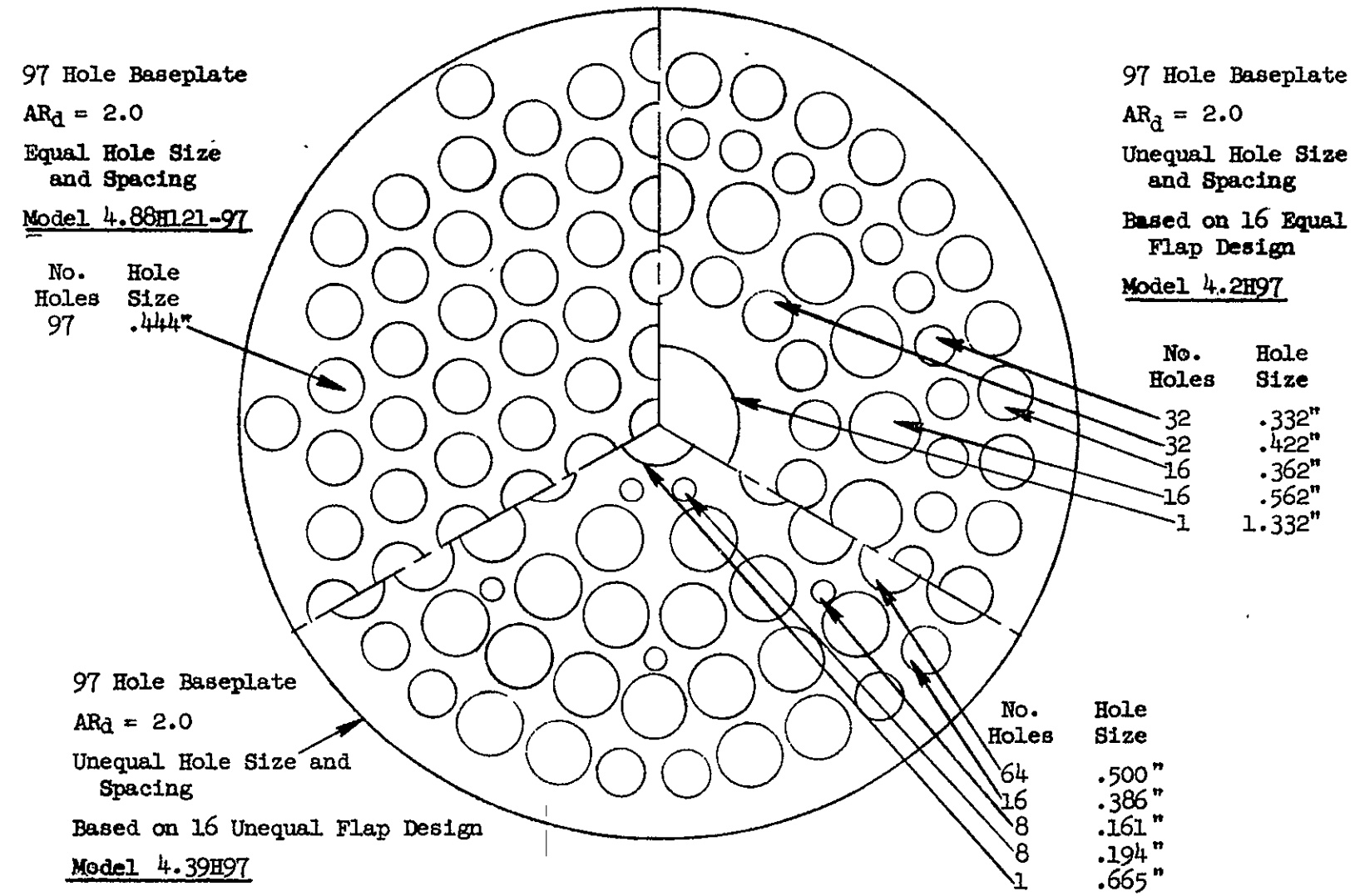

FIGURE 6-17 SCHEMATIC OF 97-HOLE BASEPLATE COMPOSITE SHOWING EQUAL AND UNEQUAL CIRCULAR HOLE SIZES AND SPACING PATTERNS

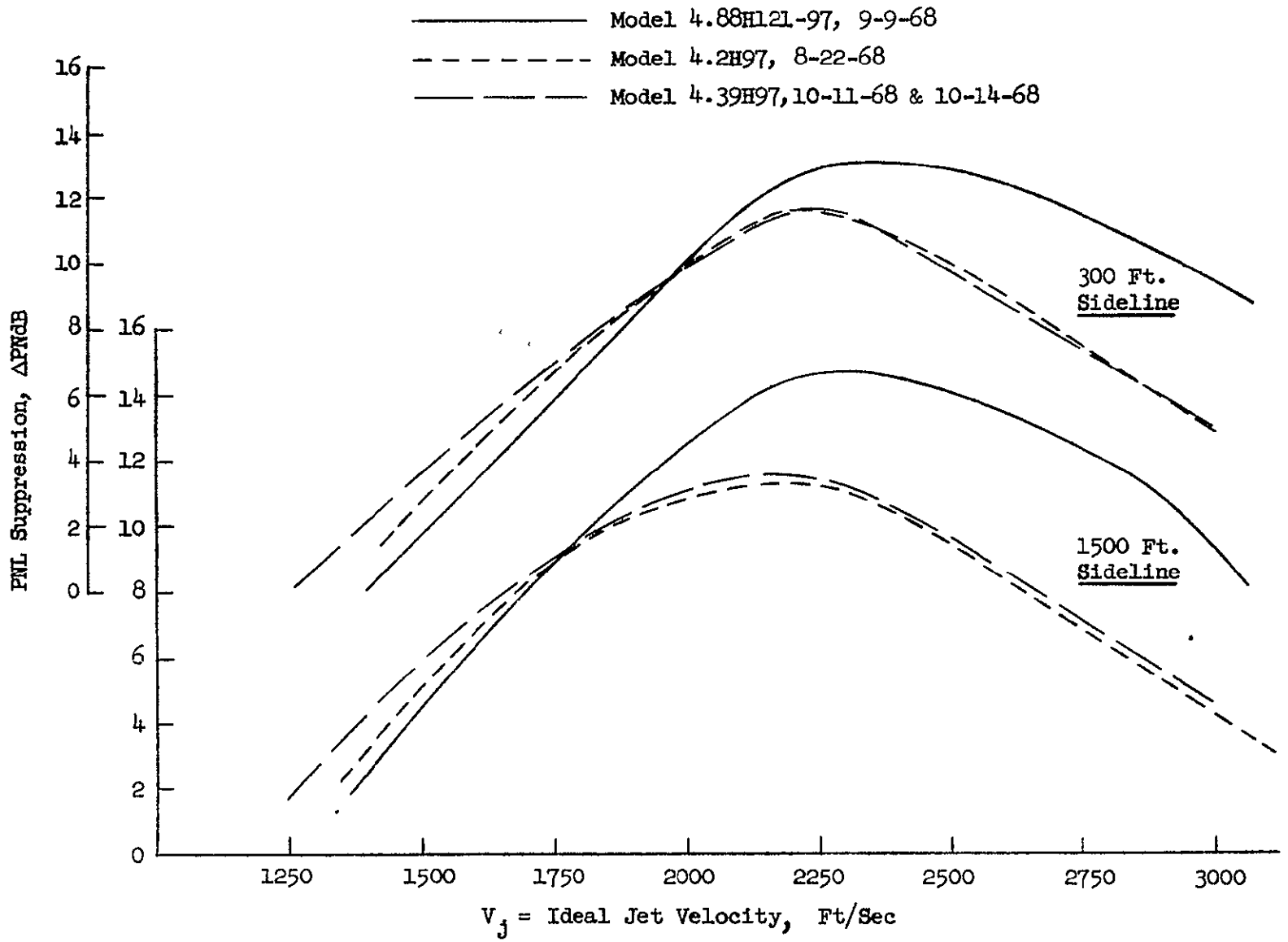

FIGURE 6-18 EFFECT OF HOLE SIZE AND SPACING ON 300 FT. AND 1500 FT. SIDELINE PNL SUPPRESSIONS FOR 97 HOLE PLATE NOZZLES

ORIGINAL PAGE IS OF POOR QUALITY

• 37 TUBES

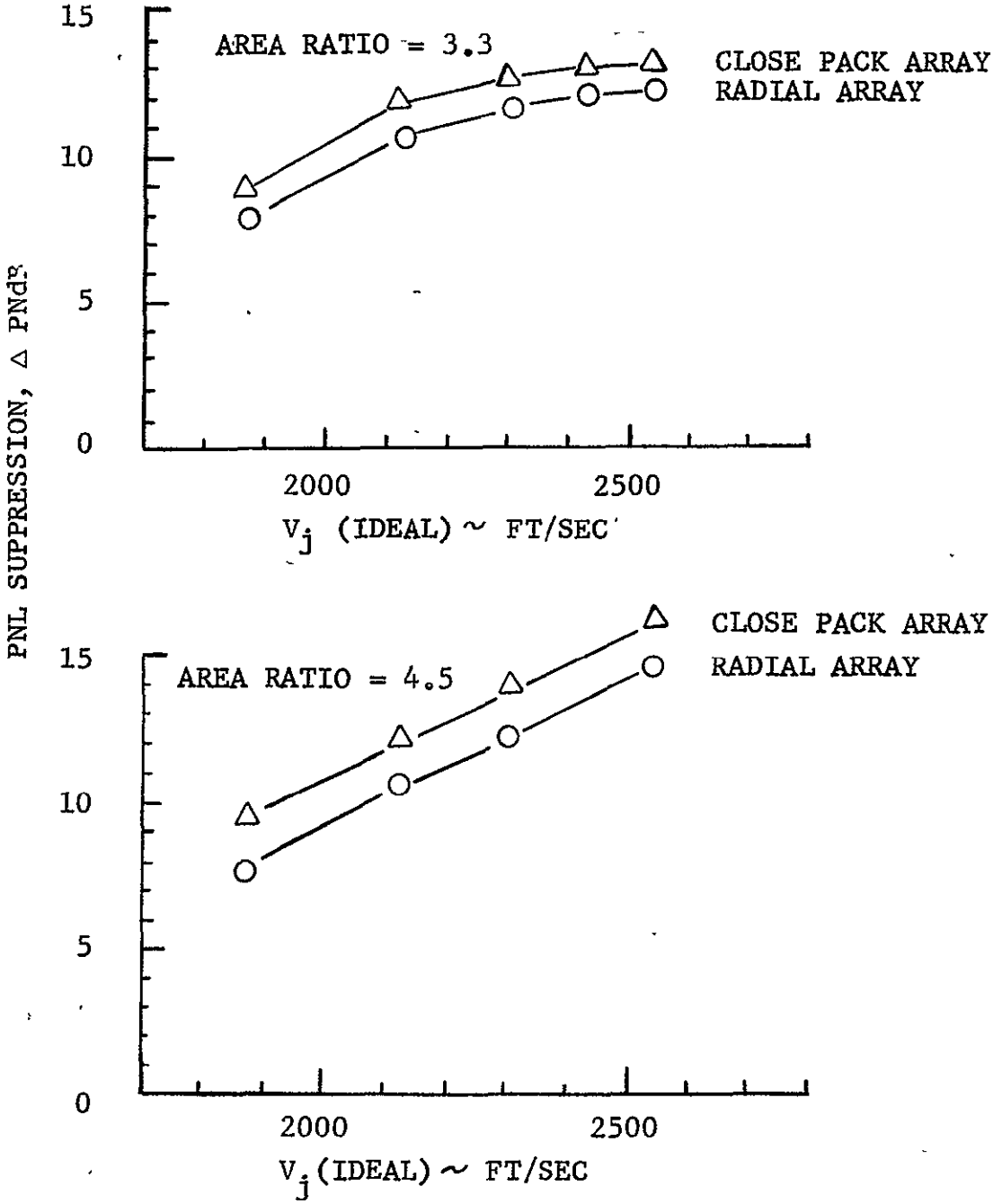

Figure 6-19 EFFECT OF TYPE OF NOZZLE TUBE ARRAY ON 2128 FT. SIDELINE NOISE SUPPRESSION

ratio = 3.19 was used. The tube pattern was uniform with equal spacing on a hexagonal pattern and tube exits were coplanar as per Figure 6-20. A total of seven models were tested by shortening the tubes in increments of 1/2, 3/4, or 1" until a baseplate remained as the last configuration, as shown schematically in Figure 6-21. The internal length to diameter ratio was thus varied from 10.47 to 1.74. Using the L_{ti} = 4.5" model as reference, suppression change due to change in tube length is shown in Figure 6-22. The curve shows variations are minor across the jet velocity range but with definite increased suppression trends in the mid-velocity range with intermediate tube length. To more closely establish the effect at mid-to-high jet velocity, Figure 6-23 shows average curves through data variations at incremental jet velocities. Indications are that an optimum design exists in the intermediate (4 to 6) L_{ti}/D_t range and a maximum gain of about 1.0 to 1.5 ΔPNL is seen from the average curves over that of a long or short tube.

- From Boeing data (Reference 13) the effect of tube length on PNL suppression is shown in Figure 6-24 for 37-tube nozzles at area ratios of 2.75 and 61-tube nozzles at area ratio = 3.3. Tube lengths of 1, 2 and 3 inches were used, however, results yield no trends with tube length. The conclusion was drawn that acoustic effect of tube length is nominal.

- Overall Conclusion - Acoustically, minor suppression changes are seen to be attributable to tube length variation, as long as the tubes are of equal size, uniformly spaced, and form a coplanar exit plane. Slight suppression gain (over baseplate or long tubes) is achieved by tube design in the intermediate L_{ti}/D_t and jet velocity. This is based primarily on the controlled General Electric test for isolation of the individual parameter.

- Aerodynamic test results for the General Electric data (Reference 8) are based on static pressure measurements on the baseplate of the models. The base pressure profiles were used to calculate the mean base pressures by integrating the measured static pressures over their

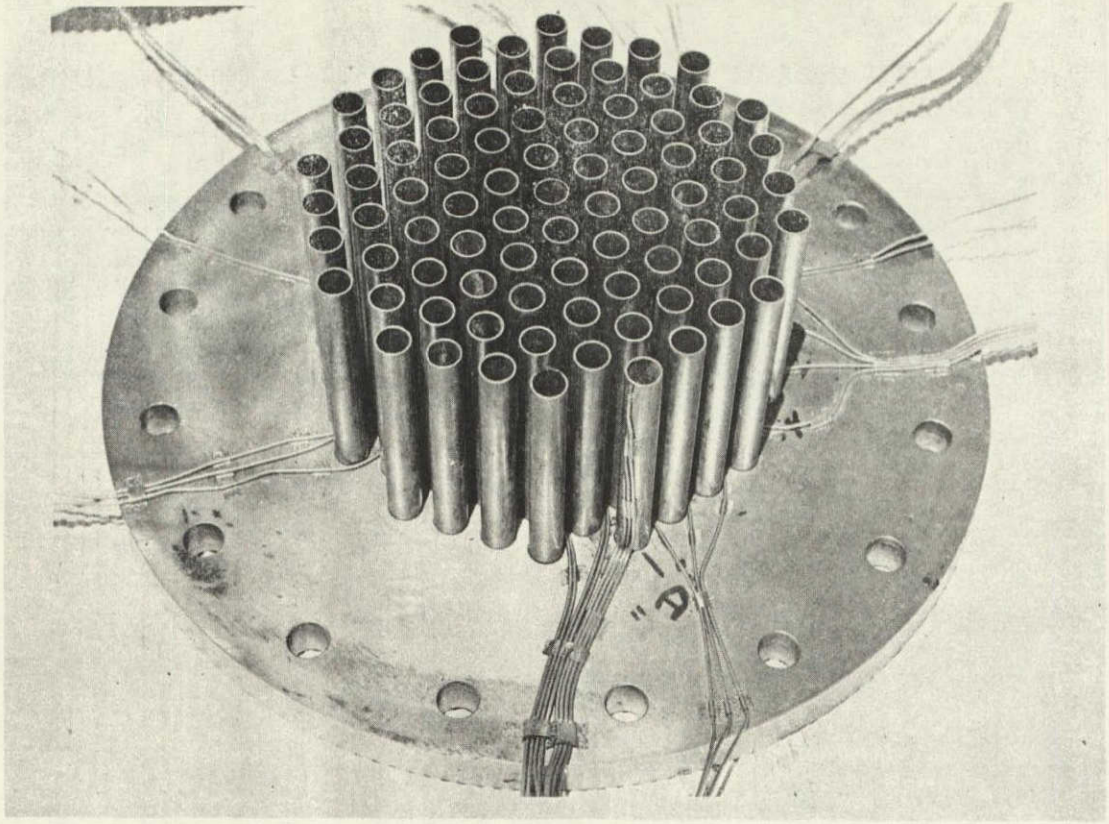

FIGURE 6-20 BASIC 85 TUBE HARDWARE CONFIGURATION USED IN THE EXTERNAL/ INTERNAL TUBE LENGTH VARIATION STUDY

ORIGINAL PAGE IS
OF POOR QUALITY

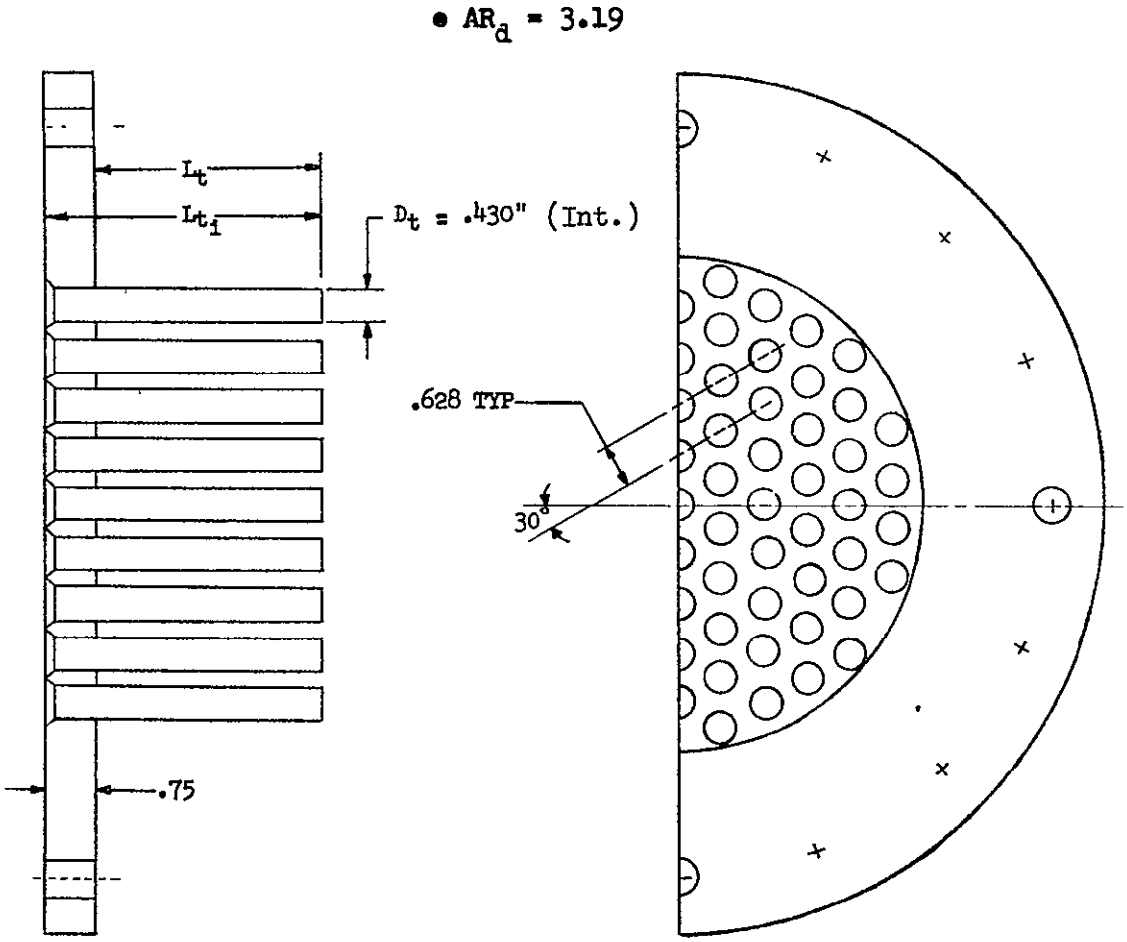

Model No.	Test Date	L_t	L_t/D_t	L_{ti}	L_{ti}/D_t
3.4T85	6-12-69	3.75"	8.72	4.5"	10.47
3.4T85-1	8-12-69	2.75"	6.40	3.5"	8.14
3.4T85-2	8-18-69	2.25"	5.23	3.0"	6.98
3.4T85-3	8-26-69	1.75"	4.07	2.5"	5.81
3.4T85-4	9-04-69	1.25"	2.91	2.0"	4.65
3.4T85-5	10-28-69	.75"	1.74	1.5"	3.49
3.4T85-6	11-21-69	0	0	.75"	1.74

FIGURE 6-21 SCHEMATIC OF 85 TUBE NOZZLE USED IN EXTERNAL/ INTERNAL TUBE LENGTH STUDY

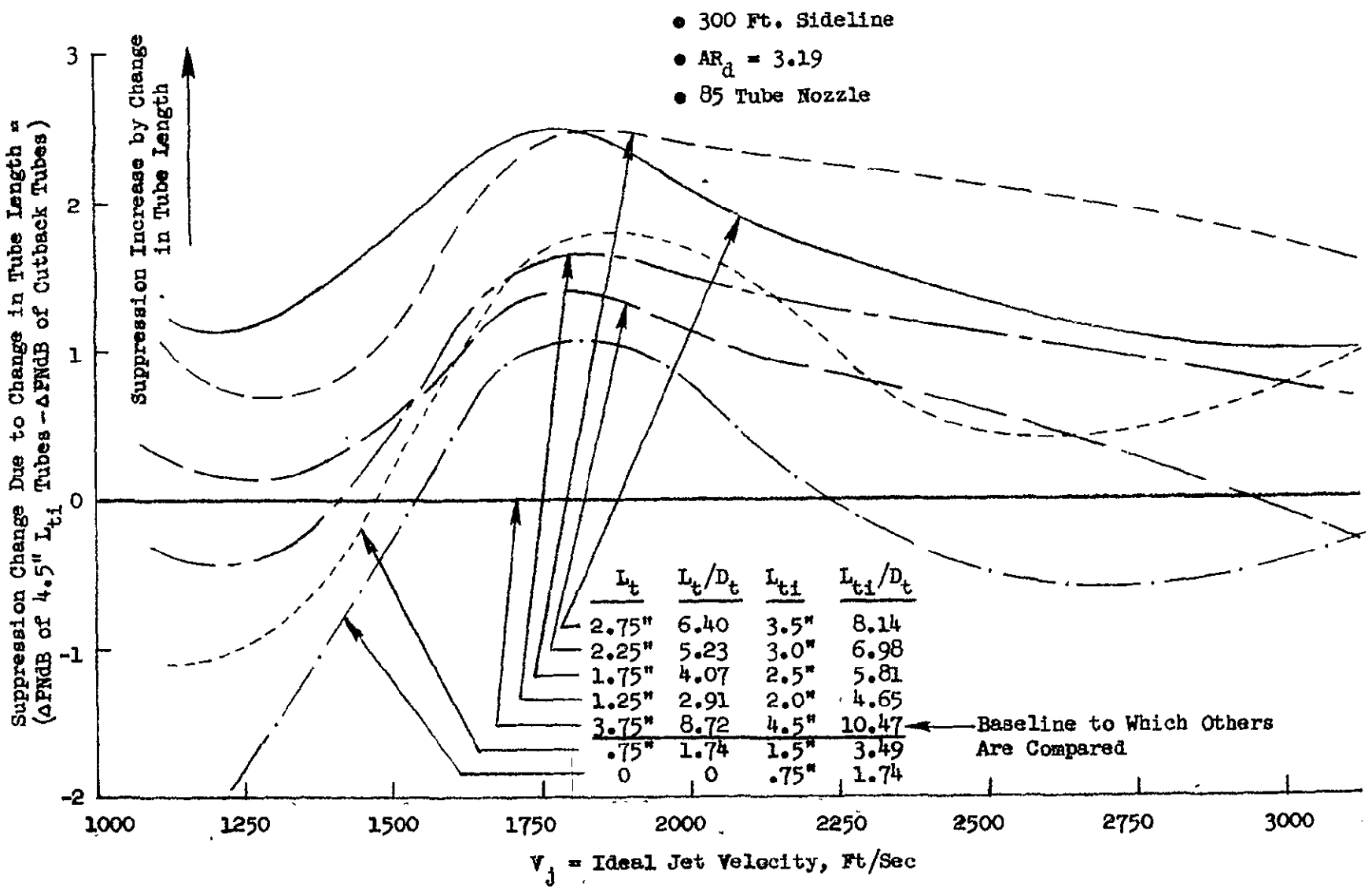

FIGURE 6-22 EFFECT OF INTERNAL/EXTERNAL TUBE LENGTH TO TUBE INTERNAL DIAMETER RATIO ON PNL SUPPRESSION

ORIGINAL PAGE IS OF POOR QUALITY

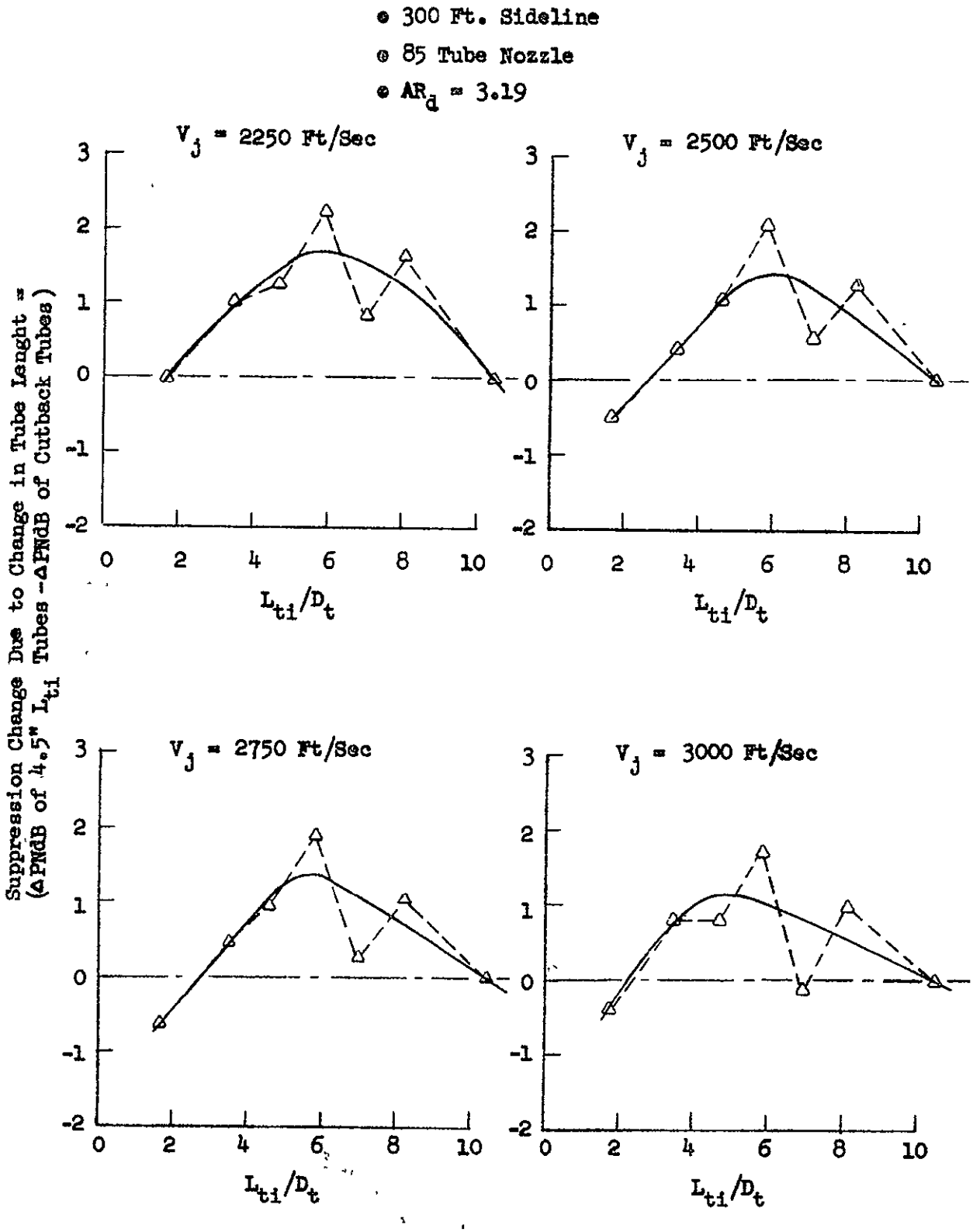

FIGURE 6-23 EFFECT OF TUBE INTERNAL LENGTH TO TUBE INTERNAL DIAMETER, L_{ti}/D_t, ON PNL SUPPRESSIONS FOR DIFFERENT JET VELOCITIES

ORIGINAL PAGE IS
OF POOR QUALITY

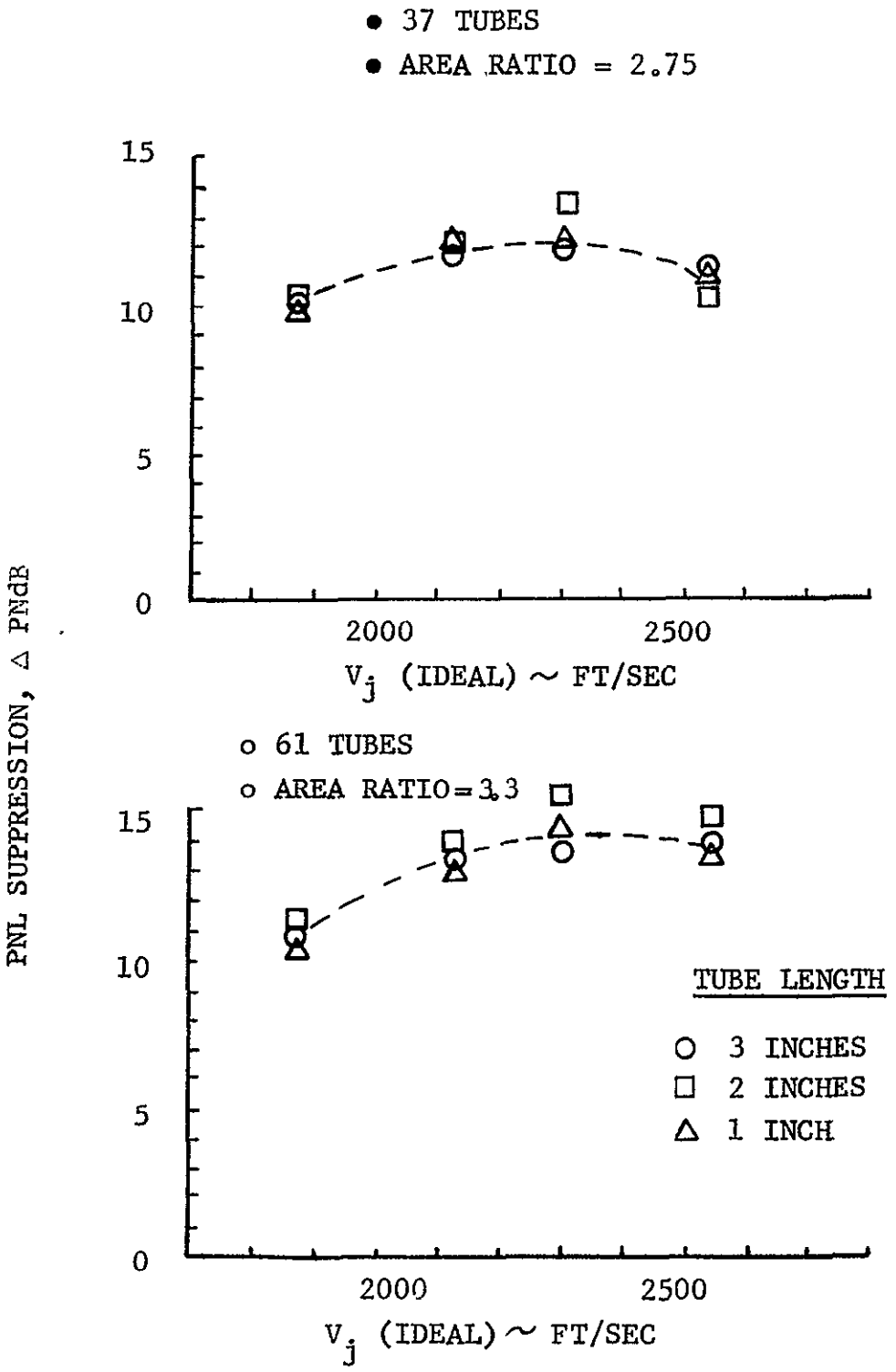

Figure 6-24 EFFECT OF NOZZLE TUBE LENGTH ON SIDELINE PERCEIVED NOISE SUPPRESSION

respective incremental base areas and then dividing the total value by the total base area acted upon. Mean base pressure ratio, $\bar{P}_B/P_o$, versus nozzle pressure ratio, P_{T8}/P_o, is presented in Figure 6-25. As the tubes were shortened, $\bar{P}_B/P_o$ decreased uniformly until $L_{ti}/D_t = 3.49$, meaning the base drag force increased. Further cutback of the baseplate model ($L_{ti}/D_t = 1.74$) significantly lowered the mean base pressure ratio.

Figure 6-26, base drag coefficient variation with P_{T8}/P_o and L_{ti}/D_t, shows baseplate drag increasing as tube length is decreased, synonymous with mean base pressure data. The change in pressure ratio and drag coefficient per incremental $\Delta L_{ti}/D_t$ is approximately constant, except for the shorter tubes which show a much greater increment of change for the same amount of cutback. In the range of $1.5 \leq P_{T8}/P_o \leq 3.4$, the change in pressure ratio has little effect on the drag coefficient except for the baseplate model. Therefore, a design curve is presented in Figure 6-27 showing base drag coefficient change as a function of L_{ti}/D_t, independent of P_{T8}/P_o for the measured range.

6.1.6 Baseplate and Tube Exit Plane Stagger

The General Electric test series and results (Reference 8) presented in Figures 6-28, 6-29 and 6-30 were to isolate the effect of a) tube bundle baseplate cant (stagger) angle, and b) tube bundle exit plane cant angle. Five models were used with combinations of tube exit and baseplate stagger from coplanar/flat to 60° each as seen in Figures 6-28 and 6-29. Each configuration had 72 tubes on a hexagonal pattern and at area ratio = 3.0. Acoustic suppression results in Figure 6-30 indicate that at high velocity a wide range of suppression is achievable, the magnitude depending strongly on tube base and exit plane orientations. If both baseplate and exit planes are staggered, suppression decreases, a larger decrease resulting from the greater stagger. For a coplanar tube bundle exit plane, suppression increases with increased canting of the baseplate.

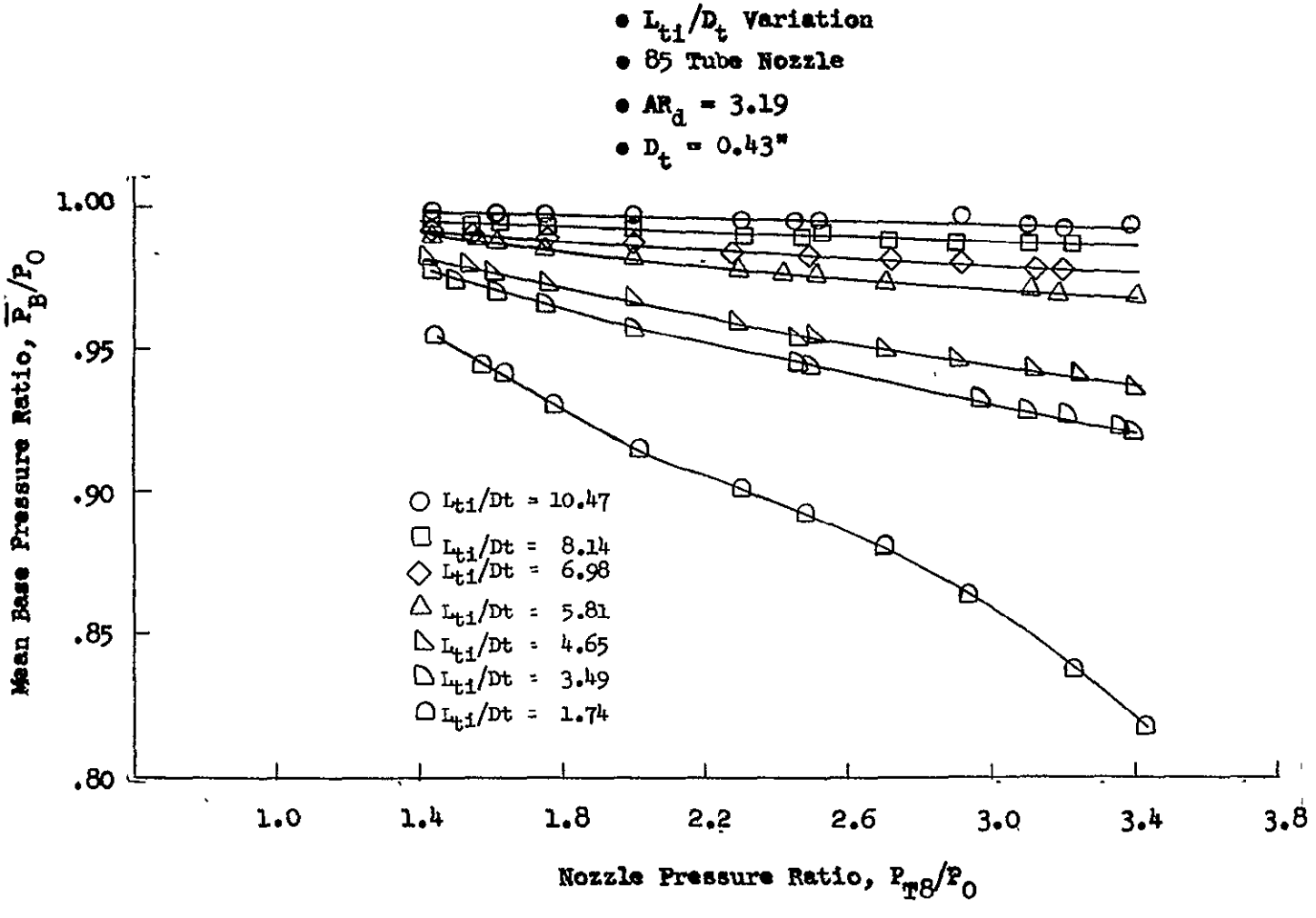

FIGURE 6-25 : EFFECT OF TUBE LENGTH TO TUBE DIAMETER RATIO ON MEAN BASEPLATE PRESSURE RATIO

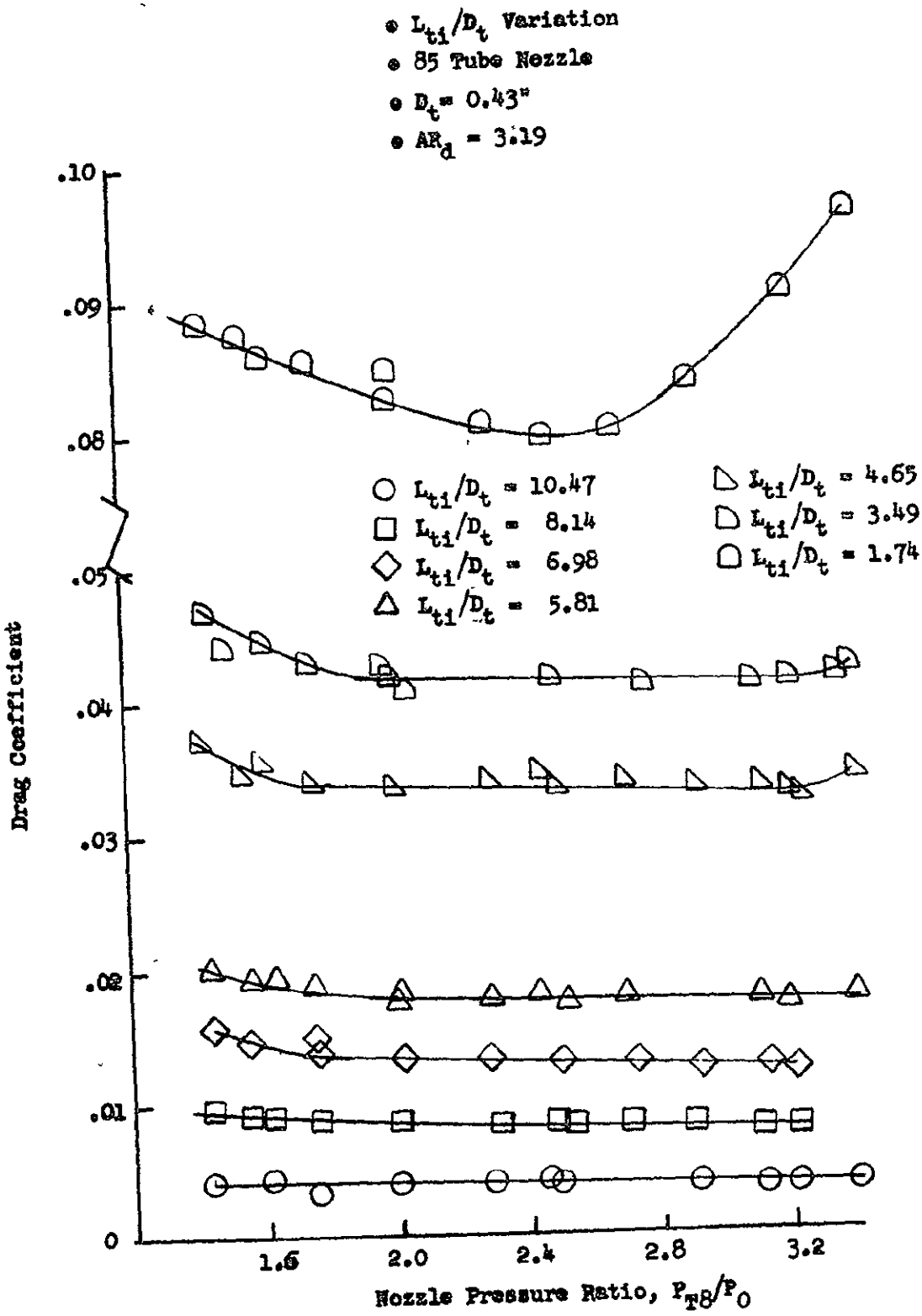

FIGURE 6-26 EFFECT OF TUBE LENGTH TO TUBE DIAMETER RATIO ON BASEPLATE DRAG COEFFICIENT

ORIGINAL PAGE IS
OF POOR QUALITY

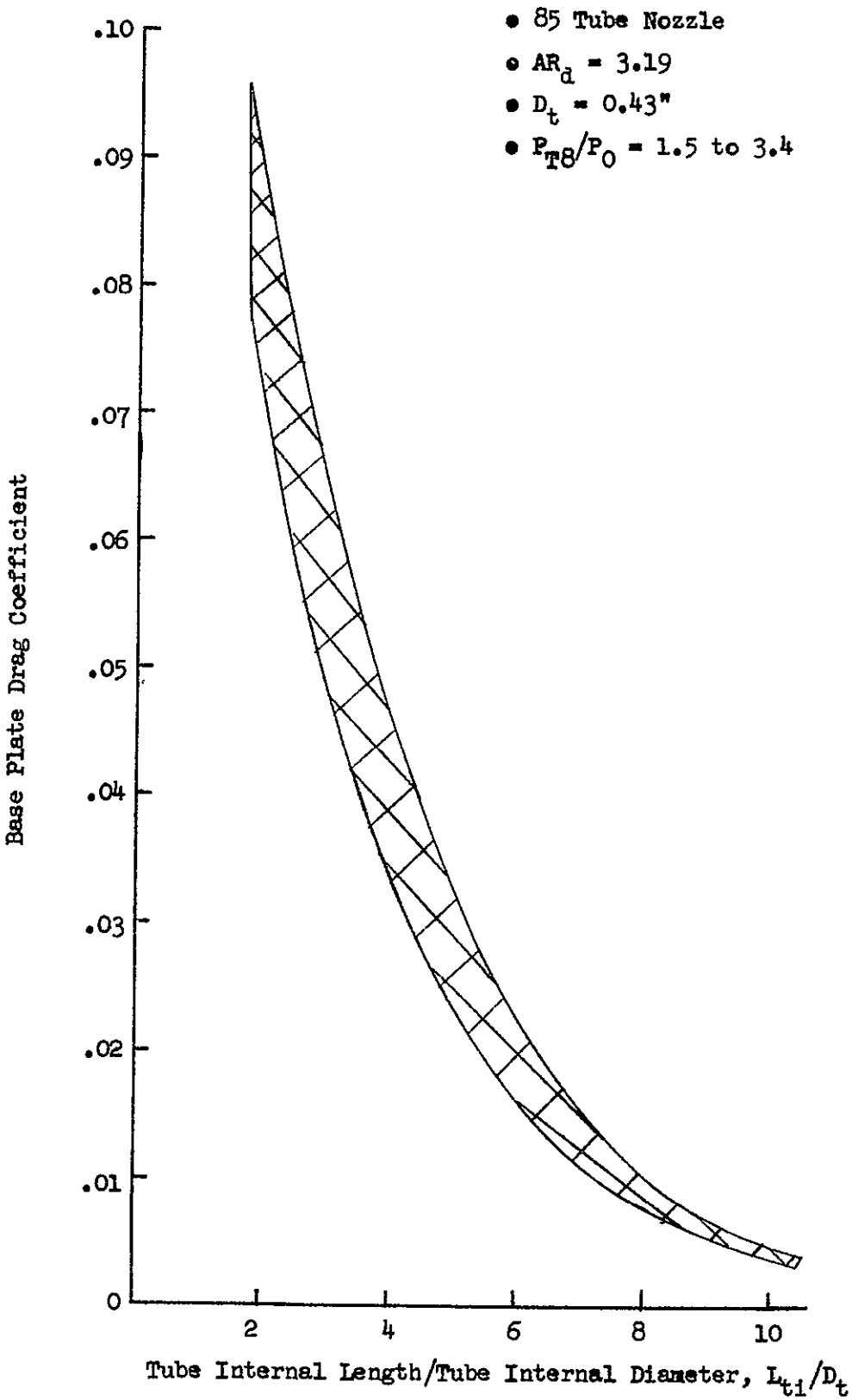

FIGURE 6-27 BASEPLATE DRAG COEFFICIENT AS A FUNCTION OF TUBE INTERNAL LENGTH TO TUBE INTERNAL DIAMETER RATIO

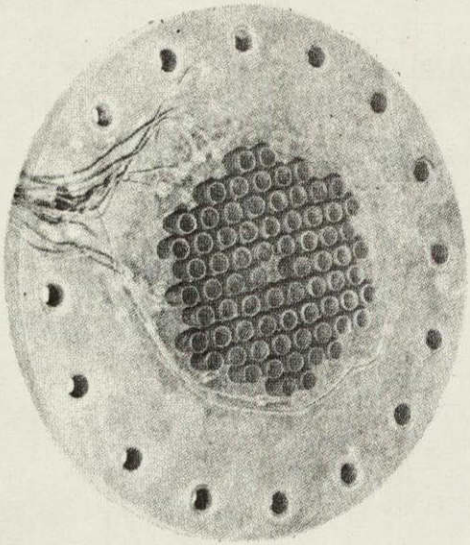

① & ② 0° Base Stagger
Coplanar Tube Exit

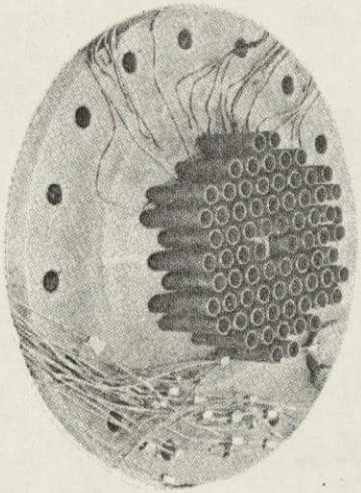

③ 30° Base Stagger
Coplanar Tube Exit

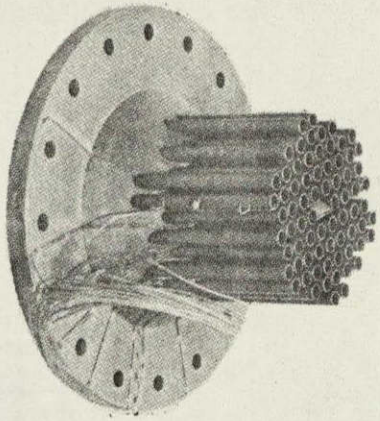

④ 60° Base Stagger
Coplanar Tube Exit

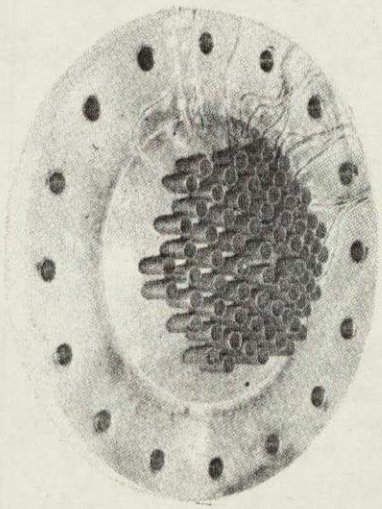

⑤ 30° Base Stagger
30° Tube Exit Stagger

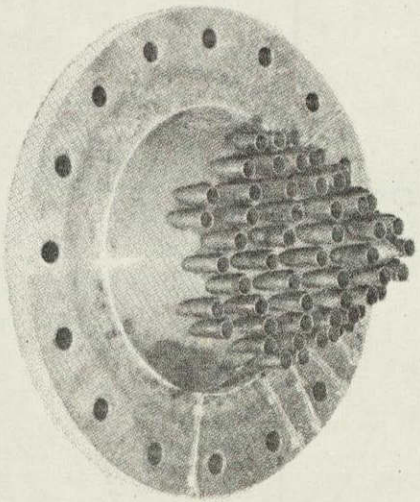

⑥ 60° Base Stagger
60° Tube Exit Stagger

FIGURE 6-28 72 TUBE NOZZLE HARDWARE FOR BASEPLATE AND TUBE EXIT PLANE STAGGER CONFIGURATIONS

ORIGINAL PAGE IS
OF POOR QUALITY

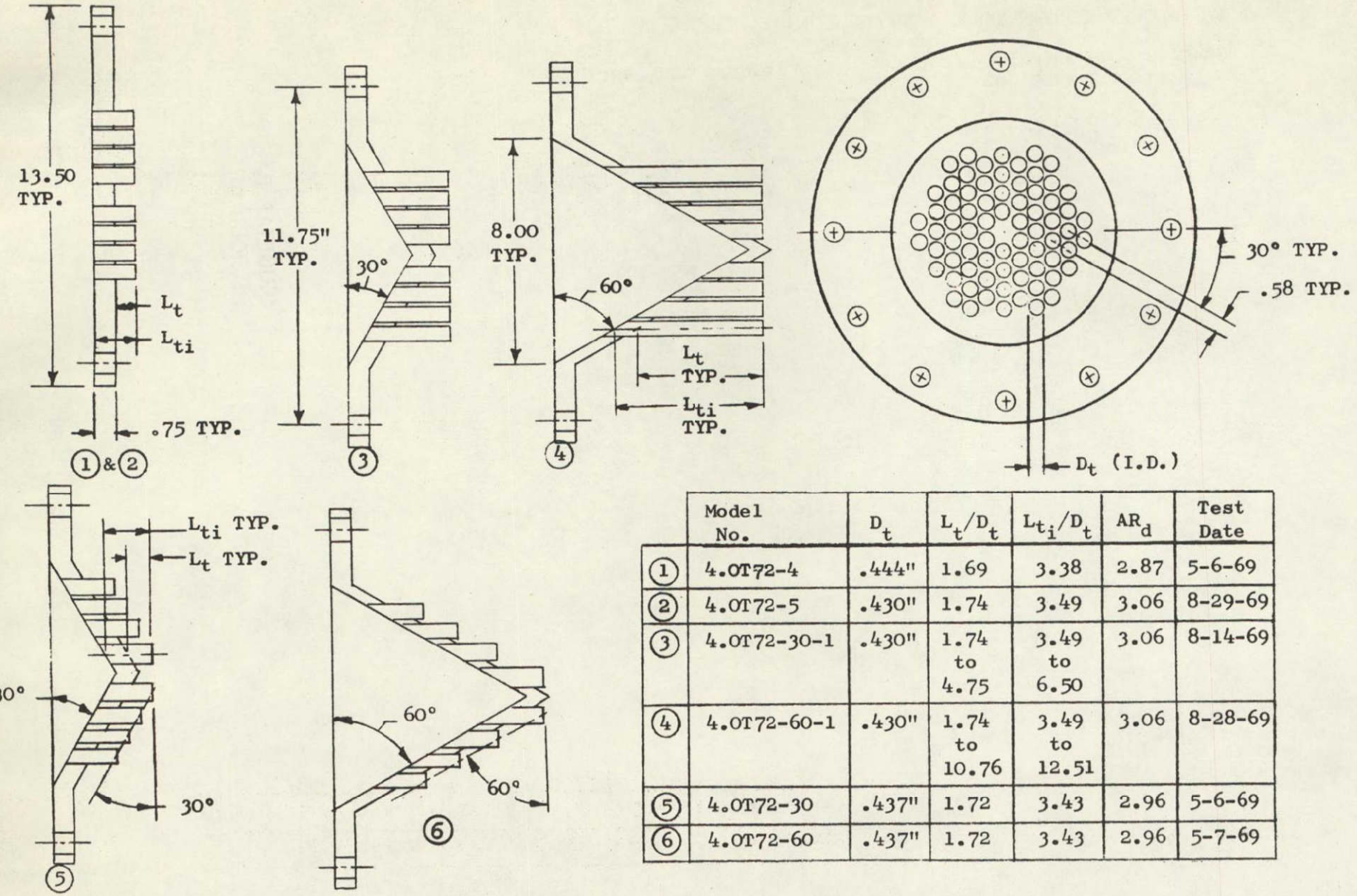

	Model No.	D_t	L_t/D_t	L_{t_i}/D_t	AR_d	Test Date
1	4.0T72-4	.444"	1.69	3.38	2.87	5-6-69
2	4.0T72-5	.430"	1.74	3.49	3.06	8-29-69
3	4.0T72-30-1	.430"	1.74 to 4.75	3.49 to 6.50	3.06	8-14-69
4	4.0T72-60-1	.430"	1.74 to 10.76	3.49 to 12.51	3.06	8-28-69
5	4.0T72-30	.437"	1.72	3.43	2.96	5-6-69
6	4.0T72-60	.437"	1.72	3.43	2.96	5-7-69

FIGURE 6-29 SCHEMATIC OF 72 TUBE NOZZLE CONFIGURATIONS FOR BASEPLATE AND TUBE EXIT PLANE STAGGER VARIATIONS

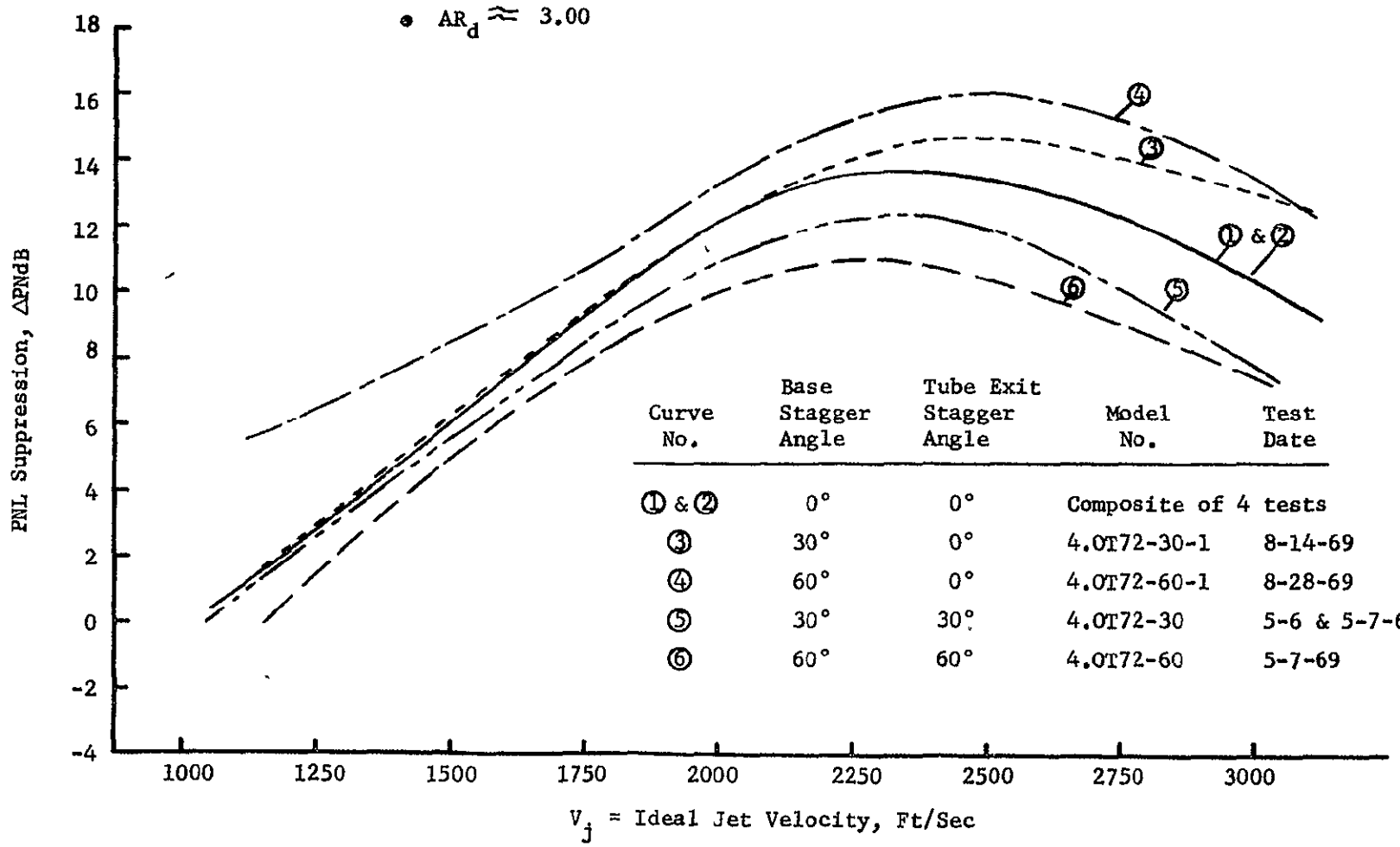

Curve No.	Base Stagger Angle	Tube Exit Stagger Angle	Model No.	Test Date
① & ②	0°	0°	Composite of 4 tests	
③	30°	0°	4.0T72-30-1	8-14-69
④	60°	0°	4.0T72-60-1	8-28-69
⑤	30°	30°	4.0T72-30	5-6 & 5-7-69
⑥	60°	60°	4.0T72-60	5-7-69

FIGURE 6-30 EFFECT OF BASEPLATE AND TUBE EXIT PLANE STAGGER ON 1500 FT. SIDELINE PNL SUPPRESSIONS FOR A 72 TUBE NOZZLE

Aerodynamic test results based on static pressure measurements on the baseplate integrated to mean base pressure ($\bar{P}_B/P_o$) distributions are shown in Figure 6-31 as a function of nozzle pressure ratio.

The flat baseplate, coplanar tube exit plane system (Models 4.0T72-4 and -5) had the lowest $\bar{P}_B/P_o$, and consequently the highest base drag coefficients, due to inability to ventilate the base area between the tubes. The 60° baseplate, coplanar tube exit system (Model 4.0T72-60-1) had the highest mean base pressure ratios, and consequently the lowest base drag. The long tube lengths at the outer periphery of the tube bundle allowed for pumping of ambient air to the center of the baseplate, pressurizing the base area and minimizing loss due to base drag.

Conclusions

- Major suppression changes are seen to be attributable to the particulars of tube exit plane and baseplate design. Within the range of geometry variance of the test series, sideline peak PNL suppression change ranged up to 5.5 PNdB at DBTF design jet velocity. Each of the models had 72 tubes and was near area ratio of 3.0 design, therefore, suppression variance was attributable only to baseplate and tube exit plane changes.
- The suppression and aerodynamic data show that if the model is staggered at both base and tube exit planes, suppression decreases and base pressure increases as stagger angle is increased.
- For a coplanar tube bundle exit plane, both base pressure and suppression increase with increased base stagger. The increased base pressure results in lower base drag and total aerodynamic thrust loss.
- The best suppressor configuration was the coplanar tube exit plane model with high base stagger angle, yielding approximately 2 ΔPNdB additional suppression at DBTF design jet velocity over the flat baseplate coplanar tube exit plane system.

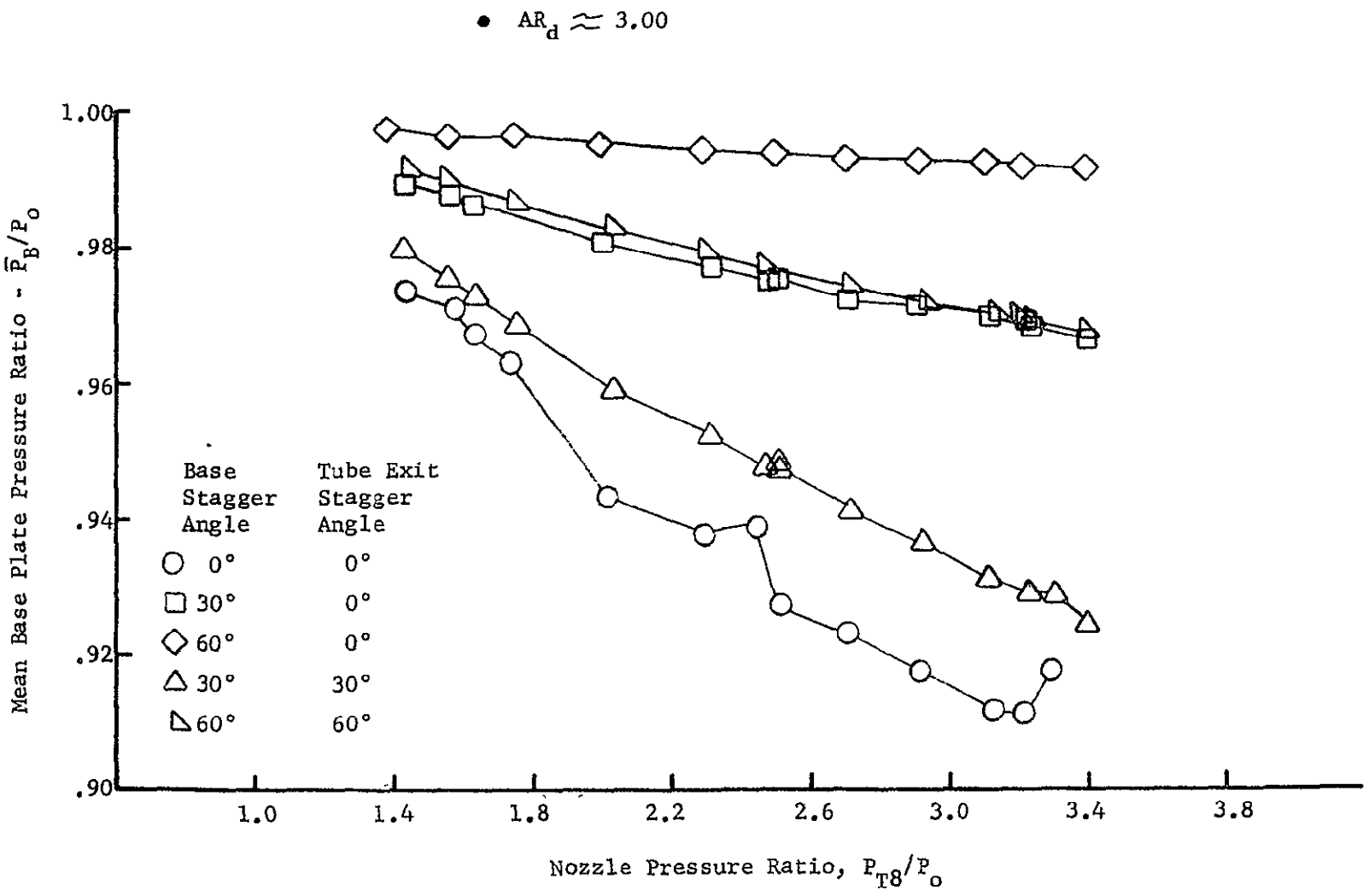

FIGURE 6-31 EFFECT OF BASEPLATE AND TUBE EXIT PLANE STAGGER ON MEAN BASEPLATE PRESSURE RATIO

6.1.7 Tube Nozzle Aerodynamic Performance Correlation

Based on review of the aerodynamic static performance data accumulated from the various referenced sources, the single most significant thrust loss mechanism was found to be the pressure drag on the base area of the suppressor. This pressure drag, in terms of average base pressure, proved to be a function of several parameters; namely, tube length, tube spacing, tube exit stagger angle, nozzle pressure ratio, and tube diameter relative to total exit area. Figure 6-32 illustrates these various parameters. It should be noted that most of the previous configurations tested by GE had tubes arranged such that all tubes were equally spaced from adjoining tubes, thus yielding a hexagonal type array, as illustrated in Figure 6-32. These data were used to analyze the effect of the above named parameters, but it has been demonstrated that the tube arrangement also effects the level of the base pressure and this could not be evaluated from the existing data.

The average base pressures for a large number of test configurations were correlated against the key model parameters, as shown in Figure 6-33. The correlation parameter, $[S^2 + (L/\cos\theta)^2]/A_8$ is an indication of the amount of base ventilation area available with respect to the nozzle flow area. The existing data is seen to collapse quite well for lines of equal nozzle pressure ratio, noting that some degree of inaccuracy was expected, simply due to the nature of the base pressure calculation which consists of integrating test pressures over a calculated base area.

Other significant loss mechanisms are tube internal friction and the P_T loss from sudden contraction of the flow from the upstream flow-chamber into the tubes. Because these losses cannot be readily measured in a test, the effect of varying geometric parameters was studied using semi-emperical methods. Tube skin friction was analyzed using turbulent boundary layer theory and average skin friction coefficients. The skin friction is a function of tube length, diameter, and flow Mach number. The entrance loss was calculated using emperical sudden contraction loss and was dependent on contraction area ratio and upstream and downstream Mach number. Examples of the parametric evaluation of skin friction loss and entrance loss are shown in Figures 6-34 and 6-35, respectively for tubes of constant flow area, i.e., the tube exit area equals the tube entrance area. These losses can be reduced significantly

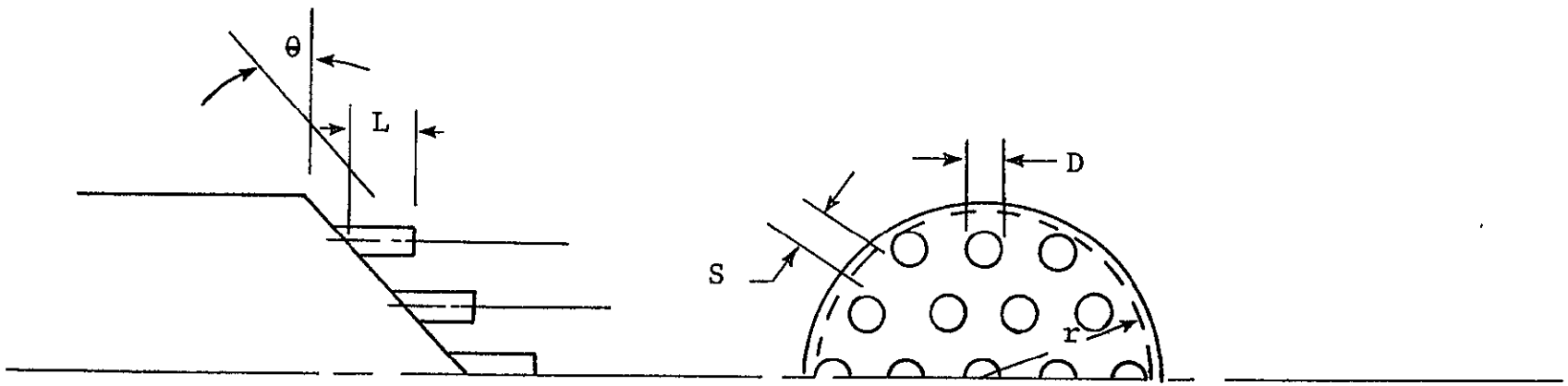

$A_{TOTAL} = \pi r^2$

D = TUBE I.D.

S = TUBE SPACING (O.D. TO O.D.)

θ = TUBE STAGGER ANGLE

L = TUBE LENGTH AT $\mathfrak{L}$

Figure 6-32 TUBE NOZZLE PARAMETERS FOR AERO PERFORMANCE CORRELATION

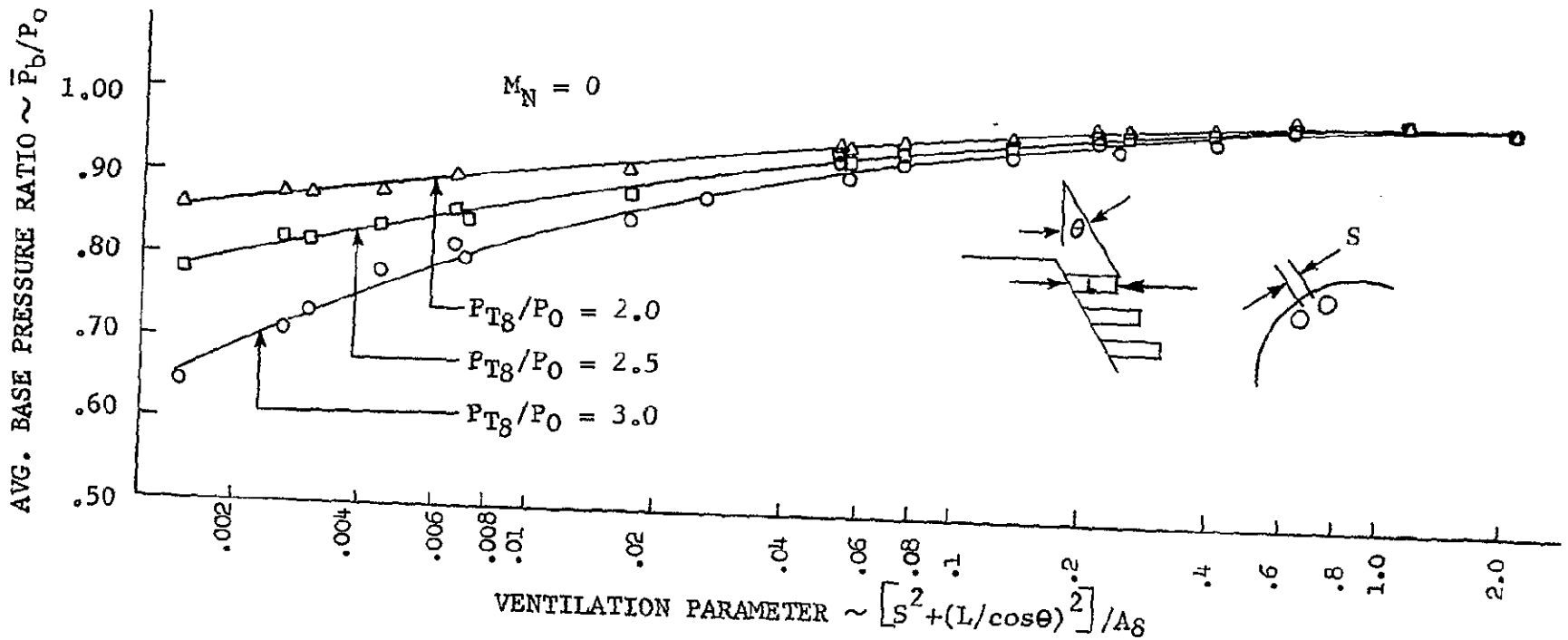

Figure 6-33 MULTI-TUBE BASE PRESSURE CORRELATION

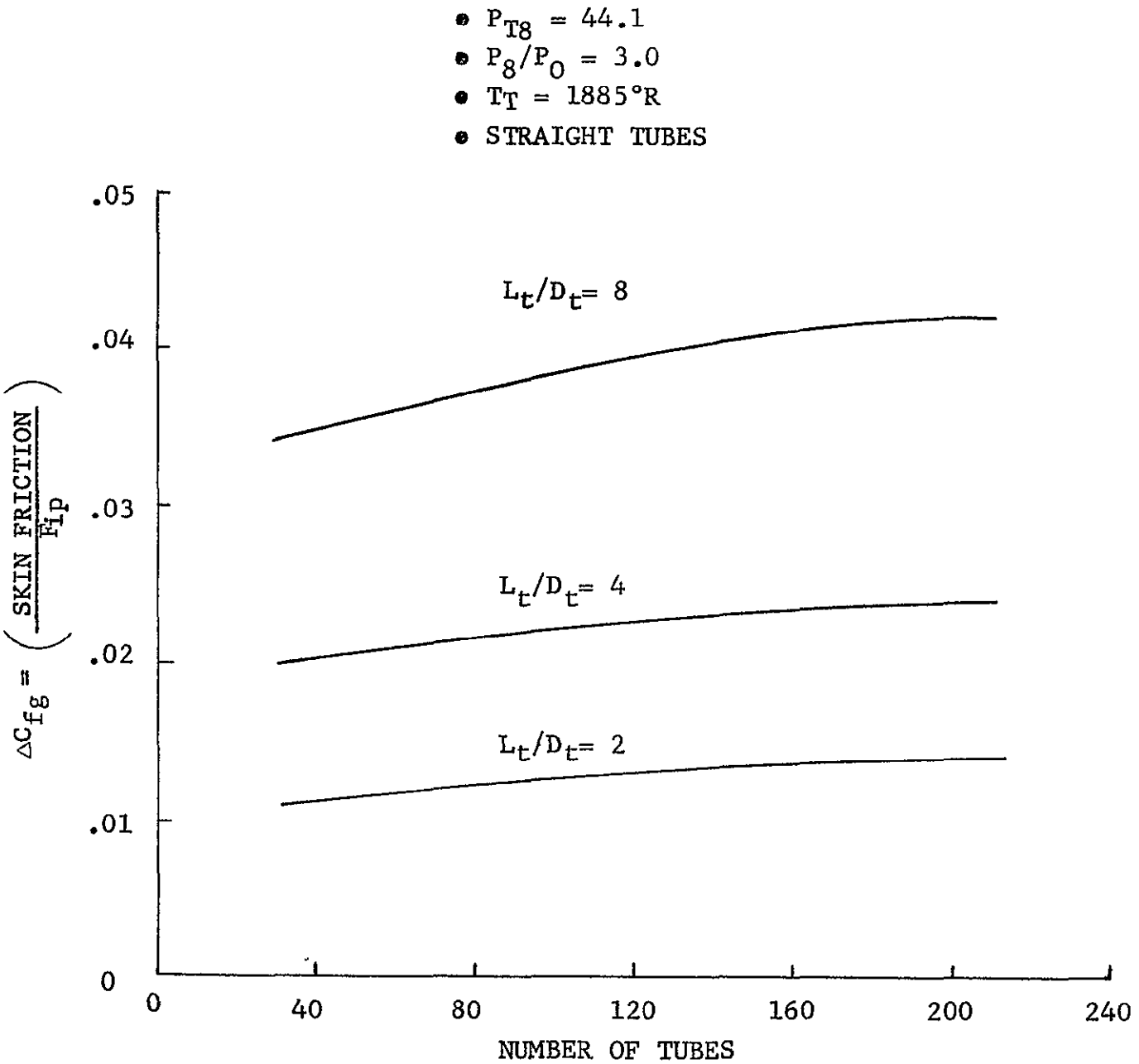

Figure 6-34 PARAMETRIC EVALUATION OF MULTI-TUBE NOZZLE INTERNAL SKIN FRICTION LOSS

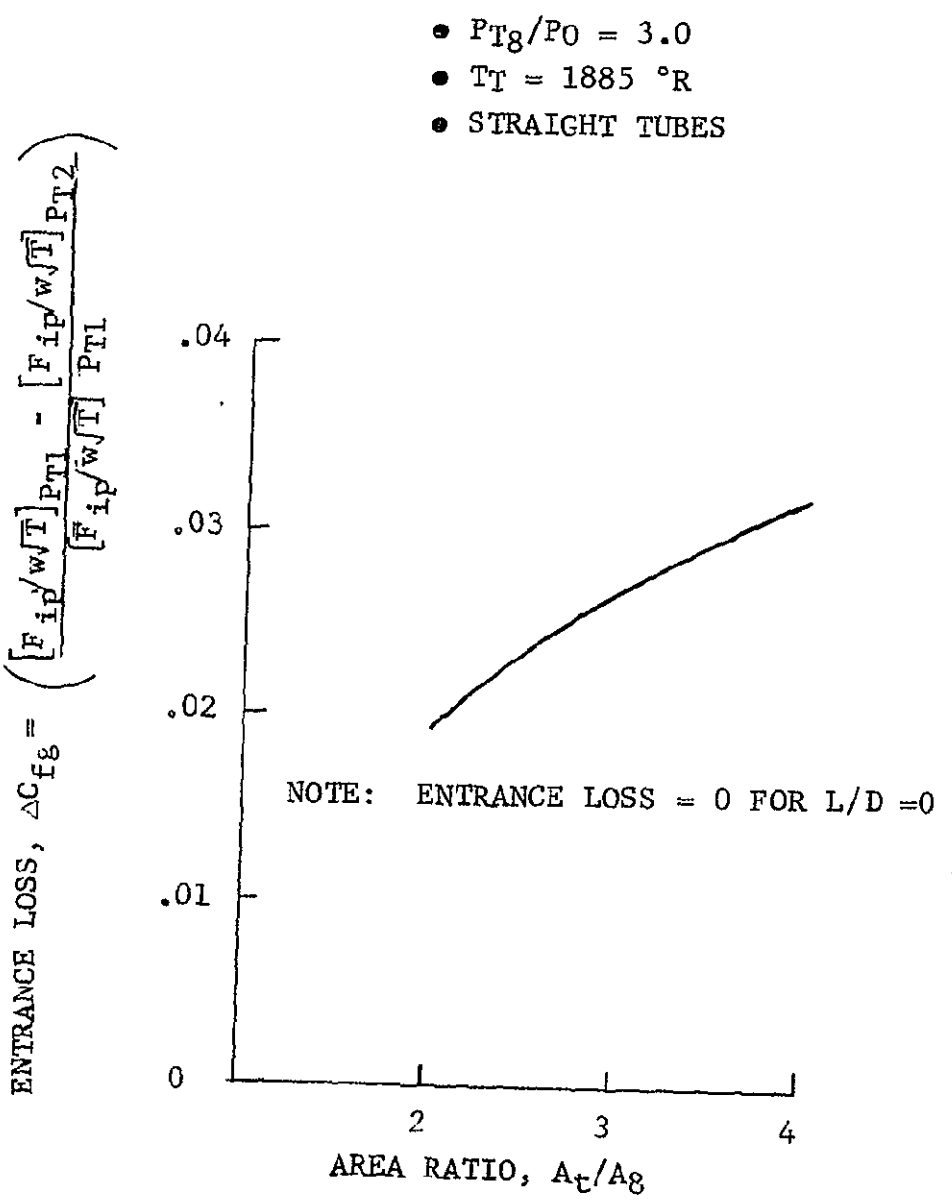

Figure 6-35 PARAMETRIC EVALUATION OF MULTI-TUBE NOZZLE TUBE ENTRANCE LOSS

by having convergent exits on the tubes. The effect of this convergence is to reduce the flow Mach number in the tubes, reducing both the skin friction and the sudden contraction pressure losses.

To evaluate the overall effect of the various design parameters, the three major loss mechanisms of base pressure, skin friction, and tube entrance may be combined to produce a total loss in thrust coefficient. Correlation of this overall loss with area ratio and tube number is shown in Figure 6-36. It should be noted that the delta thrust coefficients shown in Figures 6-34, 6-35, and 6-36 are based on the ideal thrust of the air upstream of the tube entrance plane.

The results and analysis methods used in this generalized study were applied as aerodynamic guidelines in selecting the multi-tube fan duct suppressor.

6.1.8 Selection of Multi-Tube Duct Suppressor Design

Summarizing the various conclusions derived from review of all available acoustic and aerodynamic data on multi-tube suppressors leads to the following general guidelines for design of the DBTF duct suppressor at the selected design point (see Section 4.2).

- Area ratio range should be between 2.5 and 3.0, high enough to obtain good suppression and aerodynamic performance but not entirely impractical in mechanical implementation. Favoring high area ratio should benefit the acoustic effectiveness of the treated ejector application.
- Tube number should be a minimum of 50 to 60 to obtain reasonable suppression, however, spacing of tubes within annular rows (three rows selected for final design) would probably more highly influence tube number selection.
- Try to maintain equal spacing between tubes for uniformity of plume coalescence and lower noise. Radial patterns are more efficient for baseplate ventilation, resulting in higher base pressure and aerodynamic performance, however, acoustic performance is severely jeapordized. For the duct annular suppressor, however, lack of

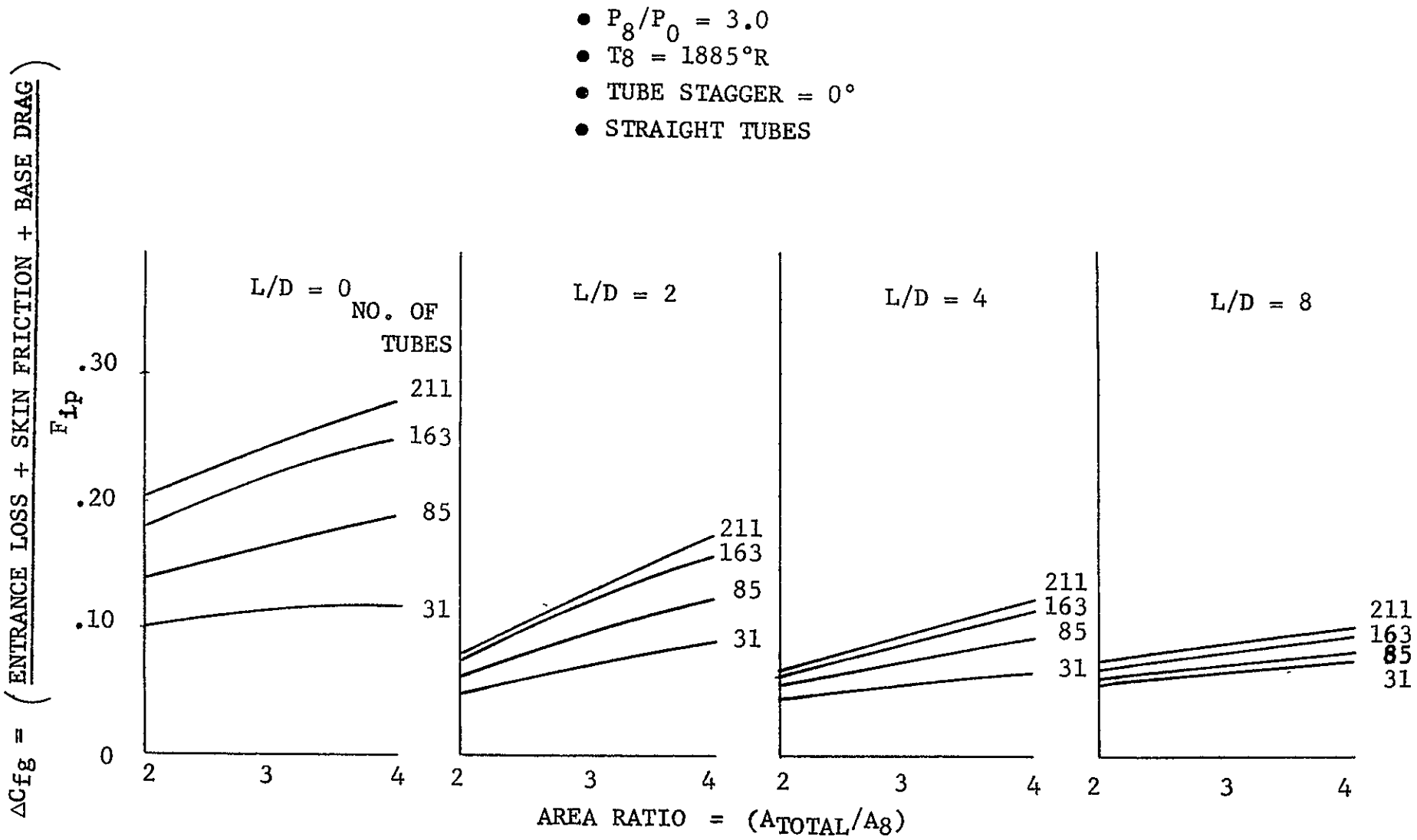

Figure 6-36 PARAMETRIC EVALUATION OF MULTI-TUBE NOZZLE TOTAL THRUST LOSS

baseplate ventilation may not be as severe a loss mechanism as for the single flow concepts previously tested. For an equivalent area ratio, the duct suppressor sets the tube base area on an annulus and results in a much shorter path for ventilating air to penetrate, as compared to the single flow non-annular suppressors.

- Tube size should also be held uniform, as long as spacing between tube centers is near equal, to assure a common plane of jet merging.
- For good base ventilation and subsequent favorable aerodynamic performance, the outer row should have long tubes. The inner tube rows should also be of reasonable length to assure ventilation to the baseplate area near the plug flowpath. For acoustic performance, tube length to diameter ratio of 4 to 5 was optimum. (The final design utilizes tubes in the outer row with a length to diameter ratio of 4.0 in an attempt to maximize base static pressures without incurring internal friction losses severe enough to offset this base pressure gain.) For practical engine design the maximum tube length would be dictated by stowage requirements in the unsuppressed mode.
- The tube exit plane should be coplanar, again for a common coalesced jet plane required for beneficial acoustic performance.
- Tube length can be gained, particularly in the outer tube rows, by canting the baseplate. Aerodynamically the baseplate stagger yields no additional performance gain for tubes which are already long, however, a trade between tube length and canting is most reasonable to obtain the desired baseplate ventilation. Canting of 30° to 45° from flat (or vertical) baseplate should be considered as reasonable, however, engine design would again dictate the limit.
- Tube ends should be convergent by approximately 30% of area [((tube inlet area/tube exit area) - 1) x 100] to a) decrease entrance loss, b) lower skin friction within the tube, and c) maintain predominately subsonic flow in the sudden contraction region of the tube entrance, eliminating shock P_T loss internal to the tube. In addition the edges formed by the tube intersections with the baseplate should be rounded to further decrease entrance loss.

- Tubes should all be directed parallel to the nozzle centerline for the DBTF design. Canting the outer tube row slightly outward could result in simulated higher aerodynamic area ratio, shown to be somewhat beneficial at the design velocity, however, the common jet merging plane would be eliminated, necessary for high suppression. Flow impingment on the secondary ejector system would also result, detrimental to aerodynamic performance. Canting the inner tube row slightly toward the centerline has been used in several previous models to aid plug pressurization for aerodynamic performance. However, in the DBTF duct application, the tubes will be ejecting along the flat of the plug and vectoring the flow would not be beneficial.

With the aid of these specific guidelines, a series of multi-tube annular arrays were designed within the limits of a) 2, 3 and 4 rows of tubes, b) area ratio = 2.75 and 3.0, c) tube number from 60 to 90 and tube exit I.D. from 0.485" to 0.402," respectively, and d) tube area convergence from 17 to 40%.

A discharge coefficient ($C_D = Ae_{18}/A_{18}$) of 0.948 was chosen, based on previous tube nozzle test data, modified for increased area convergence. The Ae_{18} of 10.842 in^2 (see Appendix A, Table A-1) thus yielded an A_{18} of 11.437 in^2. This was then used to establish the tube array physical dimensions based on the area ratio selection. Area ratio was defined as the annulus area divided by the total physical flow area (A/R = Annulus Area/No. Tubes x Area/Tube). The annulus area was defined as that between concentric circles whose radii were set as the intersection with the tube I.D.'s of the innermost and outermost tubes within the tube array at the coplanar exit plane.

Final selection from the various tube patterns designed was based on a weighted averaging of the parameters most influencing acoustic and aerodynamic performance, consistent with the previously detailed conclusions from the acoustic/aerodynamic data review. The final selection is shown schematically in Figure 6-37, with adaptive hardware to the acoustic test facility, and has the following features:

- AREA RATIO = 2.75
- 69 TUBES
- 29.4% TUBE END AREA CONVERGENCE
- COPLANAR TUBE EXITS
- ROUNDED TUBE INLETS
- ALL TUBES PARALLEL TO $\mathcal{L}$
- A_{18} = 11.437 in^2
- C_D = .948
- A_{e18} = 11.482 in^2

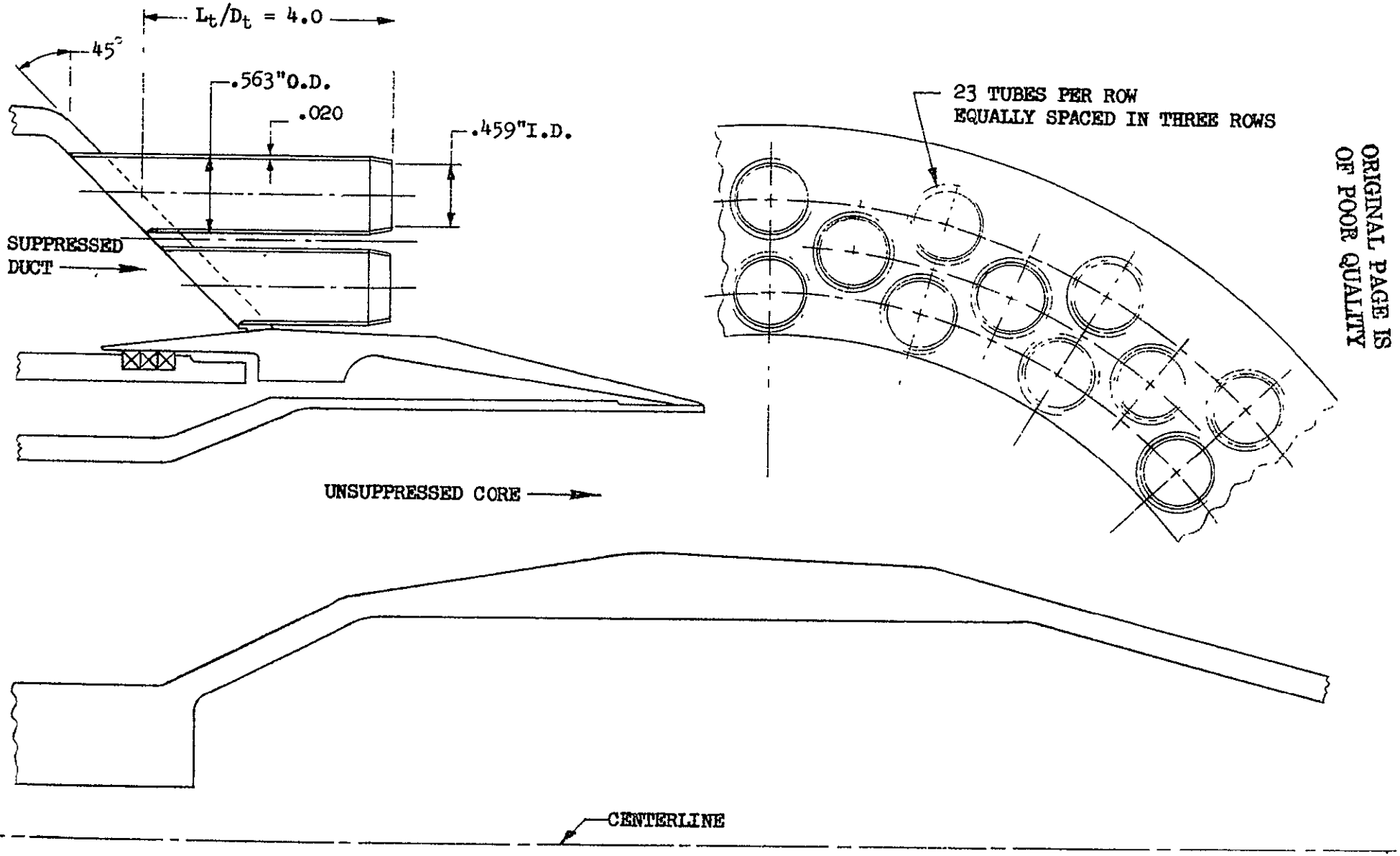

ORIGINAL PAGE IS
OF POOR QUALITY

Figure 6-37 DBTF SCALE MODEL MULTI-TUBE DUCT SUPPRESSOR

- o Area Ratio = 2.75
- o 69 tubes in three row pattern
- o Near equal spacing between tubes
- o Uniform tube characteristics with
  - a) internal diameter at exit plane = 0.459"
  - b) tube O.D. of 0.563" with 0.020" wall thickness
  - c) tube end area convergence of 29.4%
  - d) tube inlets rounded for smooth flow transition
  - e) all tubes exiting flow parallel to nozzle centerline
- o Baseplate canted at 45°
- o Coplanar tube exits
- o Tube length to diameter ratio, in outer row, of 4.0
- o C_D = 0.948 and Ae_{18} = 11.482 in^2 (design)
- o A_{18} = 11.437 in^2

A tabulation of the design areas is in Table A-1 of Appendix A. A sketch of the model system showing all related miscellaneous assembly hardware is also included in Appendix A, as well as the hardware detailed drawings.

6.2 STUDY AND DESIGN OF MULTI-CHUTE DUCT SUPPRESSOR SYSTEM

6.2.1 Acoustic/Aerodynamic Review

To effect a well integrated multi-chute duct suppressor design, the acoustic/aerodynamic trade dependencies on the following geometric parameters were considered, based on data from Ref. 8.

o Area Ratio Variation	Figures 6-38 & 6-39
o Element Number Variation	Figures 6-40 & 6-41
o Angle of Attack Variation	Figures 6-42 & 6-43
o Planform Shape Variation	Figures 6-44 & 6-45
o Spoke Versus Chute	Figures 6-46 & 6-47

The first figure of each set includes model photographs and aerodynamic results for static, M_o=0, and wind-on, M_o=.36. The second figure of each set compares 300 & 1500 ft. sideline peak PNL suppressions as a function of jet velocity and the specific geometric parameter under consideration.

ORIGINAL PAGE IS
OF POOR QUALITY

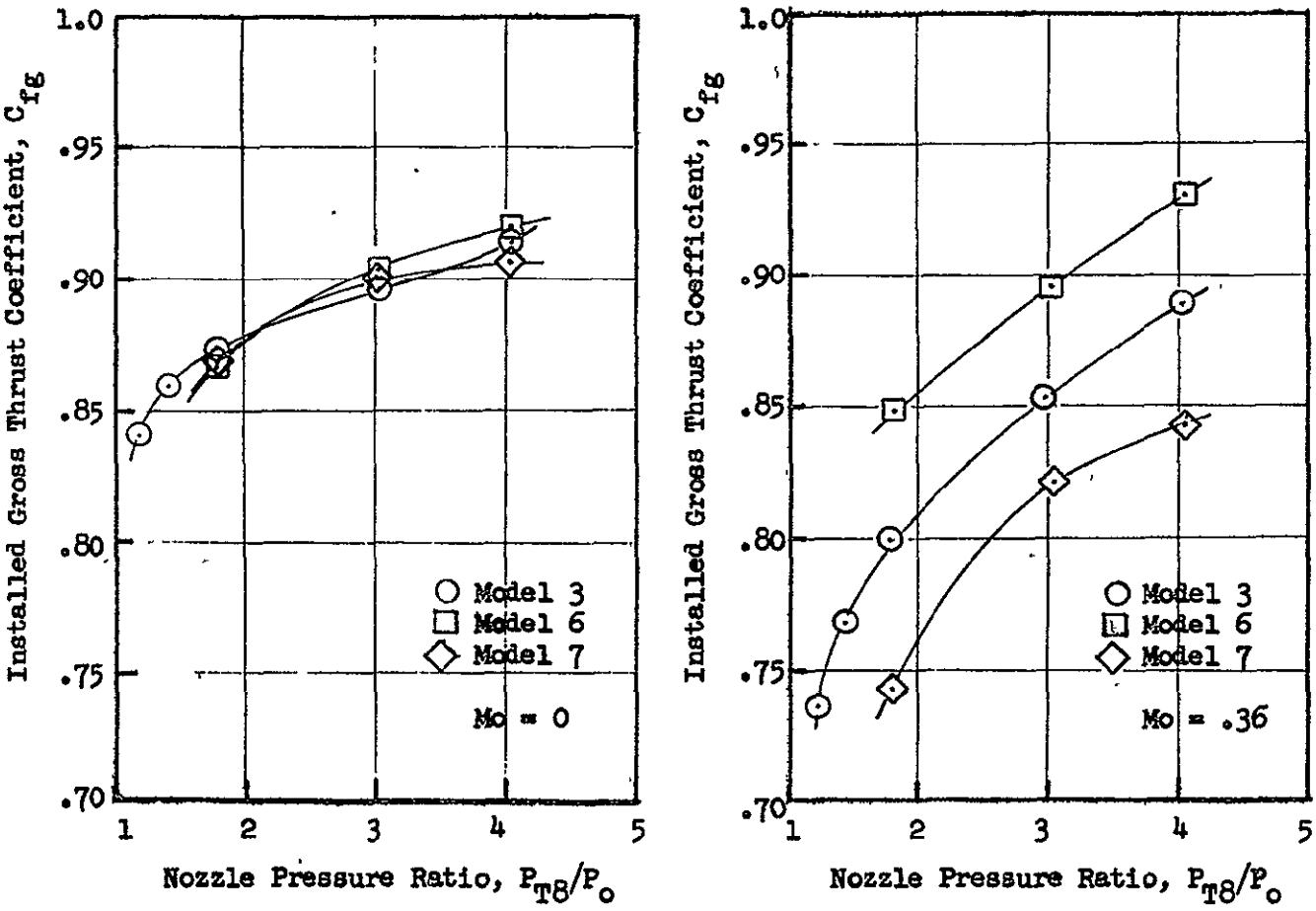

FIGURE 6-38 HARDWARE USED FOR PARAMETRIC INVESTIGATION OF AREA RATIO; AERODYNAMIC TEST RESULTS

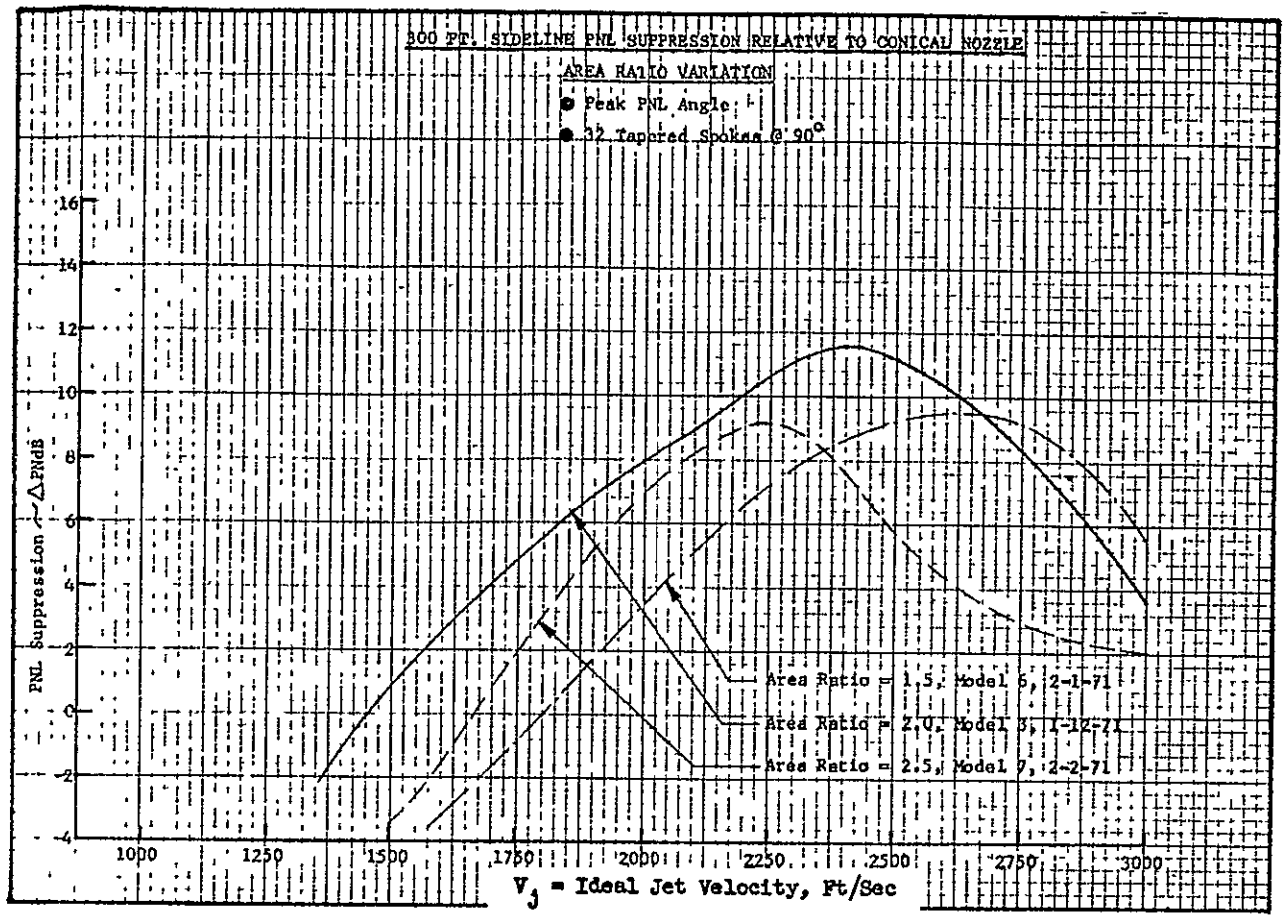

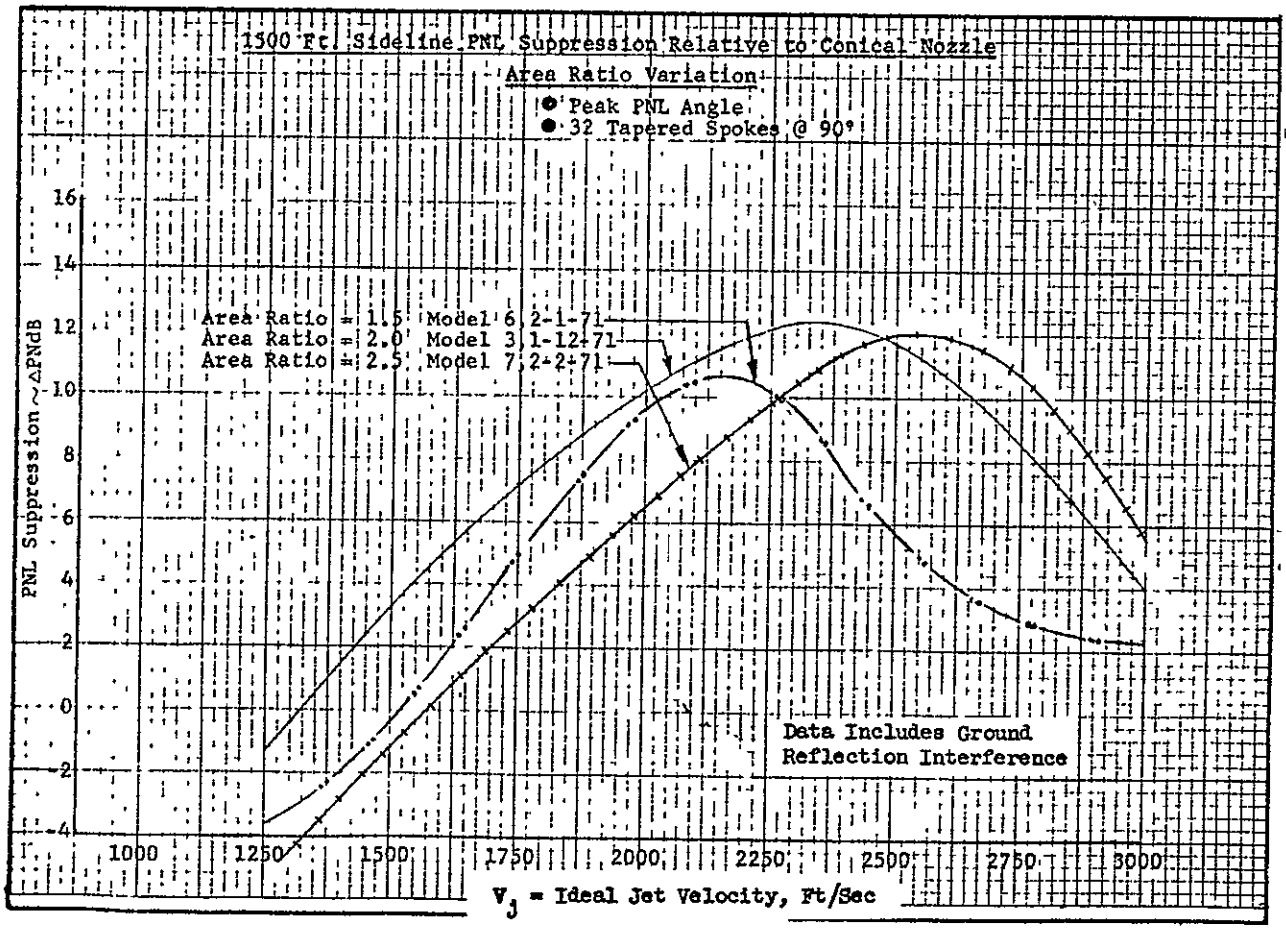

FIGURE 6-39 EFFECT OF AREA RATIO ON 300 FT AND 1500 FT SIDELINE PNL SUPPRESSION FOR PLUG NOZZLE CONFIGURATIONS

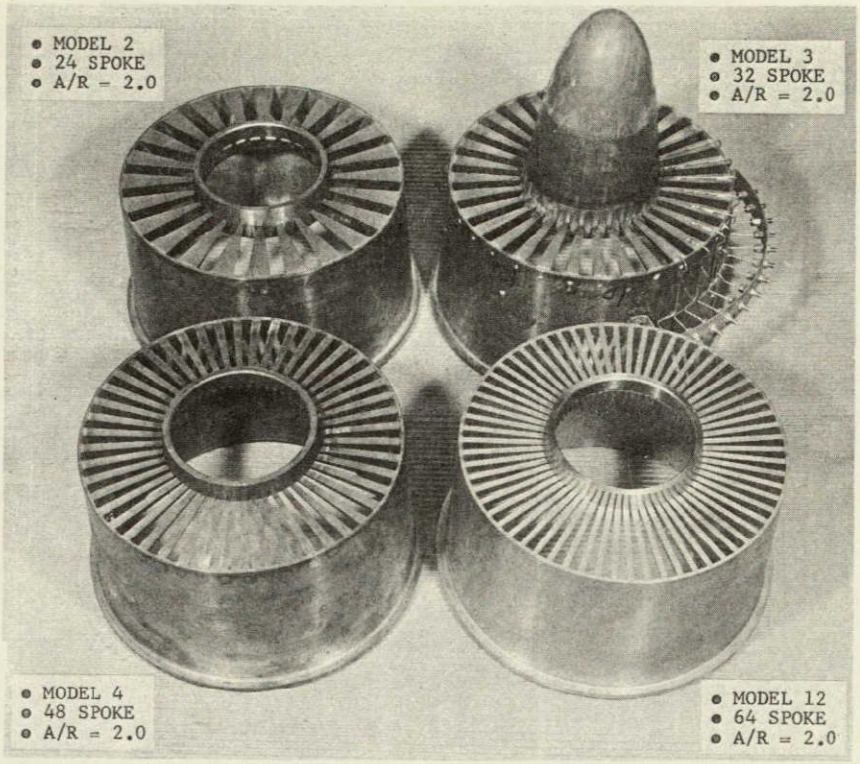

SUPPRESSOR TEST HARDWARE
SPOKE NUMBER VARIATION

ORIGINAL PAGE IS
OF POOR QUALITY

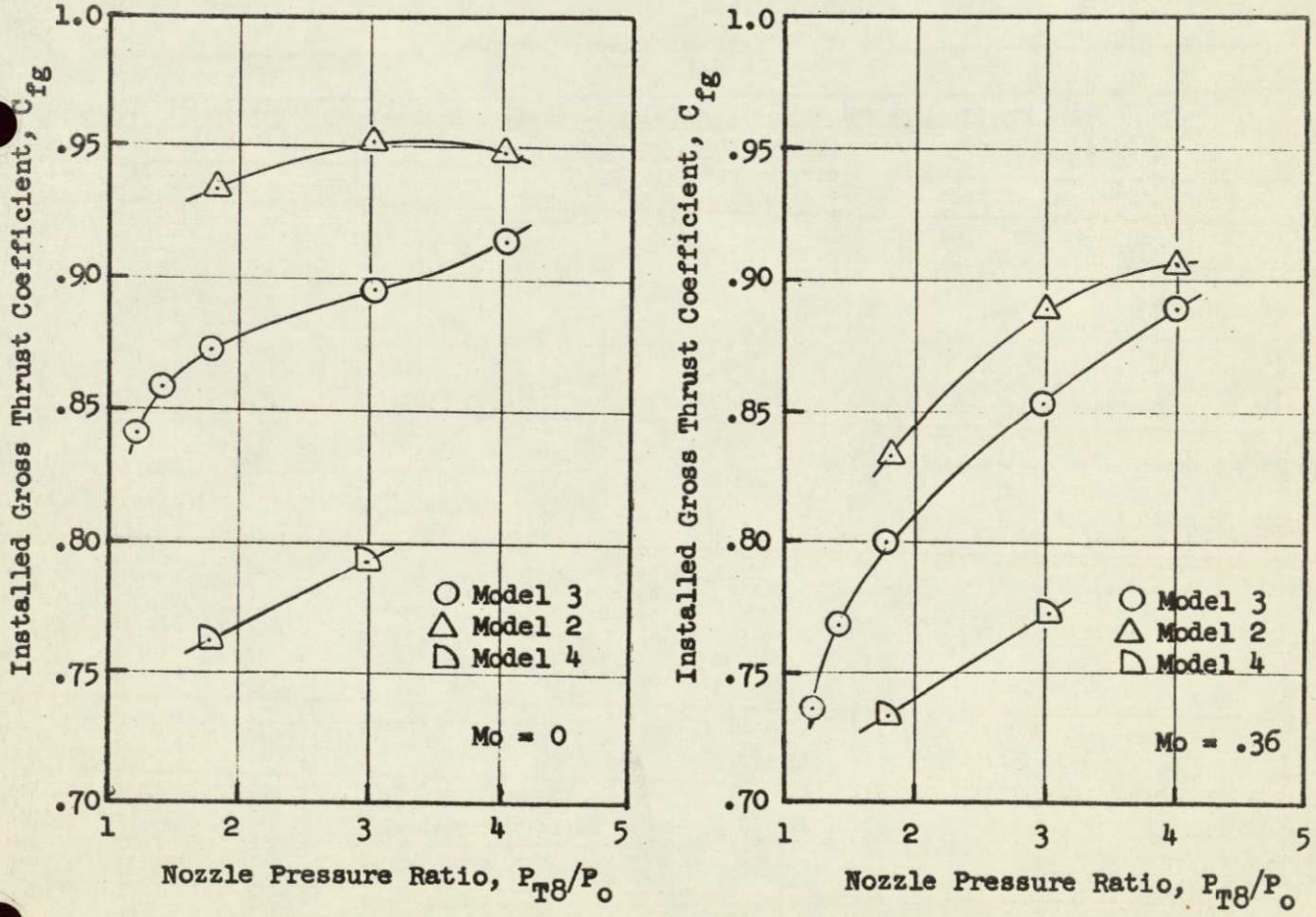

FIGURE 6-40 HARDWARE USED FOR PARAMETRIC INVESTIGATION OF SPOKE NUMBER; AERODYNAMIC TEST RESULTS

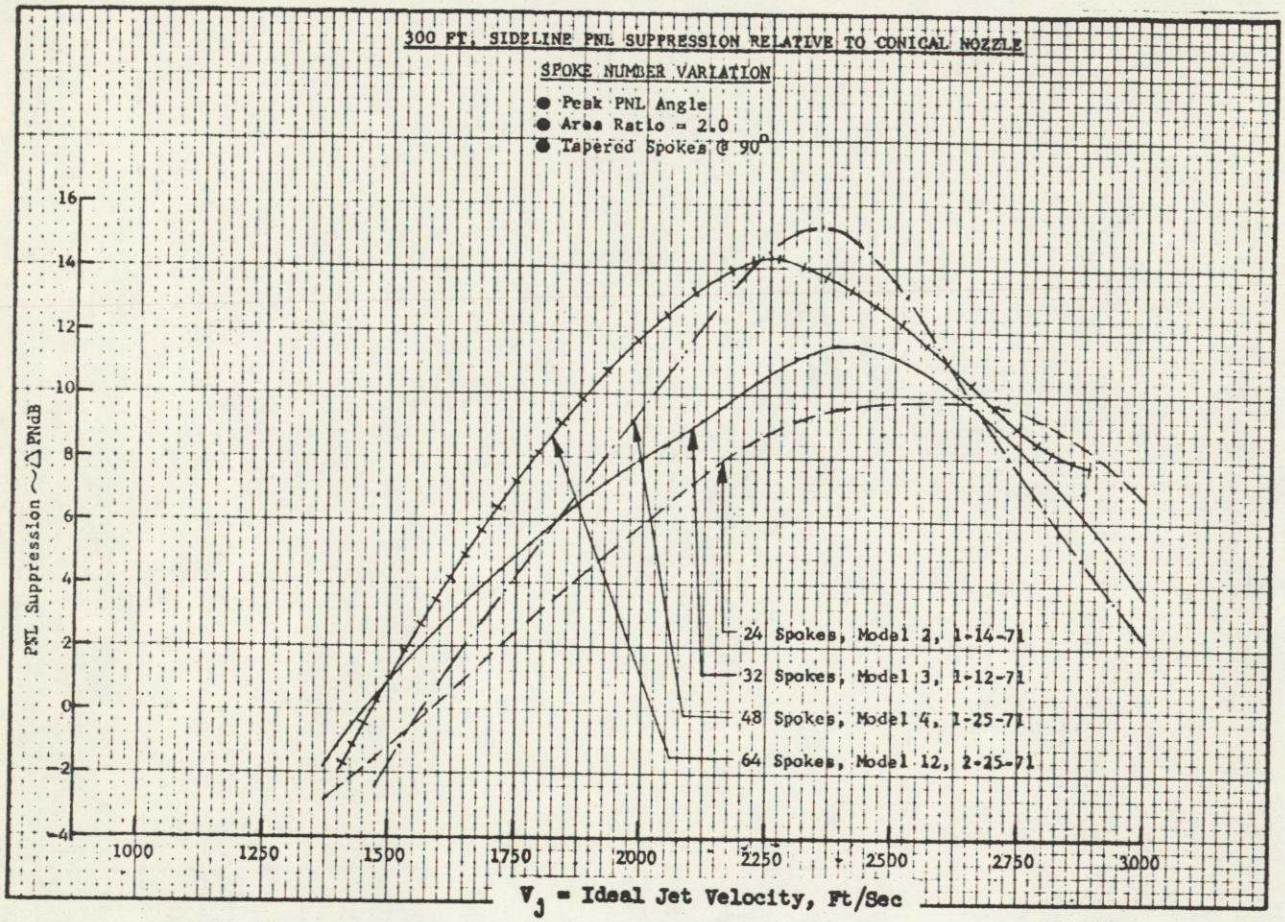

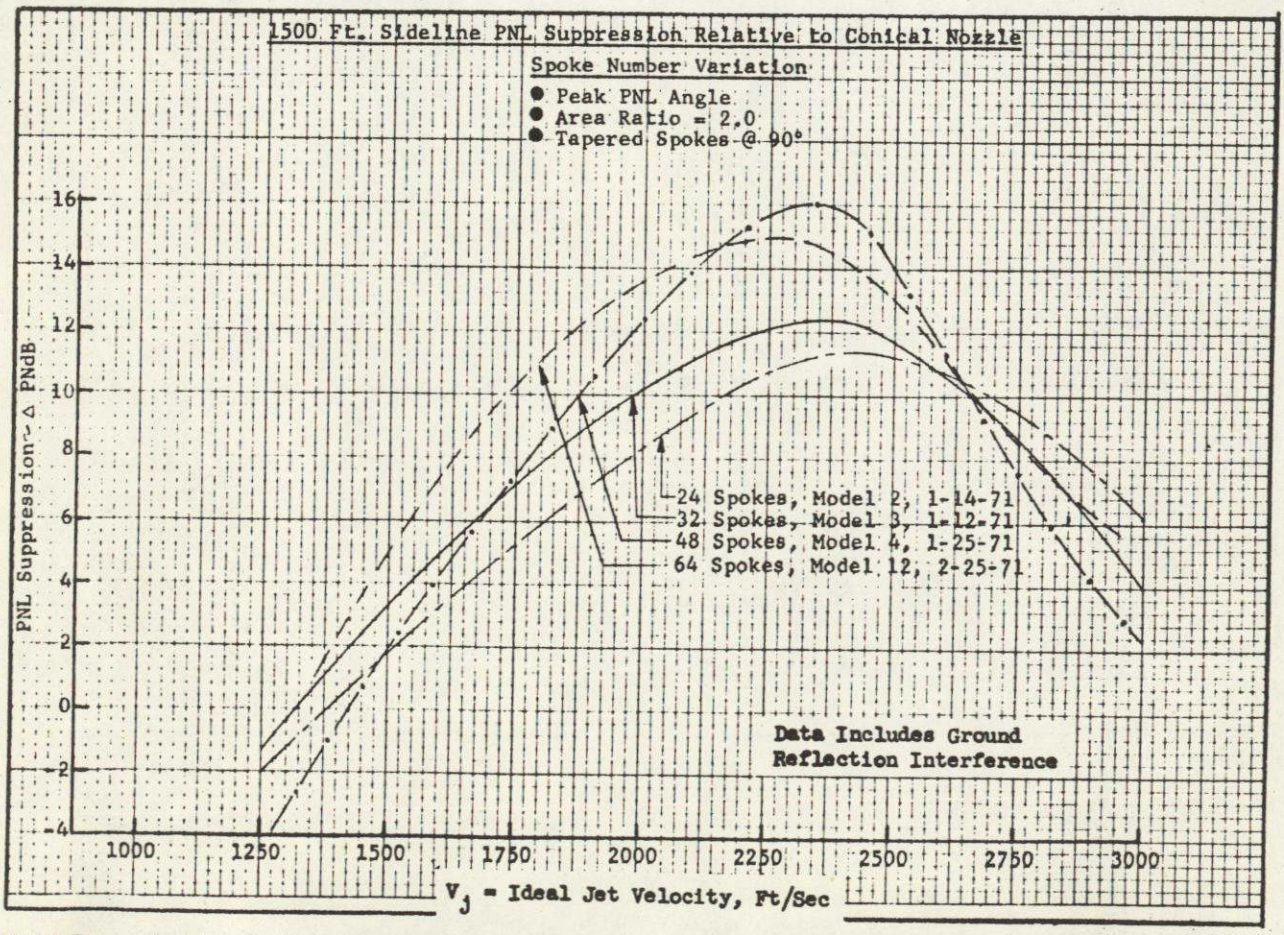

FIGURE 6-41 EFFECT OF SPOKE NUMBER ON 300 FT AND 1500 FT SIDELINE PNL SUPPRESSION FOR PLUG NOZZLE CONFIGURATIONS

ORIGINAL PAGE IS
OF POOR QUALITY

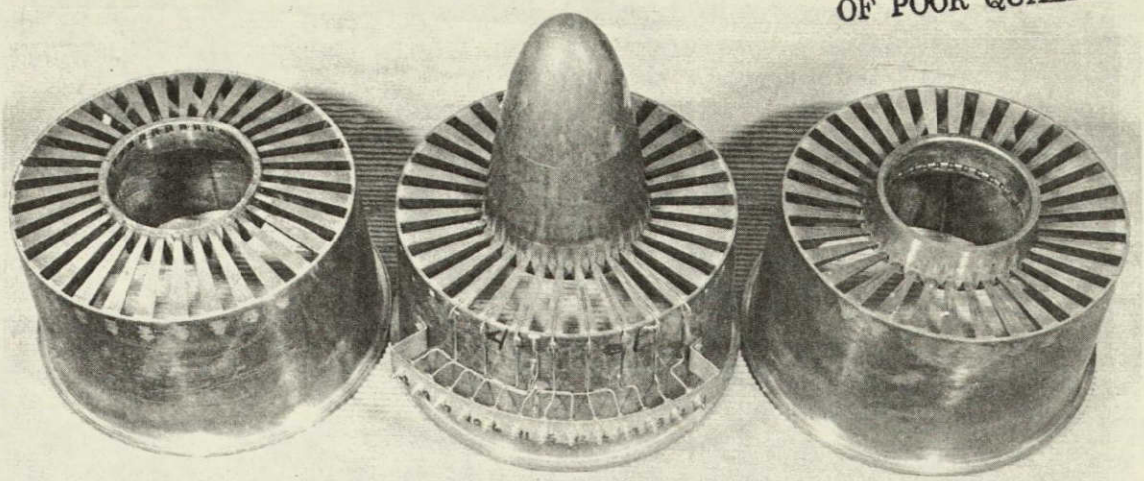

- MODEL 9
- 32 SPOKE
- A/R = 2.0
- 10° AFT

- MODEL 3
- 32 SPOKE
- A/R = 2.0
- AT 90° (Normal to Centerline)

- MODEL 8
- 32 SPOKE
- A/R = 2.0
- 10° FORWARD (Normal to Plug)

SUPPRESSOR TEST HARDWARE
SPOKE ANGLE-OF-ATTACK VARIATION

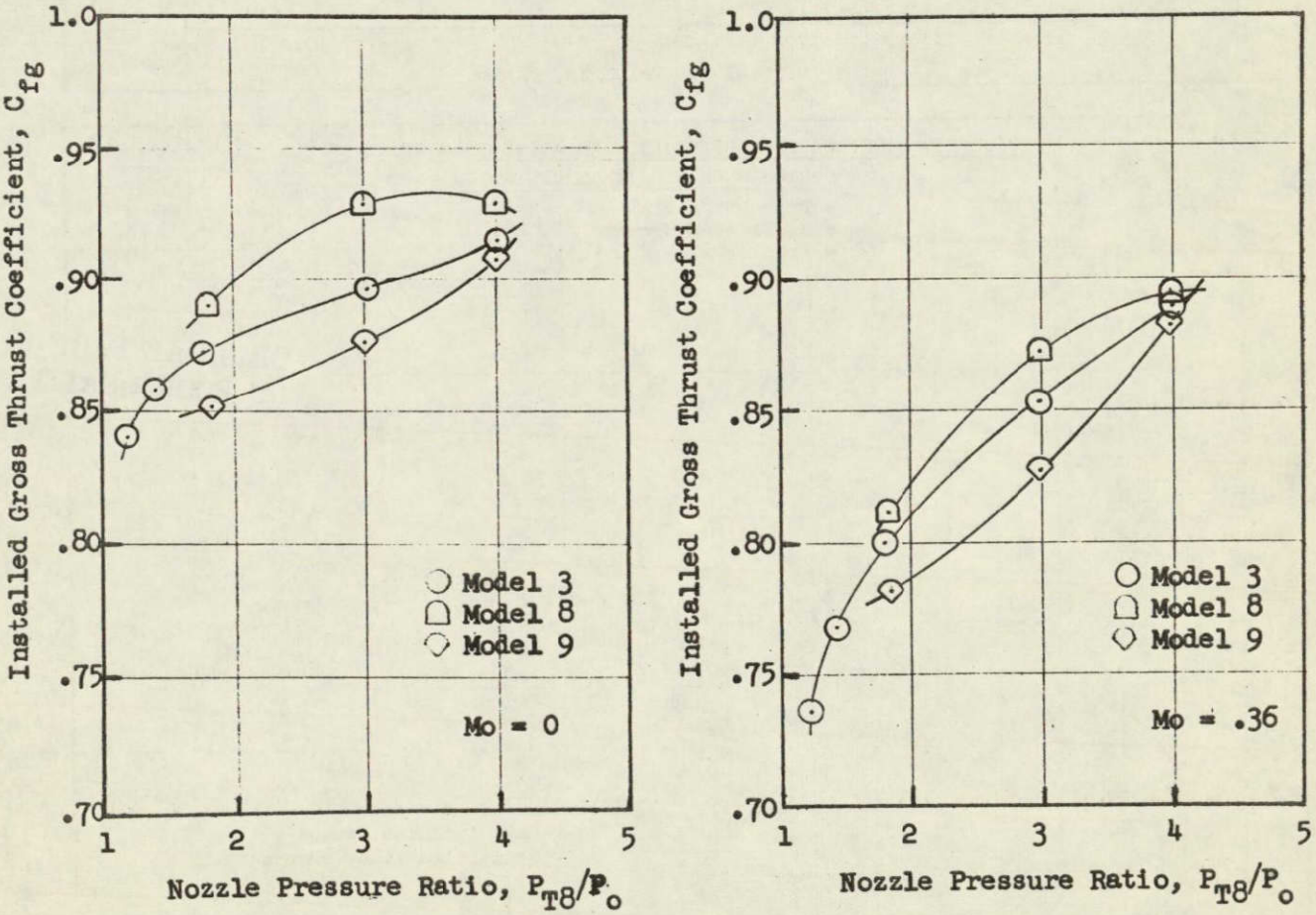

FIGURE 6-42 HARDWARE USED FOR PARAMETRIC INVESTIGATION OF SPOKE ANGLE-OF-ATTACK; AERODYNAMIC TEST RESULTS

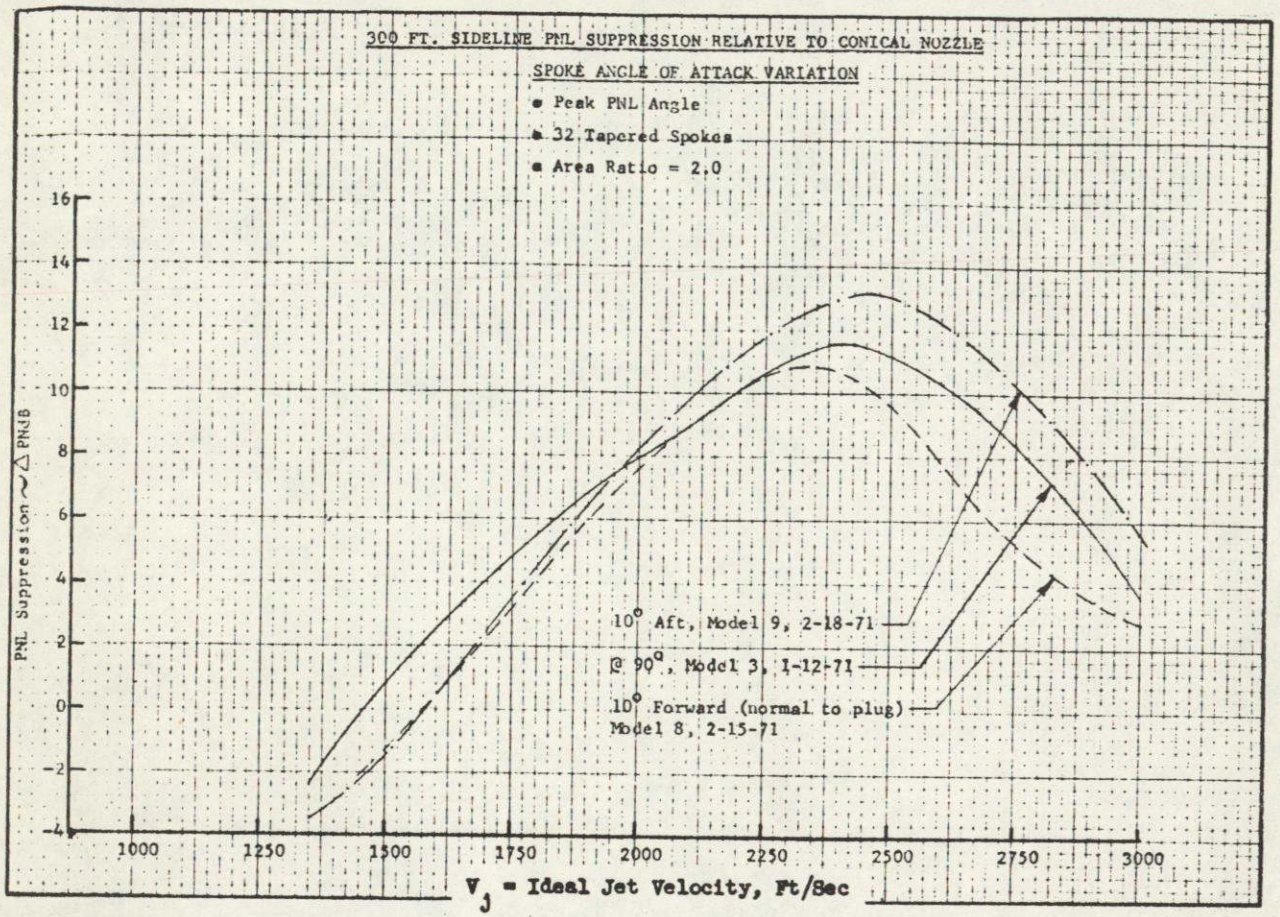

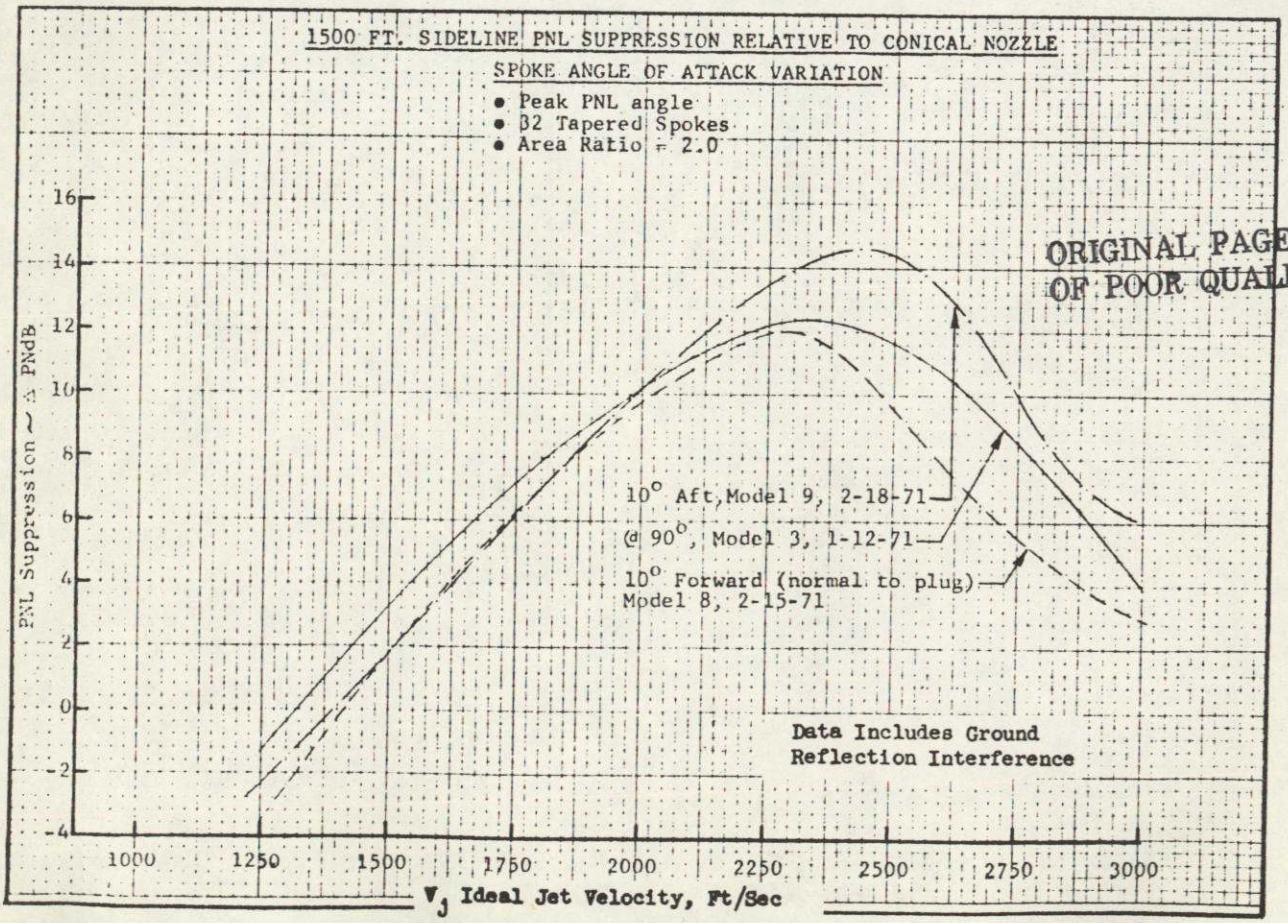

ORIGINAL PAGE IS
OF POOR QUALITY

FIGURE 6-43 EFFECT OF SPOKE ANGLE-OF-ATTACK ON 300 FT AND 1500 FT SIDELINE PNL SUPPRESSION FOR PLUG NOZZLE CONFIGURATIONS

ORIGINAL PAGE IS
OF POOR QUALITY

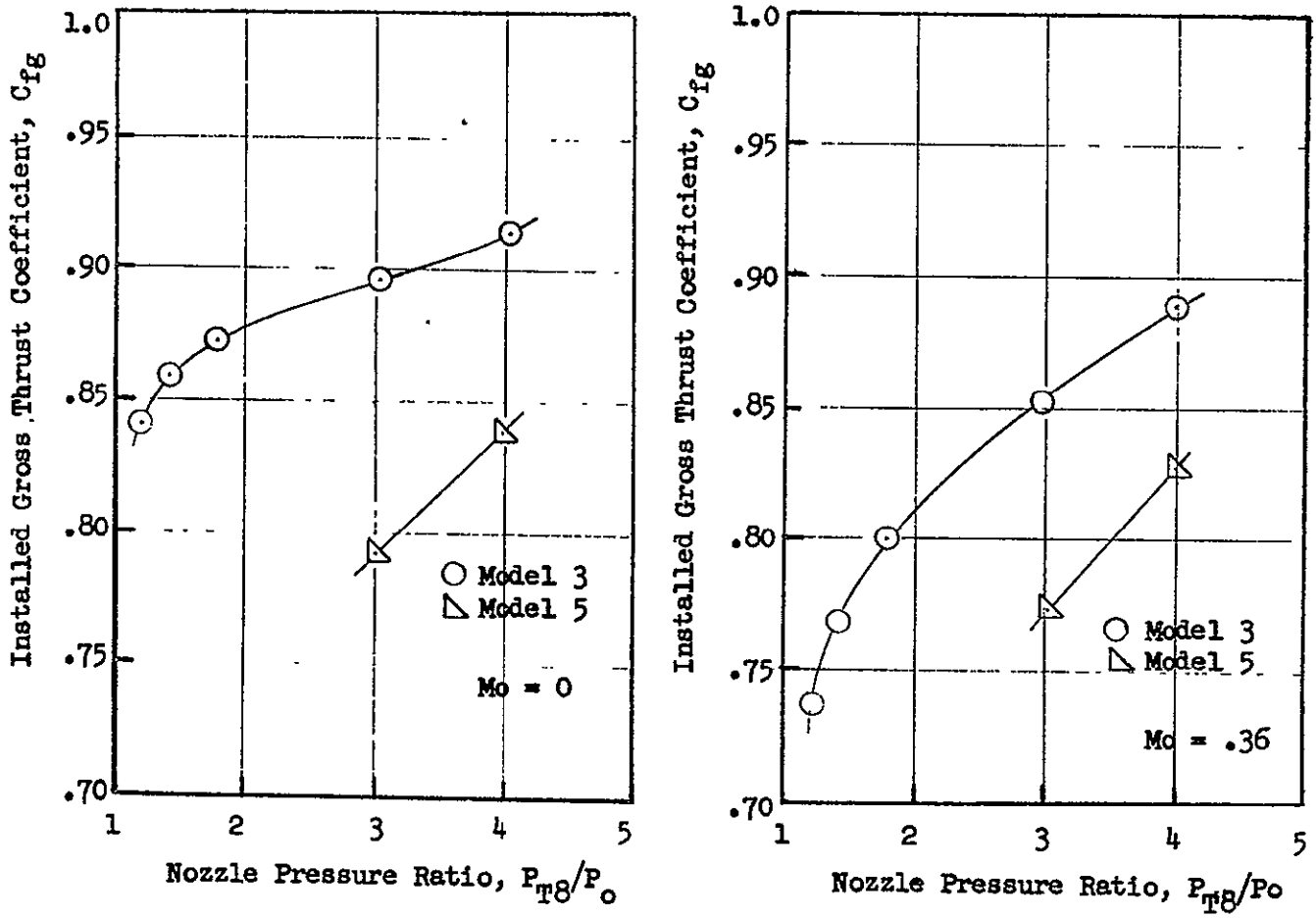

FIGURE 6-44 HARDWARE USED FOR PARAMETRIC INVESTIGATION OF SPOKE PLANFORM; AERODYNAMIC TEST RESULTS

e-y

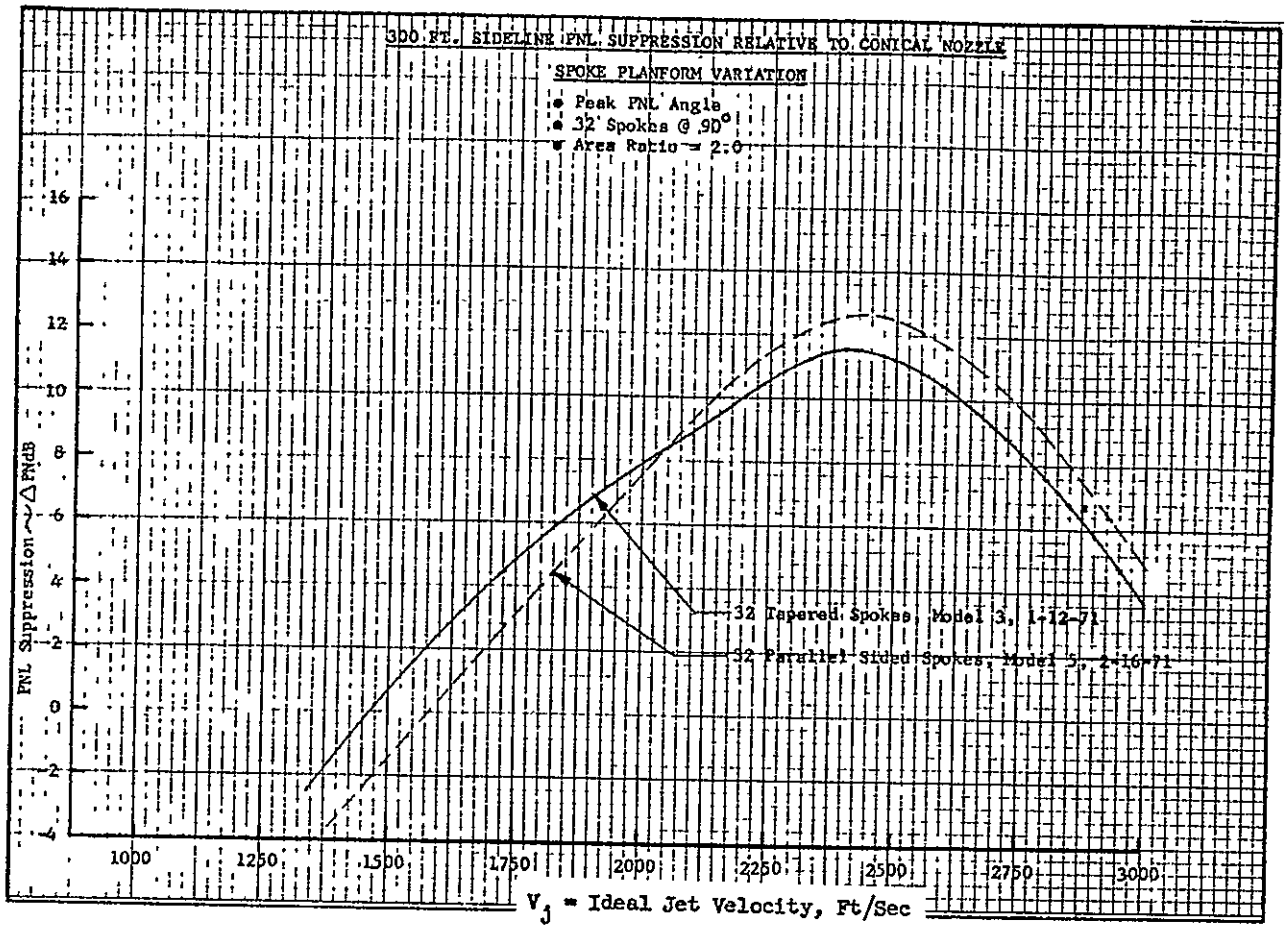

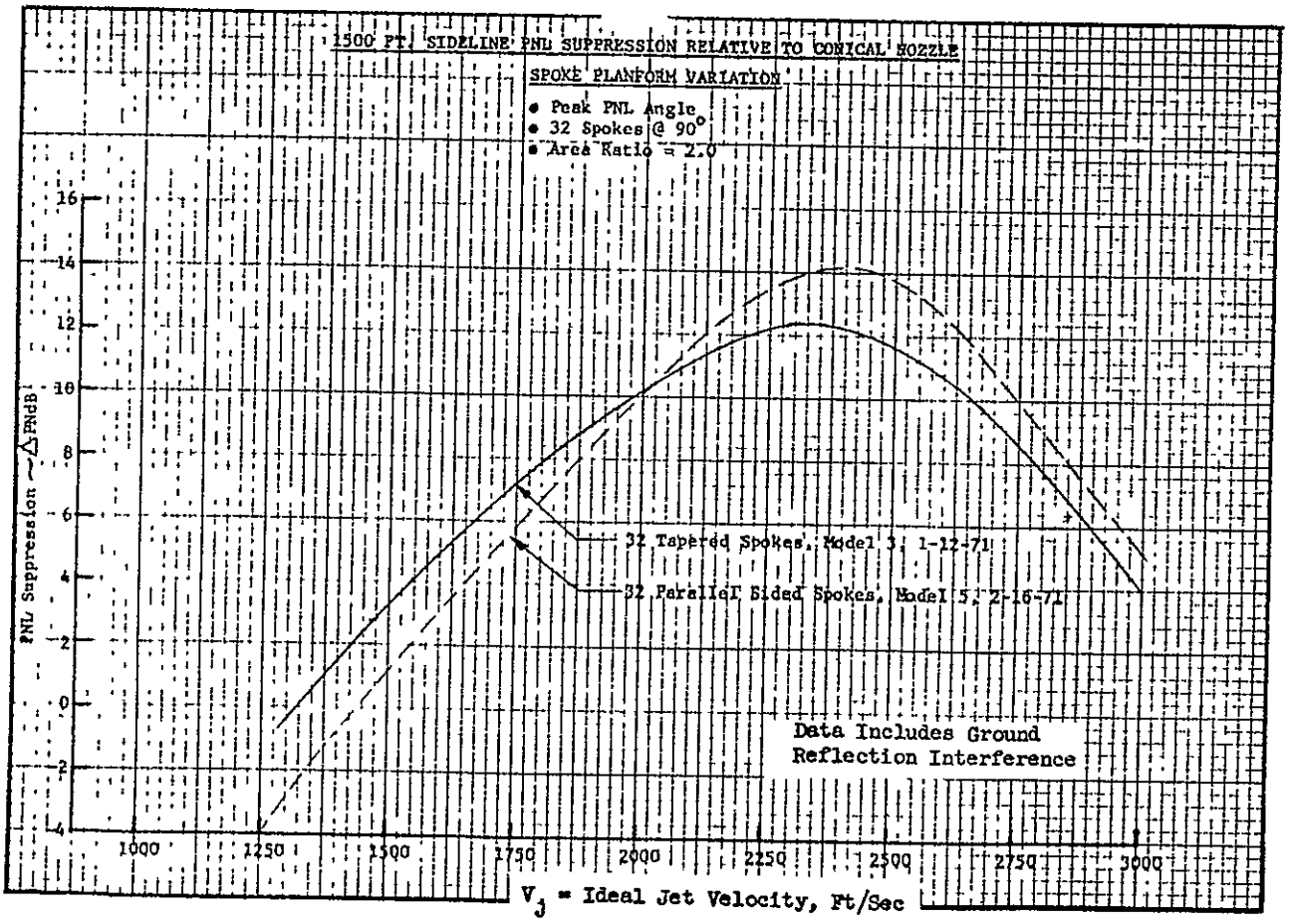

FIGURE 6-45 EFFECT OF SPOKE PLANFORM ON 300 FT AND 1500 FT SIDELINE PNL SUPPRESSION FOR PLUG NOZZLE CONFIGURATIONS

ORIGINAL PAGE IS
OF POOR QUALITY

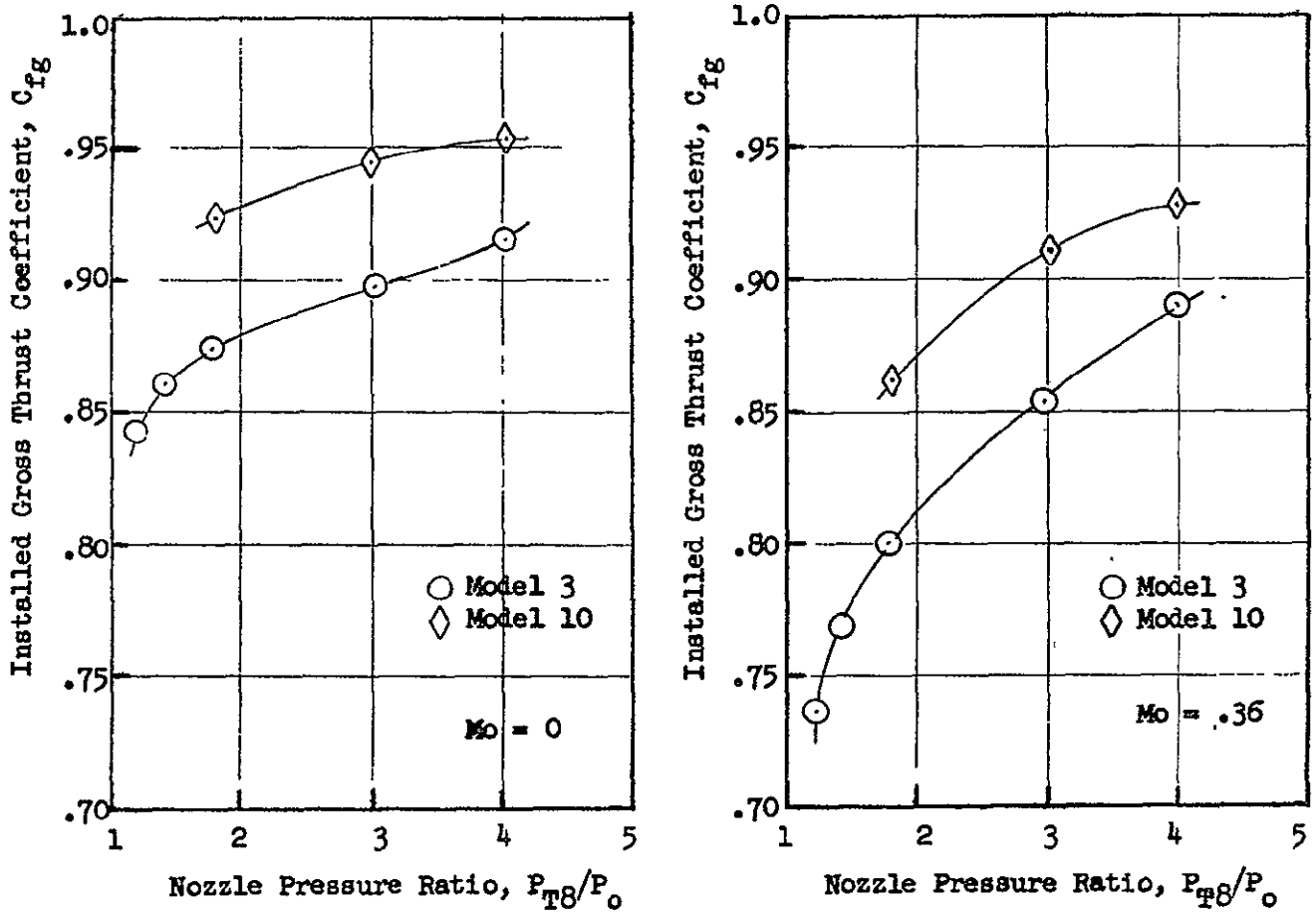

FIGURE 6-46 HARDWARE USED FOR PARAMETRIC INVESTIGATION OF CHUTES VS SPOKES; AERODYNAMIC TEST RESULTS

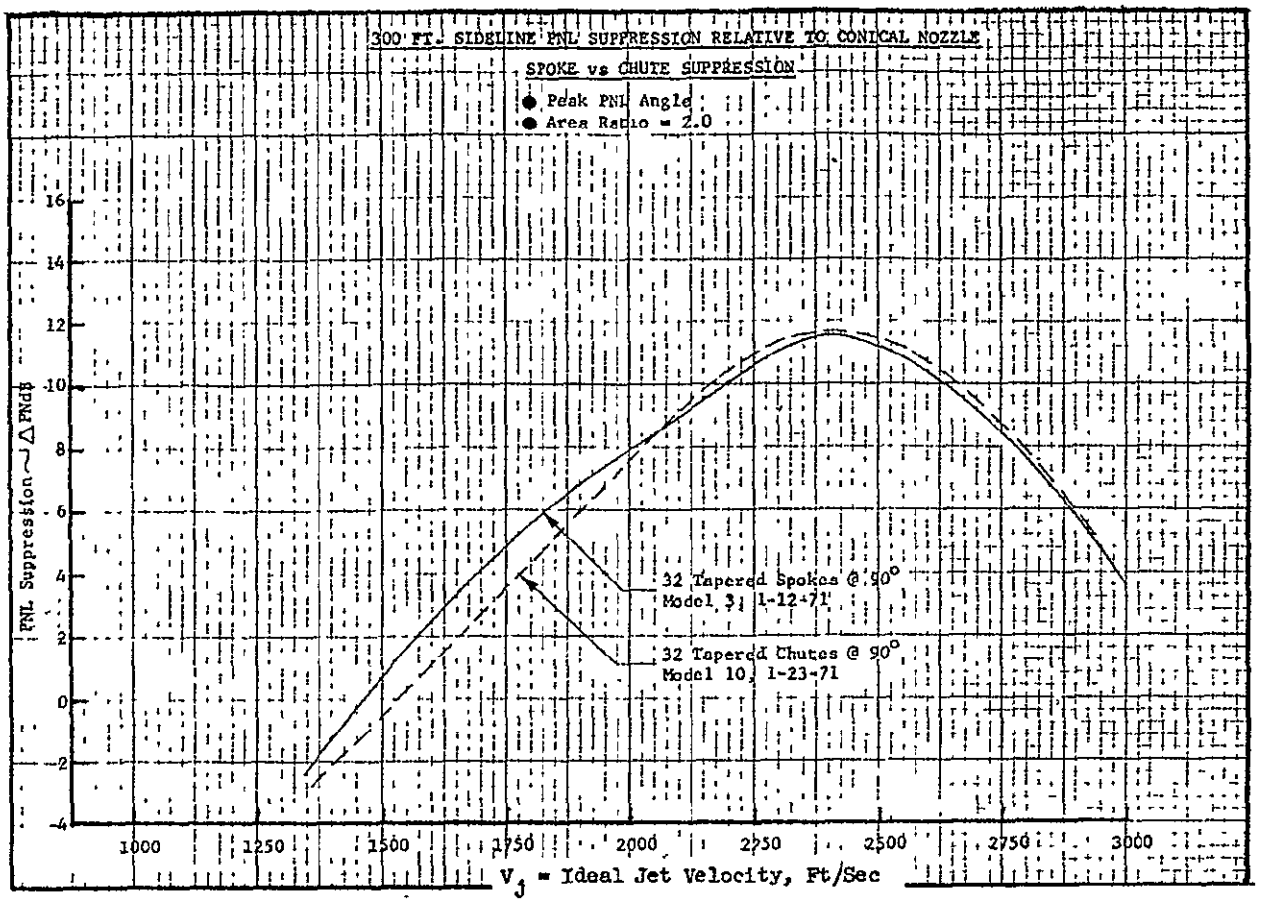

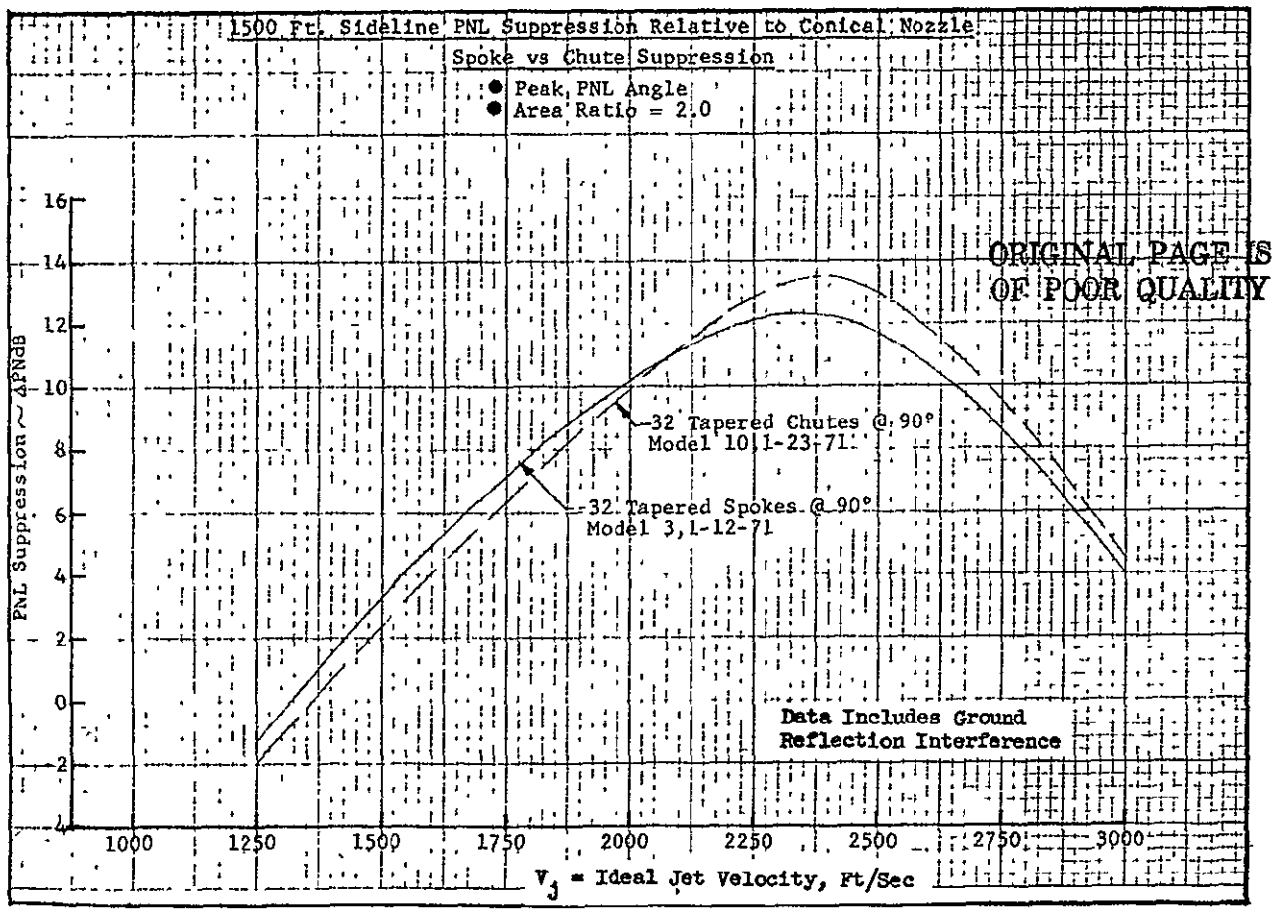

ORIGINAL PAGE IS
OF POOR QUALITY

FIGURE 6-47 EFFECT OF CHUTES VERSUS SPOKES ON 300 FT AND 1500 FT SIDELINE PNL SUPPRESSION FOR PLUG NOZZLE CONFIGURATIONS

1. Area Ratio Variation

The area ratio comparison curves of Figure 6-39 (as well as those of later curves) show that high levels of PNL suppression can be attained through use of multi-element annular plug suppressor systems. The trends at the 300 and 1500 ft. sidelines are similar to those previously measured in multi-tube suppressor tests with the velocity at which peak suppression occurs increasing with higher area ratio. The area ratio of 2.0 model has the best suppression characteristics except at high jet velocities, where area ratio of 2.5 was optimum. The area ratio of 1.5 model gave lower suppression at all velocities. This model, however, had spokes with somewhat less taper than the other models and this may have contributed somewhat to its poorer than anticipated low velocity suppression.

Figure 6-38 presents the static performance (M_o = 0.0) and effect of external Mach number on installed performance, as a function of area ratio and primary nozzle pressure ratio. The results clearly indicate the necessity for simulating the proper external Mach number in order to obtain meaningful aerodynamic performance data. At M_o = 0.36, the increase in area ratio quite rapidly decreased thrust coefficients due to the larger blockage area and longer spokes. The larger and longer spokes allowed for greater base area, particularly near the center of the nozzle, to which ambient air is not pumped for ventilation. The low base pressure on the spokes creates the largest portion of thrust loss in the form of base drag. The low pressure, combined with the larger base area, resulted in significant performance loss with increased area ratio.

2. Element Number Variation

Effect of element number on PNL suppression, Figure 6-41, again shows trends similar to those of the multi-tube test series. Peak suppression increases with greater number of elements, however, at high pressure ratio and velocity the smaller spacing between flow elements, associated with greater element numbers, appears to be acoustically detrimental. This is due to the separate flows coalescing too early at the high pressure ratios, the noise then being dominated by the coalesced jet still at high jet velocity.

Figure 6-40 shows the effect of element number on static and $M_o = 0.36$ performance. Each configuration had the same flow and blockage area. As the number of elements increased the individual element width decreased, lowering pressures on the element base considerably. This results from the flow coalescing in a shorter distance downstream of the base.

3. Angle of Attack Variation

Effect of spoke angle-of-attack variation is shown acoustically in Figure 6-43 and aerodynamically in Figure 6-42. The shift of velocity at which peak suppression occurs suggests a relationship similar to an area ratio effect. Directing the flow down the plug (Model 8 with spokes 10° forward = normal to the 10° half-angle plug) gives peak suppression at low jet velocity. In this case the flow simulates a low area ratio and individual jet streams tend to coalesce close to the nozzle exit plane. Aerodynamic performance with this model is seen to improve over the basic Model 3 nozzle, as directing the flow parallel to the plug surface pressurizes the plug. As the flow angle was increased relative to the plug surface, the static pressures on the plug surface decreased immediately aft of the suppressor throat. The decreased plug pressure was reflected in base pressure on the suppressor elements, resulting in higher base drag and lower performance. The spokes at 90° to the axis (Model 3) and 10° aft (Model 9) simulate an increased aerodynamic area ratio since the flow is initially spreading out from the plug. The highest suppression is thus realized from the 10° aft model.

4. Planform Shape Variation

Results from variation of spoke planform shape, from tapered of Model 3 to parallel-sided of Model 5, are shown as an acoustic comparison in Figure 6-45 and an aerodynamic comparison in Figure 6-44. Parallel-sided spokes gave somewhat greater high velocity PNL suppression than the tapered spokes of the same area ratio. With the tapered spokes the spacing between flow elements close to the plug is smaller, causing the core flow to coalesce quicker at high pressure ratio/jet velocity. Suppression capability is thus lowered. Aerodynamic loss is much higher for the parallel sided spoke due to the greater base area at deeper penetration where base pressures are lower.

5. Spoke Versus Chute

Acoustic comparison of the ventilated chute (Model 10) versus the solid spoke (Model 3) in Figure 6-47 indicates the entrained secondary flow through the open-ended chutes was only slightly beneficial acoustically. Aerodynamically, as seen in Figure 6-46, the chutes are far superior due to higher base pressure and corresponding lower base drag. These trends are similar to those noted for multi-tube suppressors where tube length was investigated. The higher ambient pumping rate through an array of long tubes was only slightly beneficial acoustically but considerably increased base pressures, lowering the accompanying base drag and resultant thrust decrement.

Review of the above test work, during the SST Engine Development, Contract FA-22-67-7, and further multi-spoke/chute test work within the Supersonic Transport Noise Reduction Technology Program Phase II, Contract DOT/FA72WA-2894 (Reference 8 and 14) indicates that the single most important thrust loss mechanism for spoke/chute suppressor nozzles is the pressure drag on the base area within the flow stream. Base pressure on the spokes or chutes, as is the case with multi-tube suppressor systems, is primarily a function of the amount of ventilation area which the spoke or chute has exposed to the ambient air. This ventilation area is determined principally by the suppressor area ratio and shape of the projected (planform) area of the elments, i.e., the circumferential width of the elements at the outer diameter ($W_{O.D.}$). The chutes have a further ventilation area (over the spokes) in the axial depth of the chutes (D). This additional area is exposed to ambient air at the outer diameter and gives the chute system a marked aerodynamic performance advantage over a spoke system of similar planform shape. Pumping of ambient air to fill and pressurize the base area is much easier due to the open flow channel. The chutes base area is also further removed from the main jet flow than that of a spoke, thus, lowering the influence of the low local static pressure caused from the high velocity jet. Properly shaping the chute cross section can place a large percentage of the base area forward of the throat plane away from the influence of this low static pressure region. To exemplify the difference in base pressurization between spokes & chutes, Figure 6-48 presents average base pressure as a function of nozzle pressure ratio for Model 3 & 10 of Figure 6-46. These two suppressor nozzles were identical with the exception

- AREA RATIO 2.0
- 32 ELEMENT SUPPRESSOR
- $M_0 = 0$

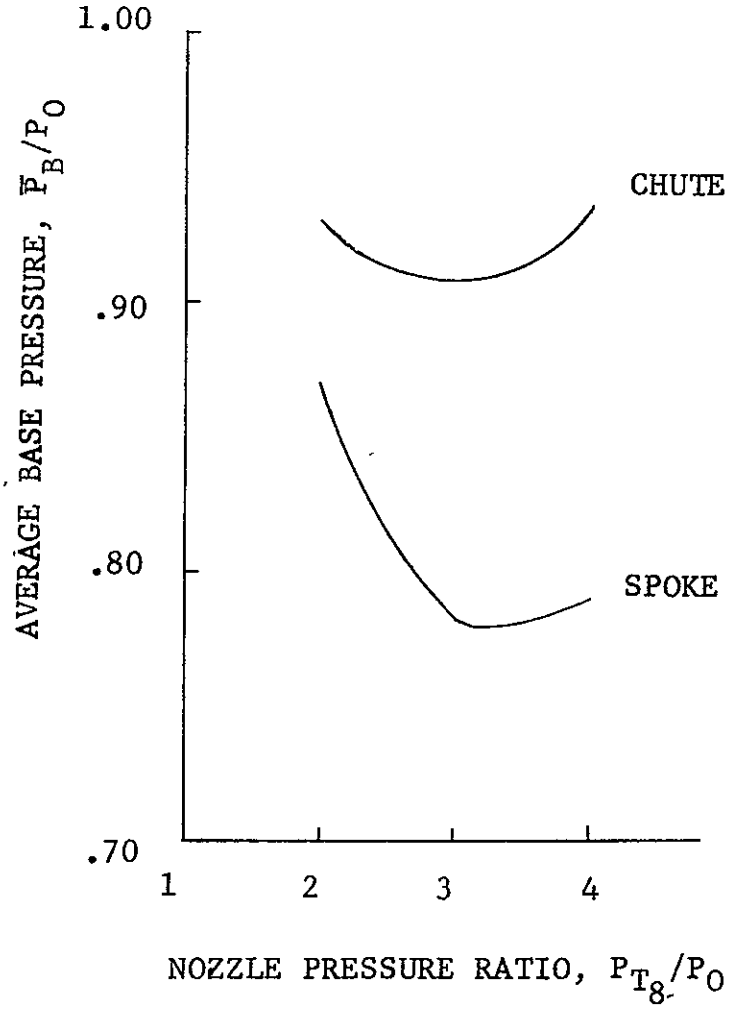

Figure 6-48 MULTI-CHUTE/SPOKE BASE PRESSURE COMPARISON

of the additional axial depth of the chute design. It becomes obvious that base pressurization and resulting base drag is the single most important thrust loss mechanism for the spoke/chute suppressor systems. As a result, the application of chutes over spokes would definitely be preferred as long as mechanical problems related to stowage in the unsuppressed mode can be overcome in a specific engine design. For the DBTF study the chute system has therefore been chosen. Section 4.0 - SYSTEM CONCEPT SECTION discusses typical schemes of chute system application to engine nozzle concepts, including the DBTF with suppressed duct stream.

6.2.2 Aerodynamic Correlation

To further investigate the influence of chute suppressor geometric parameters on base pressure and gross thrust coefficient, four single-flow multi-chute configurations tested by GE were analyzed. These were:

- 32 chute, A/R=2.0, tapered chute planform, chute exit plane perpendicular to plug centerline, 20° plug, per Figure 6-46. (Reference 8)
- 32 chutes, A/R=1.69, tapered chute planform, chute exit plane 15° foward of perpendicular to plug centerline, 30° plug. (Reference 8)
- 24 chutes, A/R=1.69, tapered chute planform, chute exit plane 15° forward of perpendicular to plug centerline, 30° plug. (Reference 8)
- 40 deep chute, A/R=2.0, near parallel chute planform, chute exit plane $\pm$ 15° to perpendicular to plug centerline, 30° plug (Reference 11, 14 and 15)

An attempt to correlate the integrated average base pressure from test data obtained on the four configurations resulted in the ventilation parameter defined in Figure 6-49. The correlation shows that to attain high base pressure, and subsequent good aerodynamic performance, the following criteria should be followed.

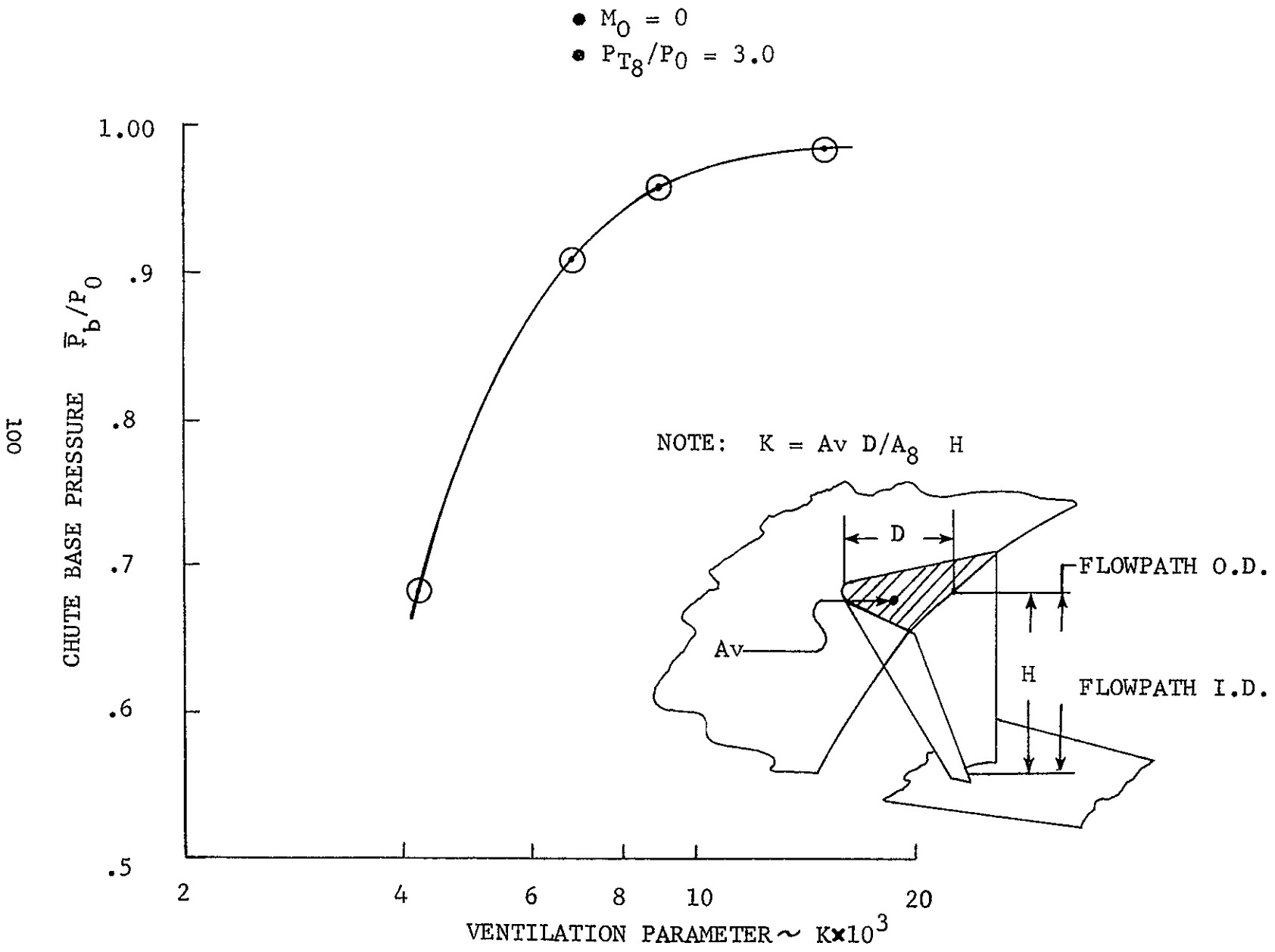

Figure 6-49 CHUTE BASE PRESSURE CORRELATION

1. The ventilating area (Av) at the flowpath O.D. should be as high as possible, attained by making the chutes wide at the O.D. as compared to the I.D. and by using a large radius at the leading edge resulting in a more rectangular shaped cross section than that suggested by the sketch of Figure 6-49.

2. The chute cross section at the flowpath O.D. should be as deep as possible (dimension D) to remove the base area from the high velocity low static pressure area near the throat plane.

3. The chute height (H) should be shallow to well ventilate as much of the base area as possible before the pumped flow turns and is expended into the main jet.

The correlation of Figure 6-49 was then used as the basis of forming design curves for the DBTF multi-chute duct suppressor. Parametric variations were made of area ratio, chute number, chute depth and chute width at the flowpath O.D. Their effects on base pressure drag were studied, resulting in the Figure 6-50 correlation of gross thrust coefficient as a function of chute width ratio, area ratio, chute number and chute depth to height ratio. This is not a general correlation but particular to the DBTF suppressed duct application where duct height at the exit plane was determined by the pre-selected duct plug flowpath and subsequent area ratio variation. This aerodynamic performance correlation then supplemented the acoustic trade data in establishing the final design.

6.2.3 Selection of Multi-Chute Duct Suppressor Design

Based on the Acoustic/Aerodynamic Review and Aerodynamic Correlation (Sections 6.2.1 & 6.2.2), guidelines for design of the multi-chute duct suppressor at the selected duct ideal jet velocity of 2415 ft/sec are summarized as follows:

1. Chutes seem to perform slightly better acoustically than spokes, attaining approximately 1 Δ PNdB greater suppression at the 1500 ft. sideline. Choice of chutes over spokes, however, precipitates more from consideration of aerodynamic performance where chutes

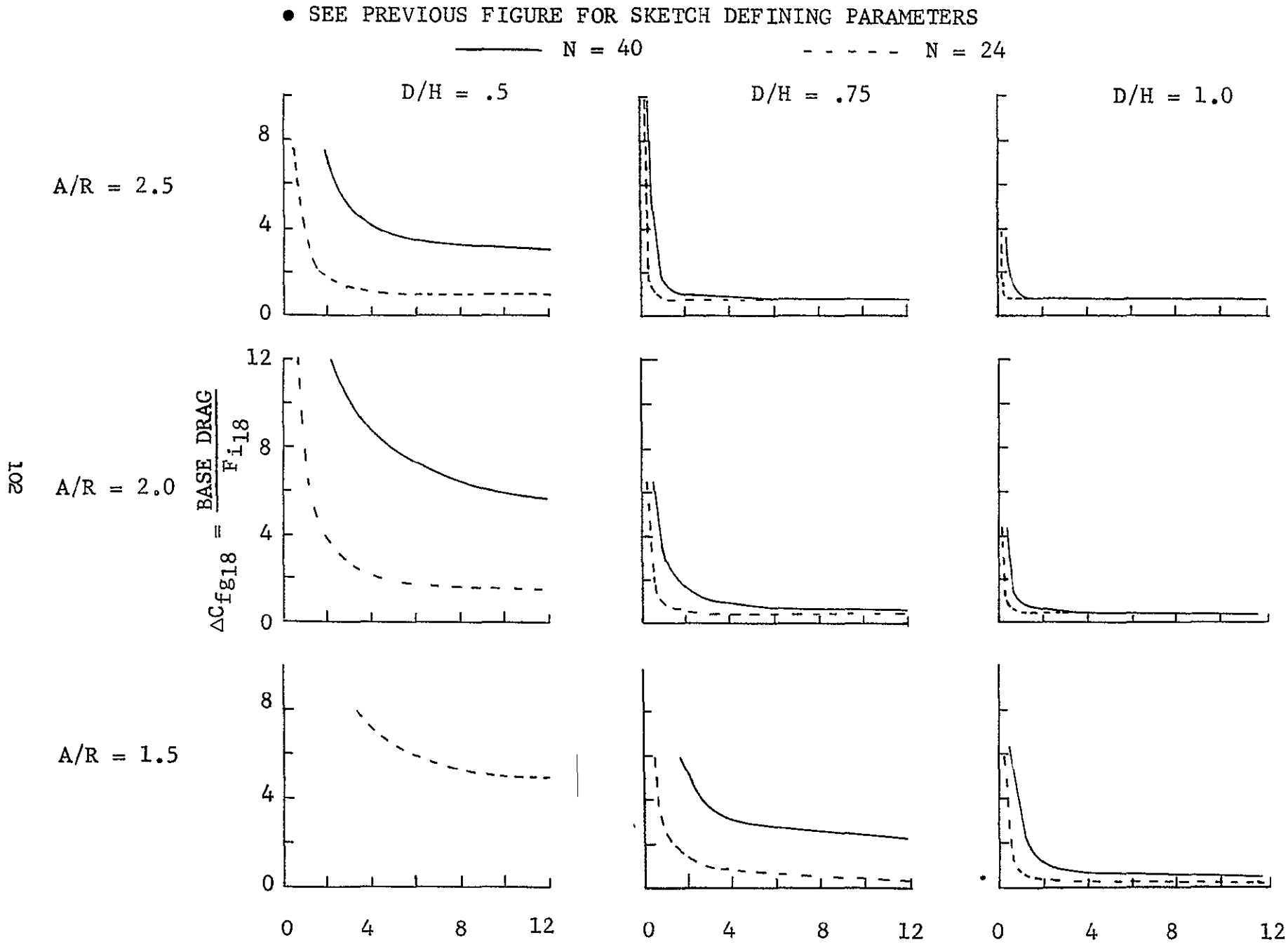

Figure 6-50 CHUTE BASE DRAG PARAMETRIC STUDY

have substantially higher performance. For a viable engine nozzle design, mechanical feasability of stowage during the unsuppressed mode is a further important consideration before selecting chutes over spokes.

2. For consideration of area ratio, the higher A/R (2.0 to 2.5 compared to 1.5) is acoustically beneficial, however, at the design point the trade between A/R = 2.0 & 2.5 is not distinctly discernable. Again, as with the multi-tube suppressor, if the optimum study design is considered as the acoustically treated ejector/duct suppressor system, the area ratio should be chosen to generate more high frequency noise than that optimum for an unejected design. The chute nozzle area ratio influence on generation of noise spectra is similar to that of tube nozzles in that the higher the area ratio, the lower the low frequency noise levels and the higher the high frequency noise levels generated. The high frequency noise generation location is close to the nozzle exit plane. An acoustically treated ejector has the potential of reducing the penalizing high frequency noise so that, together with the low frequency noise reduction achieved by the higher area ratio, greater overall suppression of PNL should result. Aerodynamically, high area ratio betters chute nozzle performance at low values of chute depth to height (D/H) ratio. At high D/H values (near 1.0) aerodynamic performance is fairly insensitive to area ratio.

3. For acoustic performance a reasonably high chute number (32 to 40) should be chosen at the design velocity of 2415 ft/sec. Very fine flow segmentation (48 to 64 spokes) did not increase suppression significantly. As with area ratio, the higher number of chutes performs superior aerodynamically for the low D/H ratios. At high D/H values (near 1.0) aerodynamic performance is fairly insensitive to chute number as long as chute width ratio is reasonable ($\geq$ 1.5).

4. As with the multi-tube designs, slanting the chute exit plane so that flow vectors outward would simulate a higher aerodynamic area ratio and result in better suppression but would probably cause flow impingement on the secondary ejector and resultant thrust loss. Slanting the chute exit plane inward so that flow vectors along the angled plug surface would normally pressurize the plug surface, resulting in higher performance, but acoustic suppression decreases due to individual jet flows merging too soon, before velocity is substantially decayed. For the DBTF suppressed duct case, the flow will be exiting the chutes on a near flat flowpath, therefore no aerodynamic benefit could be expected by inward slanting. The chutes should thus be designed with a coplanar exit plane, perpendicular to the nozzle centerline.

5. For good acoustic suppression, chute exit plane planform should be such to allow a high percentage of jet flow near the outer diameter of the annulus, as long as reasonable separation between individual jets is maintained at both the I.D. and O.D. of the annulus. Thus, the parallel sided spokes performed superior acoustically, as a greater percentage of flow area was near the annulus O.D. (See Figure 6-44). The tapered spokes allowed a more even radial flow distribution but with minimal separation between individual jets near the annulus I.D. This allowed flow coalescence before velocity was significantly decayed; therefore, loss of suppression potential.

   As seen in the aerodynamic correlation, low values of planform ratio (designated as width of chute at O.D. to width at I.D.) highly influenced aerodynamic performance. Width ratios of less than 1.0, where O.D. width is less than I.D. width, have very high thrust loss. The major base area is starved of flow from the ambient surroundings, the flow being required for pressurization.

   Both acoustic and aerodynamic performance are thus seen to be quite sensitive to planform shape. For the DBTF multi-chute suppressor, parameters other than planform should be selected, if feasible, within the range where planform becomes as least sensitive as possible.

Again from the aerodynamic correlation of Figure 6-50, this region is where area ratio and chute depth to height ratio are high, (A/R=2.5), (D/H=1.0). Parallel sided chutes ($W_{O.D.}/W_{I.D.}$ = 1.0) would be a reasonable choice within this region. However, as the correlation is not totally data substantiated, a more safe selection, past the knee of the curves, would be wiser, between $W_{O.D.}/W_{I.D.}$ of 1.0 and 2.0. Selection of chute number in this region can be done strictly for acoustic suppression as the aerodynamic correlation shows no distinction from 24 to 40 chutes.

For the specific DBTF multi-chute design the annulus I.D. was pre-fixed, based on the maximum fan plug flap travel designed into the engine nozzle system, (see Figure 5-1 of Section 5.1) linearly scaled to model size. The annulus O.D. was allowed to grow to that required to accommodate the physical area associated with the selected area ratio of 2.5. Area ratio for the chute suppressor system is defined as the ratio of total annulus area to physical flow area (A/R=Annulus Area/No. Chutes x Physical Area per Chute). To determine the annulus area requirement, a discharge coefficient, C_{D18}=.975, was chosen based on averaging the C_D's of the four previous chute test configurations (discussed in Section 6.2.2) at the takeoff design P_{T18}/P_o = 2.66. Use of this C_{D18} and the Ae_{18} of 10.842 in^2 (See Table A-1 of Appendix A) yielded an A_{18} of 11.120 in^2. Based on the area ratio definition, this A_{18} and annulus I.D. were used to establish the throat annulus O.D.

Using the above annulus physical geometry and the acoustic/aerodynamic guidelines, a series of multi-chute annular arrays were designed within the limits of a) 32 to 48 chutes, b) parallel sided chutes where $W_{I.D.}/W_{O.D.}$ = 1.0, c) radially tapered chutes where $W_{I.D.}/W_{O.D.}$ = 1.28, and d) varying chute taper in the range of $1.5 \leq W_{O.D.}/W_{I.D.} \leq 3.0$. Final suppressor selection from the various chute patterns designed was based on a weighted averaging of the parameters most influencing acoustic and aerodynamic performance, consistent with the previously detailed conclusions. The final selection is shown schematically in Figure 6-51 and has the following features.

- AREA RATIO = 2.5
- 36 CHUTES
- COPLANAR CHUTE EXITS
- RADIAL CHUTE PLANFORM

- A_{18} = 11.120 in.^{2}
- C_{D18} = .975
- A_{e18} = 10.842 in.^{2}

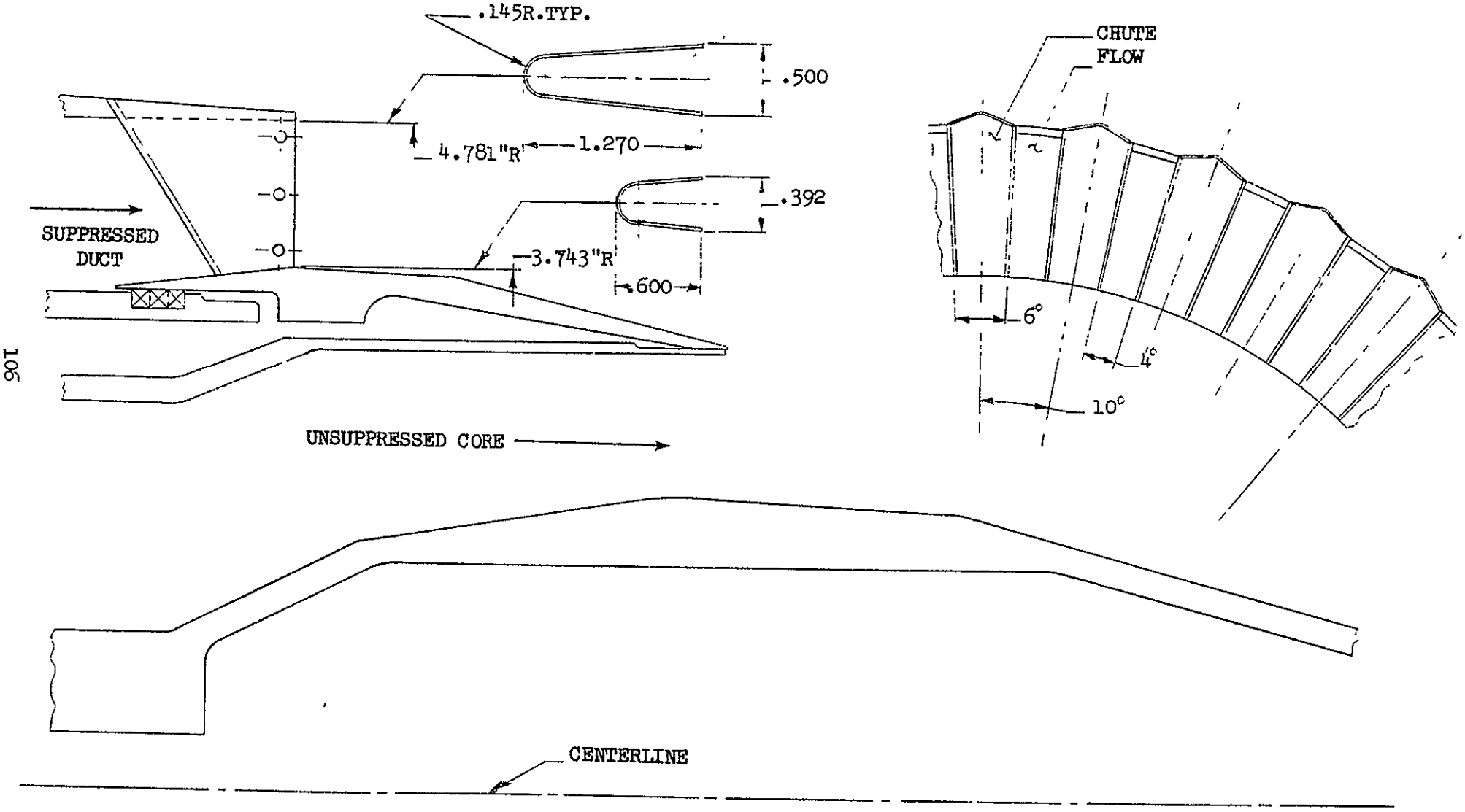

Figure 6-51 DBTF SCALE MODEL MULTI-CHUTE DUCT SUPPRESSOR

- Area Ratio = 2.5
- 36 Chutes equally spaced each 10°
- Radial chute planform at exit plane, $W_{O.D.}/W_{I.D.} = 1.28$
- Coplanar (flat) chute exit plane
- Approx. 30% area convergence from leading edge of chute at tangent point to nozzle throat plane.
- $C_{D18} = .975$
- $Ae_{18} = 10.842\ in^2$ (design)
- $Ae_{18} = 11.120\ in^2$

A tabulation of the design areas is in Table A-1 of Appendix A. A sketch of the model system showing all related miscellaneous hardware is also included in Appendix A, as well as the hardware detailed drawings.

ORIGINAL PAGE IS
OF POOR QUALITY

SECTION 7.0

EJECTORS -- HARDWALL AND ACOUSTICALLY TREATED

7.1 HARDWALL EJECTOR DESIGN

Available aerodynamics data on multi-element jet noise suppressors with secondary ejector shrouds are limited to several multi-tube, full baseplate (i.e., no plug) configurations tested by General Electric (Reference 8) and to a large number of configurations of the same general suppressor type tested by the Boeing Company (Reference 9). These test results were used, in conjunction with standard conical nozzle/ejector shroud data (References 16, 17 and 18), to develop the aerodynamic flowpath of the ejector shrouds for the subject DBTF test hardware.

The primary design consideration for the suppressor/ejector system was to provide sufficient inlet area for the ambient air entering the ejector. Insufficient inlet area results in a pump-down of base pressure on the suppressor elements or baseplate and a corresponding severe thrust loss. The previous test data indicates that the necessary inlet area may be provided by proper radial and axial placement of the ejector inlet lip. This is shown conceptually in Figure 7-1 where radial spacing is defined in terms of diameter ratio (D_{ej}/D_p) and axial spacing is defined in terms of S/D_p. Figure 7-1 also shows aerodynamic static performance results from Boeing test work (Reference 9) in terms of gross thrust coefficient versus primary nozzle pressure ratio. The primary nozzle had 31 tubes within an aera ratio of 2.5 array. Ejector radial and axial spacing geometry was varied to establish the performance changes from S/D_p of 0.0 to .125 and D_{ej}/D_p from 1.0 to 1.11. An additional data point from a General Electric test, using a 36 chute/plug nozzle and ejector system resulting with $D_{ej}/D_p = 1.0$ and $S/D_p = .061$, is also included. It is the only test data available with an annular suppressor around a plug, and exhibits good aerodynamic static performance. The combination of Boeing and General Electric data indicates that for good aerodynamic performance, sizing of the ejector inlet for proper inlet area is most critical.

ORIGINAL PAGE IS
OF POOR QUALITY

- M_o = 0.0

BOEING DOT PHASE II DATA
- 31 TUBE
- AREA RATIO 2.5

⊗ GE DOT PHASE II DATA
- 36 CHUTE/PLUG
- D_{ej}/D_p = 1.0
- S/D_p = .061

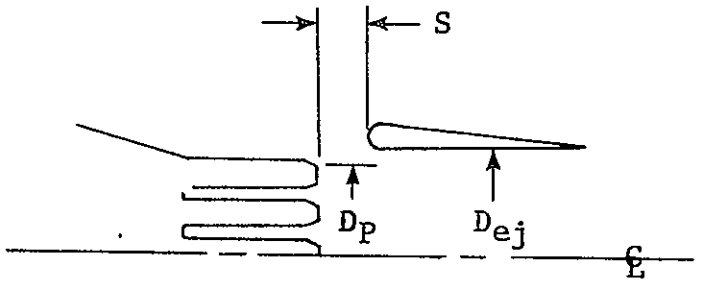

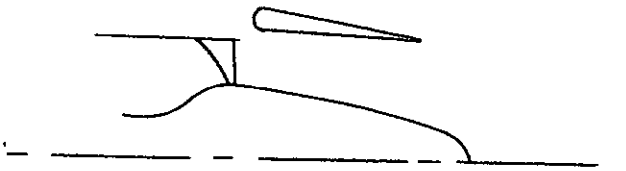

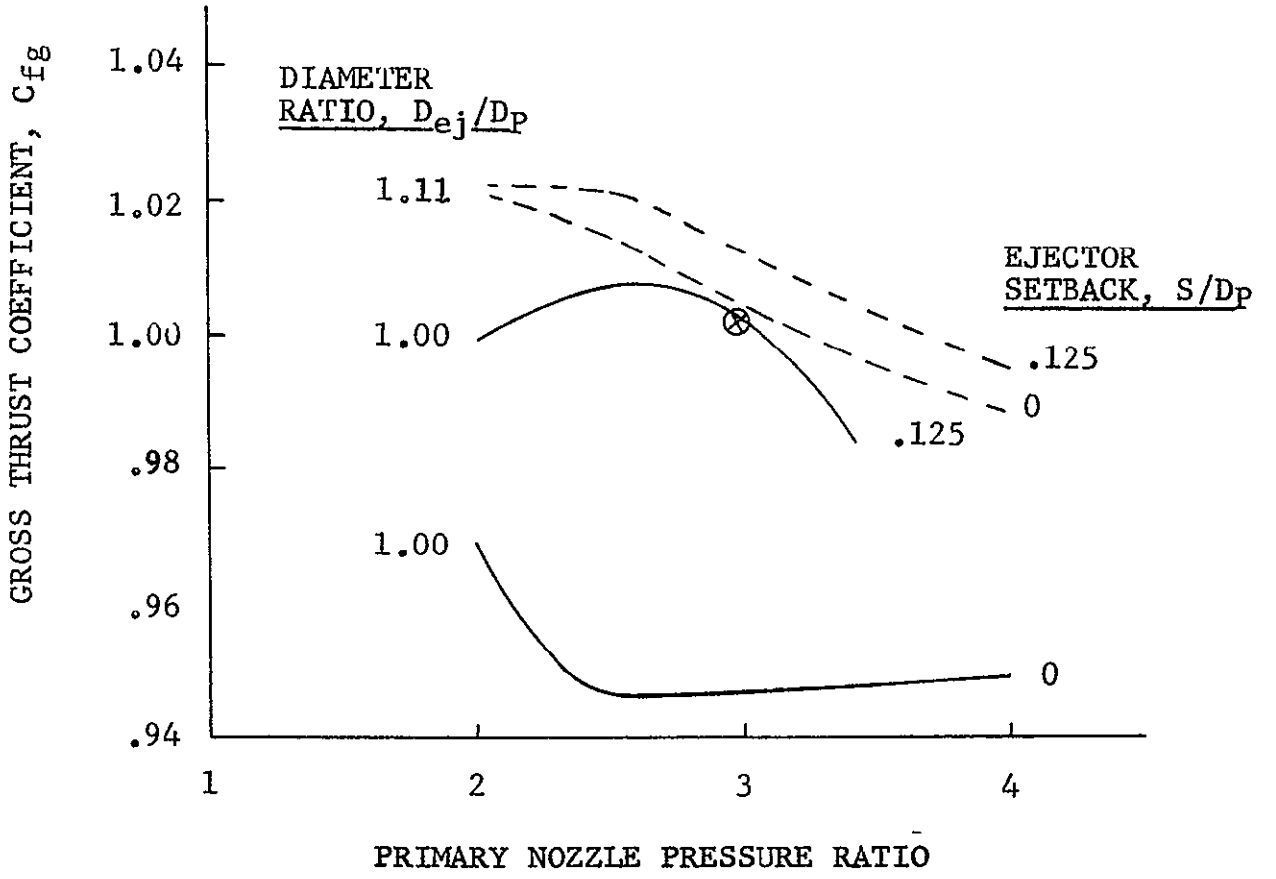

Figure 7-1 AERODYNAMIC PERFORMANCE - MULTI-ELEMENT PRIMARY WITH HARDWALL EJECTOR

Design selection for the DBTF program utilizes an ejector inlet lip at the exit plane of the multi-tube nozzle and an inlet diameter ratio (inlet lip diameter/suppressor outer diameter) of 1.11 for the multi-tube duct suppressor. A schematic of the design is shown in Figure 7-2. Details of the design are in Appendix A on Drawing No's. 101D9508 through 101D9511. Mounting this hardwall ejector to the multi-chute duct suppressor system provides an inlet diameter ratio of 1.15 as well as a higher axial spacing ratio due to ejector inlet set-back from the chute exit plane.

The second major consideration in ejector design is area distribution through the ejector. The bulk of the available suppressor/ejector data is for nozzle systems with no plug or centerbody and which utilize essentially cylindrical (constant area) ejectors. For unsuppressed conical nozzles with ejector shrouds, References 16 and 17 show performance loss can be incurred for either divergent or convergent ejectors, as compared to cylindrical shrouds at the same pressure ratio of interest. The hardwall ejector of Figure 7-2 for the DBTF dual flow plug nozzle is designed "equivalent" to a cylindrical ejector, that is, the ejector exit area equals the total inlet area. For this purpose, the definition of total inlet area for the plug nozzle with multi-element suppressors consisted of the entire fan suppressor area (base plus flow area), the core flow exit area and the ejector annulus inlet area from the suppressor outer diameter to the inlet lip. This allows the ejector shroud to converge in area by the amount of plug area in the nozzle, thus making the flow area at the exit equal to the entering flow area. The wall of the ejector shroud is straight from entrance to exit. Although this provides slight variations in the annulus flow area along the length of the shroud, it is felt that the ejector performance would not be affected. This also eliminates the need for complex wall curvature.

For acoustic suppression benefit, as a pure mechanical shield or as area available for application of acoustic treatment, long ejector length is beneficial. However, mechanical implementation into a variable engine system precludes impractical length, particularly when considering translating and stowing the ejector within the engine nacelle when not used for acoustic suppression. Thus the ejector length for the DBTF model was established

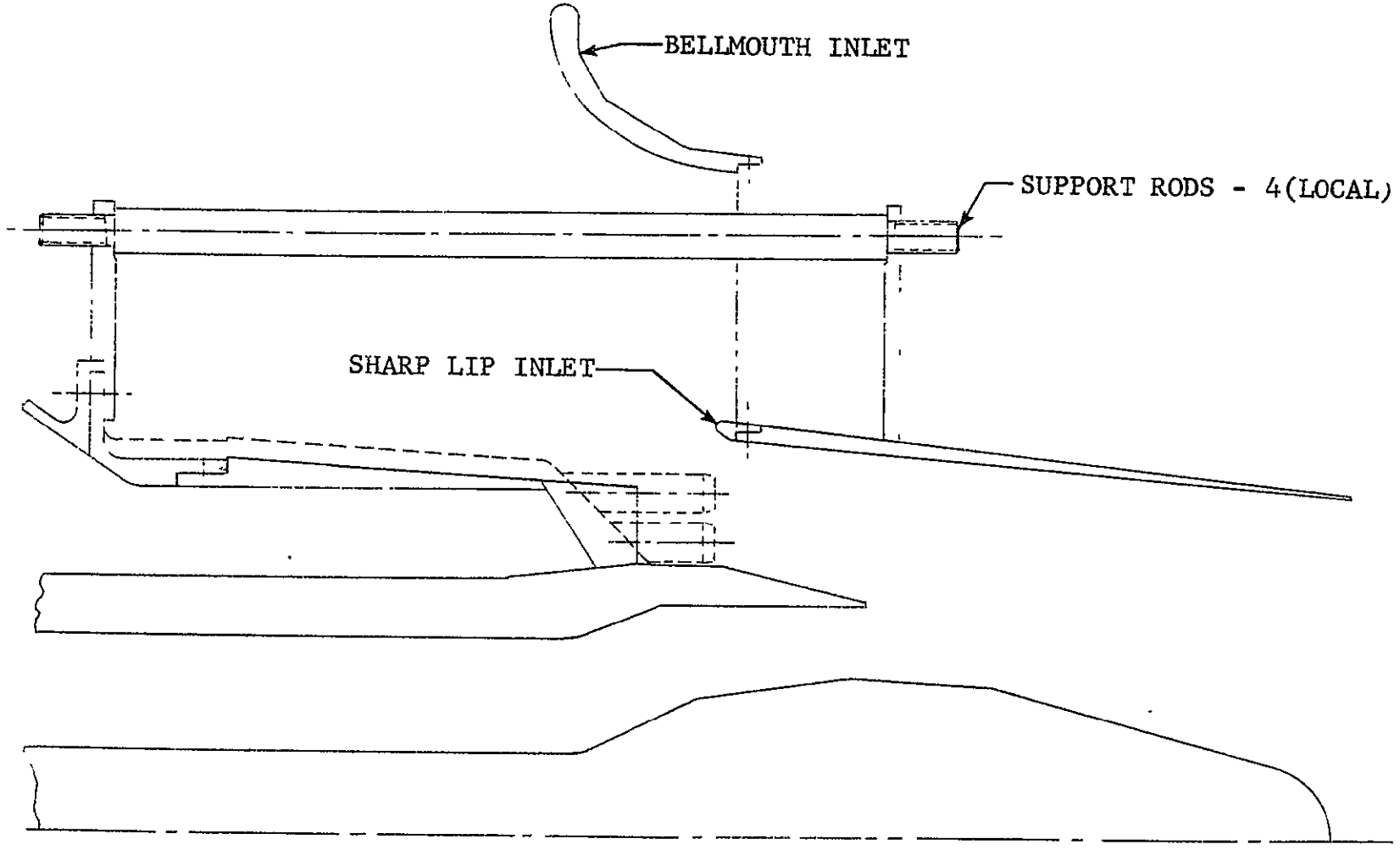

ORIGINAL PAGE IS
OF POOR QUALITY

Figure 7-2 DBTF MULTI-ELEMENT DUCT SUPPRESSOR WITH HARDWALL EJECTOR SYSTEM

through a reasonable trade between mechanical practicality and acoustic suppression potential and thus was terminated near the plug end.

Figure 7-2 also shows interchangeable sharp and bellmouth inlets for the ejector. The sharp inlet will be used for all aerodynamic static performance testing. The bellmouth inlet will be used for all acoustic tests to assure that any possible inlet separation, which could cause noise tones interfering with pure jet noise, would be eliminated.

The ejector system will be mounted through use of support flanges and four local spacer rods. These are positioned so as not to interfere with the natural airflow paths feeding the ejector inlet.

7.2 ACOUSTICALLY TREATED EJECTOR DESIGN

For application of a treated ejector, to be acoustically tested with the multi-chute and multi-tube suppressed duct configurations (Refer to Section 3.0, DESIGN OBJECTIVES, for discussion of test models), prior test work of General Electric (Reference 8) and The Boeing Company (Reference 19) were reviewed. In addition an internal treatment design review and selection program was conducted before final selection of the ejector treatment.

Schematics of test models and corresponding acoustic suppression results, for three General Electric test configurations using multi-element jet suppressors with acoustically treated ejectos, are shown in Figure 7-3 through 7-5. The primary nozzle in each system was a 37 tube array with Greatrex (segmented) tube ends. The first ejector, per Figure 7-3, was a bulk absorber design using 1" thick fiberglass packing retained with a 40% open area perforated faceplate. Suppression gain of about 5 PNdB was realized on a 300 ft sideline, over a jet velocity range of 1500 to 2500 ft/sec; attributable solely to the acoustic treatment. The second configuration, per Figure 7-4, utilized a porous "RIGIMESH" liner with a .10" deep cavity backing. Two lengths of ejector were tested. Again reasonable PNL suppression gains of 2 to 5 PNdB were realized on a 300 ft sideline, the higher suppression attained by the longer ejector. The third ejector design utilized 22.5% open area perforated sheet metal facing with Cerafelt CR-400 packing of .250" thick. Again 300 ft sideline PNL suppression gains of 4 to 5 PNdB were achieved over

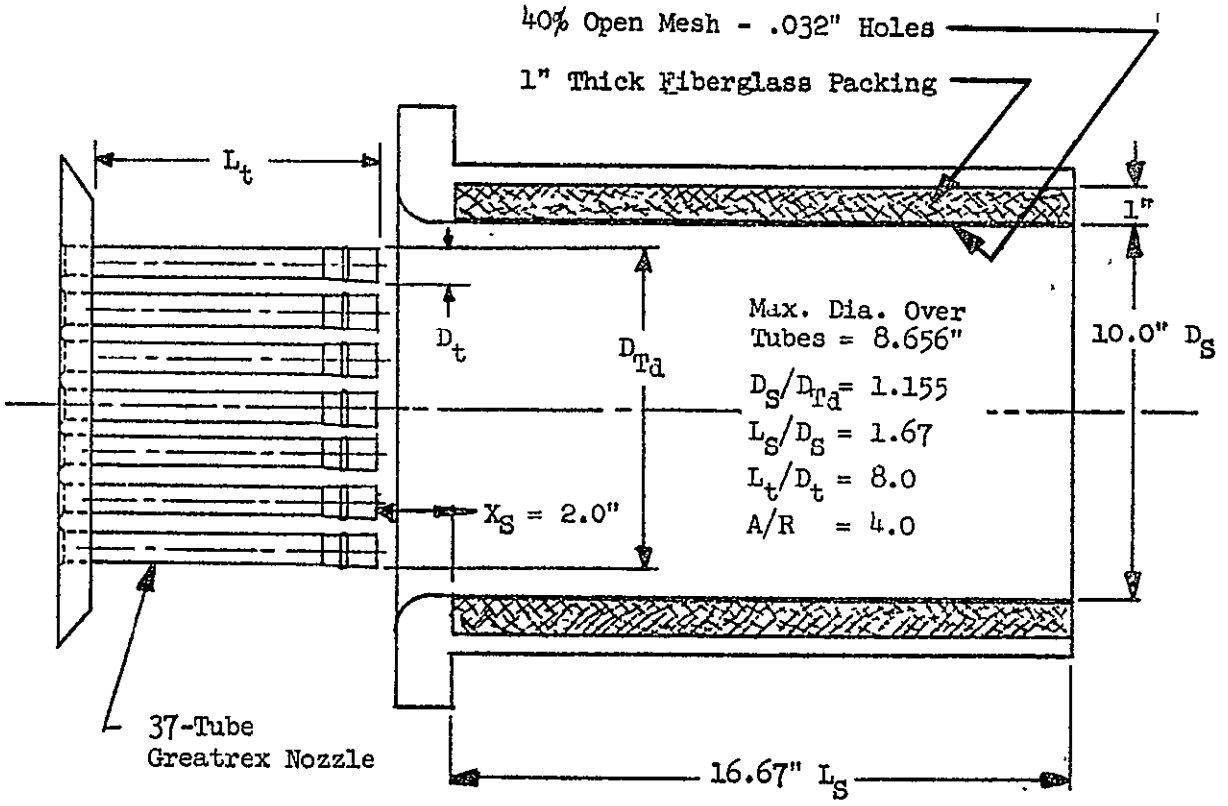

SCHEMATIC OF 37 TUBE GREATREX NOZZLE WITH FIBERGLASS LINED EJECTOR

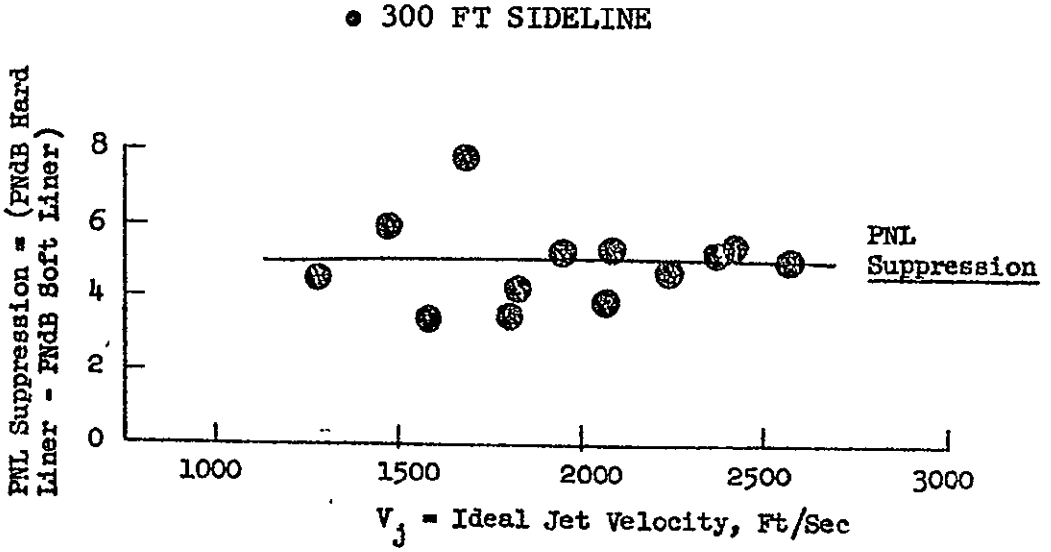

SUPPRESSION EFFECTS OF FIBERGLASS LINER ON 37 TUBE GREATREX NOZZLE

Figure 7-3 ACOUSTICALLY TREATED EJECTOR HARDWARE AND TEST RESULTS

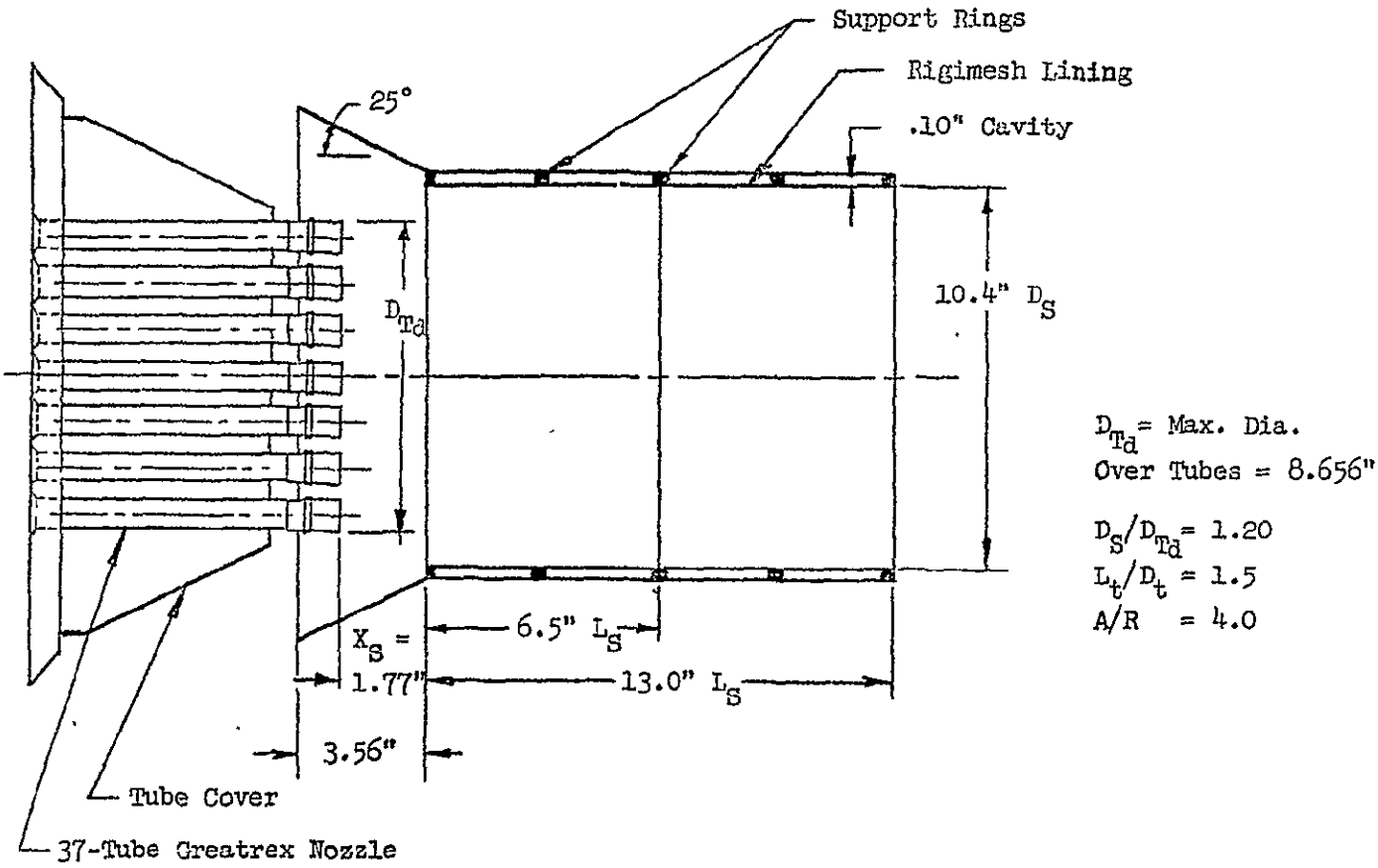

SCHEMATIC OF 37 TUBE GREATREX NOZZLE WITH RIGIMESH LINED EJECTOR

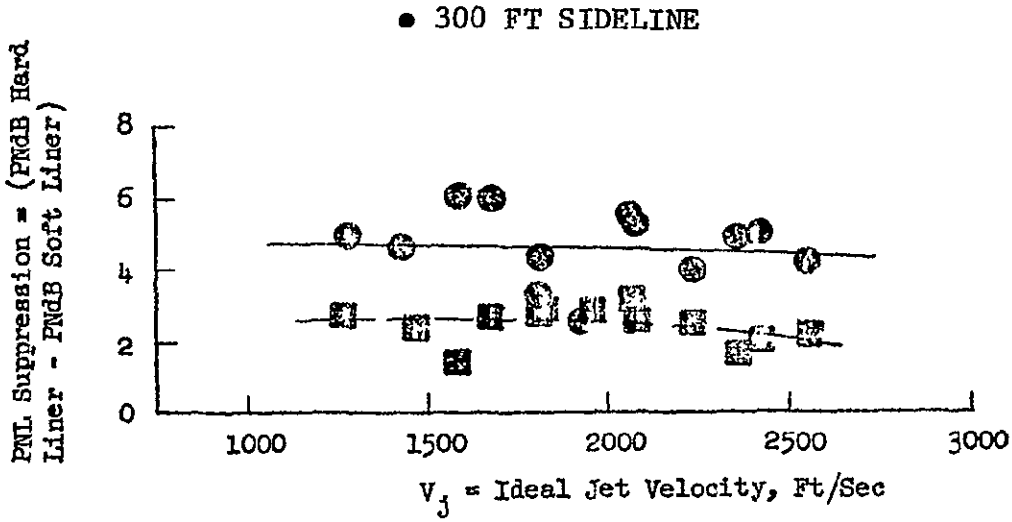

SUPPRESSION EFFECTS OF SHORT AND LONG RIGIMESH LINERS ON 37 TUBE GREATREX NOZZLE

Figure 7-4 ACOUSTICALLY TREATED EJECTOR HARDWARE AND TEST RESULTS

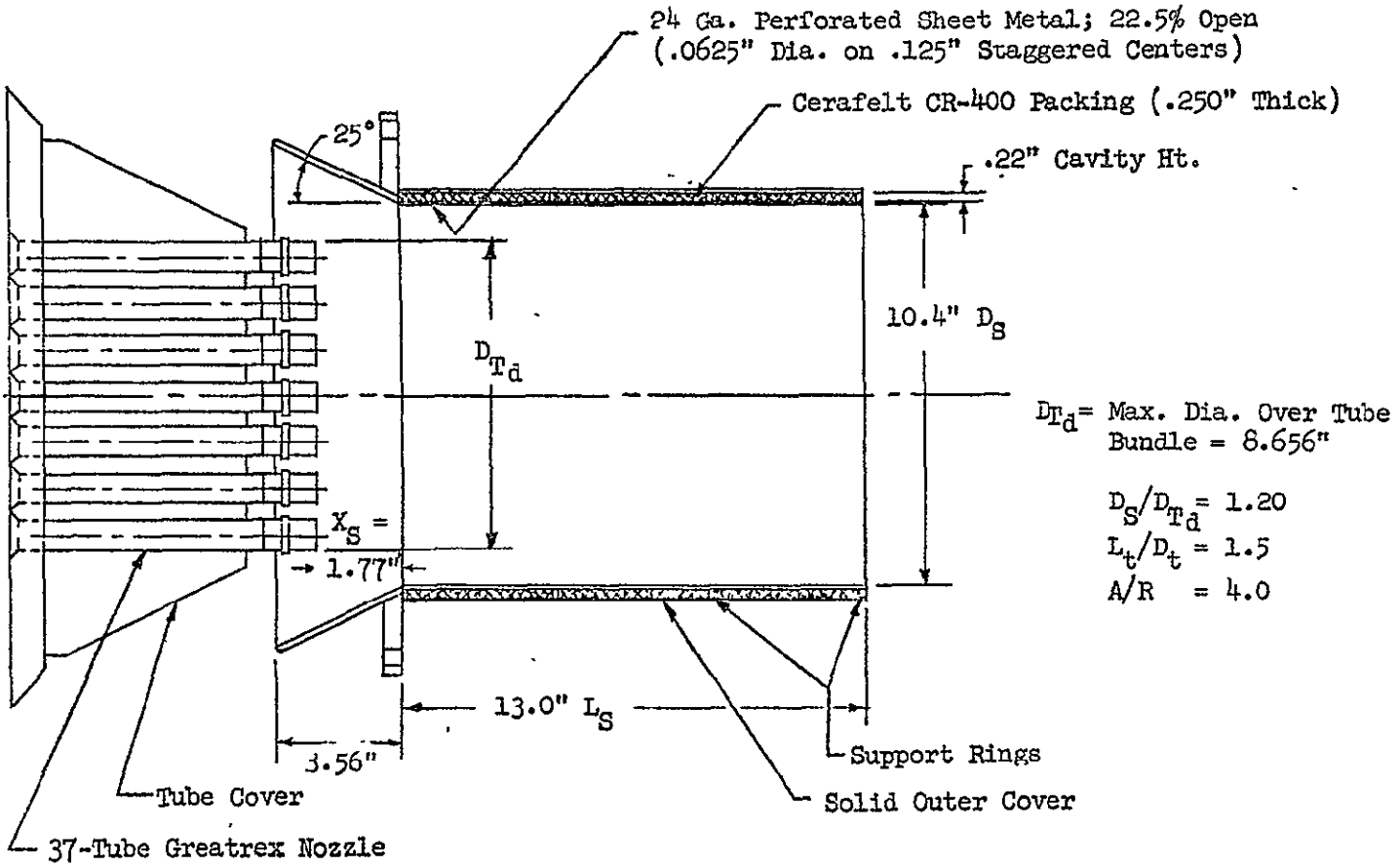

SCHEMATIC OF 37 TUBE GREATREX NOZZLE WITH PERFORATED SHEET METAL/CERAFELT PACKED EJECTOR

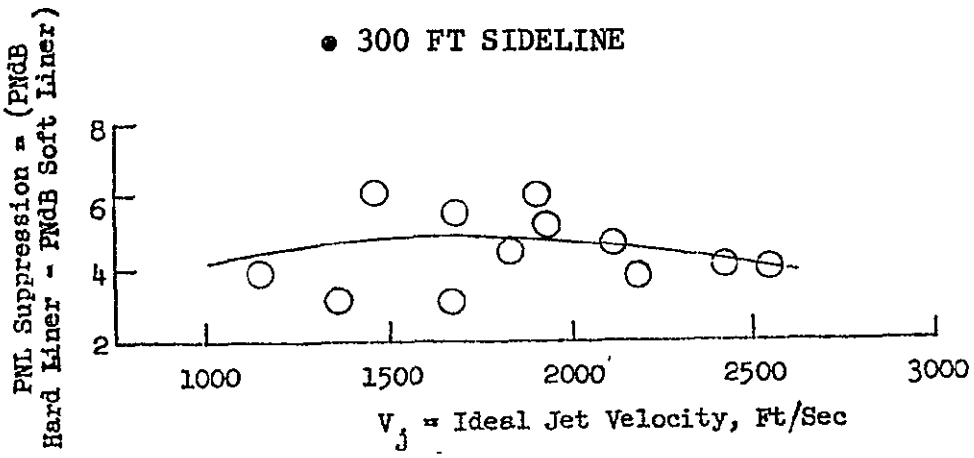

SUPPRESSION EFFECT OF 22.5% OPEN, CERAFELT PACKED LINER ON 37 GREATREX TUBE NOZZLE

Figure 7-5 ACOUSTICALLY TREATED EJECTOR HARDWARE AND TEST RESULTS

a wide jet velocity range. The suppression is again attributed directly to the acoustic treatment as the suppression is established by reference to a hardwall ejector of the same internal geometry.

In each of the three applications, the primary jet high frequency noise sources were reasonably close to the nozzle exit plane due to the high segmentation of the jet with the Greatrex tube suppressor. Likewise in each application, good suppression levels were attained by use of bulk-absorption treatment designs.

For the DBTF ejector design, the treatment review study with resultant material selection and gross tuning study for suppression of the multi-element jet spectra resulted in the following design details.

- Perforated faceplate of 37% porosity using approximately .045" diameter holes in a straight line pattern with .067" spacing between centers.
- "Kaowool" packing material – a refractory fiber material with good absorption and insulation characteristics, similar to Cerafelt; capable of sustained use at 2300° F.
- Depth of treatment cavity approximately 3/8" and filled with approximately 3 lb per cu ft density of the Kaowool packing.

The acoustic treatment design details are incorporated into a separate ejector with internal flowpath dimensions identical to those of the hardwall ejector design of Figure 7-2. The ejector outer diameters have grown to accommodate the treatment and faceplate. The bellmouth inlet is adaptable to this ejector and is planned for use during acoustic testing when applied to both the multi-tube and multi-chute suppressed duct systems.

SECTION 8.0

COANNULAR COPLANAR BASELINE SYSTEM

The conical convergent nozzle is the classic baseline for all single flow jet noise work. However, for dual flow nozzle systems, previous General Electric work has shown that a coannular coplanar convergent nozzle system without a protruding center plug is a more representative acoustic baseline. This coannular baseline nozzle represents a single conical convergent nozzle when the exit velocities are equal (same temperature and pressure), however, it is more versatile in that it also allows the velocity ratio effects to be established on a simple nozzle system. Therefore, the second baseline nozzle for the study was chosen as a coannular coplanar non-protruding-plug system. For the single flow baseline case, available acoustic data from tests of conical convergent nozzles in intended to be used, in addition to testing the dual flow baseline at equal exit velocities.

The design of the coannular coplanar baseline nozzle is shown in Figure 8-1. Design areas and discharge coefficients are tabulated in Table A-1 of Appendix A. A sketch of the model system showing all related assembly hardware is also included in Appendix A (as Figure A-4) as are the detailed model hardware drawings.

Choice of the nozzle discharge coefficients, $C_{D18} = .990$ and $C_{D8} = .994$, was based on previous test work and at the takeoff design pressure ratios of $P_{18}/P_o = 2.66$, $P_8/P_o = 1.51$. Physical throat areas, per Table A-1 in Appendix A, were used to establish the throat plane diameters, allowing for a thin lip at the core/duct interface. The total physical flow area at the coplanar throat plane is just slightly under the equivalent area of a 6" dia. nozzle, due to the high values of discharge coefficients and holding Ae_{18} and Ae_8 consistent between models rather than A_{18} and A_8. Core to duct effective area ratio (A_{e8}/A_{e18}) is 1.55, as is the design for all other models. Reasonable flowpath convergence angles are used before mating to steeper angled transition pieces which bring model flow-lines up to those of the facility instrumentation spool-pieces.

The exit plane of the coannular coplanar baseline system has been chosen to coincide with that of the coannular non-coplanar duct throat plane.

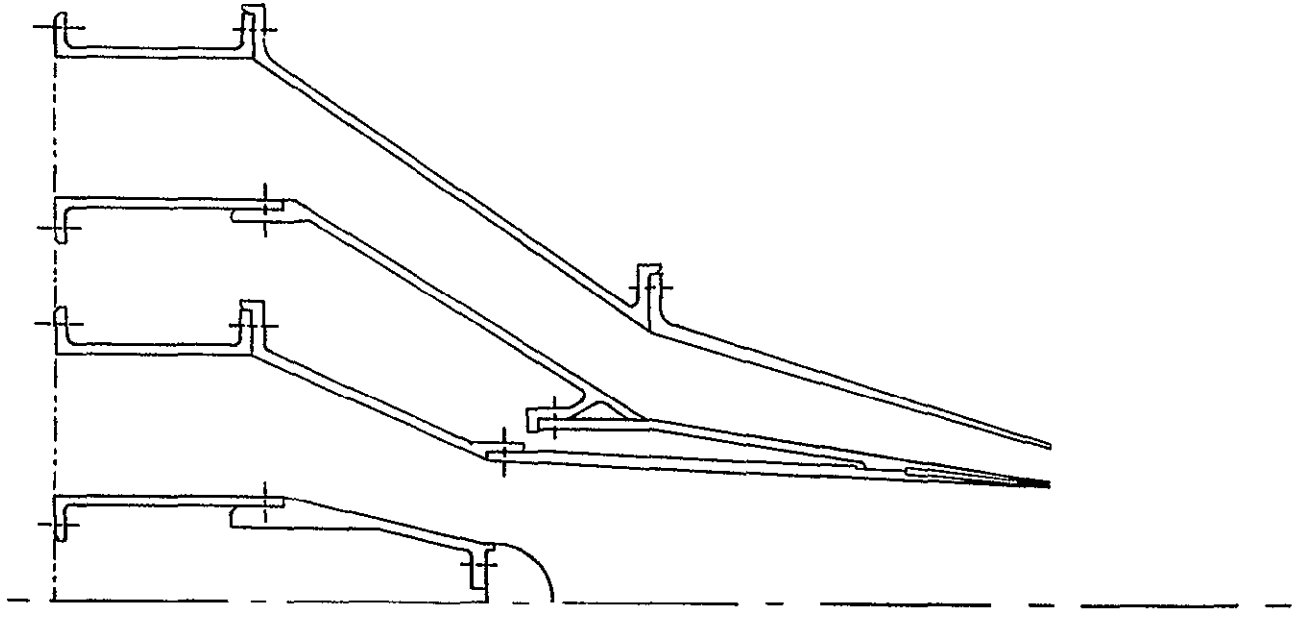

Figure 8-1 DBTF SCALE MODEL COANNULAR COPLANAR BASELINE

SECTION 9.0

MODEL HARDWARE DESIGN DEVELOPMENT

To meet the various usage intents as described in Section 3.0, DESIGN OBJECTIVES, the model hardware system and detail design became a major task within the DBTF program. The initial design criteria, imposed pastly by contractual requirements and partly by internal decision, are summarized as follows:

1) Test Conditions

a) Acoustic

	Core	Duct
T_T ∿°R	amb-1460	amb-1960
P_T/P_o	1.3-1.9	1.2-3.9
V_j ∿ft/sec	1000-1400	550-2800

$\Delta T = T_{18} - T_8$ = 0 to 1000°

V_{19}/V_9 = 0.4 to 2.0

b) Aerodynamic

	Core	Duct
T_T ∿°R	amb-1460	amb-1460
P_T/P_o	1.3-2.0	1.5-4.0

2) No water cooling of hardware.

3) Model sub-assemblies must be separable for interchangeability and repetative usage.

4) As the hardware will be exposed to large temperature gradients between the core and duct ($\Delta T = T_{18} - T_8$ = 0 to 1000°, contractual commitment) differential radial and axial growth rates will be experienced. Provisions must be made to alleviate stress concentrations, which could lead to hardware failure, by allowing independent growth of the core and duct streams' hardware, both in the radial and axial directions.

5) Models must be interchangeable between the GE JENOTS acoustic facility and the FluiDyne channel 11 facility with minimum of transition hardware.

6) Instrumentation must be provided to measure total temperature and pressure of both streams, sufficient to calculate ideal jet velocities.

7) As the models will be used for evaluation of aerodynamic static performance, flange surfaces and other potential leakage paths must be sealed as best possible. Accuracy of thrust measurements is directly proportional to flow leakage, therefore, leakage between streams or to ambient should be minimized or totally eliminated.

8) Static pressure instrumentation is to be applied to critical drag surfaces of the baseline coannular non-coplanar model and to the suppressed duct models to allow for evaluation of thrust loss constituents through pressure/area integration. Tubing for part of the instrumentation must be routed through passages within the model assembly and through hollow struts within the facility frames. Static pressure instrumentation is also to be applied to the hardwall ejector to document pressure loading and subsequent thrust gain/loss due to the ejector.

9) Models must be of flight type configurations (externally clean) to allow for possible future study of external flow effects.

Discussion of and provisions for incorporation of the above design criteria are as follows. Several initial criteria have been changed, making design requirements even more stringent.

1) The most stringent contractual requirement for mechanical integrity is imposed by the differential temperature conditions in item 1 above, i.e. $\Delta T=T_{18}-T_8$ of 0 to 1000°. However, the possibiltiy was forseen of subjecting the duct stream to the maximum design temperature of 1960° R with ambient temperature flow in the core stream, thus resulting in a ΔT of approximately 1500°. This then became the most stringent thermal design condition, as opposed to the

contractual commitment of 1000° ΔT. For gas loading on duct suppressor elements, the most severe environment would be at P_{T18}/P_o=4.0 while at T_{18} of 1960°R. Provisions have also been made to allow for test with the core stream at 1460° R and the duct stream with ambient temperature flow.

Thus the limits of operation are:

- o Duct at 1960° R - Core from ambient to 1460° R
- o Core at 1460° R - Duct from ambient to 1960° R

The final design however, does allow for core stream operation to P_{T8}/P_o of 4.0 and T_{T8} = 1460° R.

2) As jacketing for water cooling is quite complex, confidence in obtaining uniform surface cooling with water jacketing is low, and probability of success in routing instrumentation leads through water cooled sections without leakage is low, a non-water-cooled system was selected. Fabrication materials, weld and braze processes and assembly hardware items were selected to compensate for lack of cooling. The core stream I.D. and O.D. flowpath hardware is made from 300 series stainless steel (Bar stock AMS 5639C, 5647C, 5648C and 5654H, sheet stock AMS5510J, 5511B and 5524C). The duct I.D. and O.D. flowpath hardware is manufactured from Hastalloy X (Plate stock AMS5536G, Bar, Forging AMS5754F).

3) To assure interchangeability of model sub-assemblies and repetetive usage, special high temperature fastening mechanisms have been selected to eliminate seizure at elevated temperature operation. To minimize warpage at flanges between mating parts, again for assurance of sub-assemblies interchangeability, drawn fits and light interference fits are used at most flange interfaces. Provisions for back-off screws for ease of disassembly are included wherever practical.

4) To allow for differential radial and axial thermal growth rates, incorporation of provisions starts within the upstream facility frame section. A schematic of the acoustic facility hardware with the baseline coannular non-copulanar model system is shown in Figure 9-1. Independent core and duct frames have been designed, interconnected at the core O.D. and duct I.D. flowpaths with a flexing wishbone structure. The wishbone absorbs deflection due to differential thermal growth, thus eliminating high stress concentration normally inherent in single frame designs for dual flow while subjected to large thermal gradients.

The duct stream frame section adapts to the facility coannular plenum through a cylindrical outer frame support (See Figure 9-1) and a conical transition piece. Thus the duct stream outer shell supports the entire model and frame assembly. Core O.D. and duct I.D. sliding transition pieces complete the inner flowpaths from the frames to the facility coannular plenum. Sealing mechanisms are provided to eliminate leakage between streams at the interface of the core frame and coannular plenum inner supply pipe. Differential axial growth from the frame section aft through the model hardware is provided for with a sliding interface between the core O.D. and duct I.D. hardware pieces at the exit plane. Compensation for differential radial growth is also allowed for at the same exit plane interface. Sufficient radial gap is allowed such that a) when operating the core hot (1460° R) and duct at ambient, the core O.D. will grow radially into the duct I.D. hardware, but not overstress to buckling, and b) when operating the duct hot (1960° R) and core at ambient, the gap will be increased due to faster duct hardware radial growth. These allowances for differential axial and radial growth rates are also in the suppressed duct designs.

5) As the same model assemblies will be used for both acoustic and aerodynamic static performance evaluation, interchangeability between the JENOTS acoustic facility and FluiDyne's Channel 11 thrust stand is required. A schematic showing adaptation to FluiDyne's facility is shown in Figure 9-2. The acoustic facility's core and duct

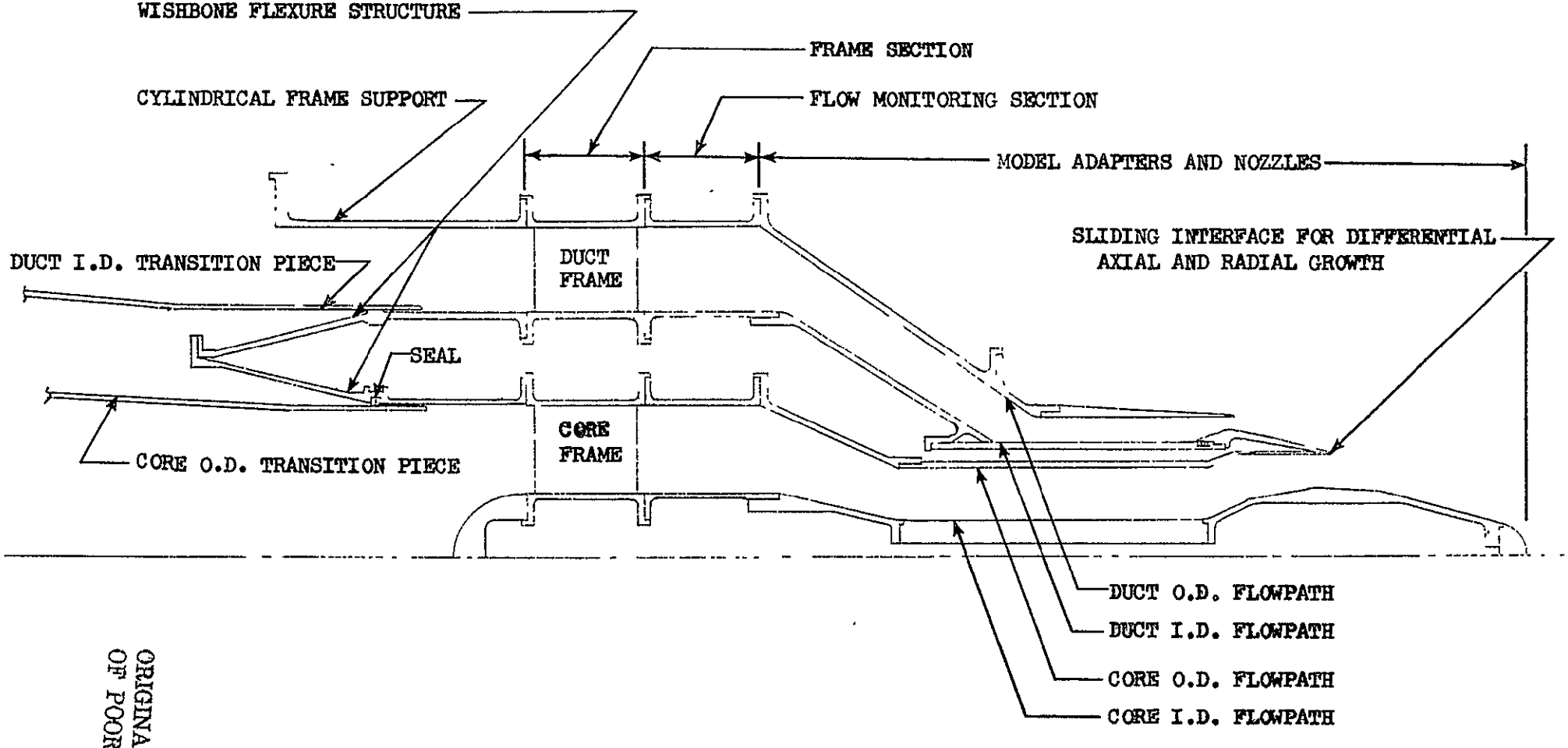

Figure 9-1 SCHEMATIC OF ACOUSTIC FACILITY HARDWARE AND BASELINE MODEL

ORIGINAL PAGE IS
OF POOR QUALITY

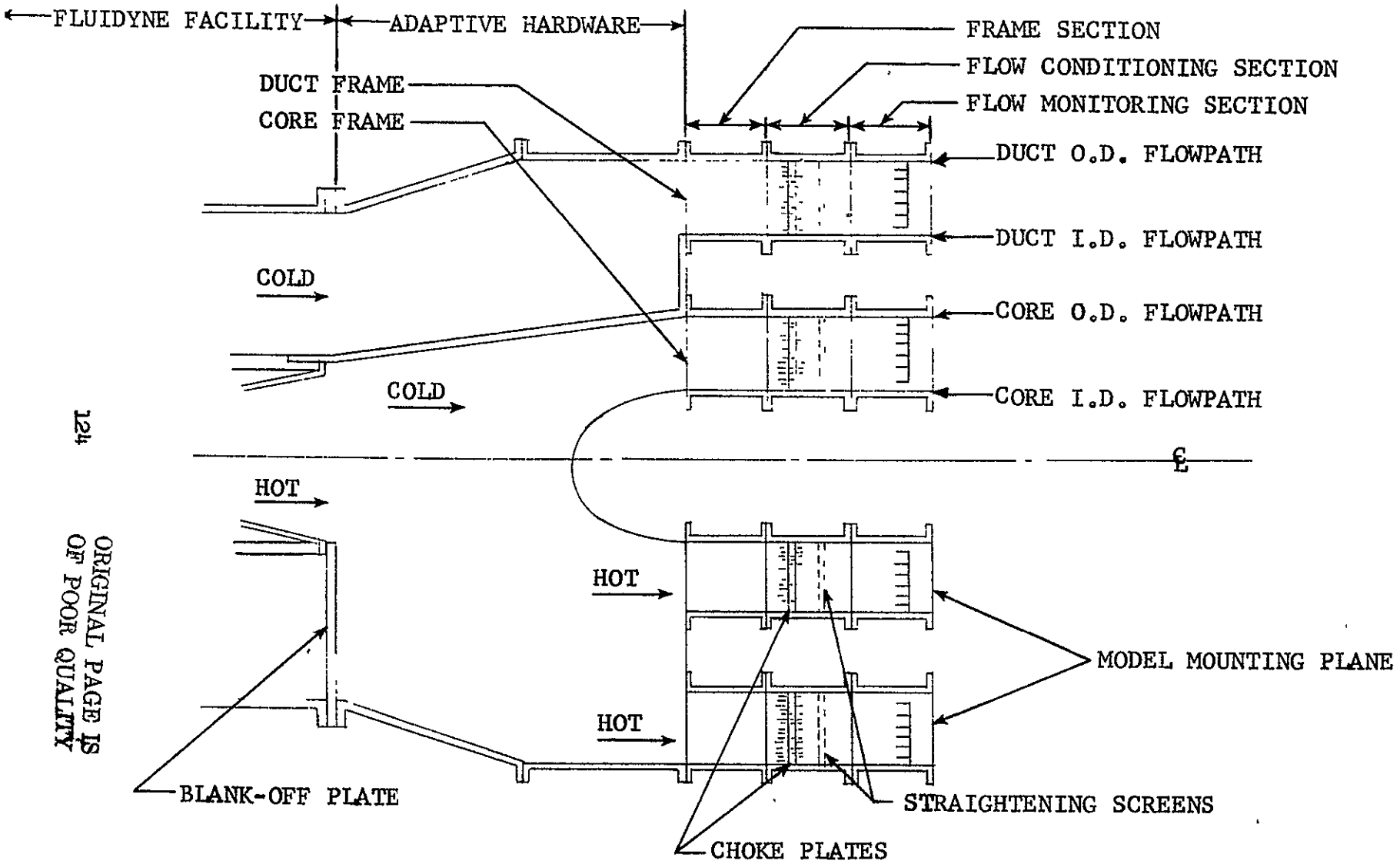

Figure 9-2 SCHEMATIC OF ADAPTION TO FLUIDYNE'S CHANNEL 11 FACILITY

ORIGINAL PAGE IS OF POOR QUALITY

frames plus outer frame support and flow monitoring instrumentation sections will be used. The flexing wishbone structure is not required as core and duct flows will be at the same temperature. Spaced between the frame section and the flow monitoring instrumentation section will be a flow conditioning section consisting of choke plates and straightening screens. The calibrated choke plates will provide the required pressure drop to supply the core and duct nozzles with correct test pressure. Additional upstream choke plates, part of the FluiDyne facility, intially reduce the supply pressure from approximately 400 to 120 psia. For ambient temperature test work, each stream will be supplied and metered independently as shown by the top half of the Figure 9-2 schematic. For hot flow aerodynamic testing, the core flow will be ducted to supply both the core and duct nozzles as shown by the lower half of the same schematic.

6) Flow monitoring instrumentation for both the acoustic and aerodynamic tests will be that designed and built as part of the new dual flow acoustic facility. As previously seen in Figure 9-2, an instrumentation section is positioned aft of the frames and flow conditioning sections for aerodynamic testing. Instrumentation within the flow metering section consists of two combination P_T/T_T rakes plus four static pressure taps in each of the two streams. A schematic of the instrumentation layout, Figure 9-3, shows the P_T/T_T rakes located midway between the wakes of the upstream struts within the core and duct streams. The static pressure taps are located just to the side of each rake to assure any flow disturbance from the rake body does not interfere with the measurements. Each P_T/T_T rake is an integral part of a removable pad such that, when inserted within the stream, no discontinuity in internal flowpath is seen other than the probe body. Three P_T and three T_T elements are on each rake, spaced on centers of equal areas, as shown schematically in Figure 9-4, i.e, core and duct annuli are divided into six equal areas and sensing elements are located at the area centers of the six equal area annuli. The two probes within each stream alternate P_T

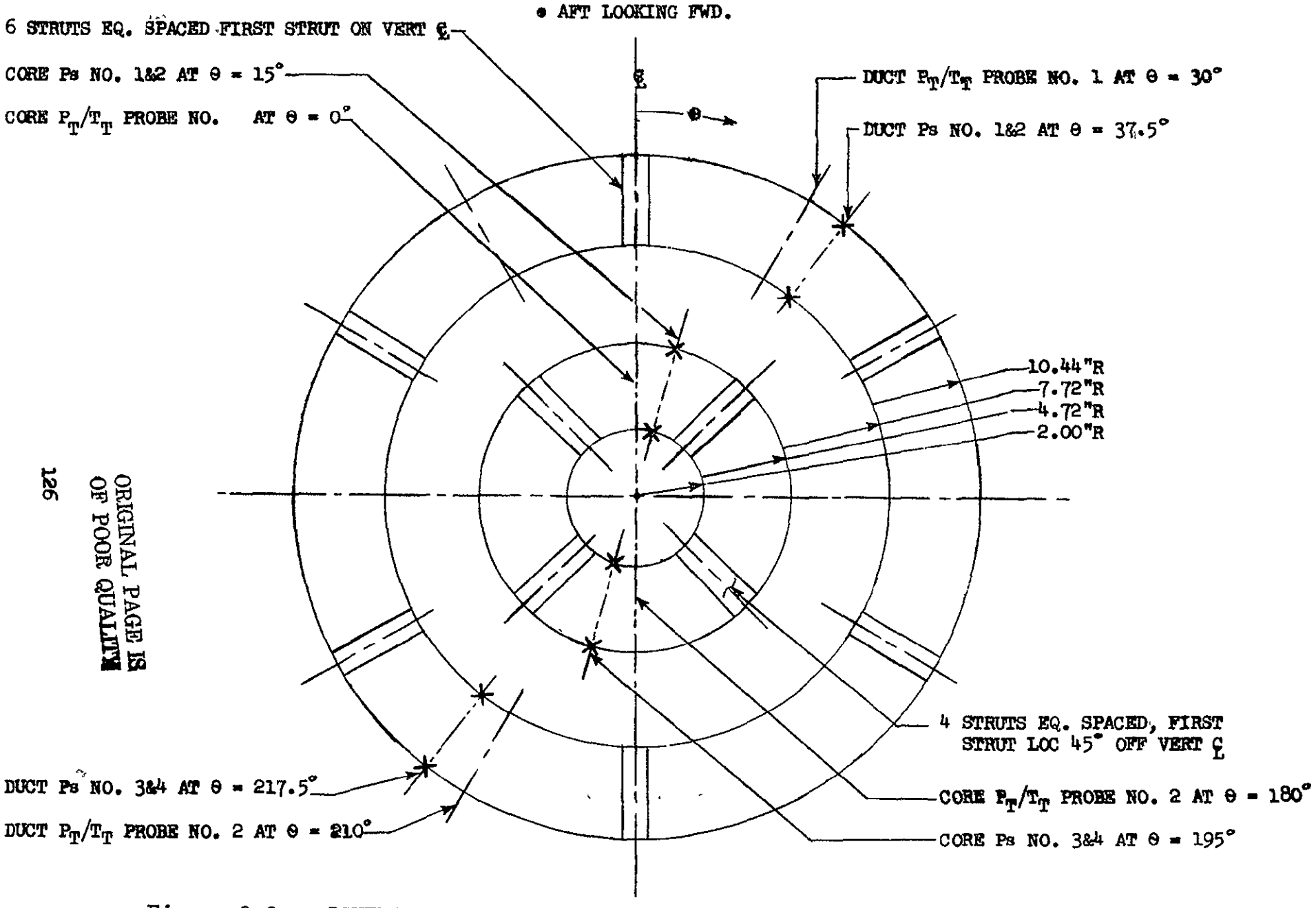

Figure 9-3 SCHEMATIC OF FLOW MONITORING INSTRUMENTATION LAYOUT

ORIGINAL PAGE IS OF POOR QUALITY

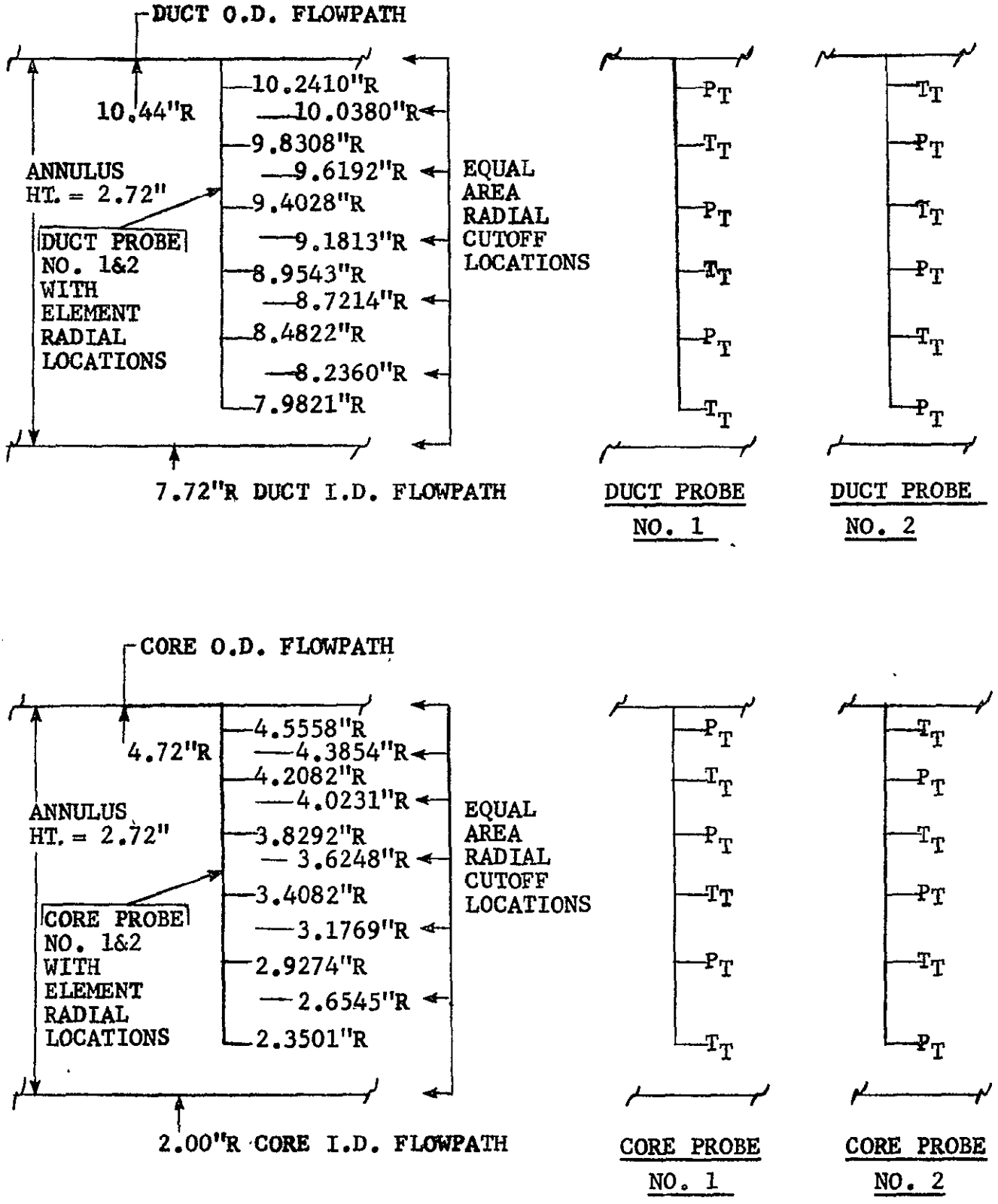

Figure 9-4 LAYOUT OF P_T/T_T RAKES DESIGN

and T_T sensing elements at each of the six radial locations. Appendix A includes probe detail drawings 665-100-1194 Sheets 1 through 3.

The use of a common flow monitoring section should, therefore, provide consistency of measurements among all test models and between the acoustic and aerodynamic test work.

7) For prevention of flow leakage between streams and from the duct stream to ambient, particularly necessary for aerodynamic static testing, several precautions have been designed into the model/adapter system.

   - o High-temperature-resisting "GRAFOIL" gaskets of .010 thickness are to be used between all radial flanges as specified in the assembly schematic Figure A-1 through A-4 of appendix A. They also will be used on upstream facility hardware at the FluiDyne facility.
   - o For axial flange areas, drawn fits and interference fits provide metal to metal contact for prevention of leakage. Additionally, radial bolts in critical locations are press fit interference.
   - o For the suppressed duct stream models, where the suppressor hardware is allowed to translate axially over the duct I.D. flowpath, as seen in Figure A-2 and A-3 of Appendix A, inconel-asbestos packing is provided to seal against leakage.

     The gasketing and packing are intended primarily for aerodynamic test work where flow leakage is critical to performance evaluation. For acoustic test work, when minor leakage does not influence acoustic noise generation, the gasketing and packing are recommended but are not mandatory.

8) Provisions have been made to route all internal static pressure tap leads through passages between the core O.D. and fan I.D. hardware pieces and internal to the core I.D. hardware, then between flow monitoring and flow conditioning hardware sections and up through slots in the frame struts. Both the core and fan plug surfaces can be instrumented in this manner. Specifics of model instrumentation are discussed in Section 10.0.

9) Contractual requirement is that model external flow-lines will be aerodynamically clean for possible use within an external flow media. This would allow the models to be evaluated for either or both acoustics and aerodynamics in a simulated flight wind-on application. A break plane has therefore been provided within each of the models four major hardware sections, (with the exception of the coannular coplanar baseline) i.e., core I.D., core O.D., duct I.D., and duct O.D., (See Figures A-1 through A-3 of Appendix A) such that adaptation to a wind tunnel sting with maintenance of smooth internal and external flowpaths is possible. The break points of the core and duct O.D. sections use interference axial fits and radial press fit bolts for elimination of leakage and for continuity of internal flowpaths.

For application of the secondary ejector, temporary bulk flanges are used for the static acoustic and aerodynamic tests. A break plane has been provided at the ejector inlet for ease of mounting to a wind tunnel sting. The bulk flanges can be machined away for an externally smooth ejector flowpath.

SECTION 10.0

MODEL INSTRUMENTATION

The models that will be tested for aerodynamic performance (all but the coannular coplanar baseline) contain static pressure instrumentation sufficient to document the major thrust loss mechanisms. Specific locations of the pressure taps are shown on the detailed drawings of Appendix A. As the core flowpath is common to all aerodynamic models, the 15 static pressure taps on the core plug (Appendix A, Drawing JNSD-121573, Sheet 1) are common. For the coannular non-coplanar baseline model, the duct plug has 12 static pressure taps as detailed in Appendix A, Drawing JNSD-122873, Sheet 1. For the multi-chute/tube duct suppressors, the duct plugs have 16 and 14 static pressure taps, respectively, as shown in Tables III and IV of Appendix A, Drawing JNSD-123173, Sheet 5. These taps are arranged in rows at several angular locations with redundant taps at various axial locations. The arrangement is designed to detect differences in plug pressure behind flow blockages (chute or portion of tube baseplate) and behind direct flowpaths (tube or between chutes).

The multi-tube suppressor is instrumented with eleven static taps at various radial locations on the baseplate, per Table II of Appendix A, Drawing JNSD-123173, Sheet 5. Redundant taps are at some radii but positioned at different circumferential locations in order to detect variations in base pressure caused by location within the tube pattern. The pressure measurements will be integrated over the base area to estimate base drag; expected to be the largest single contributor to thrust loss.

The base areas of the multi-chute suppressor are instrumented with static taps at various radial positions. The taps are located along the aft face of the leading edge of the chute as shown on Appendix A, Drawing JNSD-123173, Sheet 5, and located by Table I. The chute base pressure measurements will again be used to calculate base drag for each of the test conditions.

Each static pressure tap is to be supplied with approximately six feet of stainless steel tubing so that routing through the model assembly can be accomplished when required and tubing can be easily attached to facility readout instrumentation.

The internal surface of the hardwall ejector shroud and the sharp inlet, Appendix A, Drawings 101D9508 through 101D9511, also contains static pressure taps which will indicate the thrust and/or drag forces on the shroud.

REFERENCES

1. Kuehner, W.D., Oller, T.L., Staid, P.S., and Twiss, C.F., "High Mach Nozzles Program" Final Report, NAVAIR Contract N00019-71-C-0540 prepared by General Electric for Naval Air Systems Command, Dept. of the Navy, January 1973.

2. Kuehner, W.D., Oller, T.L., Staid, P.S., and Twiss, C.F., "High Mach Nozzle, Final Report", General Electric Technical Memo, TM 72-951, January 1973.

3. Dusa, D.J., Fashing, W., Wagenknecht, C.D., and Eckard, G.J., "Turbine Engine Exhaust Nozzle Performance Investigation - Phase I", General Electric Report No. R73AEG452, April 1974.

4. "Advanced Supersonic Propulsion System Technology Study - Task 1 Final Report", NASA Contract NAS3-16950, May 1973.

5. "Preliminary Installed Performance GE21/F3 Study B1 Propulsion System for use in Advanced Supersonic Propulsion System Technology Studies", General Electric AEG TM 73-288, April 1973.

6. "Preliminary Installed Performance GE21/F3 Study B1 (P15) Propulsion System for use in Advanced Supersonic Propulsion System Technology Studies", General Electric AEG TM 73-555, August 1973.

7. "Preliminary Installed Performance GE21/F3 Study B2 (P13) Propulsion System for use in Advanced Supersonic Propulsion System Technology Studies", General Electric AEG TM 73-553, August 1973.

8. Brausch, J.F. and Doyle, V.L., "Supersonic Transport Noise Reduction Technology Summary, Phase I, Summary of GE4/SST Acoustic Suppression Research", Report No. FAA-SS-72-42, General Electric Report No. R72-AEG-342, for Department of Transportation Contract FA-SS-71-13, December 1972.

9. "Quarterly Progress Report July - September, 1973 - SST Follow-On Program, Phase II", Boeing Commercial Airplane Company, Contract DOT-FA-72WA-2893.

10. Motsinger, R.E., Sieckman, A.R., "Prediction of Supersonic Jet Noise Reduction Using Multi-Tube Nozzle Suppressors", General Electric Report R73AEG156, March 6, 1973.

11. "Quarterly Progress Report No.3, December 1 through February 28, 1973 - Supersonic Transport Noise Reduction Technology Program - Phase II", General Electric Company, Aircraft Engine Group, Contract No. DOT-FA72WA-2894.

12. "Quarterly Progress Report No.4, March 1 through May 31, 1973 - Supersonic Transport Noise Reduction Technology Program - Phase II", General Electric Company, Aircraft Engine Group, Contract DOT-FA72WA-2894.

13. "Quarterly Progress Report April - June, 1973 - SST Follow-On Program, Phase II", Boeing Commercial Airplane Company, Contract DOT-FA-72WA-2893.

14. "Quarterly Progress Report No.2, September 1 through November 30, 1972 - Supersonic Transport Noise Reduction Technology Program - Phase II", General Electric Company, Aircraft Engine Group, Contract DOT-FA72WA-2894.

15. Harrington, D.E. and Schloemer, J.J., "Thrust Performance of Isolated Plug Nozzles With Two Types of 40 Spoke Noise Suppressor at Mach Numbers from 0 to 0.45", NASA TMX-2951, January 1974.

16. Greathouse, W.K., and Beale, W.T., "Performance Characteristics of Several Divergent - Shroud Aircraft Ejectors", NACA RM E55G21a, September 1955.

17. Greathouse, W.K., and Hollester, D.P., "Air-Flow and Thrust Characteristics of Several Cylindrical Cooling - Air Ejectors With a Primary to Secondary Temperature Ratio of 1.0", NACA RM E52L24, March 1953.

18. Kochendorfer, F.D. and Rousso, M.D., "Performance Characteristics of Aircraft Cooling Ejectors Having Short Cylindrical Shrouds", NACA RM E51E01, May 1951.

19. Atvars, J., Paynter, G.C., Walker, D.Q. and Wintermeyer, C.F. "Development of Acoustically Lined Ejector Technology for Multi-Tube Jet Noise Suppressor Nozzles by Model and Engine Tests Over a Wide Range of Jet Pressure Ratios and Temperatures", Boeing Commercial Airplane Company Report No. D6-60226 for NASA Contract NAS3-15570, November 1973.

NOMENCLATURE

A_8	Core Nozzle Physical Throat Area, in^2
A_{e8}	Core Nozzle Aerodynamics Throat Area, in^2
A_{18}	Duct Nozzle Physical Throat Area, in^2
A_{e18}	Duct Nozzle Aerodynamics Throat Area, in^2
A_9	Fully Expanded Core Jet Area, in^2
A_{19}	Fully Expanded Duct Jet Area, in^2
Alt	Altitude, ft
A/R, ARd	Suppressor Nozzle Area Ratio = Baseplate Area or Annulus Area/Total Physical Flow Area
β	Bypass Ratio = W_{18}/W_8
C_D	Discharge Coefficient = Aerodynamic Flow Area/Physical Flow Area
C_{D8}	Core Nozzle Discharge Coefficient
C_{D18}	Duct Nozzle Discharge Coefficient
D	Axial Depth of Chute Cross Section at Flowpath O.D. (see Figure 6-49), i
D_{ej}	Ejector Internal Diameter (see Figure 7-1), in.
D_p	Primary Nozzle Maximum Diameter Over Suppression Elements, in.
DBTF	Duct Burning Turbo-Fan
Fn	Thrust, lbf.
H	Chute Height between Flowpath O.D. and I.D., in.
Hz	Hertz
L_{ti}/D_t	Tube Internal Length to Diameter Ratio
M_N	Mach Number
OAPR	Engine Overall Pressure Ratio
OAPWL	Overall Power Level, dB
OASPL	Overall Sound Pressure Level, dB
P_{amb}	Ambient Pressure, psia
PR	Pressure Ratio
PR_F	Fan Pressure Ratio
P_{T8}/P_o	Core Nozzle Total to Ambient Pressure Ratio
P_{T18}/P_o	Duct Nozzle Total to Ambient Pressure Ratio
PNL	Perceived Noise Level, PNdB
$\bar{P}_B/P_o$	Mean Base Pressure Ratio

NOMENCLATURE (concluded)

SPL	Sound Pressure Level, dB
S/D_p	Ejector Axial Spacing to Primary Nozzle Diameter Ratio (see Figure 7-1)
T_{amb}	Ambient Temperature, ° R
T_T	Total Temperature, ° R
T_8	Core Stream Total Temperature, ° R
T_{18}	Duct Stream Total Temperature, ° R
V_j	Fully Expanded Jet Velocity, ft/sec
V_9	Fully Expanded Core Jet Velocity, ft/sec
V_{19}	Fully Expanded Duct Jet Velocity, ft/sec
$W_{O.D.}$	Circumferential Width of Chute Element at Annulus O.D., in.
$W_{I.D.}$	Circumferential Width of Chute Element at Annulus I.D., in.
W_8	Core Stream Weight Flow, pps
W_{18}	Duct Stream Weight Flow, pps

Appendix A - Table of Contents

Table No.	Description	Page
A-1	Design Areas and Discharge Coefficients, Engine and Model	137

Figure No.

A-1	Coannular Non-Coplanar Baseline Nozzle	138
A-2	Bypass Tube Suppressor	139
A-3	Bypass Chute Suppressor	140
A-4	Coplanar-Coannular Baseline Nozzle	141

Drawing No.

JNSD-121573 Sht. 1	Core I.D. Hardware	142
JNSD-040474 Sht. 1	Core O.D. Hardware	143
JNSD-122873 Sht. 1 and 2	Duct I.D. Hardware	144-145
JNSD-123173 Sht. 1 through 5	Duct O.D. Hardware	146-150
101D9508 through 101D9511	Hardwall Ejector with Sharp and Bellmouth Inlets	151-154
665-100-1194 Sht. 1 through 3	Combination P_T/T_T Instrumentation Rakes	155-157

TABLE A-1 DESIGN AREAS AND DISCHARGE COEFFICIENTS, ENGINE AND MODEL

• A_{e8}/A_{e18}= 1.55

	ENGINE UNSUPPRESSED COANNULAR NON-COPLANAR	MODEL 7 UNSUPPRESSED COANNULAR NON-COPLANAR	MODEL 8 UNSUPPRESSED COANNULAR COPLANAR	MODEL 2,5,6 MULTI-TUBE DUCT SUPPR. COANNULAR NON-COPLANAR	MODEL 1,3,4 MULTI-CHUTE DUCT SUPPR. COANNULAR NON-COPLANAR
CORE①					
A_{e8}, in^2	1994	16.815	16.815	16.815	16.815
C_D	.977	.977	.994	.977	.977
A_8, in^2	2041	17.211②	16.917③	17.211	17.211
DUCT					
A_{e18}, in^2	1286	10.842	10.842	10.842	10.842
C_D	.980	.980②	.990③	.948④	.975⑤
A_{18}, in^2	1312	11.064	10.952	11.437	11.120

NOTES:

① CORE NOZZLE REMAINS SAME FOR MODELS 1 THROUGH 7.

② PHYSICAL A_8+A_{18}=28.275 in^2, EQUIVALENT TO PHYSICAL AREA OF 6" DIAMETER NOZZLE.

③ USED FOR PHYSICAL DESIGN OF UNSUPPRESSED COANNULAR COPLANAR THROAT PLANE WITHOUT CORE PLUG.

④ USED FOR PHYSICAL DESIGN OF MULTI-TUBE DUCT SUPPRESSOR THROAT AT EXIT PLANE OF TUBES.

⑤ USED FOR PHYSICAL DESIGN OF MULTI-CHUTE SUPPRESSOR THROAT AT EXIT PLANE OF CHUTES.

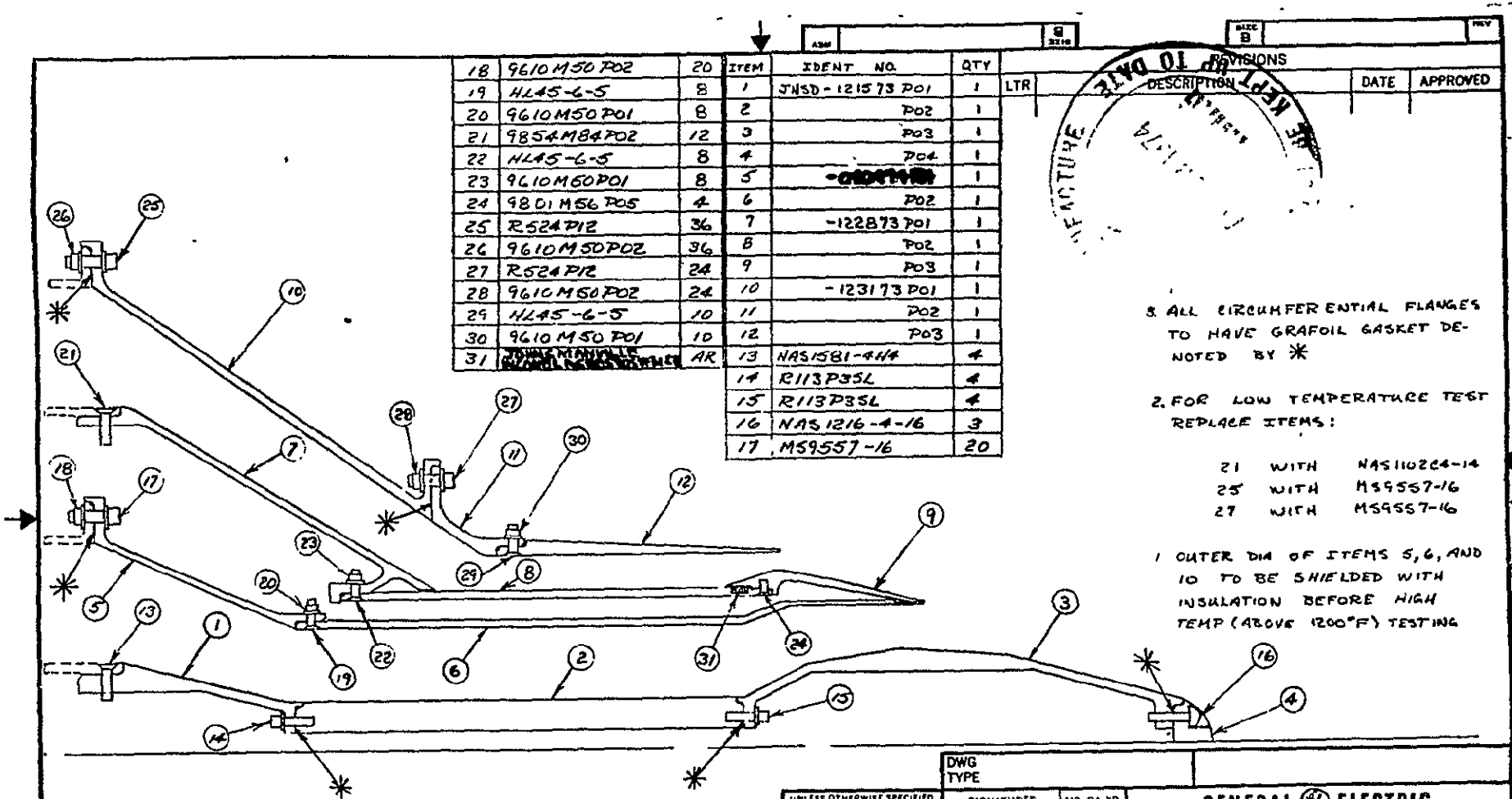

ITEM	IDENT NO.	QTY
1	JNSD-121573 P01	1
2	P02	1
3	P03	1
4	P04	1
5	[redacted]	1
6	P02	1
7	-122873 P01	1
8	P02	1
9	P03	1
10	-123173 P01	1
11	P02	1
12	P03	1
13	NAS1581-4H4	4
14	R113P35L	4
15	R113P35L	4
16	NAS1216-4-16	3
17	MS9557-16	20
18	9610M50P02	20
19	HL45-6-5	8
20	9610M50P01	8
21	9854M84P02	12
22	HL45-6-5	8
23	9610M50P01	8
24	9801M56P05	4
25	R524P12	36
26	9610M50P02	36
27	R524P12	24
28	9610M50P02	24
29	HL45-6-5	10
30	9610M50P01	10
31	[redacted]	AR

LTR	DESCRIPTION	DATE	APPROVED

3. ALL CIRCUMFERENTIAL FLANGES TO HAVE GRAFOIL GASKET DENOTED BY *

2. FOR LOW TEMPERATURE TEST REPLACE ITEMS:

21	WITH	NAS110264-14
25	WITH	MS9557-16
27	WITH	MS9557-16

1 OUTER DIA OF ITEMS 5, 6, AND 10 TO BE SHIELDED WITH INSULATION BEFORE HIGH TEMP (ABOVE 1200°F) TESTING

DWG TYPE

UNLESS OTHERWISE SPECIFIED DIMENSIONS ARE IN INCHES

ALL SURFACES ✓

MATL

SIGNATURES	MO DA YR
DRAWN	2 21 74
CHECKED	
ENGRG	
MFG	
MATL	
ISSUED	

FOR G E USE ONLY

SIMILAR TO

L/O

DR

GENERAL ELECTRIC
AIRCRAFT ENGINE GROUP CINCINNATI OHIO U.S.A.

COANNULAR NON-COPLANAR BASELINE NOZZLE

SIZE	CODE IDENT NO.	DWG NO
B	07482	FIGURE A-1

SCALE | WT CALC ACTUAL | SHEET 1 OF 1

50 1 00

PRINTS TP

138

ORIGINAL PAGE OF POOR QUALITY

GT 5038-P (3-68) PRINTED IN U.S.A.

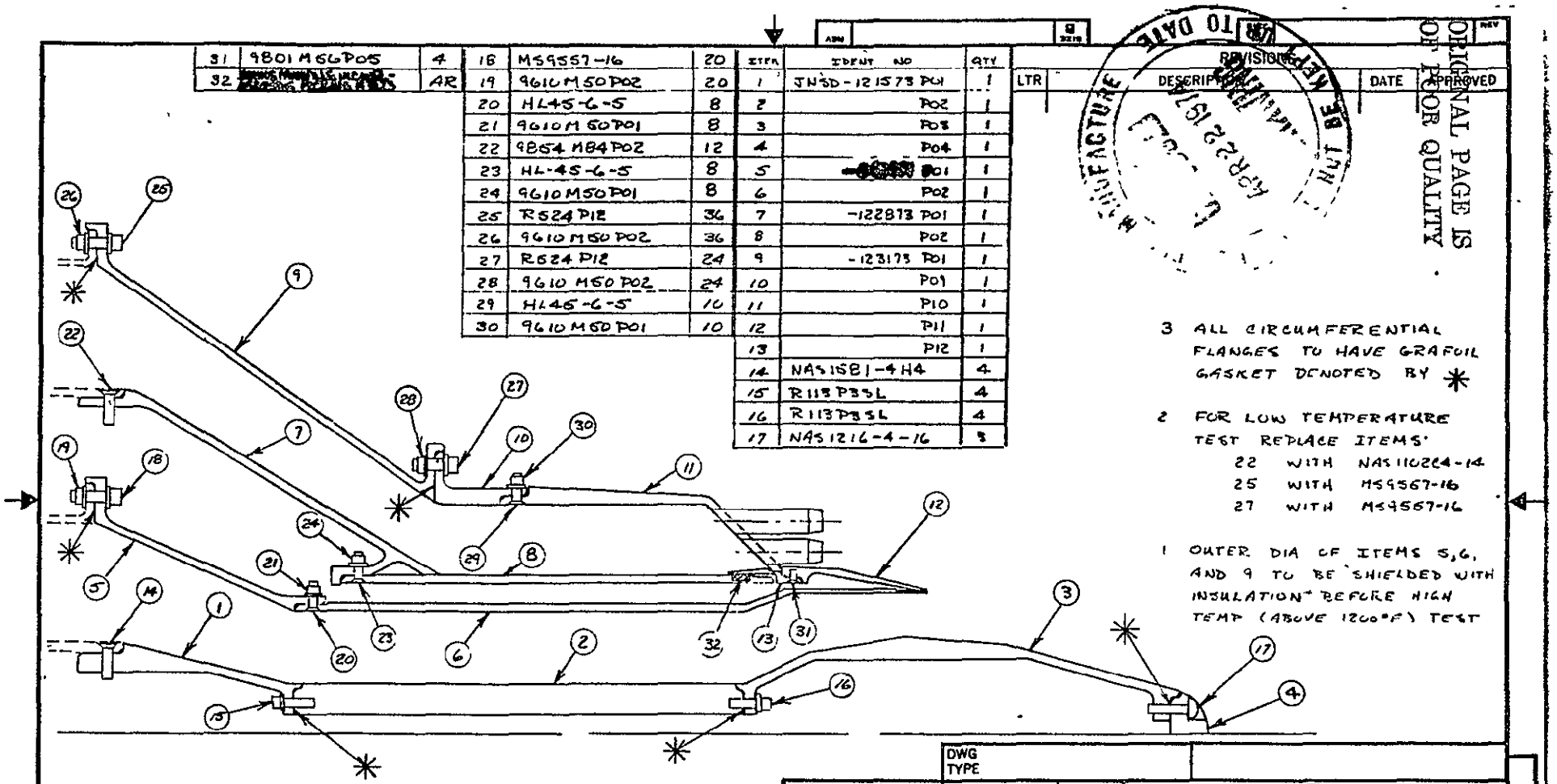

ITEM	IDENT NO	QTY
1	JN5D-121573 P01	1
2	P02	1
3	P03	1
4	P04	1
5	[illegible] P01	1
6	P02	1
7	-122873 P01	1
8	P02	1
9	-123173 P01	1
10	P01	1
11	P10	1
12	P11	1
13	P12	1
14	NAS1581-4H4	4
15	R113P35L	4
16	R113P35L	4
17	NAS1216-4-16	3
18	MS9557-16	20
19	9610M50P02	20
20	HL45-6-5	8
21	9610M50P01	8
22	9854M84P02	12
23	HL-45-6-5	8
24	9610M50P01	8
25	R524P12	36
26	9610M50P02	36
27	R524P12	24
28	9610M50P02	24
29	HL45-6-5	10
30	9610M50P01	10
31	9801M56P05	4
32	[illegible]	AR

3 ALL CIRCUMFERENTIAL FLANGES TO HAVE GRAFOIL GASKET DENOTED BY *

2 FOR LOW TEMPERATURE TEST REPLACE ITEMS:
22 WITH NAS1102C4-14
25 WITH MS9567-16
27 WITH MS9567-16

1 OUTER DIA OF ITEMS 5, 6, AND 9 TO BE SHIELDED WITH INSULATION* BEFORE HIGH TEMP (ABOVE 1200°F) TEST

LTR	DESCRIPTION	DATE	APPROVED

ORIGINAL PAGE IS OF POOR QUALITY

MANUFACTURE NOT TO BE USED AFTER APR 22 19[illegible]

DWG TYPE

UNLESS OTHERWISE SPECIFIED DIMENSIONS ARE IN INCHES

ALL SURFACES ✓

MATL

SIGNATURES	MO DA YR
DRAWN	
CHECKED	
ENGRG	
MFG	
MATL	
ISSUED	

FOR G E USE ONLY
SIMILAR TO
L/O
DR

GENERAL ELECTRIC
AIRCRAFT ENGINE GROUP CINCINNATI OHIO, U.S.A.

EXHAUST DUCT SUPPRESSOR

SIZE	CODE IDENT NO	DWG NO
B	07482	FIGURE A-2

SCALE WT CALC ACTUAL SHEET 1 OF 1

50 1 00

PRINT

GT 9035-P (5-68) PRINTED IN U.S.A.

139

FIGURE 16b

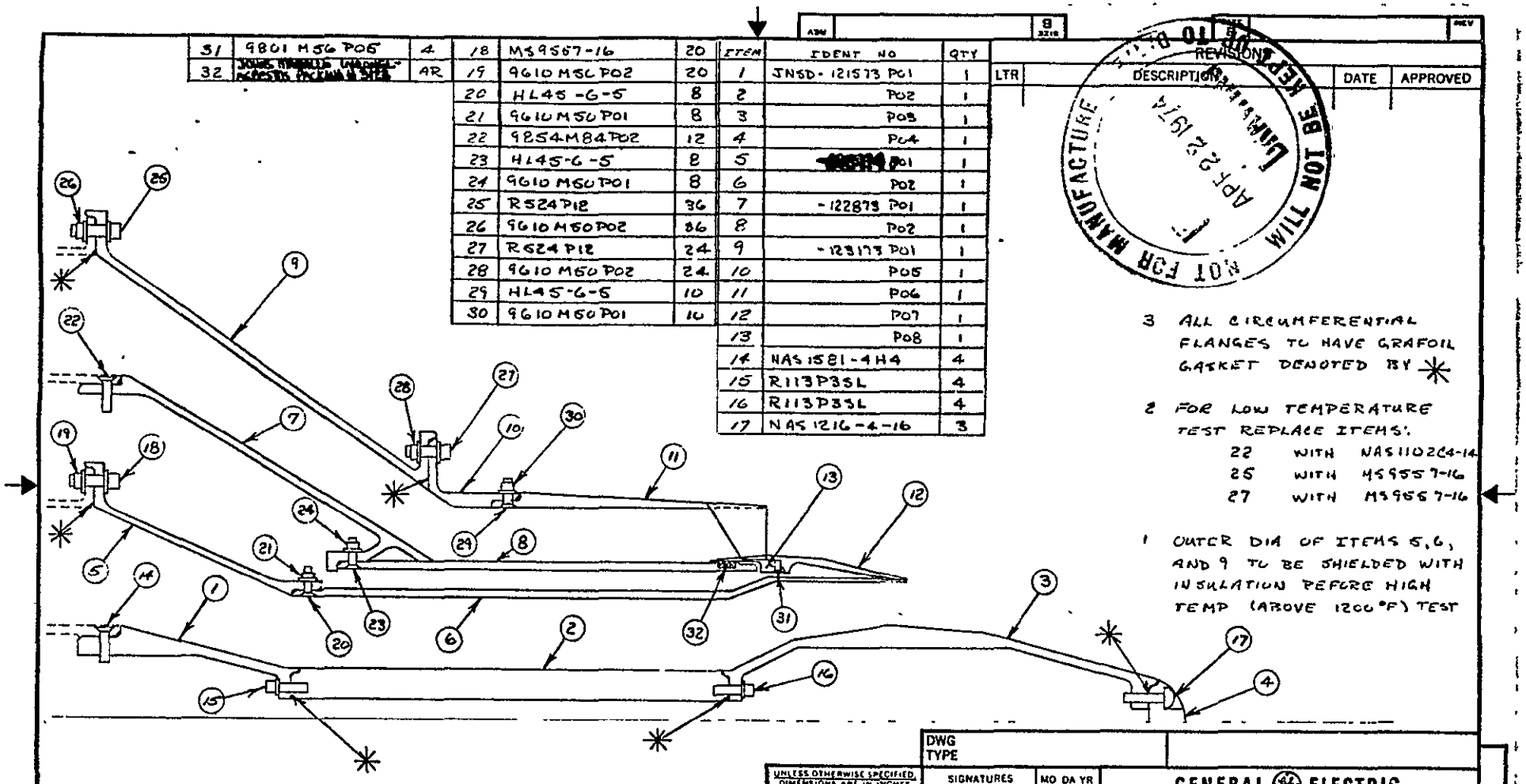

ITEM	IDENT NO	QTY
1	JNSD-121573 P01	1
2	P02	1
3	P03	1
4	P04	1
5	[redacted] P01	1
6	P02	1
7	-122873 P01	1
8	P02	1
9	-123173 P01	1
10	P05	1
11	P06	1
12	P07	1
13	P08	1
14	NAS1581-4H4	4
15	R113P35L	4
16	R113P35L	4
17	NAS1216-4-16	3
18	MS9567-16	20
19	9610M56P02	20
20	HL45-6-5	8
21	9610M50P01	8
22	9854M84P02	12
23	HL45-6-5	8
24	9610M50P01	8
25	R524P12	36
26	9610M50P02	36
27	R624P12	24
28	9610M50P02	24
29	HL45-6-5	10
30	9610M50P01	10
31	9801M56P05	4
32	JOINT, MISCELLANEOUS (ORDERED AS REQUIRED)	AR

3 ALL CIRCUMFERENTIAL FLANGES TO HAVE GRAFOIL GASKET DENOTED BY ✳

2 FOR LOW TEMPERATURE TEST REPLACE ITEMS:
22 WITH NAS1102C4-14
25 WITH MS9557-16
27 WITH MS9567-16

1 OUTER DIA OF ITEMS 5, 6, AND 9 TO BE SHIELDED WITH INSULATION BEFORE HIGH TEMP (ABOVE 1200°F) TEST

LTR	DESCRIPTION	DATE	APPROVED
	REVISIONS		

NOT FOR MANUFACTURE UNLESS RELEASED WILL NOT BE KEPT CURRENT
APR 22 1974

DWG TYPE	

UNLESS OTHERWISE SPECIFIED DIMENSIONS ARE IN INCHES	SIGNATURES	MO DA YR
	DRAWN	2-2274
ALL SURFACES ✓	CHECKED	
	ENGRG	
MATL	MFG	
	MATL	
	ISSUED	

FOR G E USE ONLY
SIMILAR TO
L/D
DR

GENERAL ELECTRIC
AIRCRAFT ENGINE GROUP CINCINNATI OHIO U S A

BYPASS CHUTE SUPPRESSOR

SIZE	CODE IDENT NO	DWG NO
B	07482	FIGURE A-3

SCALE	WT CALC ACTUAL	SHEET
		1 OF 1

PRINTS TO

50 100

140

GT 9029-P (5-68) PRINTED IN U.S.A.

FIGURE 16c

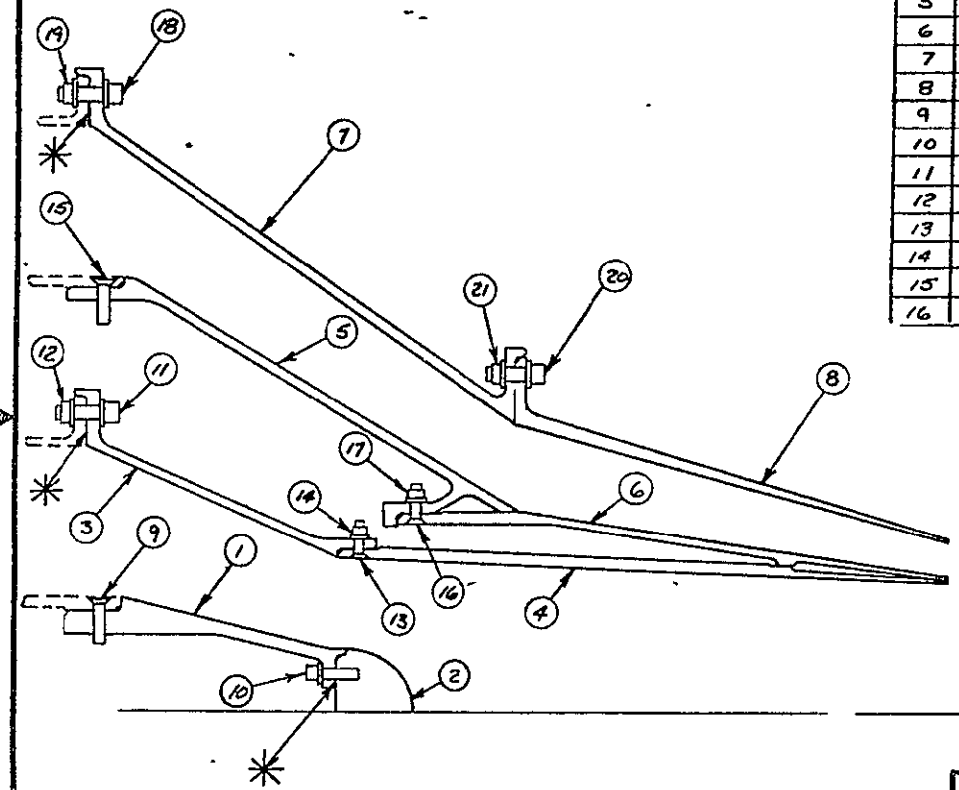

ITEM	IDENT NO	QTY
1	JNSD-121573 P01	1
2	P05	1
3	[redacted]	1
4	P03	1
5	-122873 P01	1
6	P04	1
7	-123173 P01	1
8	P04	1
9	NAS1581-4H4	4
10	R113P33L	4
11	MS9557-16	20
12	9610M50P02	20
13	HL45-6-5	8
14	9610M50P01	8
15	9864MB4P02	12
16	HL45-6-5	8
17	9610M50P01	8
18	R524P12	36
19	9610M50P02	36
20	R524P12	24
21	9610M50P02	24

REVISIONS

LTR	DESCRIPTION	DATE	APPROVED

ORIGINAL PAGE IS
OF POOR QUALITY

NOT FOR MANUFACTURE
APR 22 1974
NOT BE KEPT UP TO DATE

3 ALL CIRCUMFERENTIAL FLANGES TO HAVE GRAFOIL GASKET DENOTED BY ✳

2 FOR LOW TEMPERATURE TEST REPLACE ITEMS:
15 WITH NAS1102C4-14
18 WITH MS9567-16
20 WITH MS9557-16

1 OUTER DIA OF ITEMS 9, 4, AND 7 TO BE SHIELDED WITH INSULATION BEFORE HIGH TEMP (ABOVE 1200°F) TESTING

DWG TYPE

UNLESS OTHERWISE SPECIFIED, DIMENSIONS ARE IN INCHES
ALL SURFACES ✓
MATL

SIGNATURES	MO DA YR
DRAWN	2-27-74
CHECKED	
ENGRG	
MFG	
MATL	
ISSUED	

GENERAL ELECTRIC
AIRCRAFT ENGINE GROUP CINCINNATI OHIO U.S.A.

COPLANAR - CONNULAR BASELINE NOZZLE

SIZE	CODE IDENT NO	DWG NO
B	07482	FIGURE A-4

SCALE 50 1 00 | WT CALC ACTUAL | SHEET 1 OF 1

FOR G E USE ONLY
SIMILAR TO
L/O
DR

GY 9035-P (6-66) PRINTED IN U.S.A.

FIGURE 16d

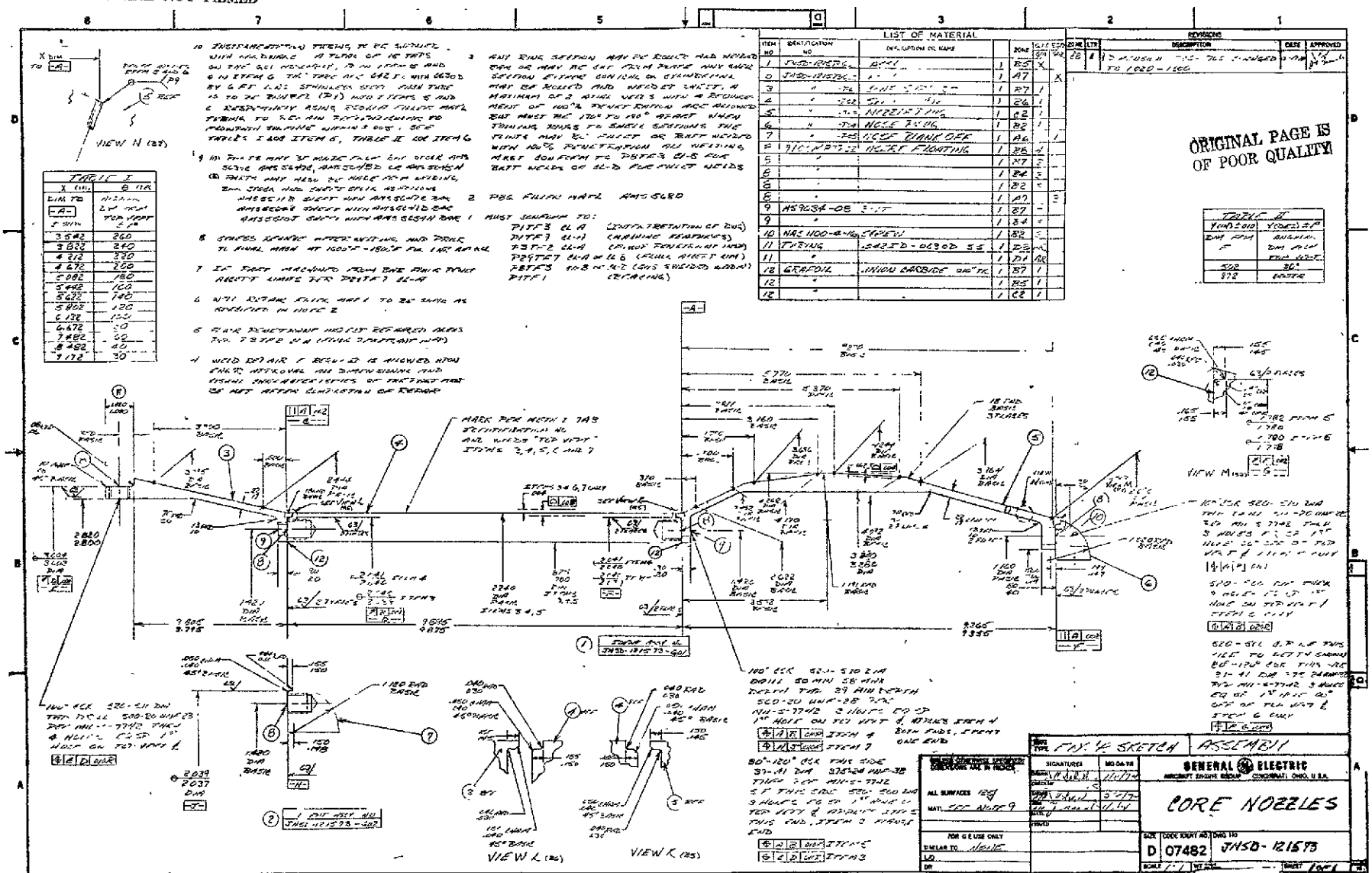

FIGURE 16e

FOLDOUT FRAME 1

ORIGINAL PAGE IS OF POOR QUALITY

FOLDOUT FRAME 2

ORIGINAL PAGE IS OF POOR QUALITY

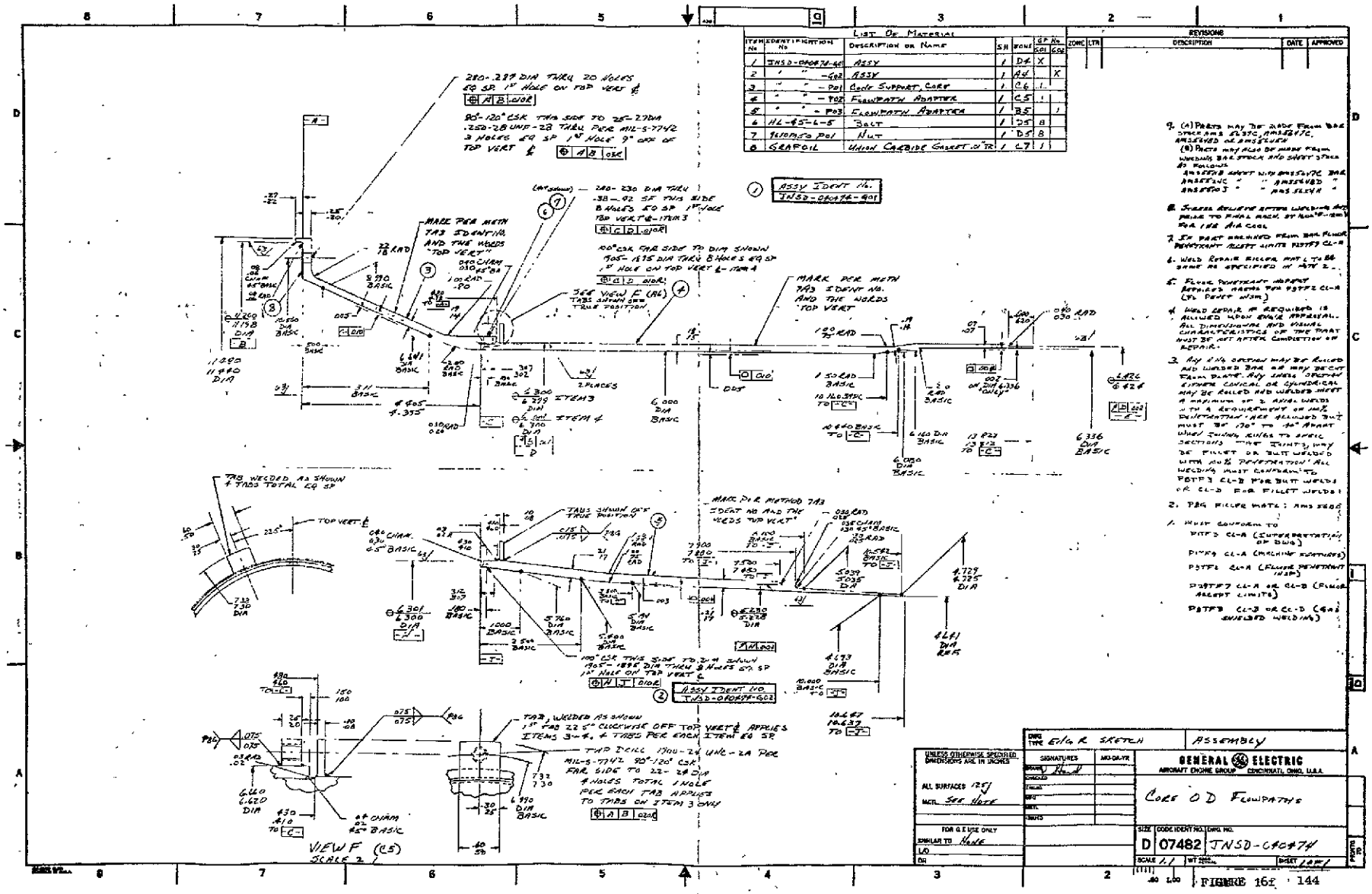

FIGURE 16. 144

FOLDOUT FRAME 1

ORIGINAL PAGE IS OF POOR QUALITY

FOLDOUT FRAME 2

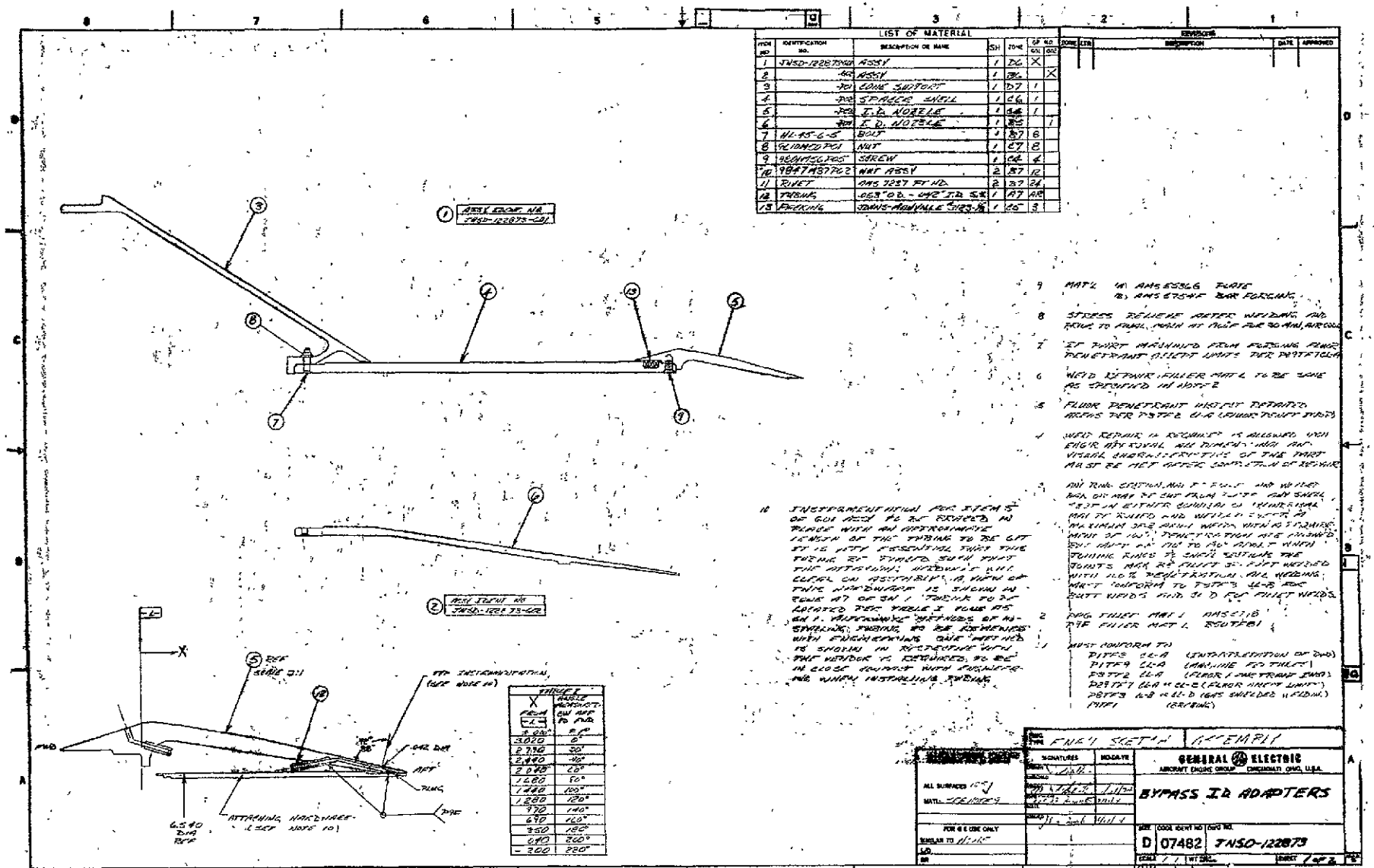

ITEM NO	IDENTIFICATION NO.	DESCRIPTION OR NAME	SH	ZONE	QP REQ GOV	QP REQ GOV
1	7NSD-122873-G01	ASSY	1	D6	X	
2	-G02	ASSY	1	D6		X
3	-701	CONE SUPPORT	1	D7	1	
4	-702	SPACER SHELL	1	C6	1	
5	-703	I.D. NOZZLE	1	C6	1	
6	-704	I.D. NOZZLE	1	B5		1
7	NL-45-6-5	BOLT	1	B7	6	
8	SU3MG5701	NUT	1	C7	8	
9	MS27039C5S	SCREW	1	C6	4	
10	9B47A87G2	NUT ASSY	2	B7	12	
11	RIVET	MS 7237 FT HD.	2	B7	24	
12	TUBING	.063"O.D. - .042"I.D. SST	1	A7	AR	
13	PACKING	JOHNS-MANVILLE 5123-75	1	D6	3	

X FROM F.S.	ANGLE RELATIVE TO AFT (CW AS VIEWED FROM FWD)
3.020	0°
2.710	30°
2.440	40°
2.095	60°
1.660	80°
1.480	100°
1.280	120°
.970	140°
.690	160°
.350	180°
.040	200°
-.300	220°

9 MATL (A) AMS 6304 PLATE (B) AMS 6304 BAR FORGING

8 STRESS RELIEVE AFTER WELDING AND PRIOR TO FINAL MACH AT 1150°F FOR 30 MIN, AIR COOL

7 ET PART MARKINGS FROM FLUORESCENT PENETRANT INSPECT LIMITS PER PARAGRAPH

6 WELD REPAIR FILLER MATL TO BE SAME AS SPECIFIED IN NOTE 2

5 FLUOR PENETRANT INSPECT DETAILED WELDS PER PARA 4.4.6 (FLUOR PENETRANT INSPECT)

4 WELD REPAIR IS ACCEPTABLE AS ALLOWED UNDER ANY REVISION AND DIMENSIONAL AND VISUAL INSPECTION OF THIS PART MUST BE MET AFTER COMPLETION OF REPAIR

3 ANY TOOL CUTTING MARKS, FAULTS AND WELDED REPAIRS MAY BE CUT FROM PARTS. CUT SHALL RESULT IN EITHER CONVEX OR CONCAVE RADII TO BLEND AND WELD. CUTTER TO MAINTAIN SPEED AND FEED WITH RESULTANT DEPTH OF CUT. PENETRATION NOT TO EXCEED .060" AND NOT TO BE ABRUPT WITH TURNING RADII TO ENSURE SMOOTH JOINTS. MACH TO FINAL PART WELDED WITH 100% PENETRATION. ALL WELDING MUST CONFORM TO PARA 3.4.3 AND BUTT WELDS PER 3.4.3.1 FOR FILLET WELDS

2 APPD FILLET MATL: AMS 5788 (OR FILLER MATL: BOLTED)

1 MUST CONFORM TO:
PIPE1 (INSTALLATION OF DWG)
PIPE2 (MACHINE TO FINAL)
PIPE3 (FLUOR PENETRANT INSP)
PIPE4 (FLUOR INSPECT LIMITS)
PIPE5 (WELDING)
PIPE (GRAVING)

10 INSTRUMENTATION PORT SIZE 5 OF 6 TO BE PROVIDED IN PLANE WITH AN APPROXIMATE LENGTH OF THE TUBING TO BE CUT SO IT IS VERY ESSENTIAL THAT THIS TUBING BE TURNED SUCH THAT THE ATTACHING HARDWARE WILL CLEAR ON ASSEMBLY. A VIEW OF THIS HARDWARE IS SHOWN IN ZONE B7 OF SH 1. TUBING TO BE LOCATED PER TABLE I FOUND AS SH 1. ALTERNATE METHODS OF WELDING TUBING TO BE REMARKED WITH ENGINEERING CASE NOT NOTED IS SHOWN IN RECEIPT OF WORK THAT HARDWARE IS CONSIDERED TO BE IN CLOSE COMPLIANCE WITH ENGINEERING WHEN INSTALLING TUBING

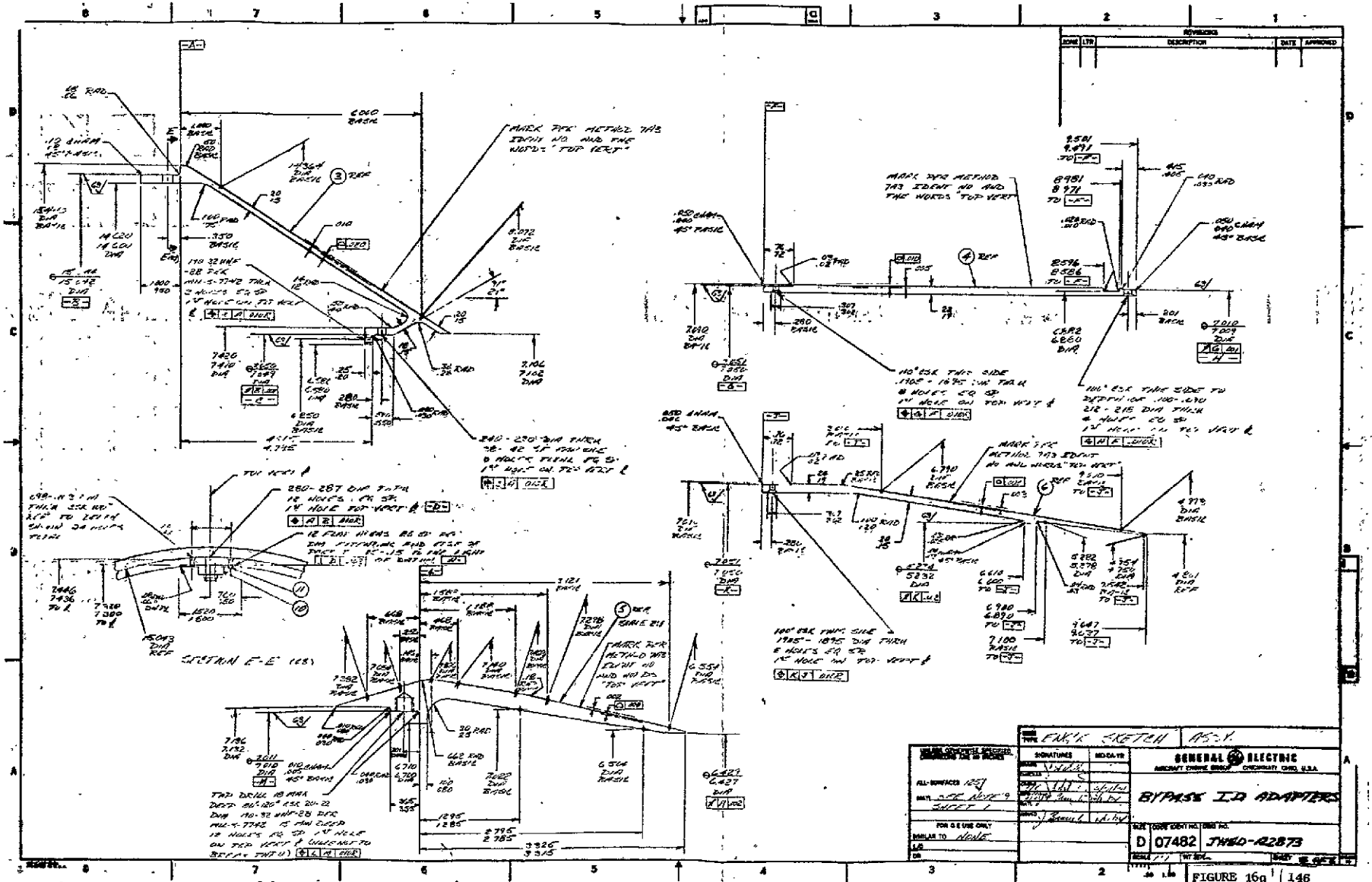

FIGURE 16g | 146

FOLDOUT FRAME 1

ORIGINAL PAGE IS
OF POOR QUALITY

FOLDOUT FRAME 2

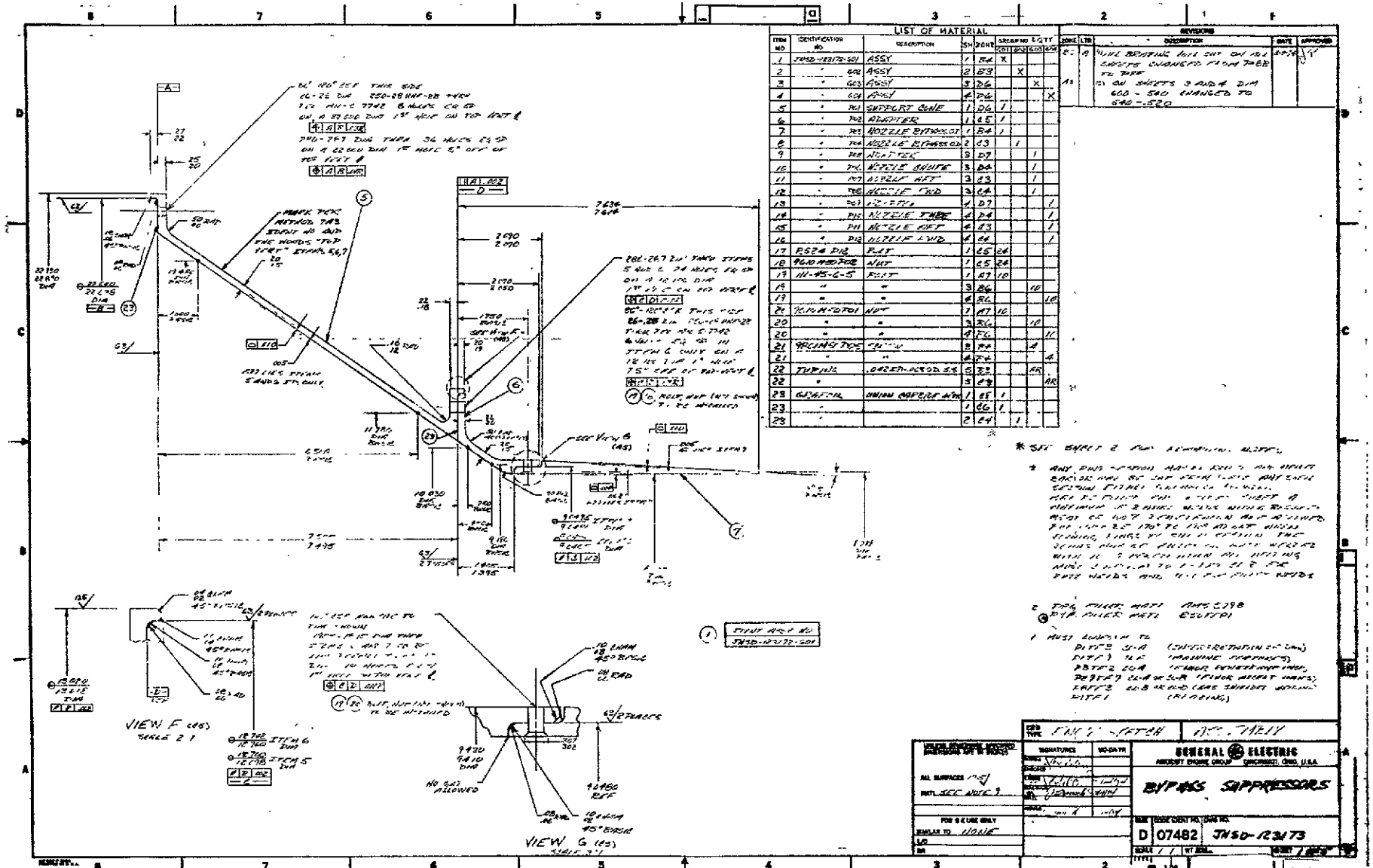

FIGURE 16h

ORIGINAL PAGE IS
OF POOR QUALITY

FOLDOUT FRAME 1

FOLDOUT FRAME 2

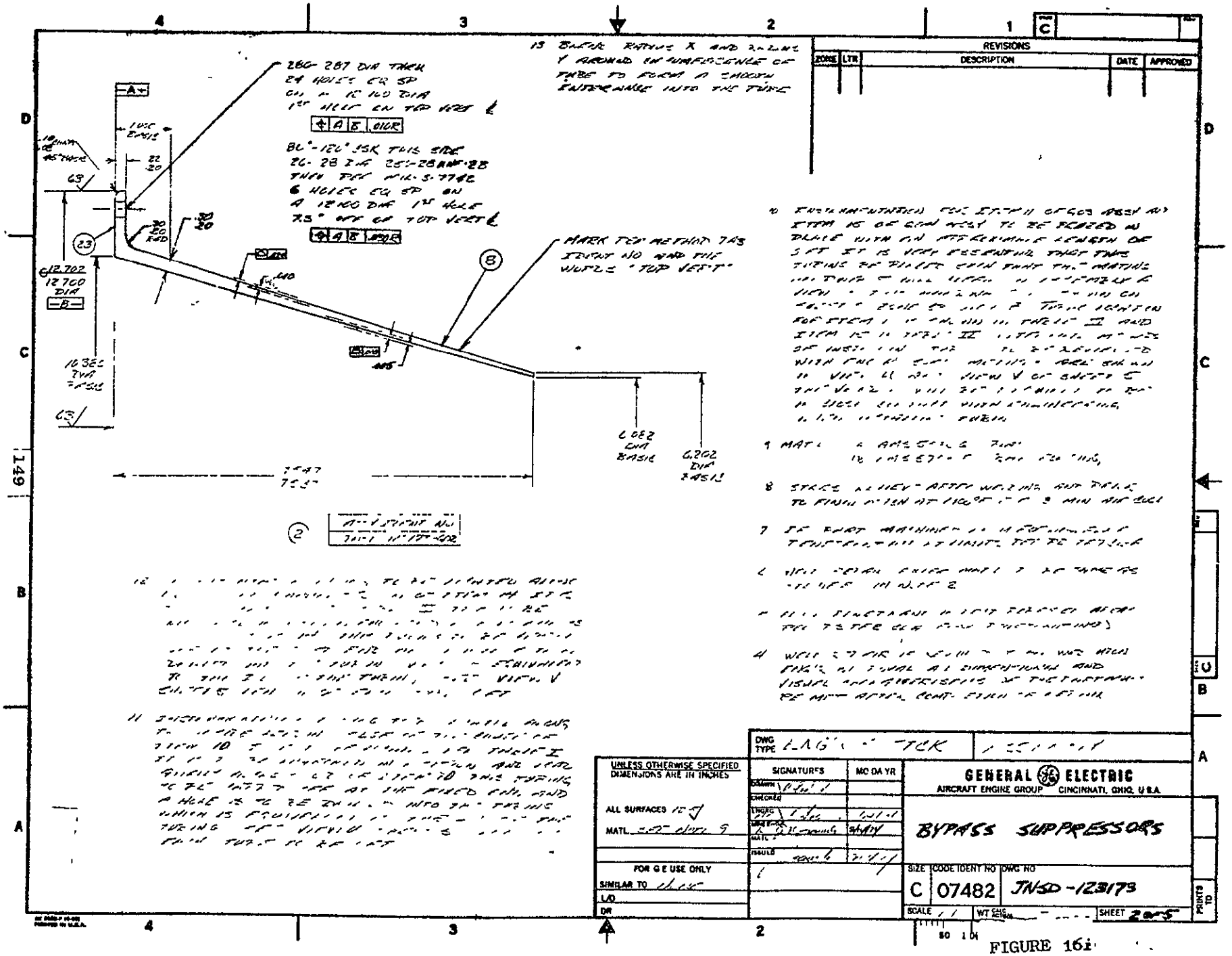

FIGURE 16i

PRECEDING PAGE BLANK NOT FILMED

PRECEDING PAGE BLANK NOT FILMED

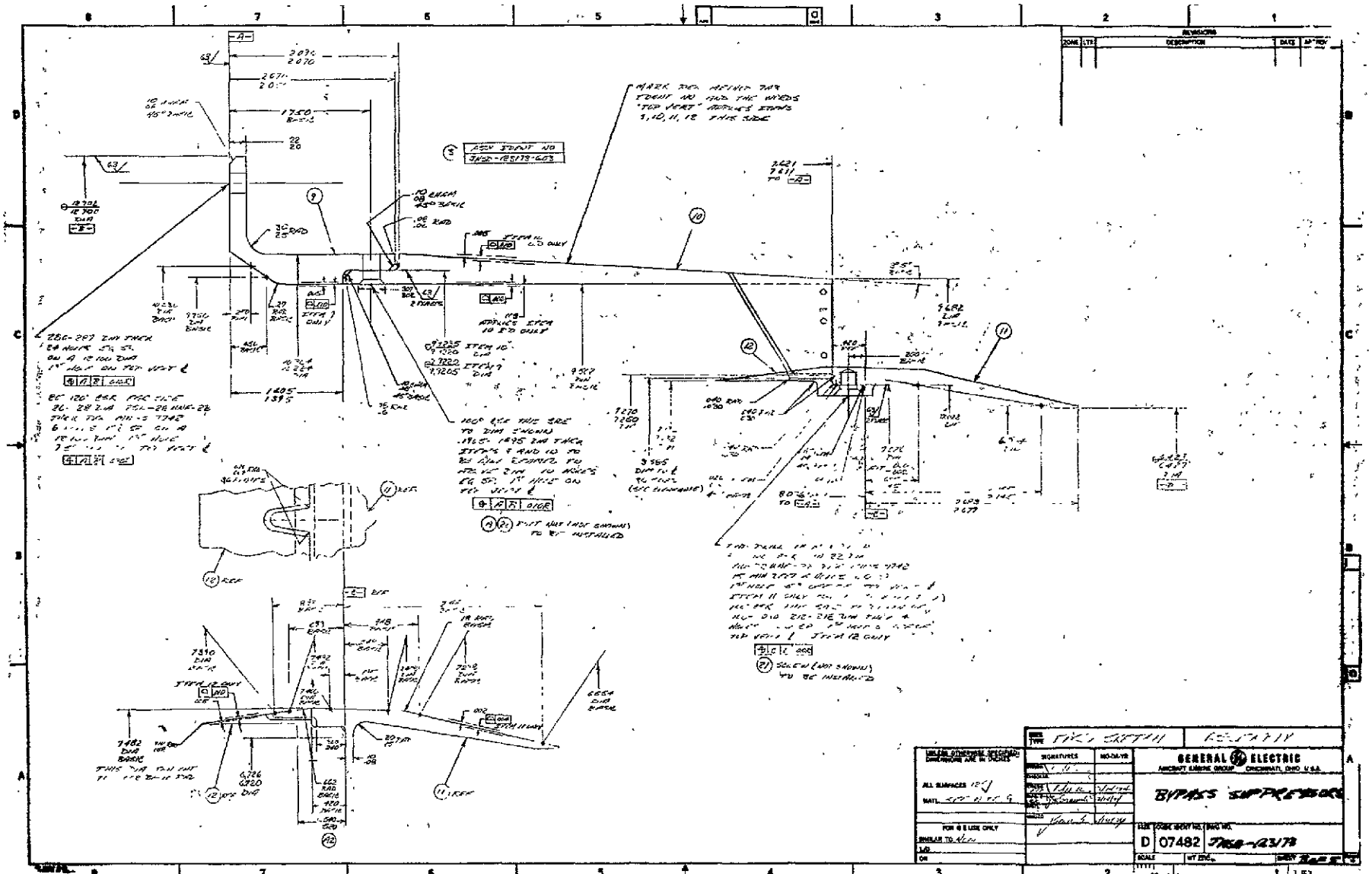

FIGURE 16j

FOLDOUT FRAME 1

ORIGINAL PAGE IS
OF POOR QUALITY

FOLDOUT FRAME 2

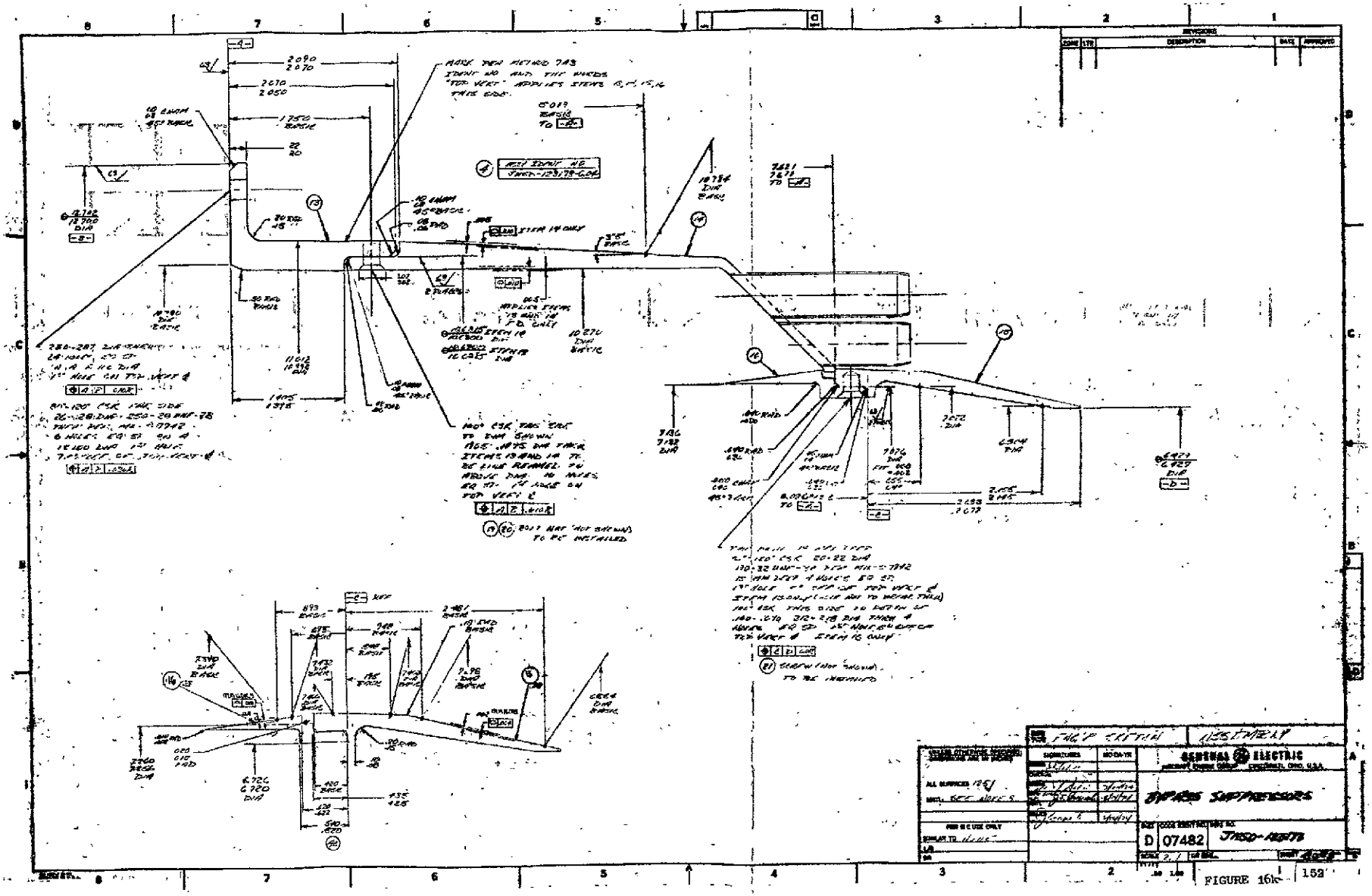

FIGURE 16k

ORIGINAL PAGE IS
OF POOR QUALITY

FOLDOUT FRAME 1

FOLDOUT FRAME 2

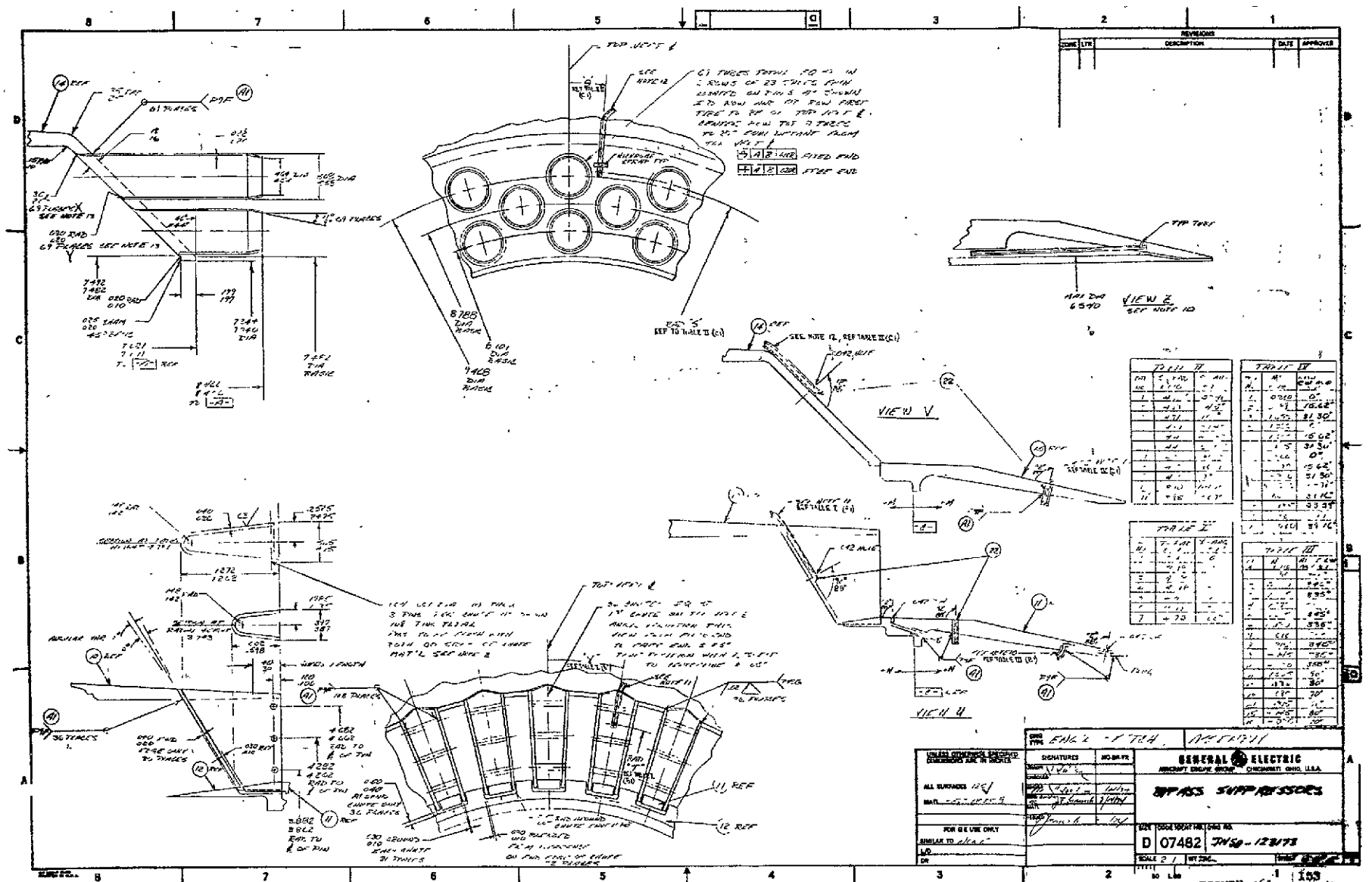

FIGURE 161

FOLDOUT FRAME 1

ORIGINAL PAGE IS OF POOR QUALITY

FOLDOUT FRAME 2

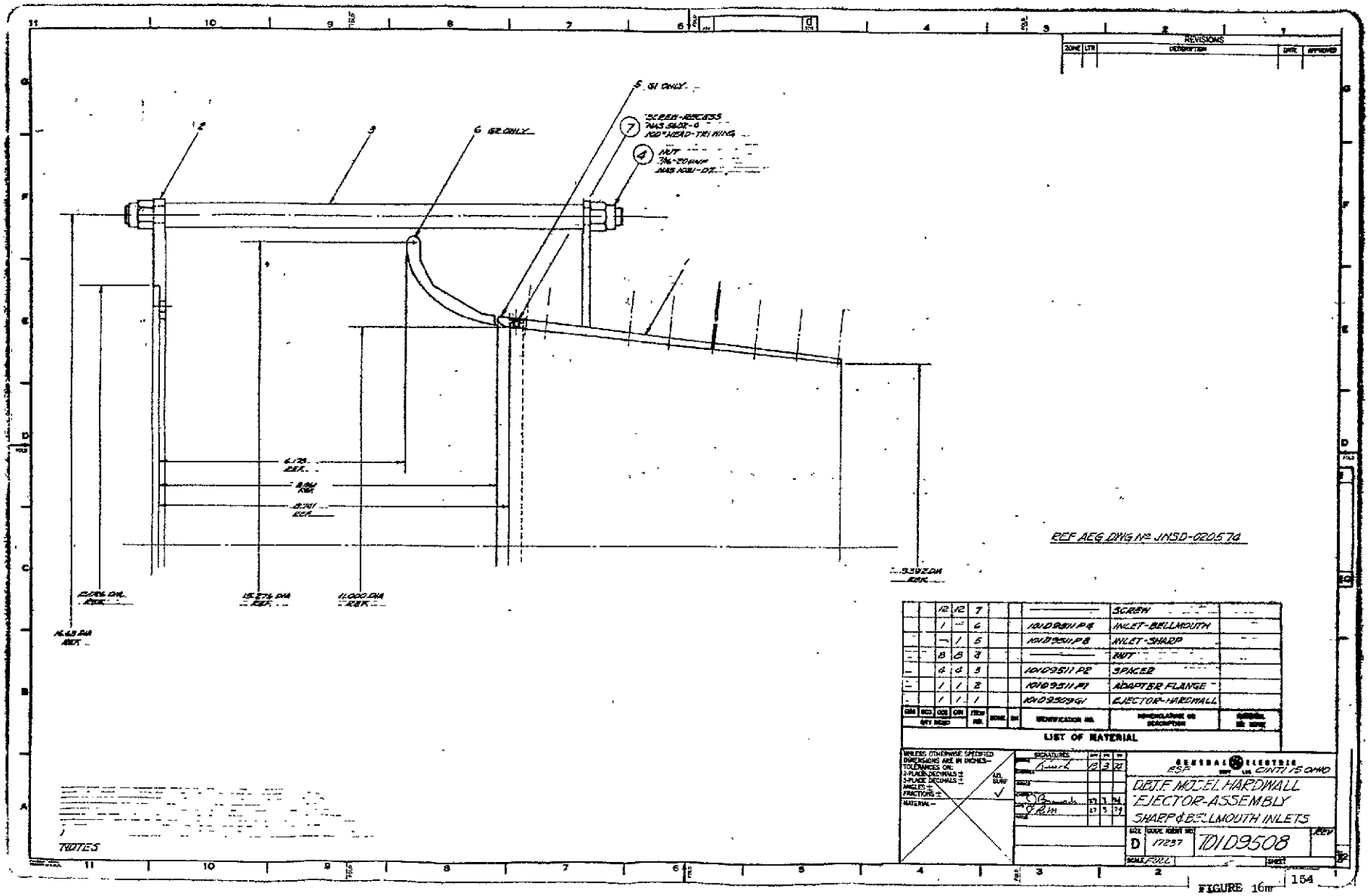

FIGURE 16m

FOLDOUT FRAME 1

ORIGINAL PAGE IS
OF POOR QUALITY

FOLDOUT FRAME 2

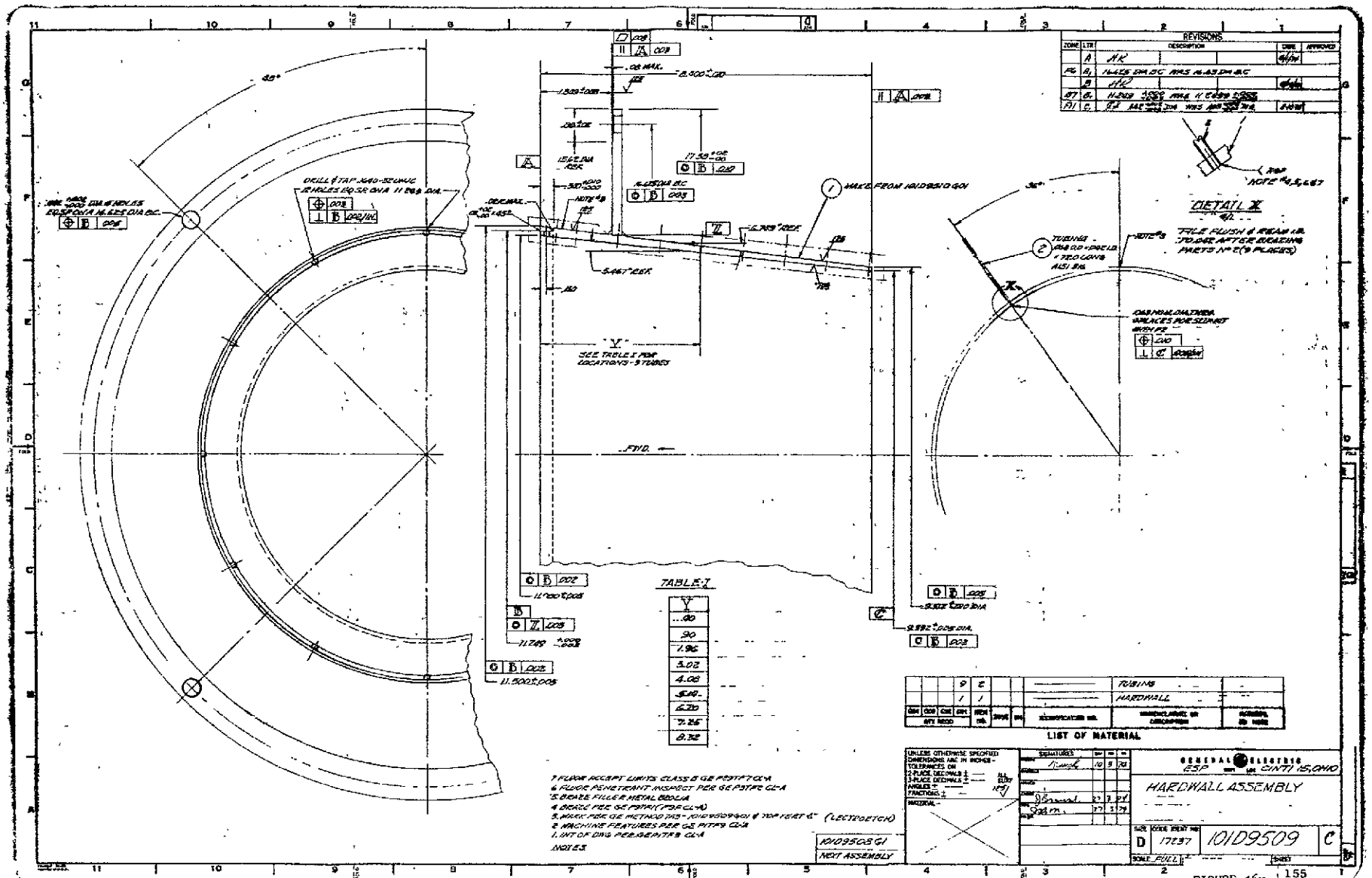

FIGURE 16n

FOLDOUT FRAME 1

ORIGINAL PAGE IS
OF POOR QUALITY

FOLDOUT FRAME 2

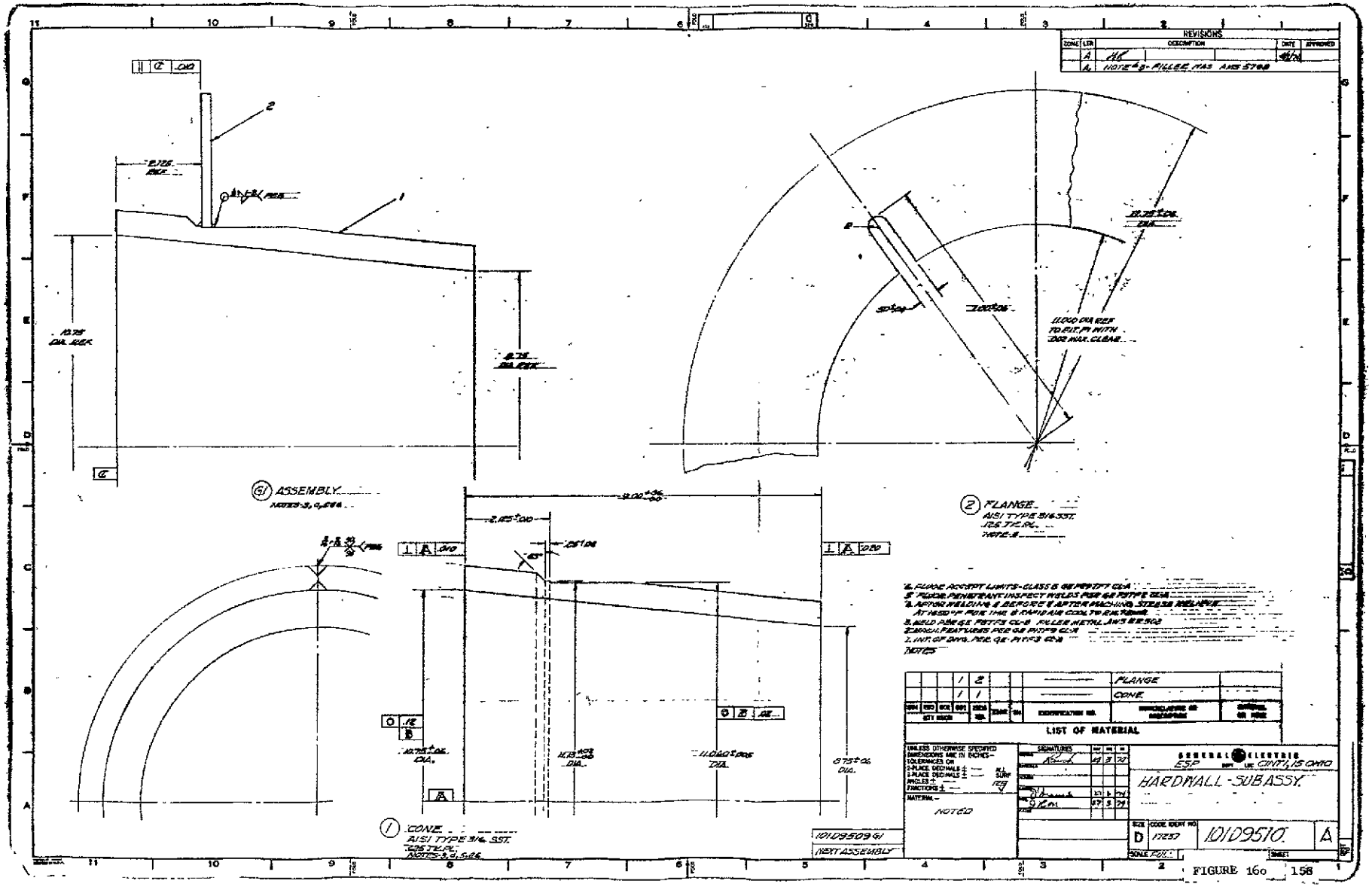

FIGURE 16o 158

FOLDOUT FRAME 1

ORIGINAL PAGE IS
OF POOR QUALITY

FOLDOUT FRAME 2

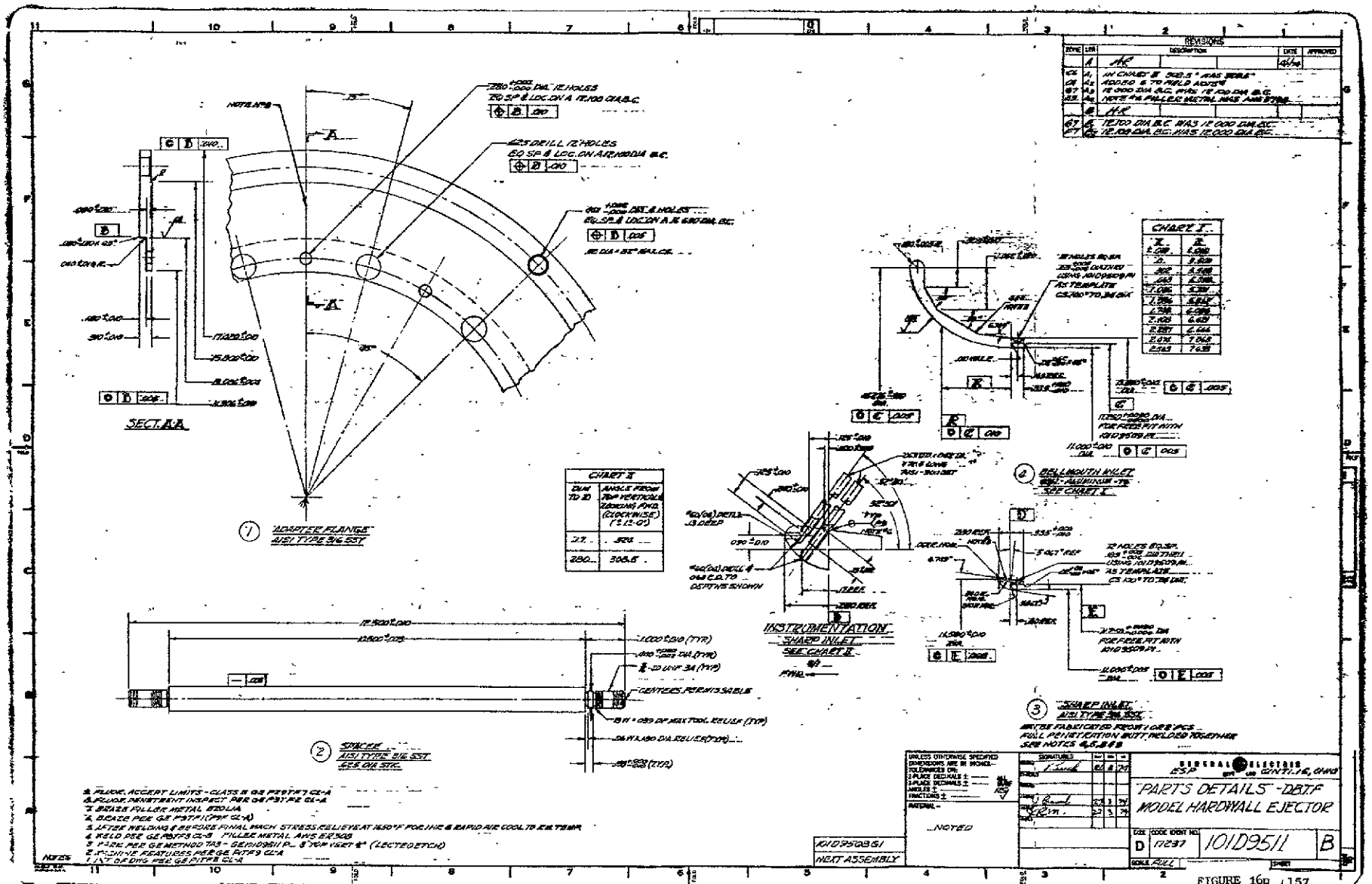

FIGURE 16p 157

FOLDOUT FRAME 1

ORIGINAL PAGE IS
OF POOR QUALITY

FOLDOUT FRAME 2

ORIGINAL PAGE IS
OF POOR QUALITY

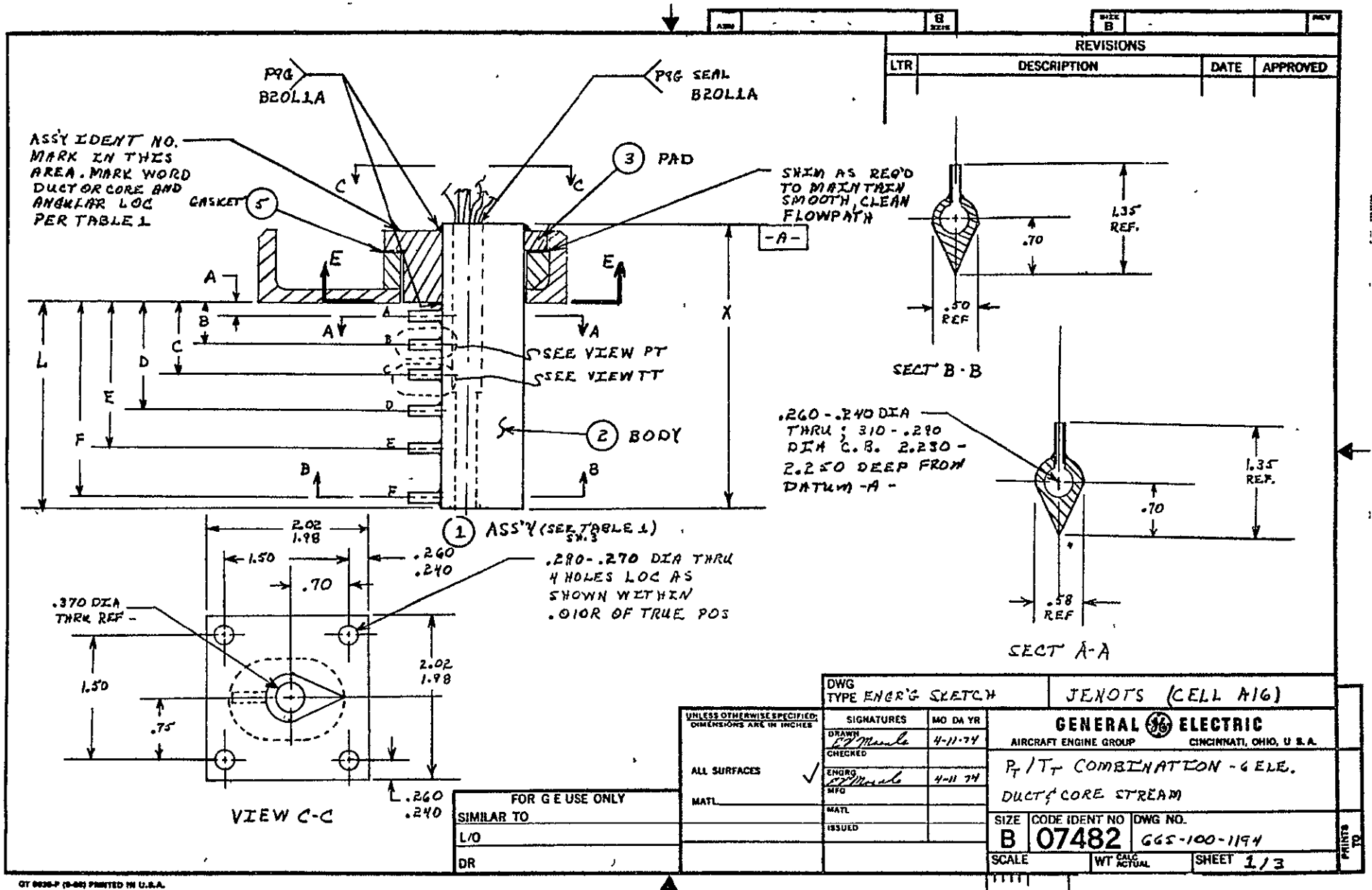

FIGURE 16r

PRECEDING PAGE BLANK NOT FILMED

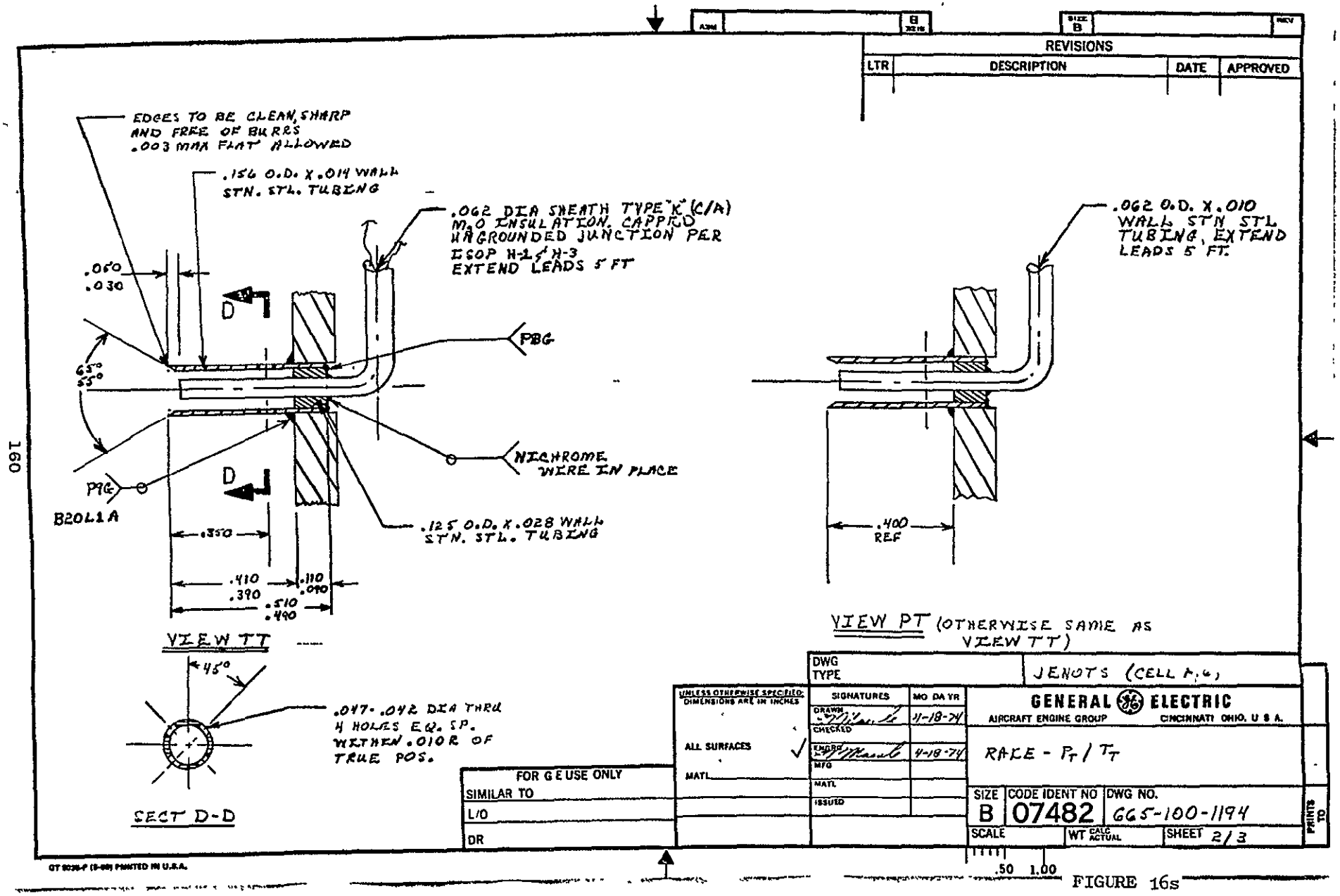

160

FIGURE 16s

ASS'Y / LENGTH	(DUCT) G01 (30°) DIM	VIEW	(DUCT) G02 (210°) DIM	VIEW	(CORE) G03 (0°) DIM	VIEW	(CORE) G04 (180°) DIM	VIEW	TOLERANCE
A	.199	PT	.199	TT	.164	PT	.164	TT	±.010
B	.609	TT	.609	PT	.512	TT	.512	PT	±.010
C	1.037	PT	1.037	TT	.891	PT	.891	TT	±.010
D	1.486	TT	1.486	PT	1.312	TT	1.312	PT	±.010
E	1.958	PT	1.958	TT	1.793	PT	1.793	TT	±.010
F	2.458	TT	2.458	PT	2.370	TT	2.370	PT	±.010
L	2.600	—	2.600	—	2.500	—	2.500	—	±.020
X	3.600	—	3.600	—	3.500	—	3.500	—	±.020
Y	.847 -.837		.847 -.837		.667 -.657		.667 -.657		—
R	10.440		10.440		4.720		4.720		±.005

TRBLE 1: RAKE DIM AND LOC

REVISIONS

LTR	DESCRIPTION	DATE	APPROVED

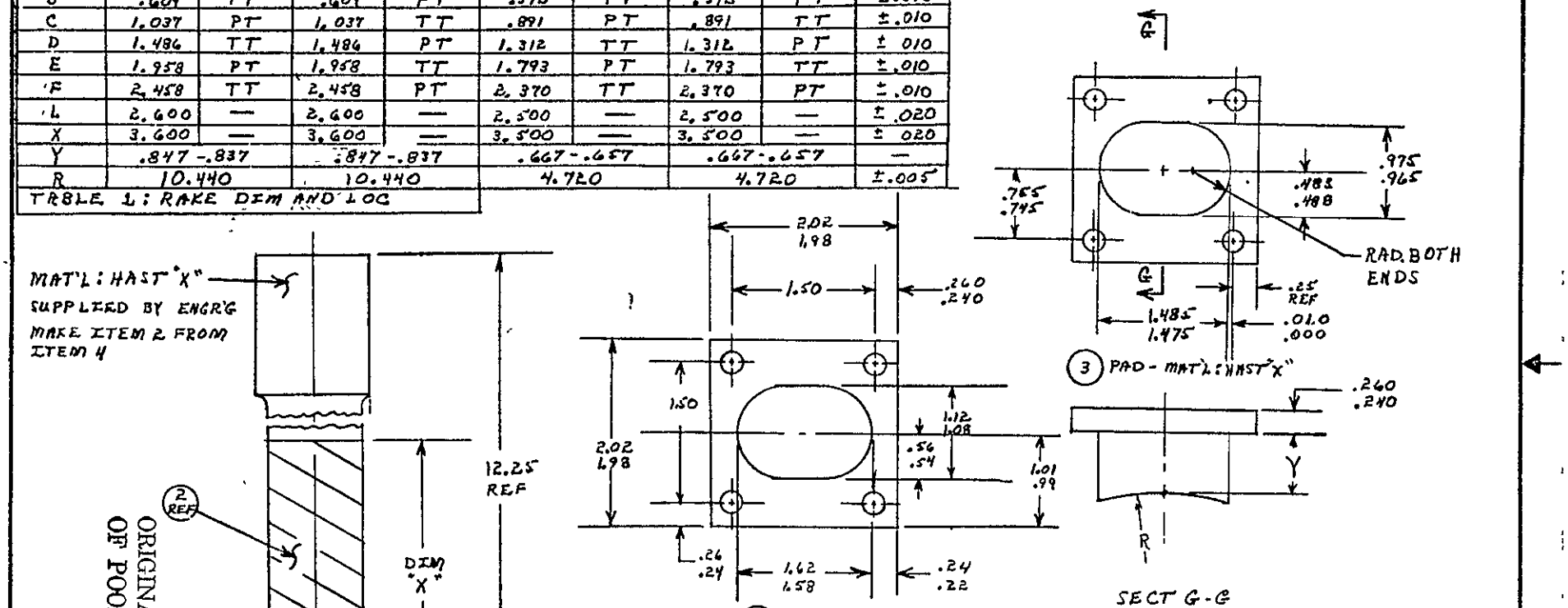

ORIGINAL PAGE IS OF POOR QUALITY

DWG TYPE ENGR'G SKETCH		JENOTS (CELL A16)
UNLESS OTHERWISE SPECIFIED DIMENSIONS ARE IN INCHES	SIGNATURES	MO DA YR
	DRAWN	4-18 74
	CHECKED	
ALL SURFACES ✓	ENGR	4-18-74
MATL AS NOTED	MFG	
	MATL	
	ISSUED	
FOR G E USE ONLY: SIMILAR TO		
L/O		
DR		

GENERAL ELECTRIC
AIRCRAFT ENGINE GROUP — CINCINNATI, OHIO, U.S.A.

RAKE - P_T / T_T

SIZE	CODE IDENT NO	DWG NO
B	07482	G65-100-1194

SCALE | WT CALC / ACTUAL | SHEET 3/3

PRINTS TO

50 100

FIGURE 16t

FLUIDYNE ENGINEERING CORPORATION

HOT/COLD FLOW MODEL TESTS TO DETERMINE STATIC PERFORMANCE OF DUCT NOISE SUPPRESSION NOZZLES

by
Robert A. Kirschbaum
Richard G. Brasket

Conducted for
General Electric Company
Aircraft Engine Group
Cincinnati, Ohio 45215

General Electric Purchase Order No. 200-4XX-14G31451
FluiDyne Report 1008
July 1974

Approved: Richard G. Brasket
Richard G. Brasket, Group Head
Propulsion Test Operation

Owen P. Lamb
Owen P. Lamb
Vice President

SUMMARY

This report presents the results of hot/cold flow model tests conducted to determine static performance of several dual-flow exhaust nozzles with duct noise suppression. The test program was conducted by FluiDyne Engineering Corporation for General Electric Company under Purchase Order No. 200-4XX-14G31451. The model tests were performed in the Channel 11 static thrust stand at the FluiDyne Medicine Lake Aerodynamic Laboratory.

Five configurations of a dual-flow plug-nozzle model were tested. The baseline configuration represented a co-annular unsuppressed duct-burning turbofan nozzle. Two configurations used noise suppressors deployed in the fan duct (either 69 tubes or 36 spokes). Two more configurations were obtained by adding an ejector shroud to each of the suppressor designs.

Facility checkout tests were made using two standard ASME long-radius metering nozzles. These tests demonstrated facility data accuracy at flow conditions similar to the dual-flow nozzle tests.

Test conditions included fan nozzle pressure ratios from $\lambda_{18} = 1.5$ to 4 and core nozzle pressure ratios from $\lambda_8 = 1.3$ to 2. The model air was generally at ambient temperature (cold-flow). One configuration, the multi-tube suppressor with ejector, was also tested with the model airflows heated to 1000°R and 1460°R. The test program totaled 59 data points, including 15 ASME nozzle tests.

Test results include nozzle thrust coefficients, fan and core nozzle discharge coefficients, and surface static pressure distributions.

TABLE OF CONTENTS

		Page
SUMMARY		i
TABLE OF CONTENTS		ii
LIST OF FIGURES		iii
DEFINITION OF SYMBOLS		iv
1.0	INTRODUCTION	1
2.0	FACILITY DESCRIPTION	2
3.0	MODEL DESCRIPTION	4
3.1	General Electric Dual-Flow Nozzles	4
3.2	Standard ASME Nozzles	6
4.0	DATA ANALYSIS PROCEDURES	7
4.1	Flow Rates	7
4.2	Discharge Coefficients	10
4.3	Thrust Measurement	11
4.4	Thrust Coefficient	13
4.5	Pressure and Temperature Data	15
4.6	Force Balance Calibration	15
5.0	PRESENTATION OF RESULTS	18
5.1	ASME Checkout Tests	18
5.2	General Electric Suppressor Nozzle Tests	19

REFERENCES

FIGURES

DATA AND CALCULATIONS (under separate cover)

LIST OF FIGURES

Figure	Description
1	Channel 11 Facility Layout
2	ASME Checkout Test Assembly
3	Model Adapters Assembly
4a-e	Model Photographs
5a	Station Notation, Cold-Flow Model Tests
5b	Station Notation, Hot-Flow Model Tests
5c	Station Notation, ASME Checkout Tests
6	Run Schedule and Tabulation of Major Test Results
7a-c	Test Results, ASME Nozzle Tests
8a-c	Thrust Coefficients
9a-c	Fan Nozzle Discharge Coefficients
10a-c	Core Nozzle Discharge Coefficients

DEFINITION OF SYMBOLS

A	Cross-section area, $in.^2$
c	Real-gas A/A* correction factor, dimensionless
C_x	Axial balance readout, counts
C_D	Discharge coefficient, dimensionless
C_T	Static thrust coefficient, dimensionless
D	Diameter
F	Stream thrust, lb.
f	Exit stream thrust parameter, dimensionless
g	Acceleration of gravity, 32.174 $ft./sec.^2$
G	Real-gas stream thrust correction factor, dimensionless
H	Axial thrust component, lb.
H_x	Axial balance force, lb.
K	Critical weight flow parameter, $°R^{1/2}/sec.$
K_x	Axial balance force calibration factor, lb./count
L	Calibration load, lb.
m	Mass flow rate, slugs/second
P	Pressure, static unless otherwise specified by subscript, psia
ΔP	Static pressure difference across seal, psi
r	Radial distance, in.
R_N	Reynolds number, dimensionless
T	Temperature, °R
v	Velocity, ft./sec.
W	Weight flow rate, lb./sec.
y	Distance from wall
δ	Boundary layer thickness
γ	Ratio of specific heats, dimensionless
Δ	Incremental quantity
λ	Pressure ratio, P_t/P_a, dimensionless
θ	Meridian angle measured clockwise looking upstream, degrees
ρ	Density, $slugs/ft.^3$

Subscripts

a	Ambient
e	Exit
i	Ideal
t	Total conditions
w	Wall
∞	Freestream
1,2,4,5,8,18	See Figures 5a-5c

Superscripts

*	Sonic condition

1.0 INTRODUCTION

This experimental study was conducted to determine aerodynamic performance of five model configurations of a duct-burning turbofan exhaust nozzle with noise suppression. The test program was defined by General Electric Technical Memorandum 74-39, "Test Specification - Dual Flow Nozzle with Duct Noise Suppression Model Test for NASA Duct-Burning Turbofan Jet Noise Program." Test objectives were to determine nozzle thrust coefficients, discharge coefficients for each of the two streams, and static pressure distributions on the model surfaces. Technical liaison for General Electric was performed by Mr. Paul S. Staid and Mr. John F. Brausch.

The model hardware was supplied by General Electric. Model-to-facility adapters, and additional flow conditioning elements, were designed and fabricated by FluiDyne. Model tests were conducted in FluiDyne's two-temperature-flow static thrust stand (Channel 11) with the model exhausting directly to atmosphere.

This report describes the test facility, test models, data acquisition and analysis procedures, and presents the test results. Test conditions and major test results are tabulated in Figure 6 and are plotted in Figures 7-10. Detailed data and calculations are tabulated in the Appendix.

2.0 FACILITY DESCRIPTION

The tests were performed in Channel 11 at FluiDyne's Medicine Lake Aerodynamic Laboratory. Channel 11 is a two-temperature flow static thrust stand used to determine performance of exhaust nozzles in which the two exhaust flows are at different temperatures. Nozzle thrust is determined from force measurement with a strain gage force balance. The general arrangement of Channel 11 is shown in Figure 1. Photographs of test model installations are presented in Figure 4.

The airflows for both the cold and hot passages of a test nozzle are obtained from the facility high-pressure dry air storage system. Air for the cold passage is throttled, metered through a long-radius ASME nozzle, ducted to the cold passage of the test nozzle, and finally exhausted to atmosphere. Air for the hot passage is throttled, passed through a regenerative storage heater, mixed with unheated bypass flow to achieve a desired temperature, metered through a long-radius ASME nozzle, ducted to the hot passage of the test nozzle, and finally exhausted to atmosphere.

The air heater used for the hot flow contains alumina pebbles which are preheated to approximately 1250°F with a combustion heater. The heater capacity is nominally 40 lbs./sec. at 1200°F.

The model assembly is supported by a strain gage force balance and is isolated from the facility piping by two elastic seals; see schematic in Figure 5. Calibration of the balance and seals is described in Section 4.6.

The ASME meter at Station 1 is water-cooled to protect the elastic seal from thermal effects. Since the cooling water is confined to the upstream (i.e., non-metric) hardware only, no tare forces are introduced by the water supply lines.

Facility instrumentation is provided to calculate mass flow rates at Stations 1 and 4, and to calculate the exit thrust produced by the test nozzle; details are described in Section 4.0. The data were recorded with Polaroid cameras and digital printers.

3.0 MODEL DESCRIPTION

3.1 General Electric Dual-Flow Nozzles

The test models were furnished by General Electric. Model-to-facility adapters, including flow conditioning elements, were designed and fabricated by FluiDyne. An assembly drawing of the model adapters is shown in Figure 3. Photographs of model assemblies are shown in Figures 4a-4e.

The upper portion of Figure 3, and Figure 5a, shows the arrangement of the adapters for cold dual-flow tests (Runs 16 through 54). The fan nozzle flow was metered, ducted to an annular passage, and passed through two screens before entering the fan nozzle. Charging station instrumentation for the fan nozzle (indicated in Figure 3) consisted of 6 area-weighted total pressure ($P_{t_{18}}$) probes, 6 area-weighted total temperature ($T_{t_{18}}$) probes, and 2 static pressure taps on each of the inner and outer walls. The temperatures were measured with shielded C/A thermocouples. The rakes were located at $\theta = 30°$ and $210°$ (3 P_t and 3 T_t in each of the two probe assemblies).

The core nozzle flow was metered and passed through a choke plate and two screens before entering the core nozzle. Charging station instrumentation for the core nozzle was similar to that described above for the fan, with two probe assemblies located at $\theta = 0°$ and $180°$.

The lower portion of Figure 3, and Figure 5b, shows the arrangement of the adapters for the five hot-flow tests. In this arrangement, the total flow was metered at Station 1 and ducted through a jet breaker to a common plenum supplying air to both the fan and core nozzles. The open area of the core passage choke plate (relative to the fan nozzle throat area) produced the proper flow split between the core and fan nozzles. Charging station instrumentation for the hot tests was the same as described above, except

that one T_{t_8} thermocouple was used to control the flow temperature and was, therefore, not recorded.

The test nozzles were assembled from interchangeable model components to form five test configurations. The core nozzle was common to all configurations.

Configuration 7, Figure 4a, was a "baseline" or unsuppressed nozzle, having axisymmetric co-annular core and fan nozzles.

Configuration 1, Figure 4b, employed 36 "chutes" to provide multiple jets at the fan nozzle exit.

Configuration 3, Figure 4c, was obtained by adding an axisymmetric ejector shroud to Configuration 1.

Configuration 2, Figure 4d, employed 69 tubes (.522 inch ID cylinder, 10° half-angle contraction, .4594 inch ID at exit).

Configuration 5, Figure 4e, was obtained by adding the ejector shroud to Configuration 2. The ejector mounting flange was modified between tests of Configurations 3 and 5, as shown in the photographs.

Geometric throat areas calculated from specified dimensions were $A_8 = 17.2108$ in.^{2} (common to all configurations), $A_{18} = 11.1555$ in.^{2} for the baseline model, $A_{18} = 11.1202$ in.^{2} for chutes, and $A_8 = 11.437$ in.^{2} for the tubes.

Static pressure instrumentation on the model surfaces consisted of 15 taps on the common core plug, 12 taps on the baseline fan plug, 23 taps on the chute/fan plug assembly, 25 taps on the tube/fan plug assembly, and 11 taps on the ejector. The pressure tubes were connected to mercury manometers with plastic stripatube lines.

3.2 Standard ASME Nozzles

Facility demonstration and checkout tests were performed using two standard ASME long-radius flow metering nozzles (Figures 2 and 4a). The 5.5 inch nozzle was mounted in line with the upper meter of the facility force measuring system, and was tested with cold flow. The 4 inch nozzle was mounted inline with the lower meter, and was tested with both cold and hot flows. The two ASME nozzles were tested separately and simultaneously.

4.0 DATA ANALYSIS PROCEDURES

The following subsections describe the data analysis procedures used in the present test program. Station notations are defined in Figure 5.

4.1 Flow Rates

The mass flow rates through the test nozzles were determined using choked ASME long-radius metering nozzles. For most of the model tests, as shown in Figure 5a, the core nozzle flow rate was calculated at Station 1 and the fan nozzle flow rate was calculated at Station 4, using the following equations.

$$W_1 = W_8 = \frac{K_1 C_{D_1} A_1 P_{t_1}}{\sqrt{T_{t_1}}}$$

$$W_4 = W_{18} = \frac{K_4 C_{D_4} A_4 P_{t_4}}{\sqrt{T_{t_4}}}$$

Special hot-flow calibration tests were run with Configuration 5 to determine the discharge coefficient of the fan nozzle (tubes), by blanking off the primary passage, and discharging the entire metered flow through the tubes. Fan nozzle discharge coefficients determined by these calibration tests included effects of thermal growth of the hot tubes.

For the hot dual-flow tests of Configuration 5, Figure 5b, the total flow rate was metered at Station 1. The fan nozzle flow rate was then calculated using tube discharge coefficients determined by the above-described hot calibration tests. The core flow rate was then calculated by subtracting the calculated fan nozzle flow from the metered total flow.

The critical flow factor, K , was calculated as a function of total pressure and total temperature.

$$K = 0.52820 + a\,T_t + b\,T_t^2 + c\,T_t^3 + 0.186 \times 10^{-4} \times P_t \times e^{-.0067\,(T_t - 500)}$$

where: $a = 0.1654 \times 10^{-4}$

$b = -0.2119 \times 10^{-7}$

$c = 0.6008 \times 10^{-11}$

T_t is in °R and P_t is in psia.

This equation was obtained by curve-fitting tabulated values in Reference 1; the curve-fit is accurate to within $\pm$ 0.03% for $0 < P_t < 30$ atmospheres and $460 < T_t < 700$°R, and is accurate to within $\pm$ 0.1% for $0 < P_t < 40$ atmospheres and $460 < T_t < 1800$°R.

C_{D_4} was calculated using a semi-empirical equation

$$C_{D_4} = \left(1 - 0.184\, R_{N_4}\right)^{-0.2}$$

and varied from 0.990 to 0.993 for the present tests.

C_{D_1} was calculated from a similar equation, modified for the hot tests to account for a thermal boundary layer. This thermal boundary layer results from watercooling of the Station 1 meter.

$$C_{D_1} = 1 - \left(0.184\, R_{N_1}^{-0.2}\right)\left(1.574 - 0.574\, T_{t_1}/T_w\right)$$

The above equation was derived assuming constant static pressure in the boundary layer, a 1/7 power velocity profile, thermal boundary layer thickness equal to velocity boundary layer thickness, and a density distribution in the boundary layer defined by

$$\frac{\rho}{\rho_\infty} = \frac{T_\infty}{T_w} - \left(\frac{T_\infty}{T_w} - 1\right)\left(\frac{y}{\delta}\right)^{1/7}$$

T_w, the wall temperature at the nozzle throat, was estimated from heat-balance calculations of heat transfer from the air stream to the cooling water. T_w values calculated for the present hot tests varied from 122° to 240°F. $R^w_{N_1}$ was calculated using a mean temperature, $(T_w + T_{t_1})/2$. C_{D_1}, calculated using the above equation, varied from 0.991 to 0.998 for the present tests. Given sufficient wall cooling, C_{D_1} may exceed unity (Reference 2).

The above equation for C_{D_1} is believed to be correct within $\pm$ 0.002, on the basis of results from facility demonstration tests. These demonstration tests include test series with either a 2.5-inch or a 4-inch diameter ASME nozzle located downstream of the water-cooled Station 1 meter. The downstream nozzle was essentially at adiabatic conditions (thin-wall construction, backside insulated). Flow rates calculated at Station 1 (using the above C_{D_1} equation) agreed within $\pm$ 0.25% with flow rates calculated at the downstream nozzle (using adiabatic wall C_D), thereby indicating the adequacy of the C_{D_1} equation.

A_4, the geometric throat area of the Station 4 meter, was 4.909 in.^{2}. A_1, the geometric throat area of the Station 1 meter, was calculated assuming thermal expansion from 70°F to T_w. The largest value of A_1 calculated for the present tests was 3.8113 in.^{2}, representing a thermal expansion area change of 0.31% from the nominal area of 3.7996 in.^{2}.

P_{t_1} and P_{t_4} were measured on Heise bourdon-tube gages. T_{t_1} and T_{t_4} were measured with shielded chromel/alumel thermocouples and recorded on the facility Vidar system (analog to digital converter, printer).

Calculated flow rates (lbm./sec.) for the present tests were in the ranges

$$3 < W_1 < 20 \qquad 5 < W_4 < 20 \ .$$

4.2 Discharge Coefficients

Discharge coefficient is defined as the ratio of actual flow rate through a nozzle, to the ideal isentropic flow rate at the overall nozzle pressure ratio. Overall nozzle pressure ratios are defined as $\lambda_8 = {}^{P}t_8/P_a$ and $\lambda_{18} = {}^{P}t_{18}/P_a$.

$$C_{D_{18}} = \frac{W_{18}\sqrt{T_{t_{18}}}}{K_{18}A_{18}P_{t_{18}}(A^*/A)_{18}} \quad \text{and} \quad C_{D_8} = \frac{W_8\sqrt{T_{t_8}}}{K_8A_8P_{t_8}(A^*/A)_8}$$

K_{18} and K_{8} were evaluated using a previous equation, as functions of $P_{t_{18}}$, $T_{t_{18}}$ and P_{t_8}, T_{t_8}. $T_{t_{18}}$ and T_{t_8} were measured on shielded chromel/alumel thermocouples, and were defined as the averages from the area-weighted probes. $P_{t_{18}}$ and P_{t_8} were measured on multiple-tube mercury manometers and were defined as the averages from the area-weighted probes.

The throat area of the 5.498-inch ASME nozzle was $A_{18} = 23.741$ in.^{2}. The throat area of the 4.000-inch ASME nozzle, when measured at room temperature, was $A_8 = 12.566$ in^2. For the hot tests, this area was calculated as 12.75 in^2, assuming thermal expansion from 70°F to a recovery temperature, T_w. T_w was calculated assuming isentropic expansion and a recovery factor of 0.89, i.e.,

$$T_w/T_{t_8} = (T_8/T_{t_8}) + 0.89\ (1 - T_8/T_{t_8}).$$

Throat areas for the noise suppression nozzles are listed in Section 3.0.

A*/A, the isentropic area ratio, is used to correct the ideal flow rate when the nozzle is unchoked. A*/A for the cold tests was calculated using equations valid for $\gamma = 1.4$, obtained from Reference 3.

$$A^*/A = 3.86393\lambda^{-0.71429}\sqrt{1 - \lambda^{-0.28571}} \quad \text{for } \lambda \leq 1.8929$$

and

$$A^*/A = 1 \quad \text{for } \lambda \geq 1.8929.$$

A^*/A for hot tests was obtained by correcting the $\gamma = 1.4$ value for "real gas effects," to account for γ being significantly less than 1.4. The correction was derived by curve-fitting tabulated values from Reference 4; no corrections are indicated for $T_t < 900°R$. First, the critical pressure ratio was expressed as a function of total temperature:

$$1/\lambda^* = 9.667 \times 10^{-6} \times T_t\,(°R) + 0.5196$$

if $\lambda \geq \lambda^*$, then $A^*/A = 1$. If $\lambda < \lambda^*$ and $900 < T_t < 1260°R$,

$$c = 1 + \left(\frac{1}{\lambda} - \frac{1}{\lambda^*}\right) 5.728 \times 10^{-5} (T_t - 900).$$

If $\lambda < \lambda^*$ and $1260 < T_t < 1800°R$,

$$c = 1 + \left(\frac{1}{\lambda} - \frac{1}{\lambda^*}\right) \left[2.615 \times 10^{-5} (T_t - 1260) + 0.020621\right].$$

Finally,

$$A^*/A = c \times \left[(A^*/A) \text{ at } \gamma = 1.4\right].$$

For the present tests, c (denoted c* on computer output sheets) varied from 1.000 to 1.004.

4.3 Thrust Measurement

The net static thrust of an exhaust nozzle is defined as the axial exit momentum of the exhaust flow, plus the excess of exit pressure over ambient pressure times the exit area.

$$H = mv_e + (P_e - P_a) A_e .$$

The net static thrust of an exhaust nozzle model was determined in the present test program by applying the momentum equation to the control volume shown in Figure 5. The analysis of forces applied to the control volume includes

entering stream thrusts (F_1 and F_4), a balance force (H_x), various pressure-area terms and seal tare forces, and the exit stream thrust, $(H + p_a A_e)$. Summing forces,

$$H = F_1 + F_4 + p_2 (A_2 - A_1) + p_5 (A_5 - A_4) - p_a (A_2 + A_5) - H_x .$$

The stream thrust at Station 4 is the exit stream thrust of a choked long-radius ASME nozzle, and was calculated as:

$$F_4 = G_4 (1 + 1.4 C_{D_4} C_{T_4}) .52828 P_{t_4} A_4 .$$

Use of $\gamma = 1.4$ and $P^*/P_t = .52828$ in the above equation imply an ideal gas. The factor G, derived from tabulated values in References 1 and 4, corrects the stream thrust from that of an ideal gas to that of a real gas.

If $T_t < 560°R$, $G = 1.00012 + 6.8338 \times 10^{-6} \times P_t$ (psia) .

If $T_t > 560°R$, $G = 1.0044 - (4.196 - .0059 P_t) (T_t + 460) \times 10^{-6}$

C_{D_4} has already been discussed; C_{T_4} was calculated in an analogous manner,

$$C_{T_4} = 1 - 0.109 R_{N_4}^{-0.2}$$

This equation is a semi-empirical expression of the thrust coefficient of an ASME nozzle at a pressure ratio of $\lambda = 1.8929$ (corresponding to $P^*/P_t = .52828$). For the present tests, G_4 varied from 1.0004 to 1.0013, and C_{T_4} varied from 0.994 to 0.996.

The stream thrust at Station 1 was calculated as:

$$F_1 = G_1 (1 + 1.4 C_{D_1} C_{T_1}) .52828 P_{t_1} A_1 .$$

Each variable in this equation has been previously described, except C_{T_1}. C_{T_1} was calculated in a similar manner as C_{T_4}, but was modified for hot tests to account for the thermal boundary layer described in the discussion of C_{D_1} in Section 4.1:

$$C_{T_1} = 1 - (0.109\, R_{N_1}^{-0.2})\,(0.828 + 0.172\, T_{t_1}/T_w) .$$

The above equation was derived using the same assumptions as in the derivation of C_{D_1}. C_{T_1} for the present tests varied from 0.992 to 0.996.

Static pressures p_2 and p_5 were measured on mercury manometers and bourdon-tube gages. Ambient pressure (p_a) was measured on a Hass mercury manometer (barometer). A_5 and A_2, the geometric reference areas for the seals, were 12.6924 and 7.0686 in^2, respectively.

4.4 Thrust Coefficient

The static thrust coefficient of an exhaust nozzle is defined as the ratio of the measured nozzle net thrust, to the ideal thrust of the actual mass flow when expanded isentropically from P_t to P_a.

$$C_T = \frac{H}{m\, v_i}$$

For the present dual-flow tests, the ideal thrust was calculated as the sum of the fan nozzle ideal thrust and the core nozzle ideal thrust:

$$C_T = \frac{H}{m_{18} v_{i_{18}} + m_8 v_{i_8}}$$

Ideal thrust was calculated using a dimensionless ideal thrust function, $m_i v_i / P_t A^*$, which is a function of both λ and γ.

$$m_i v_{i_{18}} = (A^*/A)_{18} \; C_{D_{18}} A_{18} P_{t_{18}} \; (m_i v_i / P_t A^*)_{18}$$

$$m_8 v_{i_8} = (A^*/A)_8 \; C_{D_8} A_8 P_{t_8} \; (m_i v_i / P_t A^*)_8$$

where

$$(m_i v_i / P_t A^*) = \gamma \left[\frac{2}{\gamma + 1}\right]^{\frac{\gamma}{\gamma - 1}} \sqrt{\frac{\gamma + 1}{\gamma - 1}} \sqrt{1 - \lambda^{\frac{1 - \gamma}{\gamma}}}$$

$$= 1.81162 \sqrt{1 - \lambda^{-0.28571}} \quad , \quad \text{for } \gamma = 1.4 \; .$$

For the cold tests, γ was taken to be 1.400. For the hot tests, however $\gamma \neq 1.4$, and therefore $(m_i v_i / P_t A^*)$ obtained from the above equation was corrected to account for "real gas effects" by multiplying by the ratio

$$\frac{(m_i v_i / P_t A^*) \quad \text{for real gas}}{(m_i v_i / P_t A^*) \quad \text{for } \gamma = 1.4}$$

This ratio was calculated from tabulated values in Reference 4; for the present range of test conditions this factor was obtained from a curve-fit expression

$$.9957 - 5.81 \times 10^{-5} \times (T_t \; , \; °R - 1000) + 1.25 \times 10^{-3} \times (\lambda - 1)$$

and varied between .9937 and .9971 for the core nozzle, and between .9952 and .9996 for the fan nozzle.

Thrust data from the ASME nozzle tests were also expressed in terms of the dimensionless exit stream thrust parameter,

$$f_9 = \frac{H + P_a (A_8 + A_{18})}{P_{t_8} A_8 + P_{t_{18}} A_{18}}$$

4.5 Pressure and Temperature Data

Pressure instrumentation for facility pressures and charging station pressures were described previously. All other pressures in the model were measured using multiple-tube mercury manometers. Model pressure data were reduced to absolute pressures (psia) and dimensionless ratios ($P/P_{t_{18}}$, P/P_{t_8}, P/P_a). The results are tabulated on computer output sheets, contained in the Appendix.

Facility and charging station temperature data were obtained using shielded chromel/alumel thermocouples, and were recorded on the facility Vidar system. Temperatures were expressed in °F or °R, or both.

4.6 Force Balance Calibration

The force balance calibration determines the output characteristics of both the force balance flexure and the elastic seals which provide pressure-tight expansion joints between the metric model assembly and the non-metric facility structure. The output of the strain-gage flexure is very linear with applied load, but the seals provide an additional force which is a function of both axial load and seal pressure. Most of this force carryover results from radial seal deflections required to support the static pressure differentials across the seals when the ducts are pressurized. Consequently, the seal and balance assembly is calibrated under simulated operating conditions of axial load (deflection) and seal differential pressures. The calibration for this mixed flow facility is further complicated by the fact that the vertical location of the applied horizontal load during a test is a function of the hot/cold flow split and nozzle pressure ratios; the calibration must, therefore, duplicate both the magnitude and location of the net force which was experienced during a test. As a result of these requirements, it has been found expedient to calibrate "on-point," that is, to determine the balance output characteristics while simultaneously reproducing the horizontal force, force vertical location, and seal pressures experienced at a specific test point.

The horizontal force and force location for each test point are not known exactly until the on-point calibration is completed. The initial test data are, therefore, reduced (by computer) using a preliminary calibration. The computer is programmed so that, as it reduces the initial test data, it also prints out the required calibration information (calibration load and load location), such that an accurate on-point calibration can then be made.

Calibration consists of blanking off both air ducts in the metric part of the system so that the seals can be pressurized internally as they are during a test. The seals are then pressurized to simulate running levels and a horizontal load is applied (at the proper vertical location) which gives the same balance output as that experienced at the particular test point being simulated. The apparent balance force, H_x, (which contains the seal force carryover) is then calculated as follows:

$$H_x = L + \Delta P_2 A_2 + \Delta P_5 A_5$$

where:

- L is the applied calibration load
- A_2 is the hot flow seal duct area
- A_5 is the cold flow seal duct area
- ΔP_2 is the pressure difference across the hot duct seal
- ΔP_5 is the pressure difference across the cold duct seal

This force is divided by the balance output (counts) to get a calibration factor, K_x:

$$K_x = \frac{H_x}{C_x}$$

The calibration factor, K_x, is relatively constant and makes accurate interpolation between calibration points possible. Even with the so-called "on-point" calibration, the applied load is varied slightly during calibration to give the trend of K_x versus C_x.

The proper value of K_x is then multiplied by the actual balance output, C_x, from a test point to get the apparent horizontal load, H_x. This is substituted into the equation for thrust, H, presented in Section 4.3.

5.0 PRESENTATION OF RESULTS

Test conditions and major test results are tabulated in Figure 6 and are plotted in Figures 7-10. Detailed data and calculations, including tabulated static pressure distributions, are contained in a separate Data Appendix.

The tabulation in Figure 6 includes: Configuration number and description, run number, actual values of the independent test variables (λ_{18}, λ_8 , T_t), and the major test results (C_T, C_{D_8}, $C_{D_{18}}$). For the ASME nozzles, f_9 is also tabulated.

5.1 ASME Checkout Tests

Three combinations of standard ASME nozzles were tested to demonstrate facility data accuracy. The test results are tabulated in Figure 6 and are plotted in Figures 7a-c.

Target performance curves for the ASME nozzles are shown in the figures. These predictions are based on semi-empirical equations from Reference 5, and were obtained by an analysis of ASME nozzle exit surveys conducted by FluiDyne in 1965.

The test results were statistically analyzed in terms of bias (average difference between actual and predicted values) and scatter (standard deviation of the data from the biased curve). This analysis is summarized in the following table.

		Bias, %				Standard Deviation, %			
Runs	Type	$C_{D_{18}}$	C_{D_8}	C_T	f_9	$C_{D_{18}}$	C_{D_8}	C_T	f_9
1-5	5.5" cold	-.11		-.03	-.08	.07		.07	.03
6-10	5.5" + 4", cold	-.06	-.11	-.13	-.12	.10	.11	.06	.06
11-15	4" hot		.08	-.12	-.30		.16	.08	.06

5.2 General Electric Suppressor Nozzle Tests

Major results from the suppressor nozzle tests are tabulated in Figure 6, sheets 2 and 3. Thrust coefficients are plotted versus fan nozzle pressure ratio in Figures 8a-c.

Fan nozzle and core nozzle discharge coefficients are plotted versus their respective pressure ratios in Figures 9a-c and 10a-c. Discharge coefficients greater than 1.00 at low nozzle pressure ratios are due to throat static pressures being less than ambient.

REFERENCES

1. Johnson, R. C., "Real-Gas Effects in Critical-Flow-Through Nozzles and Tabulated Thermodynamic Properties." NASA TN D-2565. 1965.

2. Massier, P. F., Back, L. H., Noel, M. B., and Saheli, "Viscous Effects on the Flow Coefficient of a Supersonic Nozzle." AIAA Journal, Volume 8, No. 3, March 1970, pp. 605-607.

3. Ames Research Staff, "Equations, Tables and Charts for Compressible Flow." NACA Report 1135. 1953.

4. Jordan, D. P., and Mintz, M. D., "Air Tables." McGraw-Hill Book Company, New York. 1965.

5. Siegfried, R. G., and Kuchar, A. P., "A Standard for Exhaust Nozzle Tests." General Electric ESAD Technical Brief 71006. April 6, 1971.

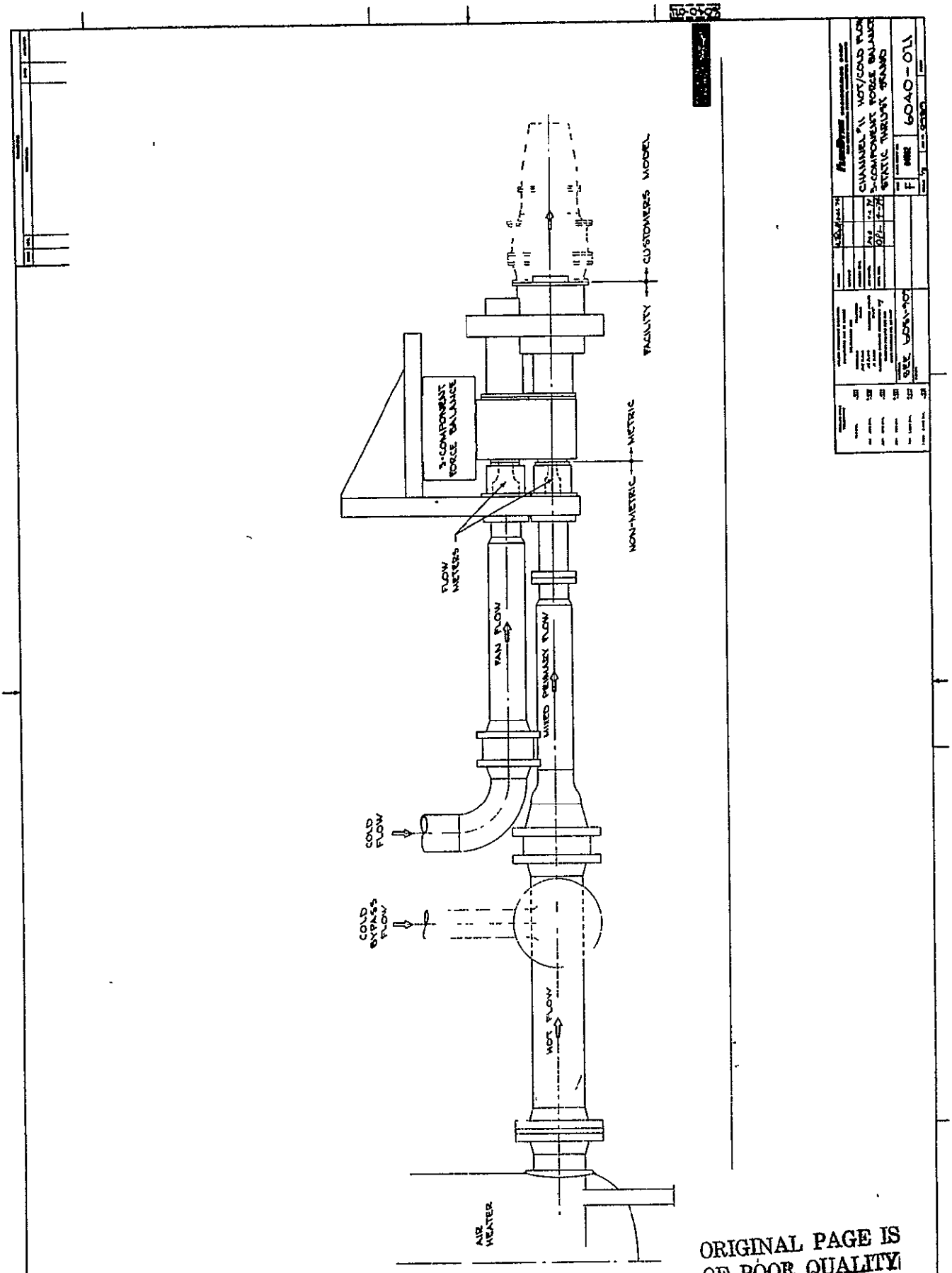

FIGURE 1. CHANNEL 11 FACILITY LAYOUT

ORIGINAL PAGE IS
OF POOR QUALITY

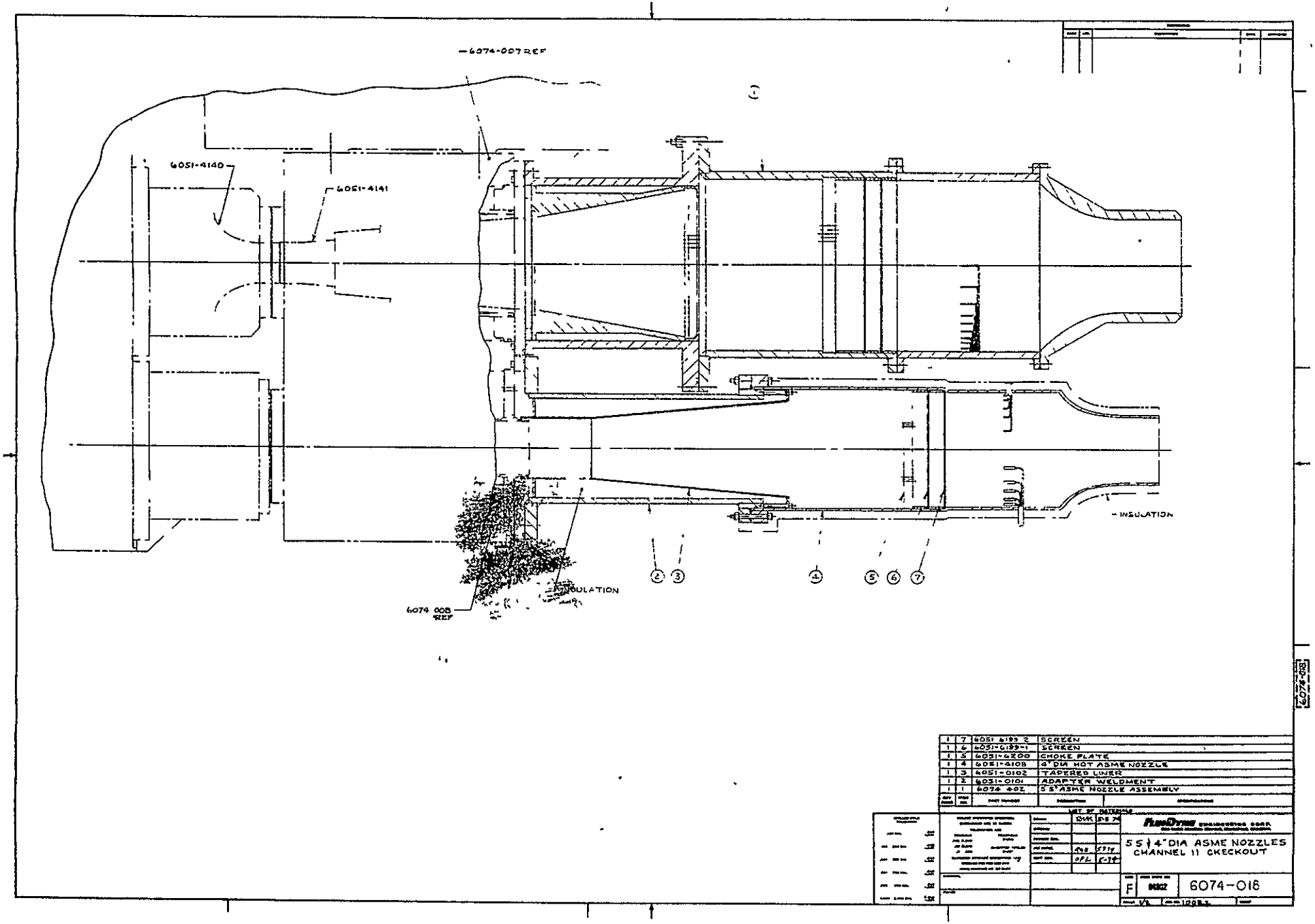

FIGURE 2. ASME CHECKOUT TEST ASSEMBLY

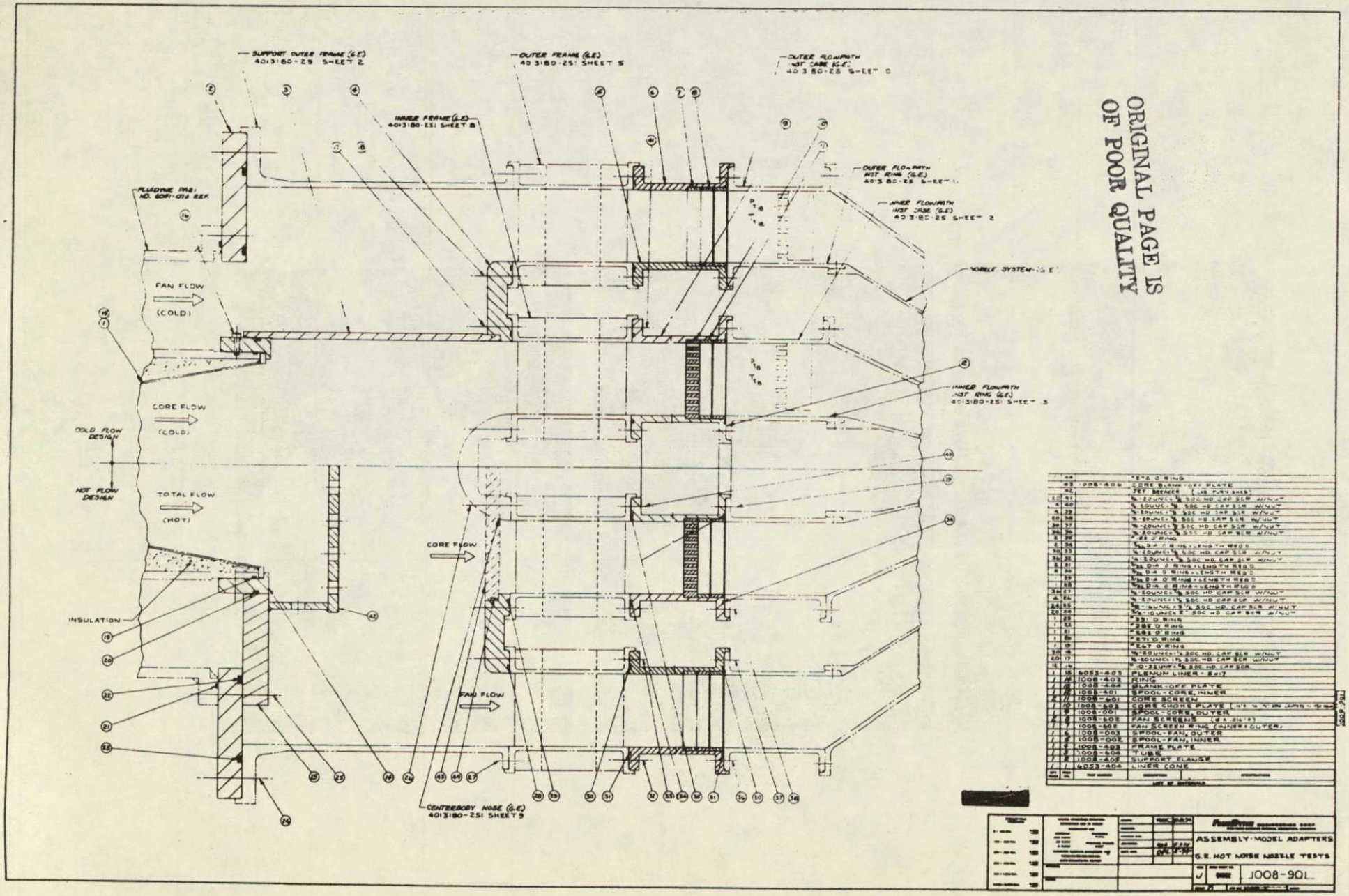

ORIGINAL PAGE IS
OF POOR QUALITY

FIGURE 3. MODEL ADAPTERS ASSEMBLY

FLUIDYNE ENGINEERING CORPORATION

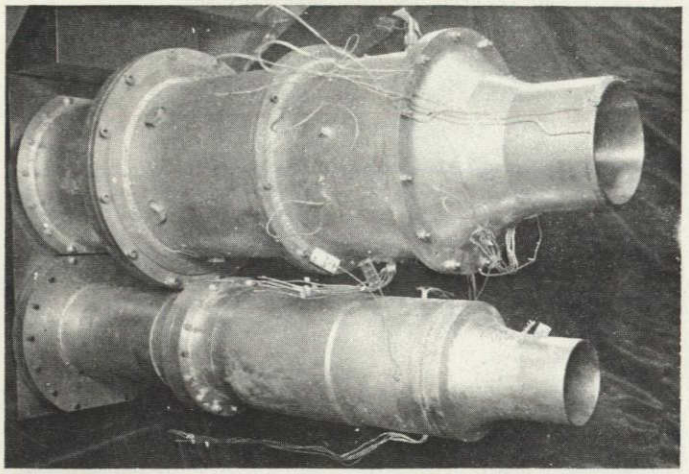

5.5" and 4"
ASME nozzles

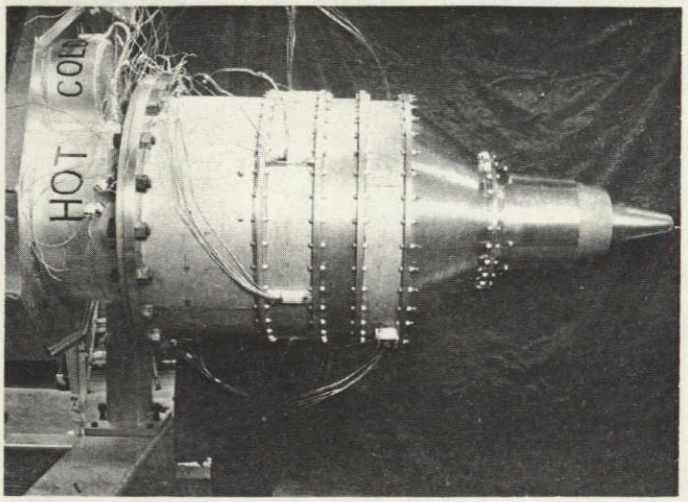

Configuration 7
(baseline)

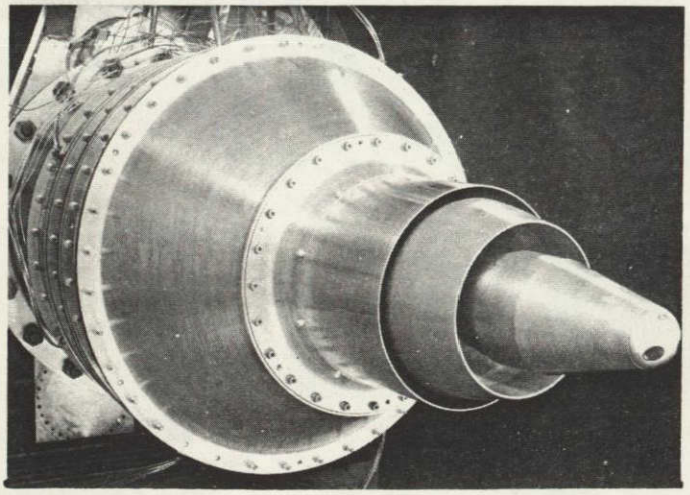

Configuration 7
(baseline)

FIGURE 4a. MODEL PHOTOGRAPHS

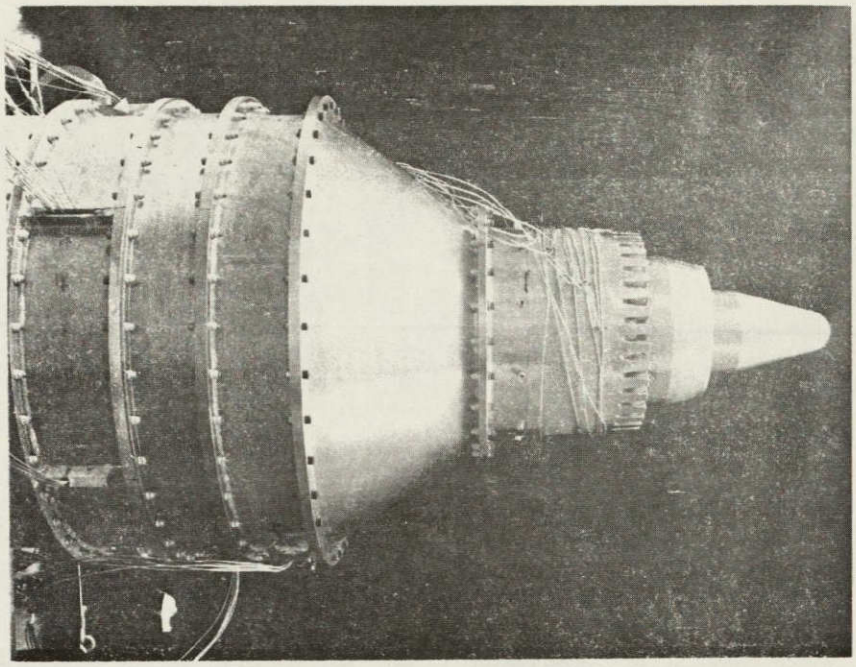

ORIGINAL PAGE IS
OF POOR QUALITY

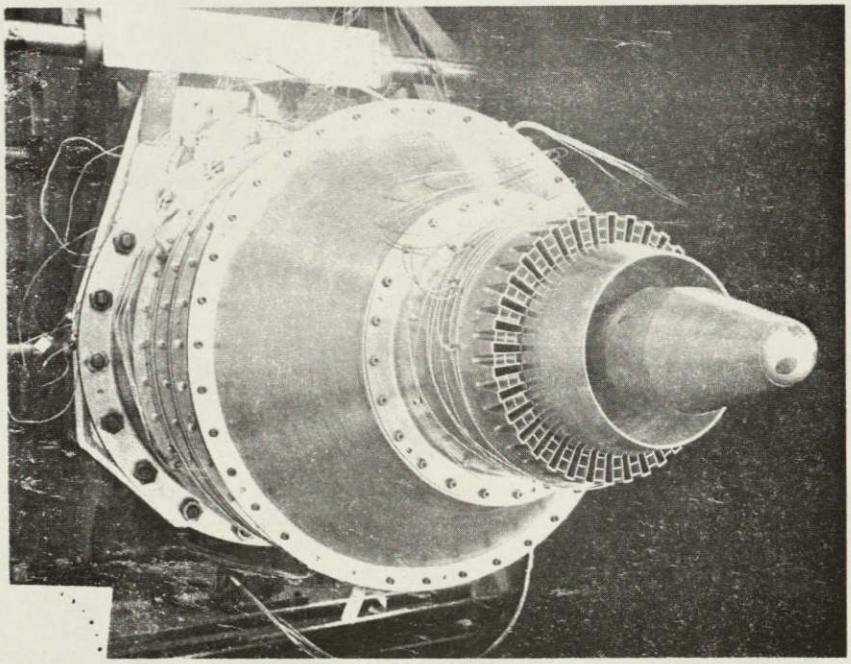

FIGURE 4b. MODEL PHOTOGRAPHS,
CONFIGURATION 1 (CHUTES)

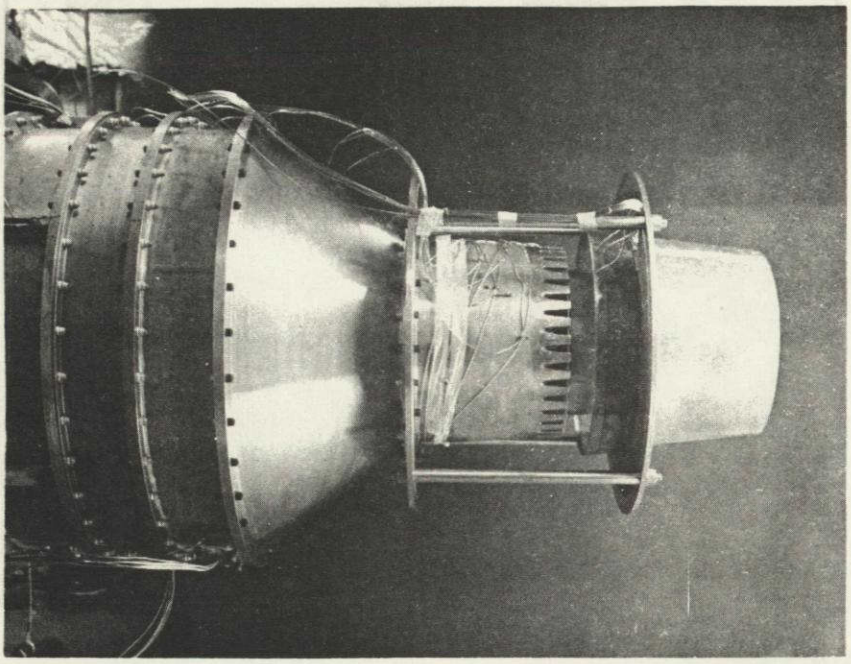

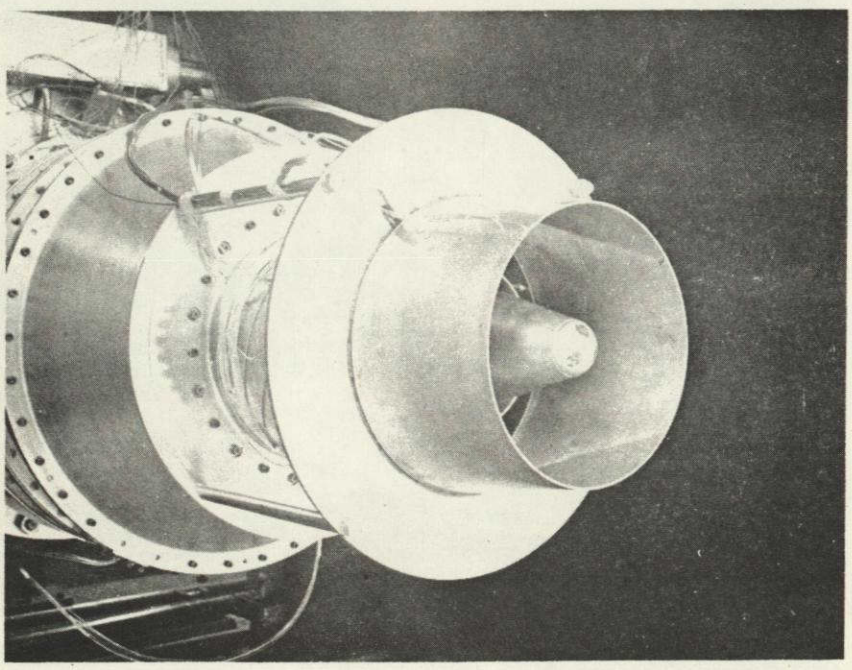

FIGURE 4c. MODEL PHOTOGRAPHS,
CONFIGURATION 3 (CHUTES & EJECTOR)

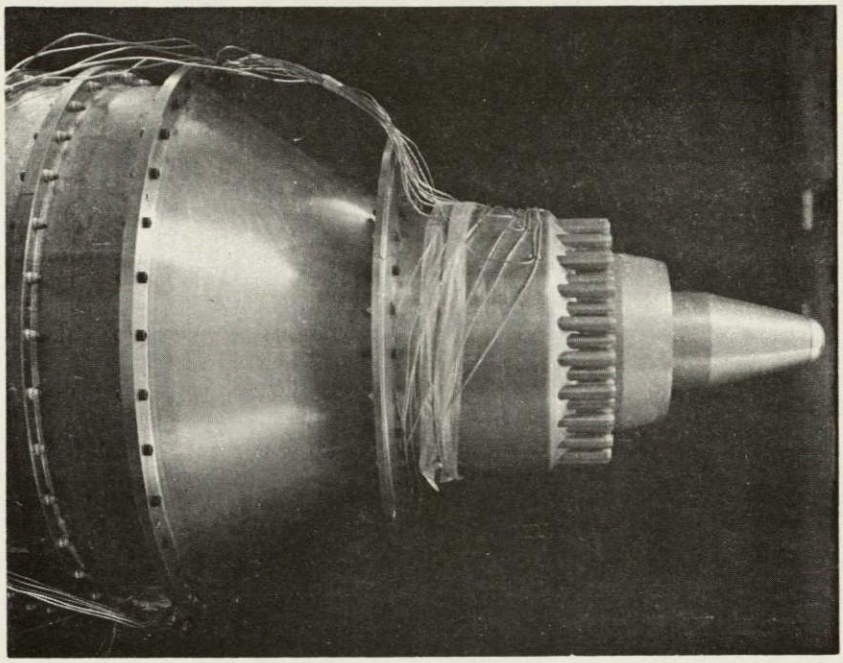

ORIGINAL PAGE IS
OF POOR QUALITY

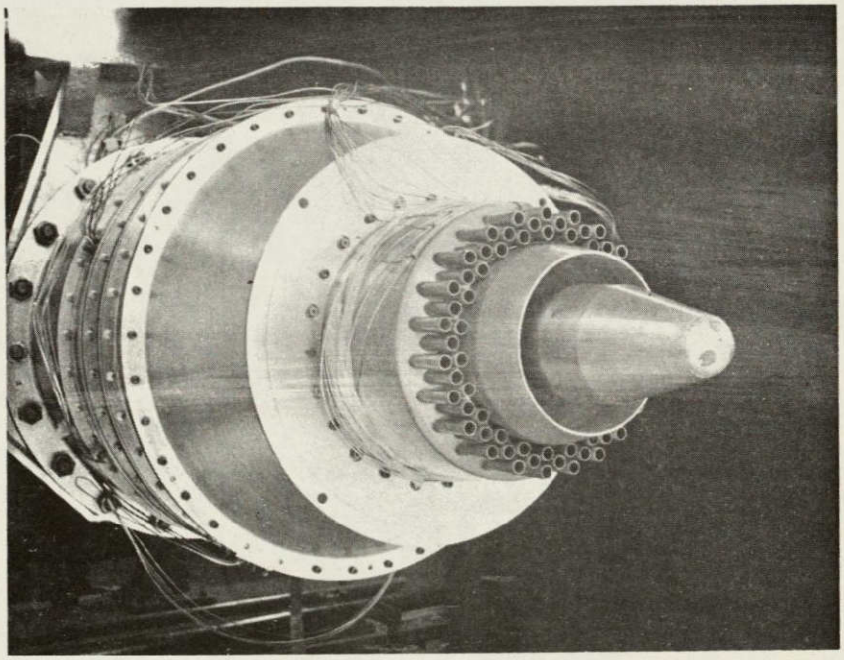

FIGURE 4d. MODEL PHOTOGRAPHS,
CONFIGURATION 2 (TUBES)

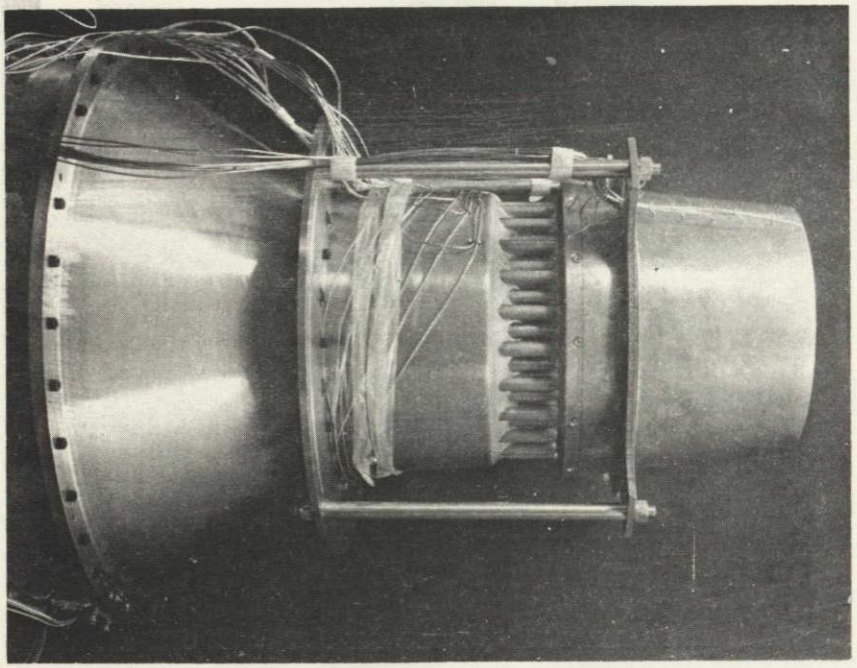

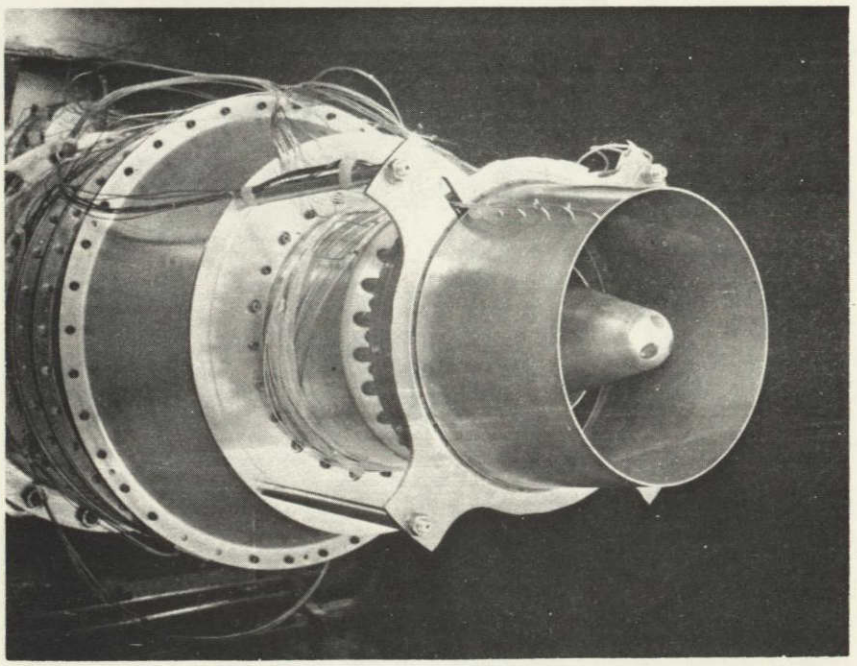

FIGURE 4e. MODEL PHOTOGRAPHS,
CONFIGURATION 5 (TUBES & EJECTOR)

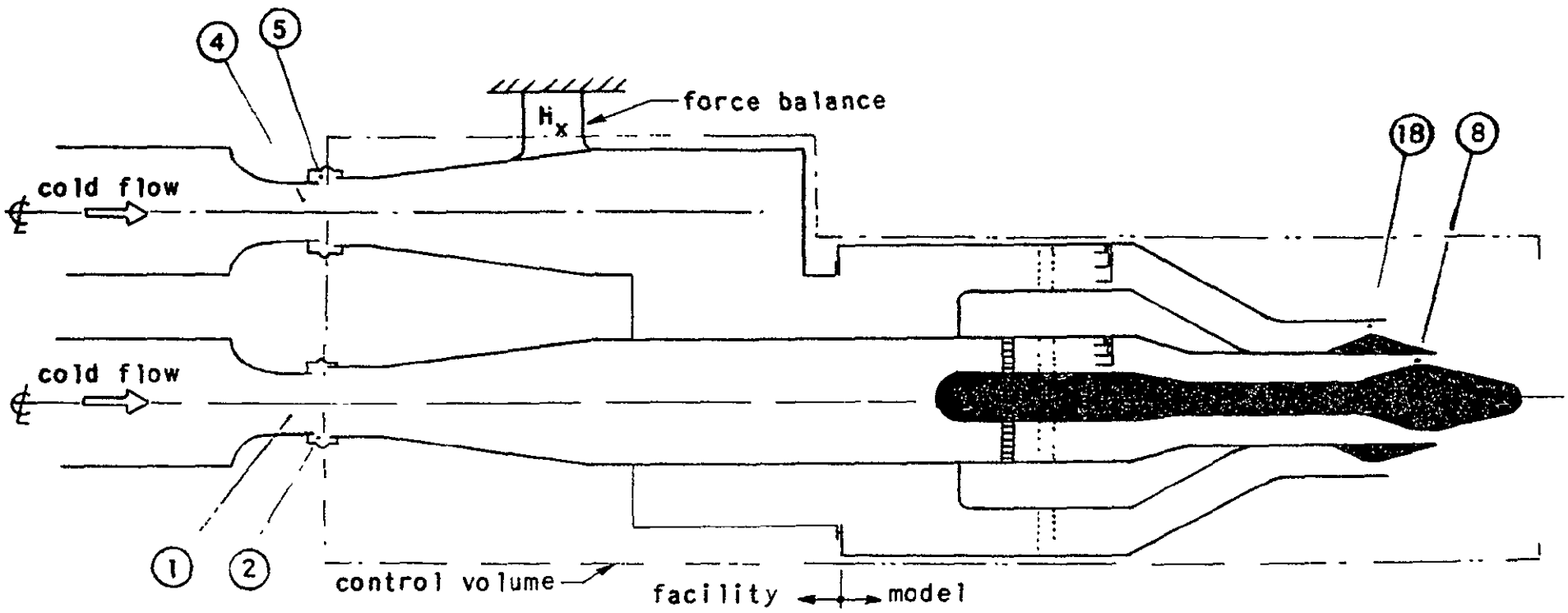

Station	Description
1	ASME meter throat (core flow)
2	flexible seal (core flow)
4	ASME meter throat (fan flow)
5	flexible seal (fan flow)
8	core nozzle
18	fan nozzle

FIGURE 5a. STATION NOTATION, COLD-FLOW MODEL TESTS

FLUIDYNE ENGINEERING CORPORATION

ORIGINAL PAGE IS
OF POOR QUALITY

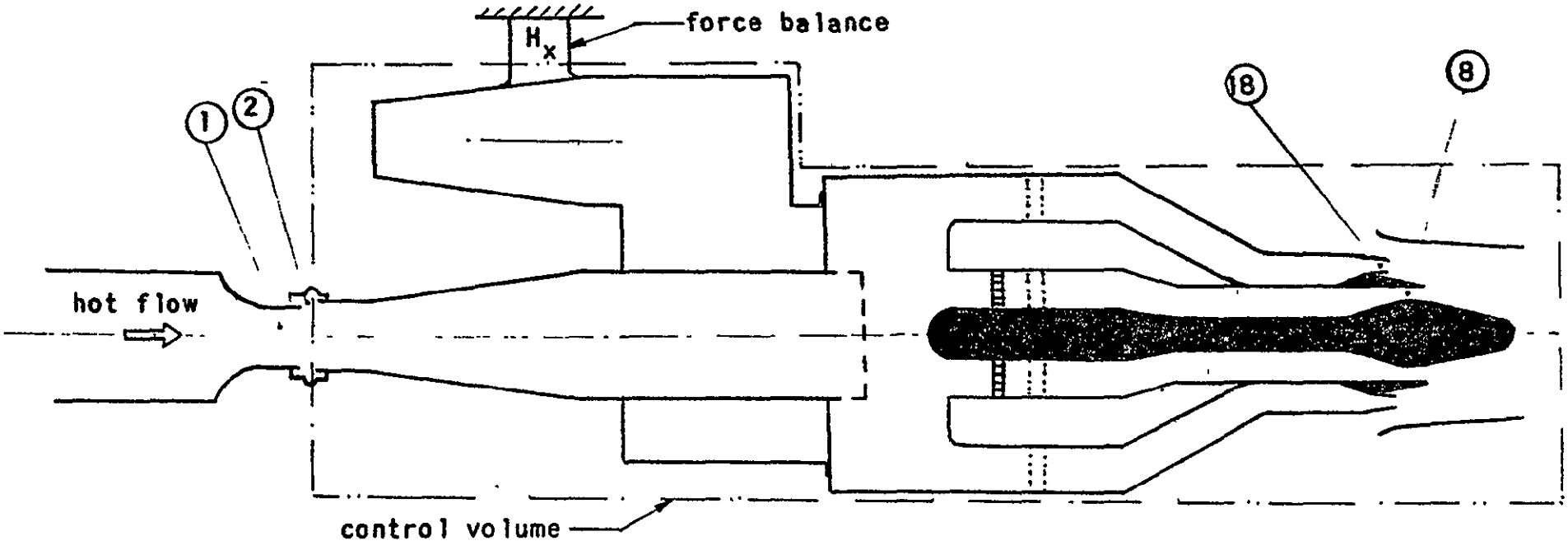

Station	Description
1	ASME meter throat (total flow)
2	flexible seal (total flow)
8	core nozzle
18	fan nozzle

FIGURE 5b. STATION NOTATION, HOT-FLOW MODEL TESTS

FLUIDYNE ENGINEERING CORPORATION

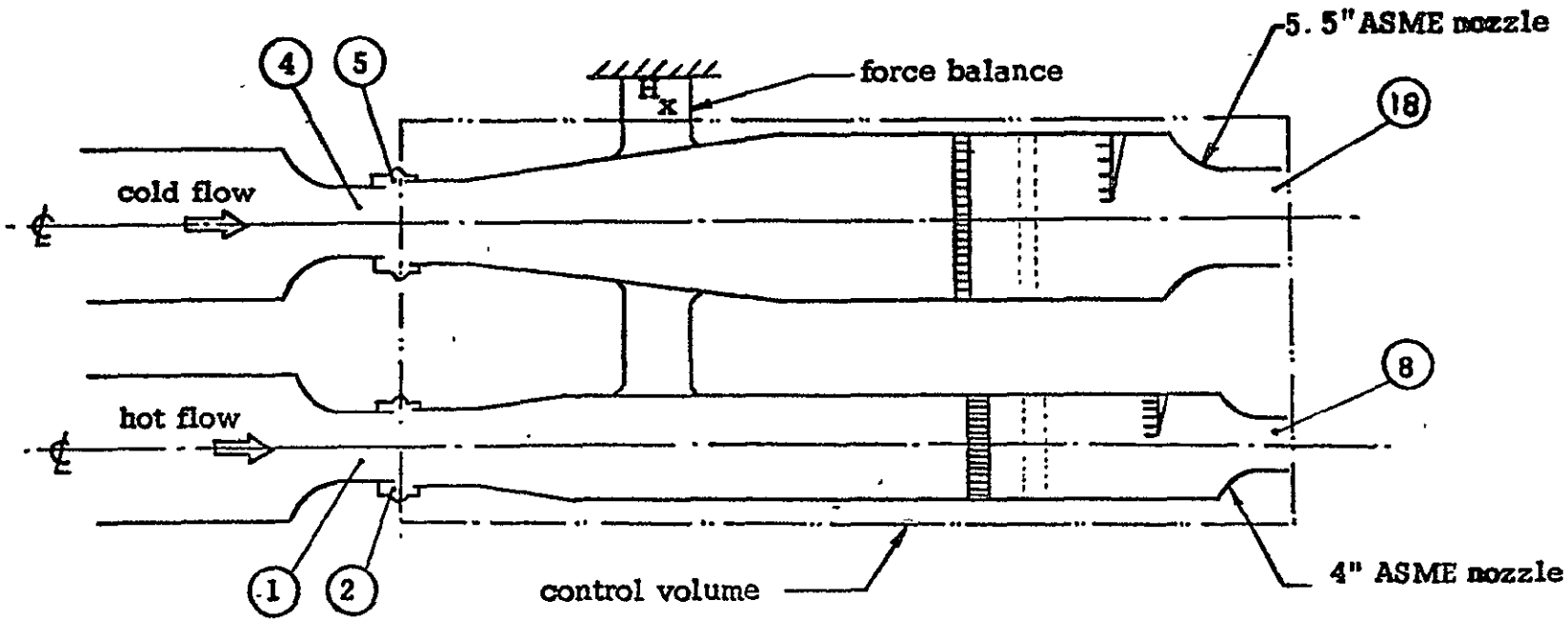

Station	
1	ASME Meter Throat (core flow)
2	Flexible Seal (core flow)
4	ASME Meter Throat (fan flow)
5	Flexible Seal (fan flow)
18	5.5 Cold ASME Nozzle Throat
8	4" Hot ASME Nozzle Throat

FIGURE 5c. STATION NOTATION, ASME CHECKOUT TESTS

ORIGINAL PAGE IS
OF POOR QUALITY

Configuration	Run No.	λ_{18}	λ_8	C_T	$C_{D_{18}}$	C_{D_8}	f_9
5.5" ASME	1	1.522		.9945	.9885		1.2335
cold, upper	2	1.838		.9943	.9896		1.2559
	3	2.040		.9941	.9907		1.2561
	4	2.285		.9957	.9908		1.2573
	5	2.549		.9946	.9909		1.2571
5.5" ASME	6	1.521	1.490	.9927	.9896	.9872	1.2308
cold, upper	7	1.834	1.791	.9927	.9913	.9890	1.2551
+	8	2.048	1.986	.9932	.9892	.9903	1.2546
4" ASME	9	2.288	2.237	.9949	.9913	.9910	1.2569
cold, lower	10	2.547	2.494	.9939	.9918	.9899	1.2566
4" ASME	11		1.498	.9912		.9851	1.2244
hot, lower	12		2.002	.9913		.9896	1.2490
$T_{t_8} \approx 1460°R$	13		2.501	.9931		.9903	1.2507
	14		3.013	.9902		.9910	1.2519
	15		4.249	.9765		.9903	1.2517

FIGURE 6. RUN SCHEDULE AND TABULATION OF MAJOR TEST RESULTS

(Sheet 1 of 8)

FLUIDYNE ENGINEERING CORPORATION

Configuration	Run No.	λ_8	λ_{18}	C_T	C_{D_8}	$C_{D_{18}}$
7	16	1.312	1.490	.9741	.9431	1.0238
baseline	17	1.308	3.077	.9722	.8494	.9866
	18	1.308	4.034	.9660	.8398	.9896
	19	1.886	1.574	.9663	.9864	1.0096
(cold flow)	20	1.890	3.081	.9642	.9565	.9864
	21	1.895	4.033	.9618	.9453	.9878
1	22	1.297	1.548	.9534	.9943	.9469
chutes	23	1.298	2.272	.9601	.9922	.9687
	24	1.298	3.064	.9567	.9923	.9735
	25	1.298	4.035	.9481	.9461	.9755
	26	1.888	1.547	.9575	.9867	.9493
	27	1.895	2.270	.9602	.9850	.9685
(cold flow)	28	1.897	3.071	.9575	.9839	.9698
	29	1.897	4.033	.9496	.9836	.9767
3	30	1.298	1.541	.9837	1.0356	.9556
chutes	31	1.301	2.273	.9943	1.0544	.9709
+	32	1.298	3.061	.9953	1.0724	.9740
ejector	33	1.301	4.036	.9828	1.0445	.9772
	34	1.893	1.541	.9716	.9849	.9534
	35	1.893	2.247	.9822	.9855	.9685
(cold flow)	36	1.893	3.060	.9827	.9847	.9714
	37	1.895	4.036	.9747	.9853	.9758

FIGURE 6. RUN SCHEDULE AND TABULATION OF MAJOR TEST RESULTS
(Sheet 2 of 3)

FLUIDYNE ENGINEERING CORPORATION

Configuration	Run No.	λ_8	λ_{18}	C_T	C_{D_8}	$C_{D_{18}}$
2	38	1.302	1.552	.9442	1.0008	.9202
	39	1.304	2.243	.9507	.9971	.9424
tubes	40	1.301	3.048	.9506	1.0004	.9426
	41	1.301	4.033	.9456	1.0030	.9446
	42	1.897	1.542	.9493	.9848	.9213
(cold flow)	43	1.897	2.250	.9517	.9848	.9440
	44	1.895	3.061	.9526	.9855	.9447
	45	1.901	4.038	.9458	.9851	.9456
5	46	1.300	1.545	.9449	1.0450	.9389
	47	1.299	2.255	.9591	1.0768	.9417
	48	1.299	3.257	.9689	1.0975	.9428
tubes	49	1.298	4.035	.9802	1.1168	.9445
+	50	1.645	3.258	.9682	.9970	.9442
ejector	51	2.001	1.544	.9533	.9813	.9432
	52	1.996	2.246	.9600	.9840	.9427
(cold flow)	53	1.996	3.254	.9703	.9845	.9442
	54	1.997	4.029	.9833	.9845	.9450
5 $T_{t_8} \approx T_{t_{18}} \approx 1000°R$	55	1.273	2.215	.9511	1.0893	.9432
	56	2.129	4.001	.9858	1.0048	.9457
5 $T_{t_8} \approx T_{t_{18}} \approx 1460°R$	57	1.296	2.242	.9501	1.0574	.9544
	58	1.727	3.213	.9611	1.0041	.9556
	59	2.148	4.017	.9810	1.0013	.9567

*

*Notes: 1) $C_{D_{18}}$ from hot-flow calibration tests.

2) Both C_{D_8} and $C_{D_{18}}$ are based on cold throat areas.

FIGURE 6. RUN SCHEDULE AND TABULATION OF MAJOR TEST RESULTS

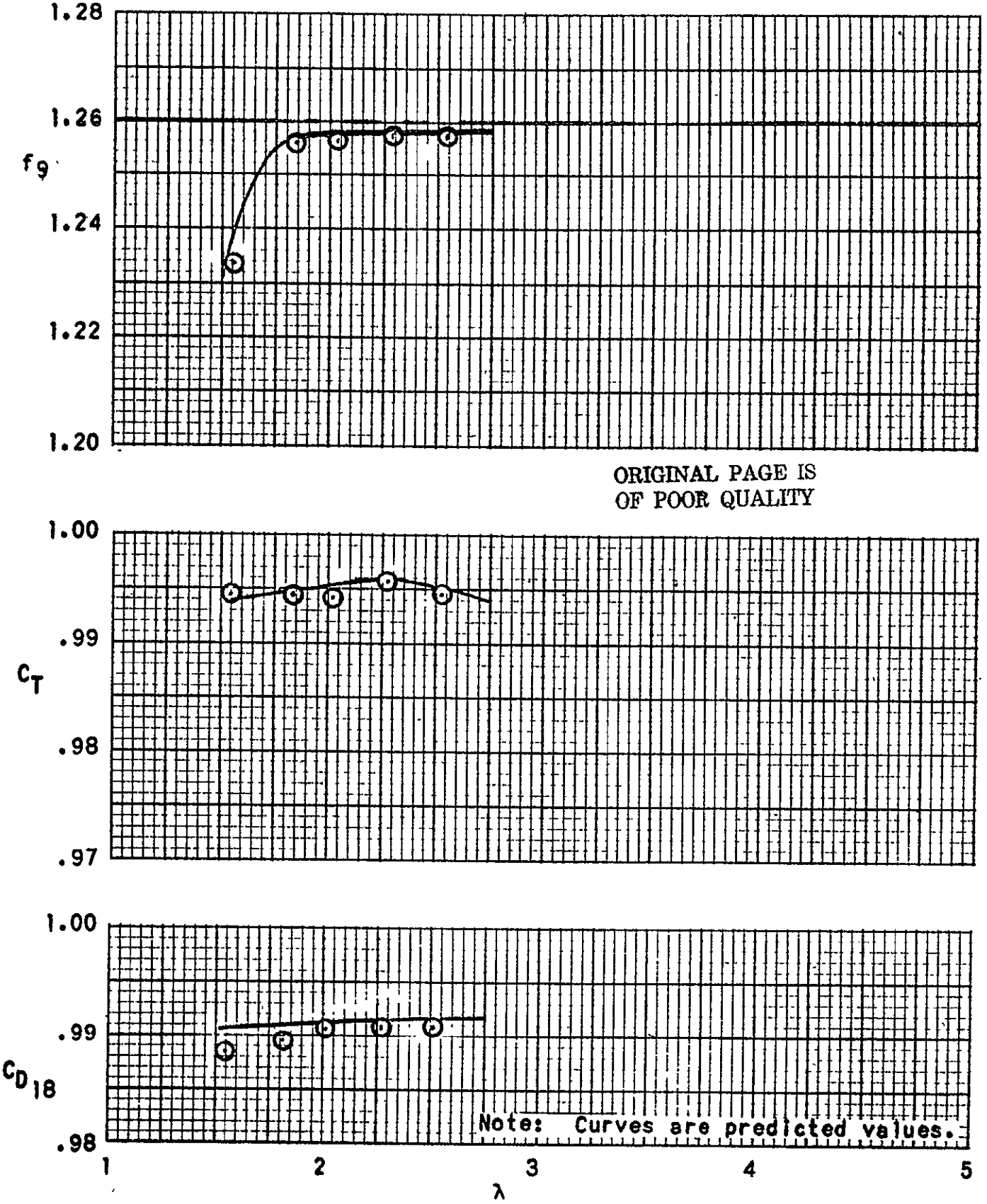

ORIGINAL PAGE IS
OF POOR QUALITY

FIGURE 7a. TEST RESULTS, 5.5" COLD ASME NOZZLE

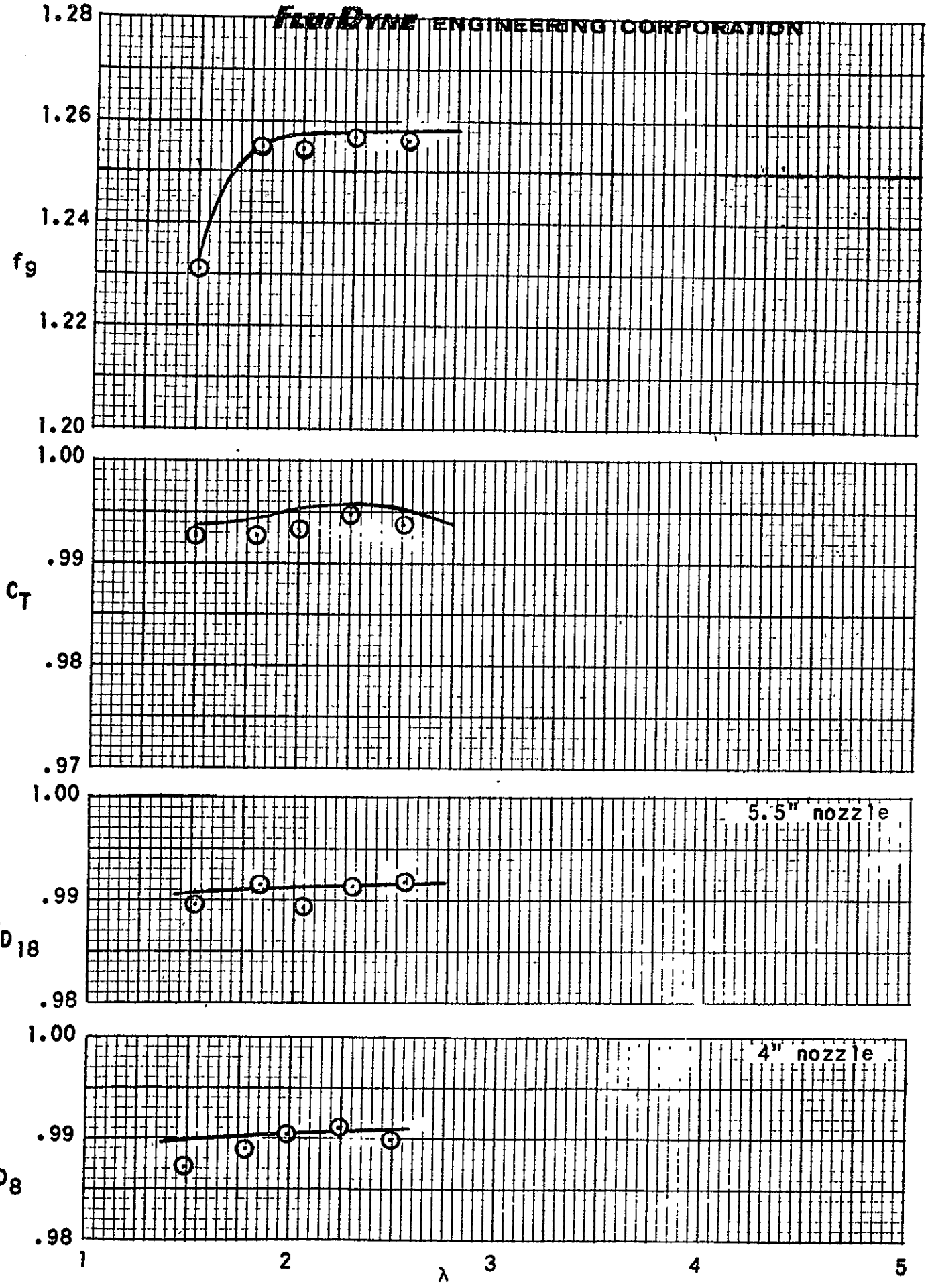

FIGURE 7b. TEST RESULTS, 5.5" AND 4" COLD ASME NOZZLES

ORIGINAL PAGE IS
OF POOR QUALITY

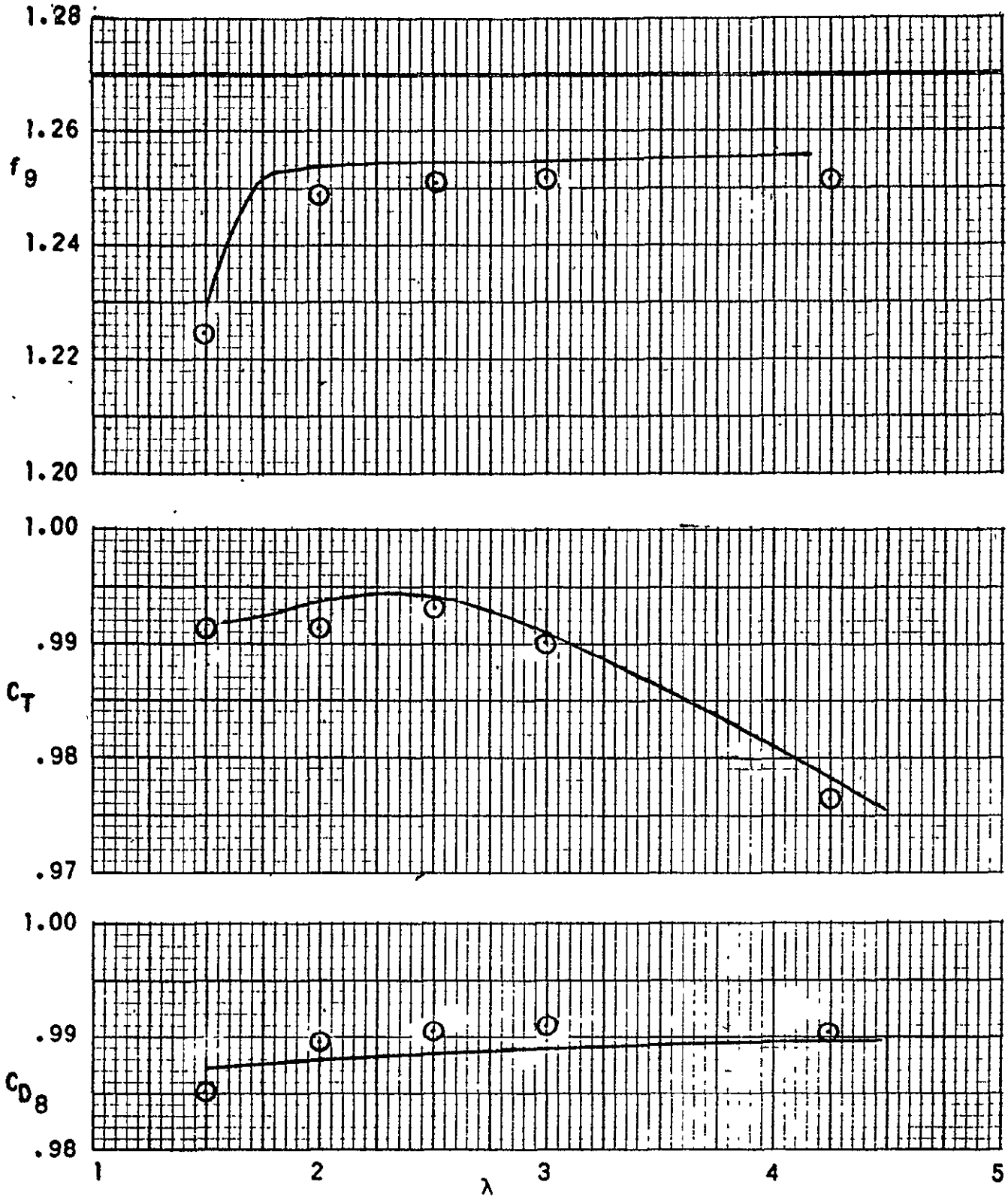

FIGURE 7c. TEST RESULTS, 4" HOT ASME NOZZLE

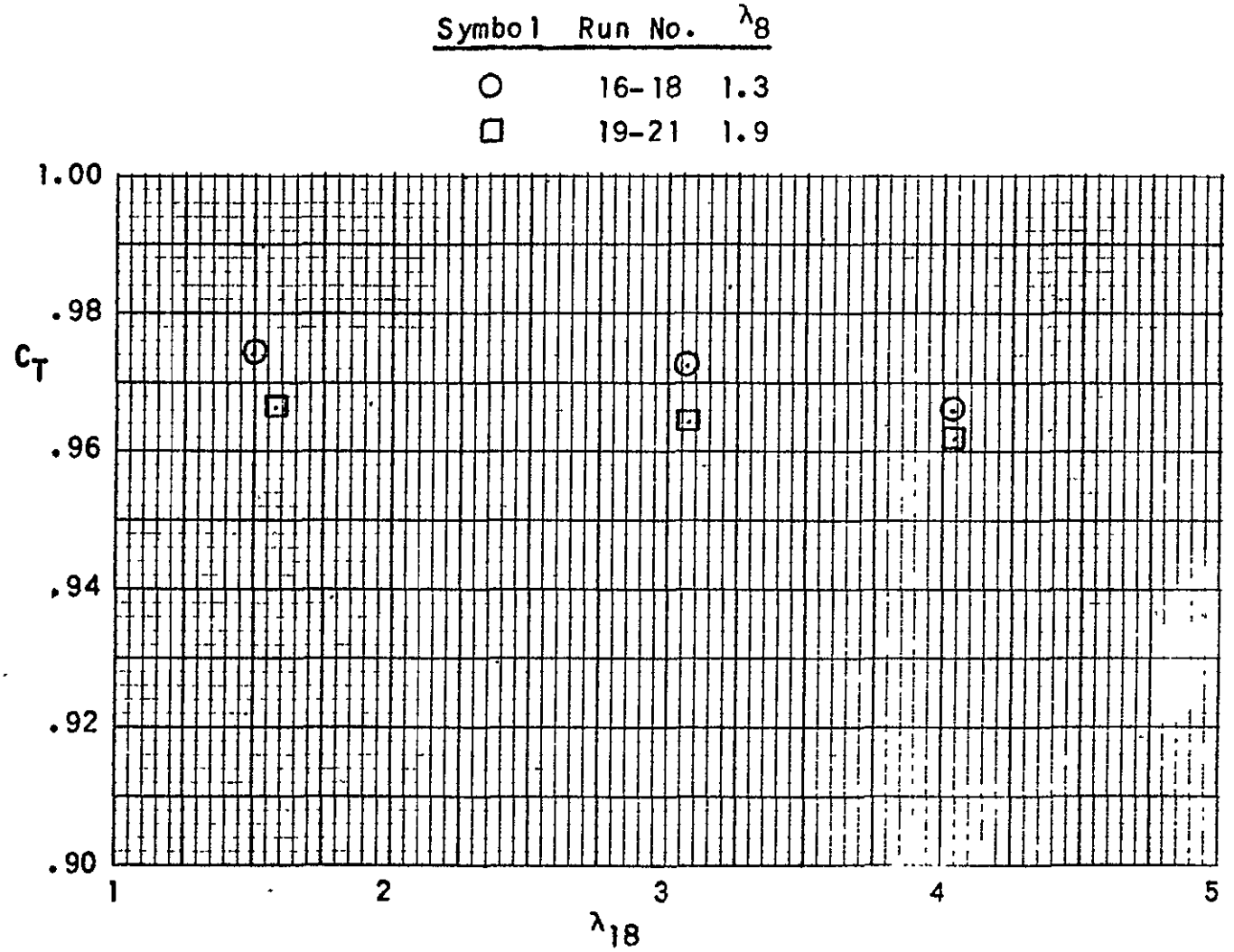

FIGURE 8a. THRUST COEFFICIENTS, CONFIGURATION 7 (BASELINE)

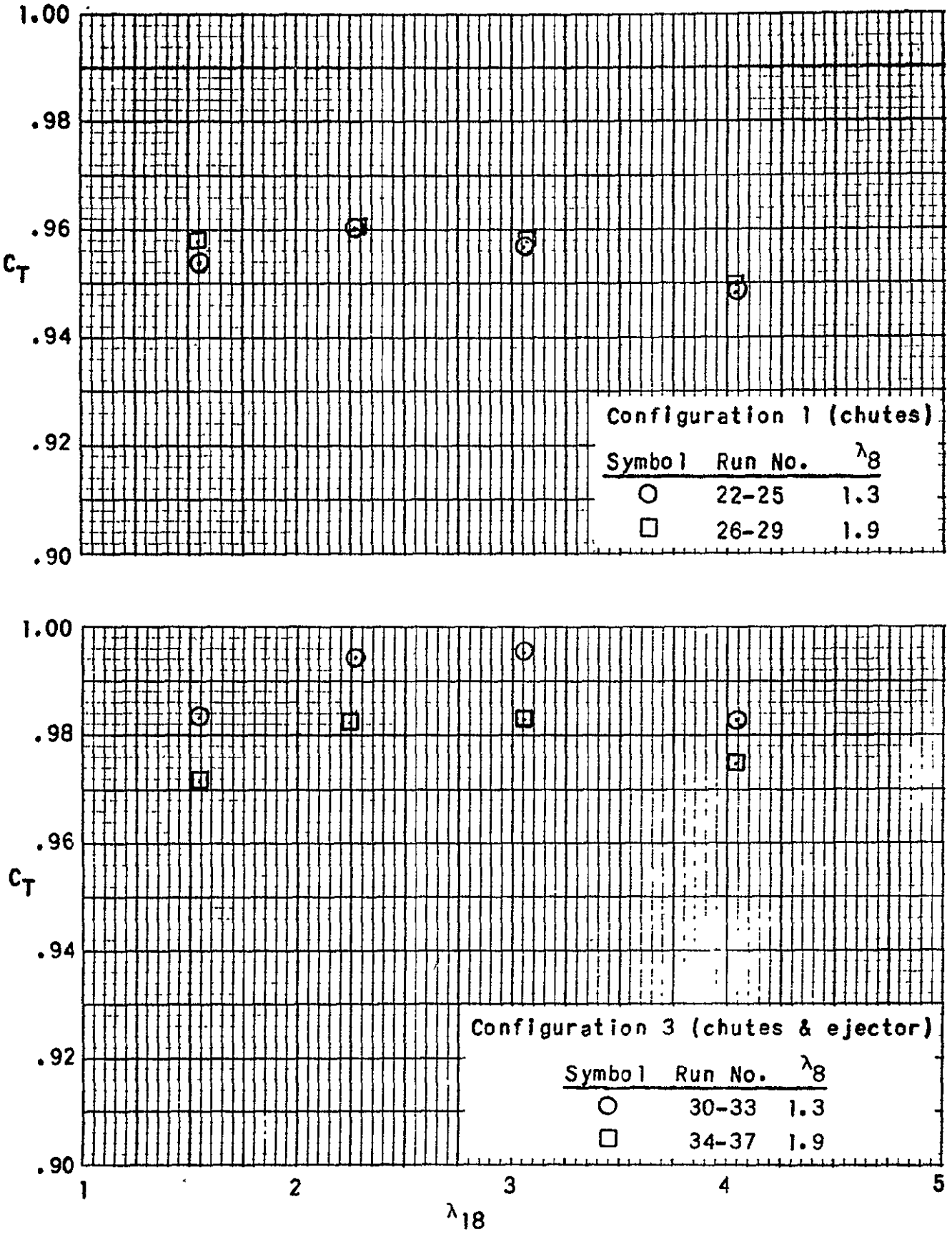

FIGURE 8b. THRUST COEFFICIENTS, CONFIGURATIONS 1 AND 3

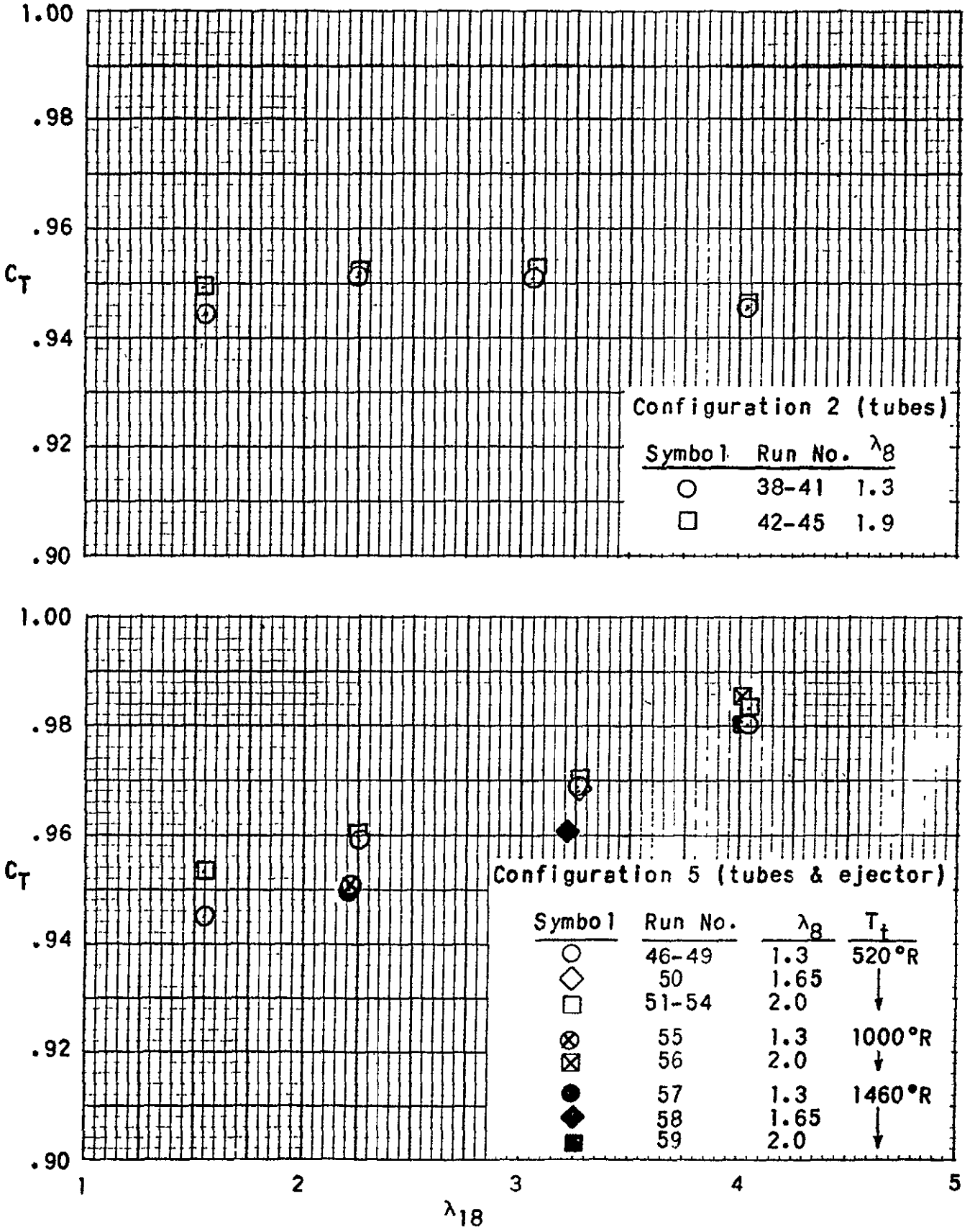

FIGURE 8c. THRUST COEFFICIENTS, CONFIGURATIONS 2 AND 5

ORIGINAL PAGE IS
OF POOR QUALITY

Symbol	Run No.	λ_8
○	16-18	1.3
□	19-21	1.9

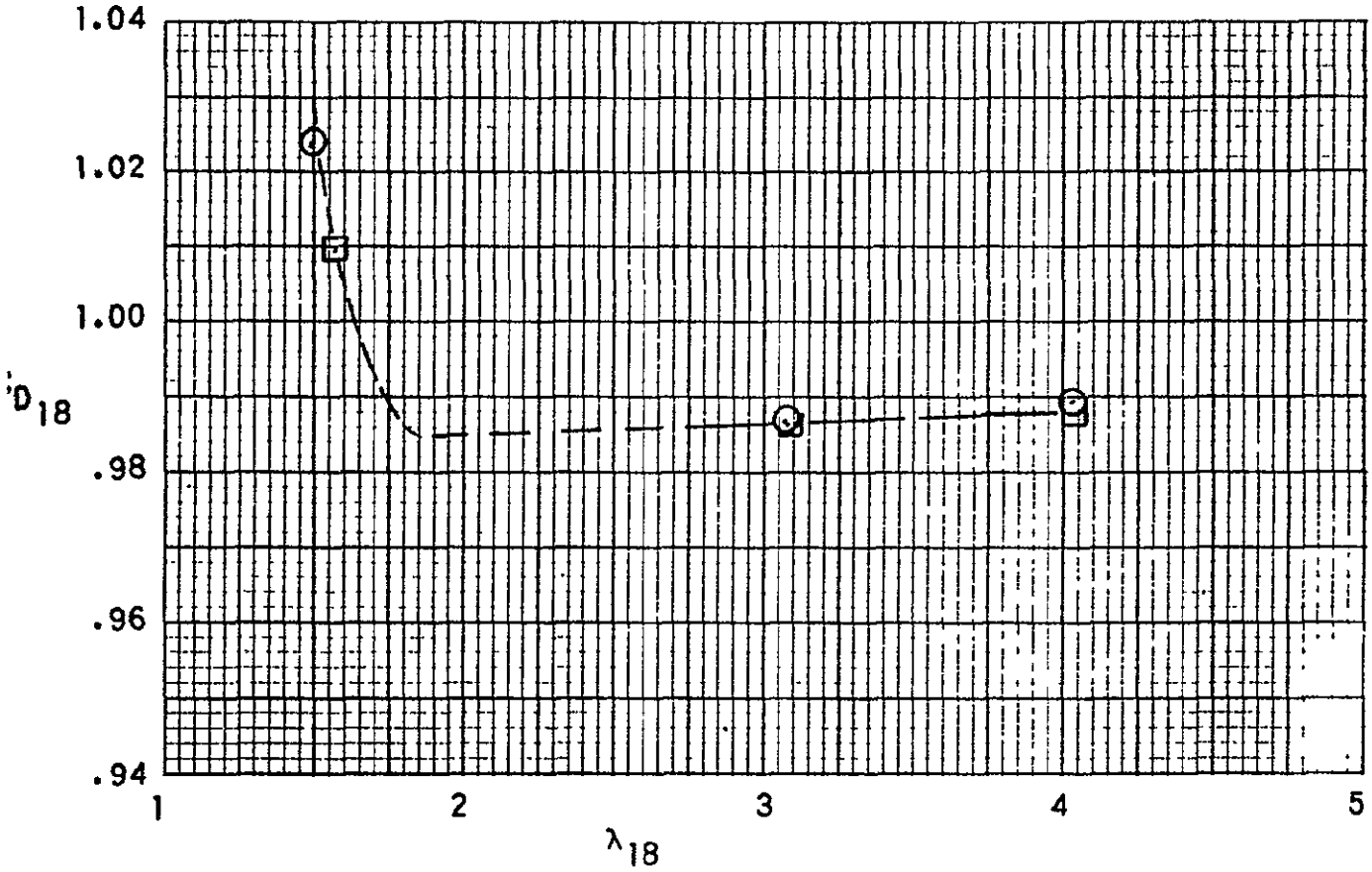

FIGURE 9a. FAN NOZZLE DISCHARGE COEFFICIENTS, CONFIGURATION 7 (BASELINE)

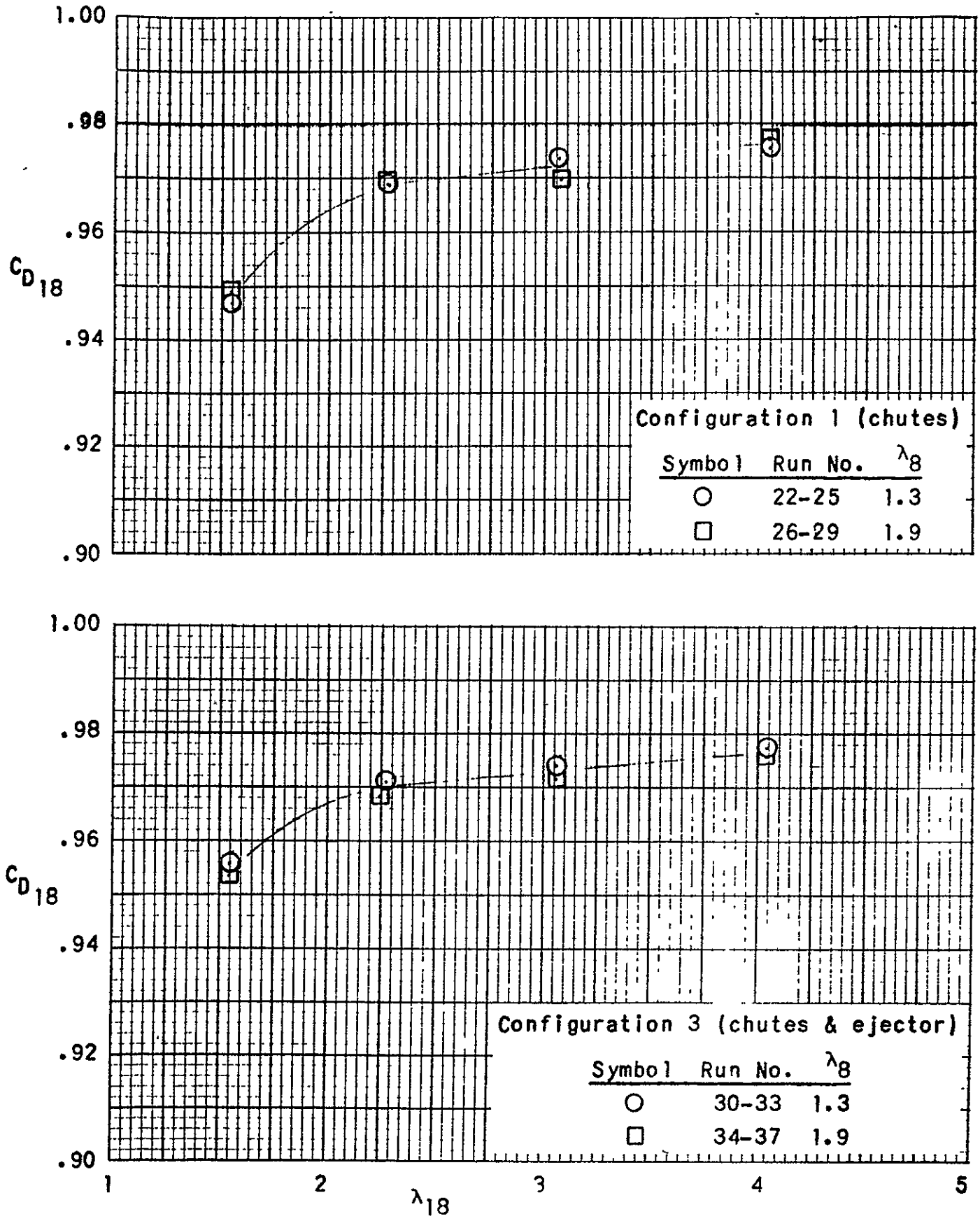

FIGURE 9b. FAN NOZZLE DISCHARGE COEFFICIENTS, CONFIGURATIONS 1 AND 3

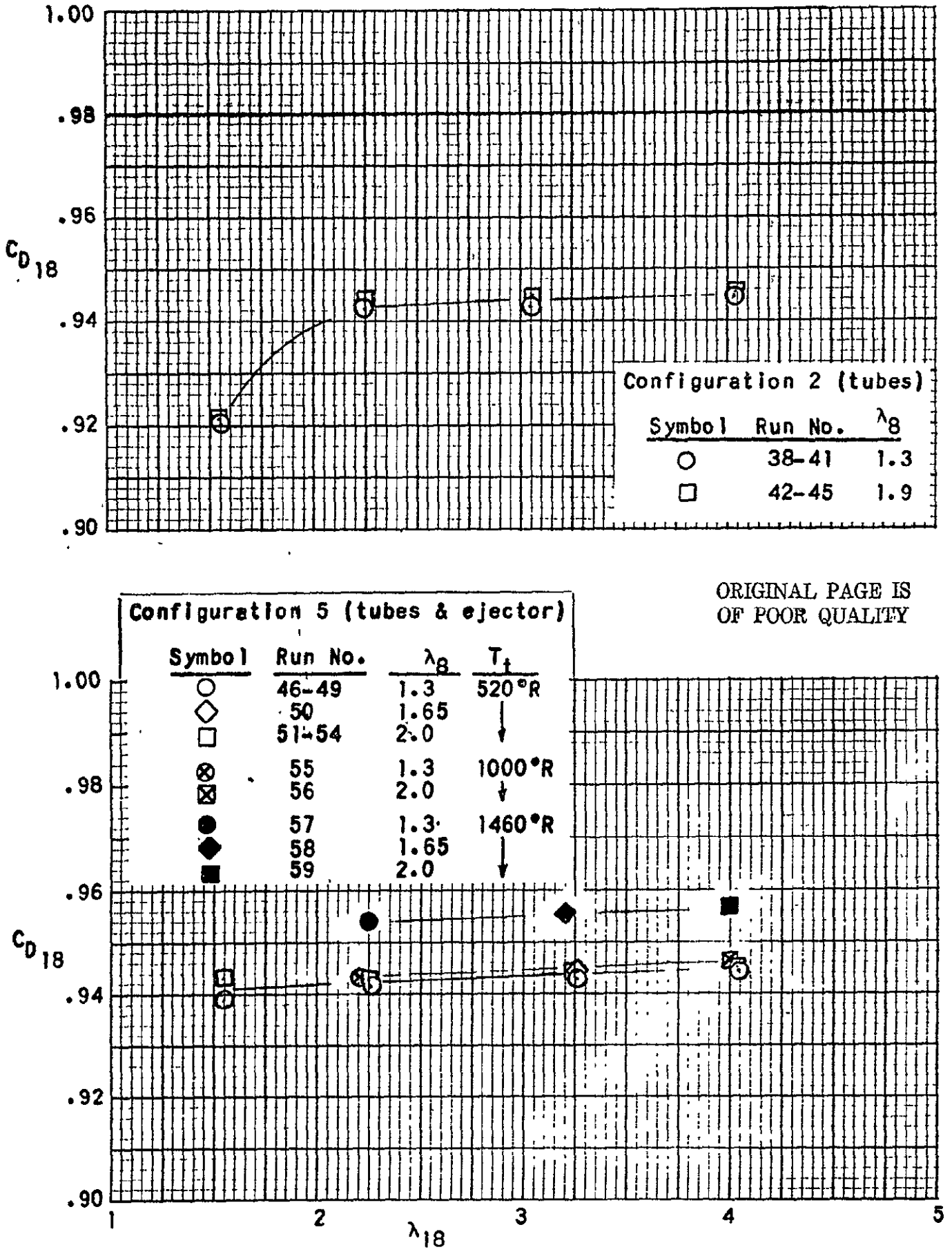

ORIGINAL PAGE IS
OF POOR QUALITY

FIGURE 9c. FAN NOZZLE DISCHARGE COEFFICIENTS, CONFIGURATIONS 2 AND 5

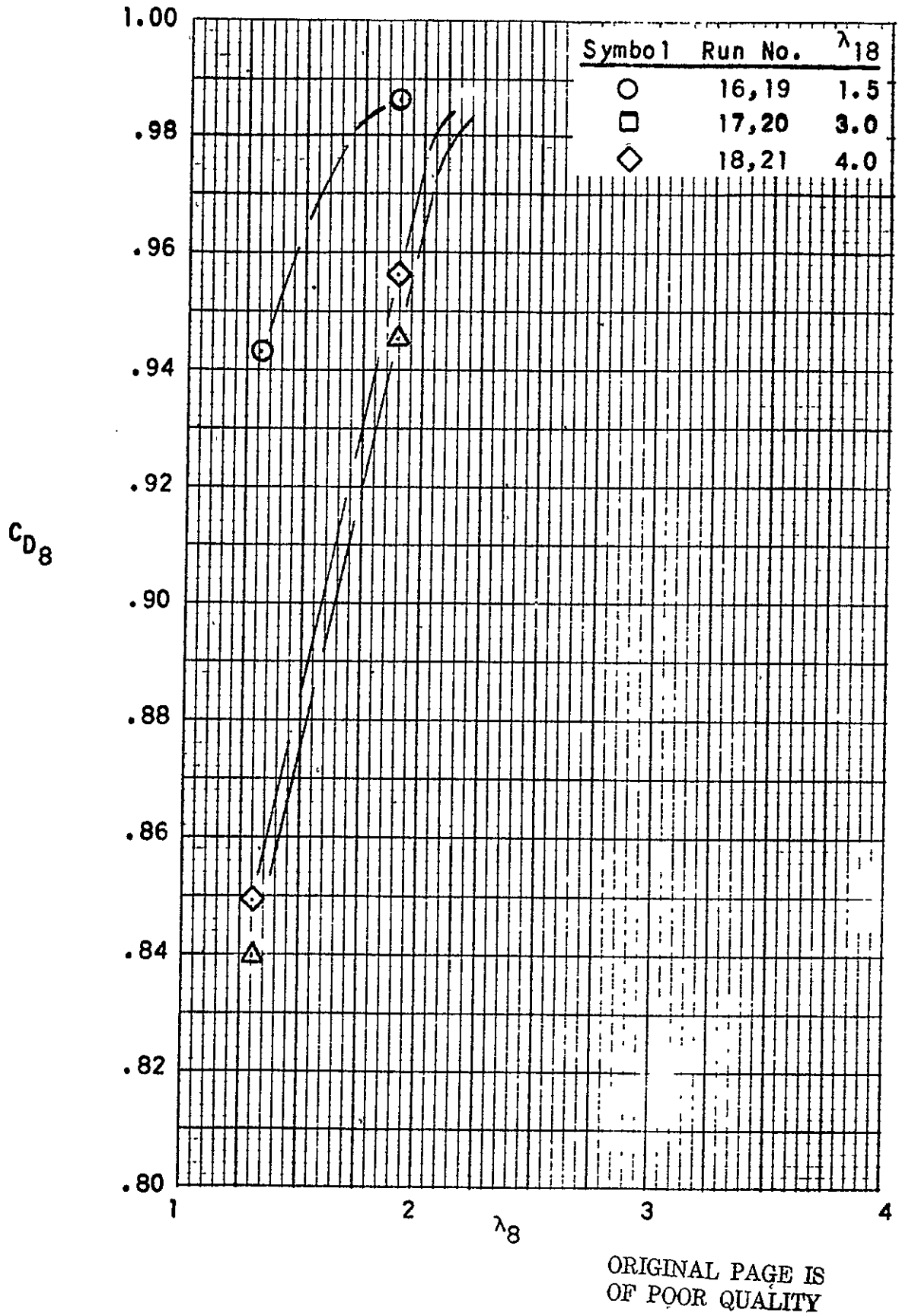

ORIGINAL PAGE IS
OF POOR QUALITY

FIGURE 10a. CORE NOZZLE DISCHARGE COEFFICIENTS, CONFIGURATION 7 (BASELINE)

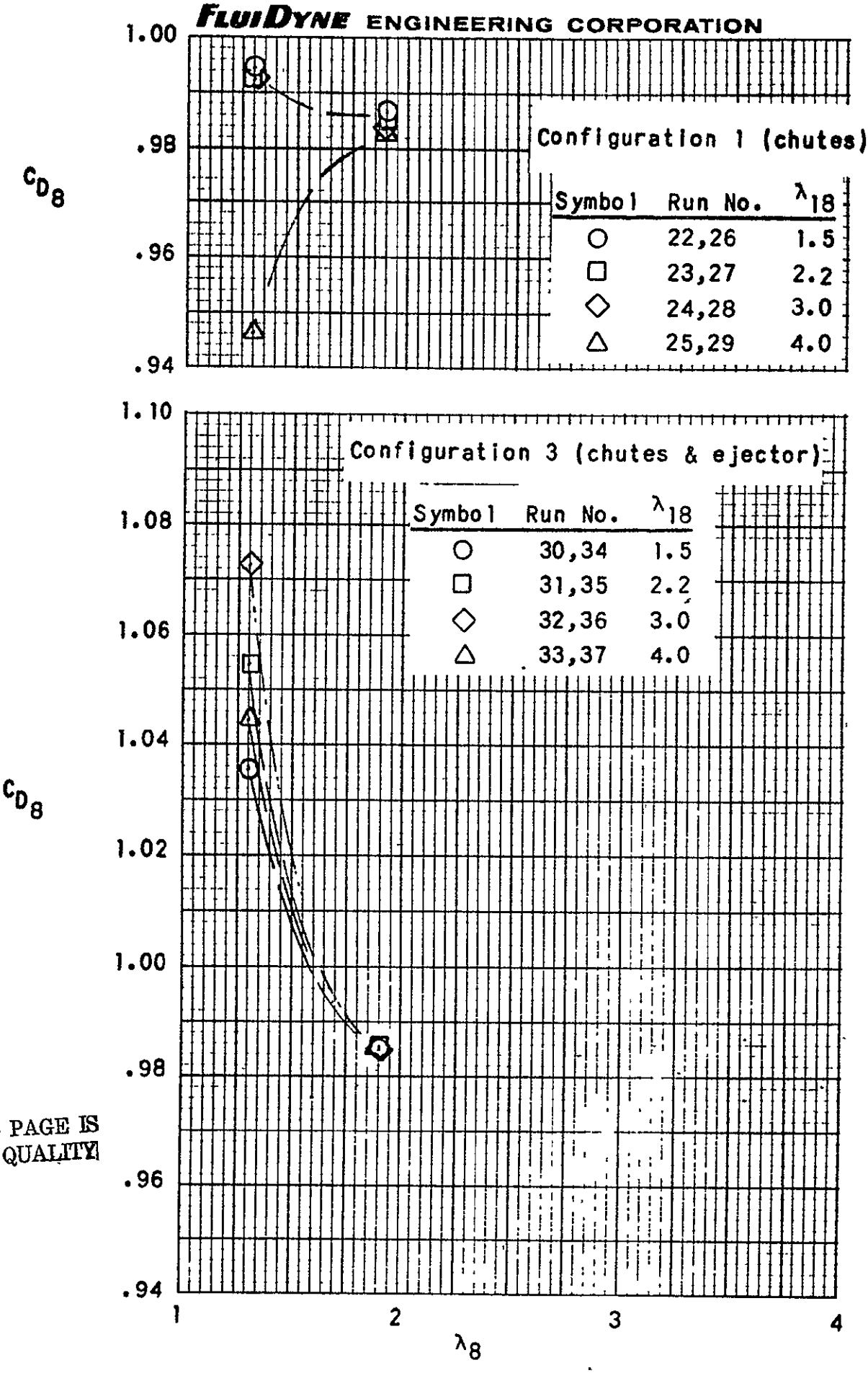

ORIGINAL PAGE IS
OF POOR QUALITY

FIGURE 10b. CORE NOZZLE DISCHARGE COEFFICIENTS, CONFIGURATIONS 1 AND 3

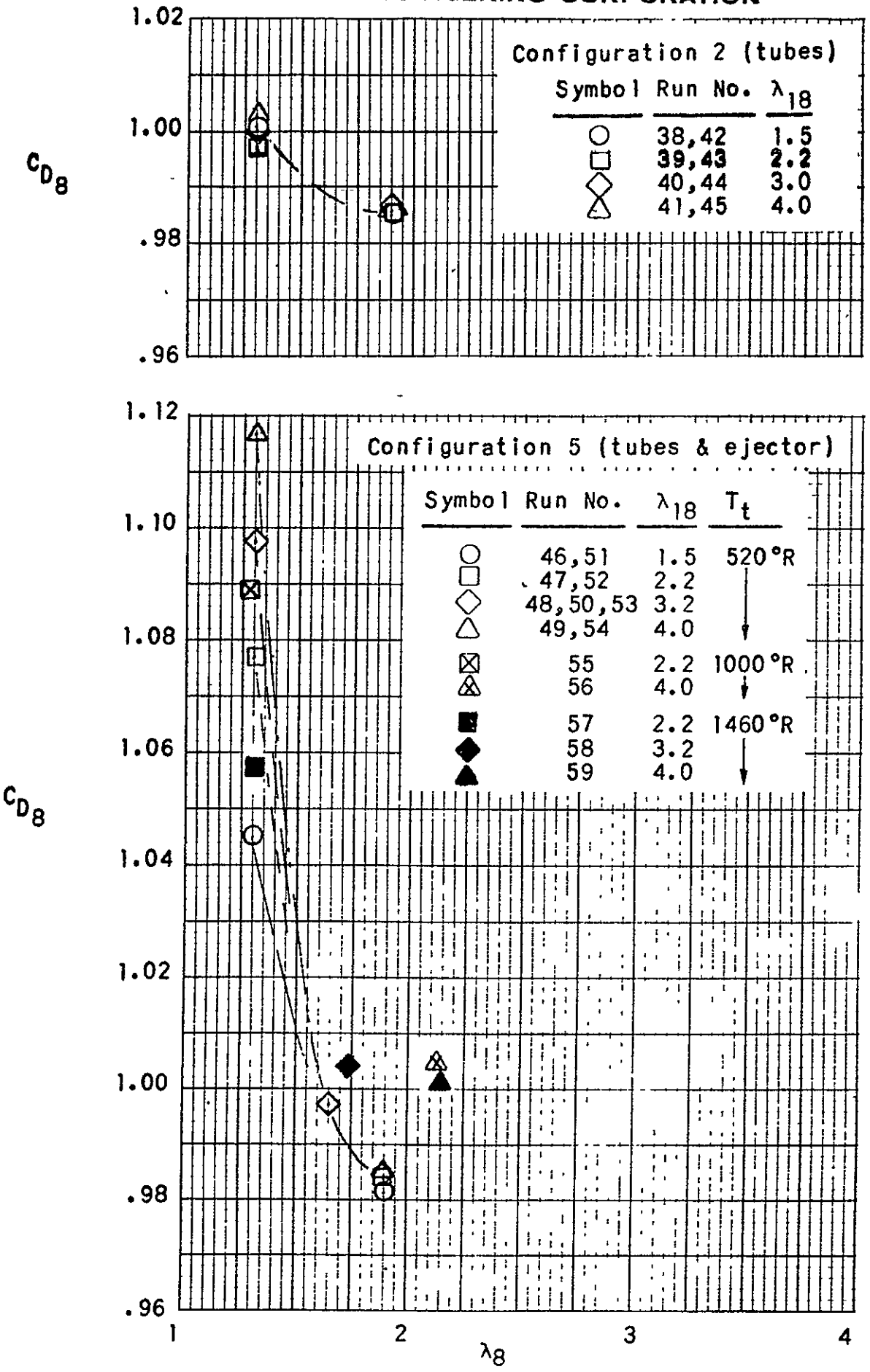

FIGURE 10c. CORE NOZZLE DISCHARGE COEFFICIENTS, CONFIGURATIONS 2 AND 5